*Hydrogen ingestion flash in Sakurai's object: Development of a split convection zone*

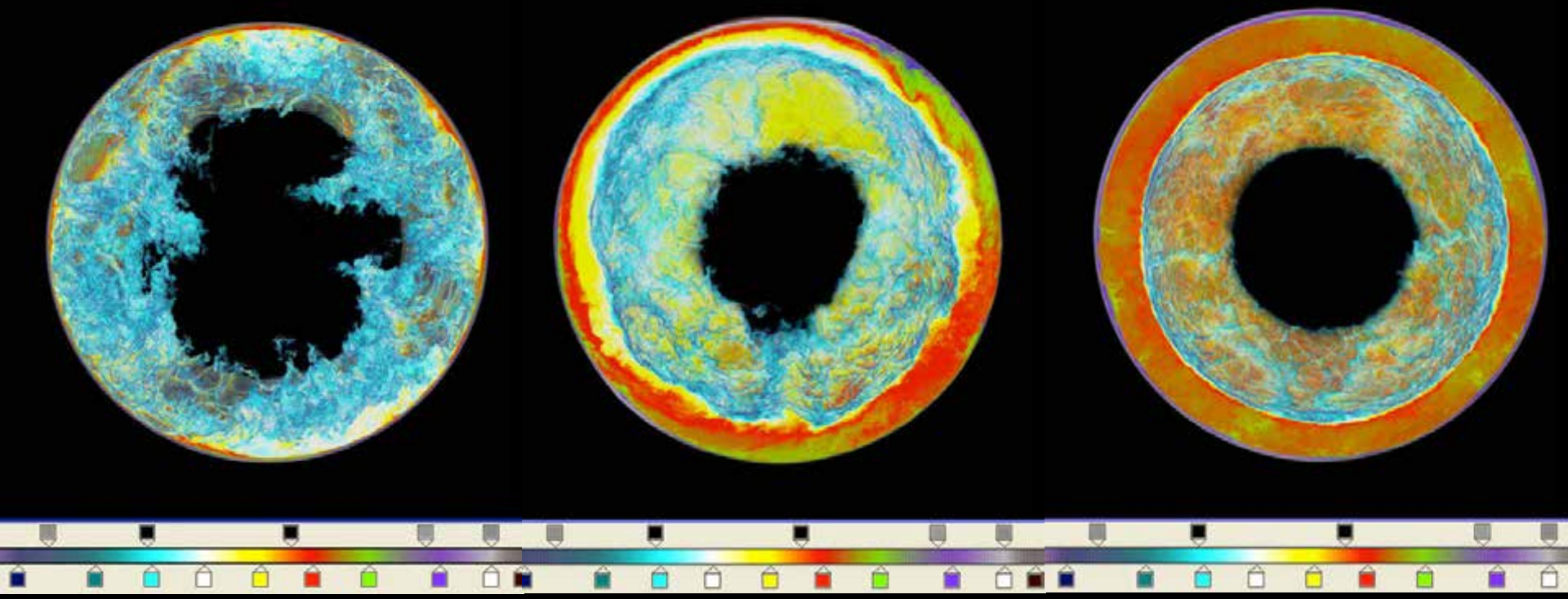

# 3-D Simulations of Hydrogen Ingestion Flashes in AGB Stars as Sites for *i*-process Nucleosynthesis

**Paul Woodward, Jagan Jayaraj, Pei-Hung Lin, Michael Knox**
**Stou Sandalski, University of Minnesota**

**Falk Herwig, University of Victoria**

# The Team:

## @ lcse.umn.edu

Paul Woodward, astrophysics, algorithms, codes.
Jagan Jayaraj (now at Sandia, Albuquerque),
Pei-Hung Lin (now at Livermore),
computer science, domain-specific compilers.
Mike Knox, making everything work.
Stou Sandalski, new code modifications.

## @ uvic.ca

Falk Herwig, astrophysicist, stellar evolution. Our guru.

## @ lanl.gov

Chris Fryer, Gabe Rockefeller, astrophysicists, stellar evolution & stellar explosions.
William Dai, computational physicist, algorithms, codes.

## Extreme Strong Scaling:

- Last year, as friendly users, we took our code for compressible turbulent mixing in inertial confinement fusion and ran a problem with $10560^3$ grid cells for about 85,000 time steps in 41 hours on 702,000 cores on Blue Waters at 1.5 Pflop/s sustained (32-bit).
- This year, we did something much harder:
  we ran with $1536^3$ cells for 5.7 million time steps on 443,232 cores at 0.42 Pflop/s sustained (64-bit).
- Each node hosted 8 MPI ranks, each with 4 threads.
- Just $64^3$ cells per node, and $32^3$ cells per MPI rank.
- Restartable context of only 50 MB per MPI rank.
- 26 time steps per second!
- A dump every 3 minutes for 4 days!
- Glorious stereo movies immediately via GPU nodes.

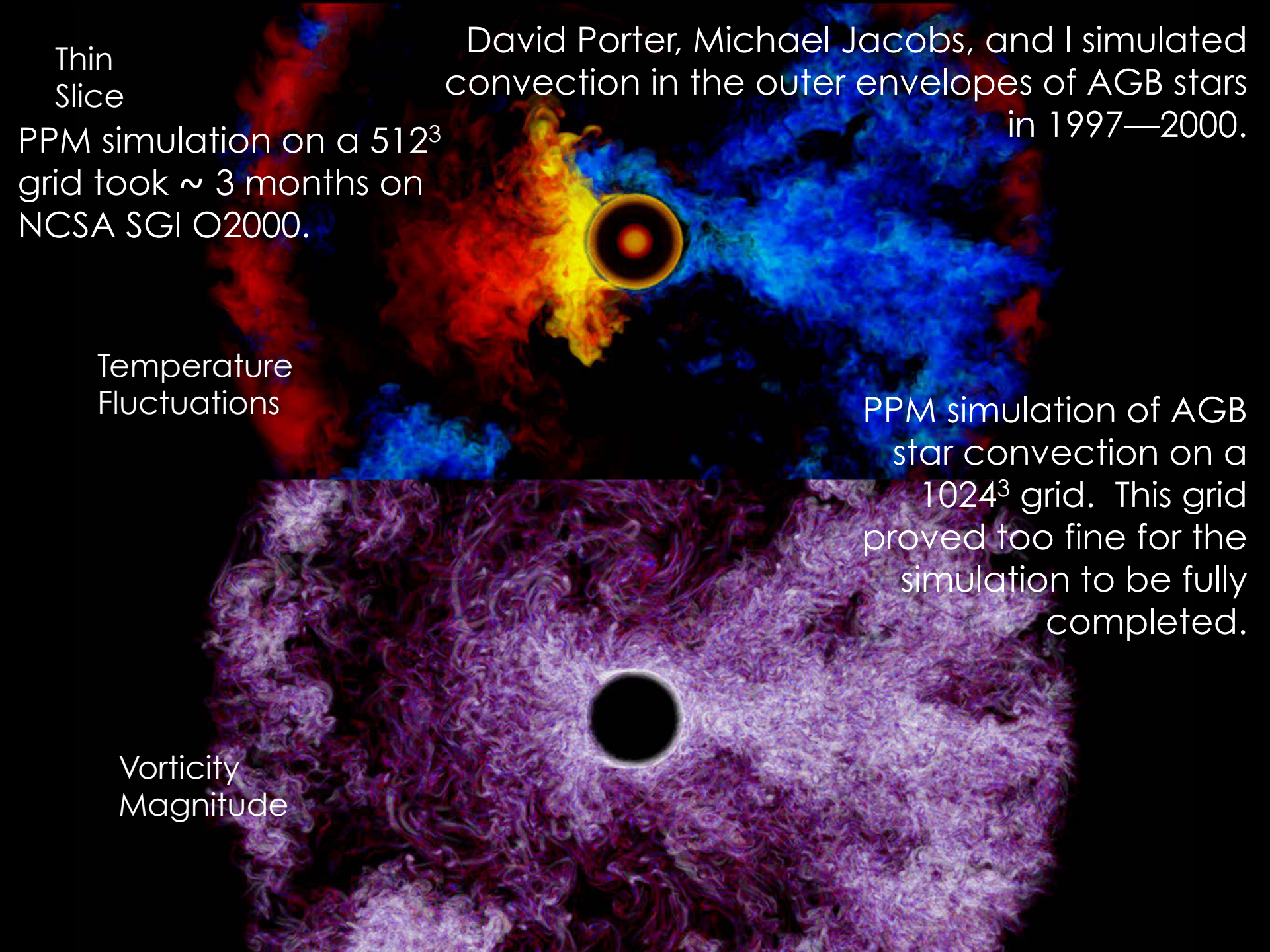
Thin
Slice
David Porter, Michael Jacobs, and I simulated convection in the outer envelopes of AGB stars in 1997—2000.
PPM simulation on a $512^3$ grid took ~ 3 months on NCSA SGI O2000.
Temperature
Fluctuations
PPM simulation of AGB star convection on a $1024^3$ grid. This grid proved too fine for the simulation to be fully completed.
Vorticity
Magnitude

## *Very Late Thermal Pulse:*

AGB star at end of life, having expelled almost all of outer giant envelope, has a last helium shell flash.

Helium shell flash lasts about 2 years.

At height of flash is day-long hydrogen ingestion flash.

The nucleosynthesis is highly sensitive to the hydrogen entrainment rate, subsequent mixing, and transport.

Positive nonlinear feedback from burning ingested fuel.

Deep convection zone results in global oscillatory modes.

This demands a fully 3-D treatment.

## *Context (typical shell convection zone):*

Carbon/oxygen degenerate core of radius ~ 9 Mm.

Helium shell flash convection zone to ~ 18 Mm.

Unburned hydrogen entrained at top of conv. zone.

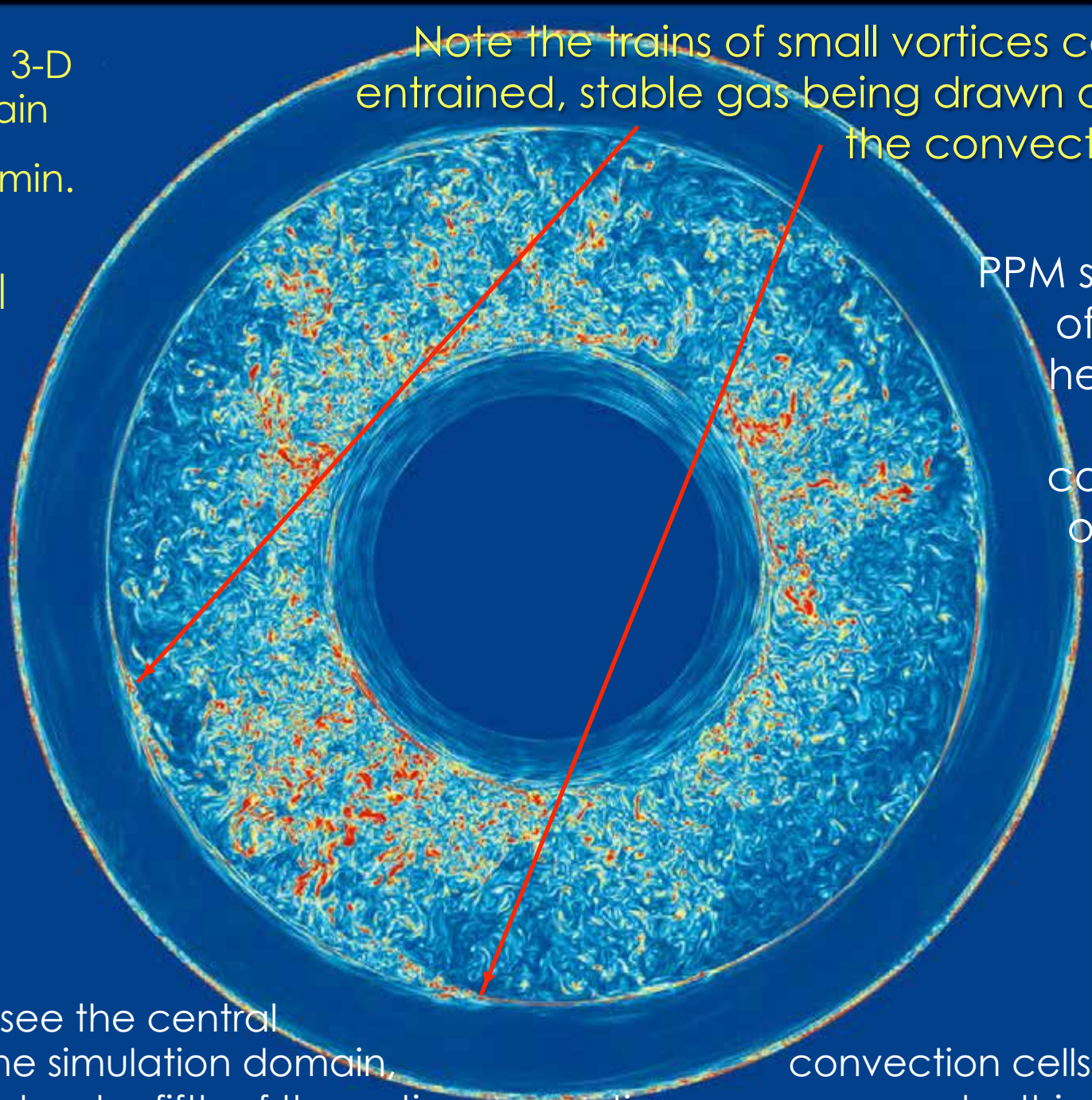
Slice of 3-D Domain
t = 400 min.
|∇×u|
Note the trains of small vortices containing entrained, stable gas being drawn down into the convection zone.
PPM simulation of VLTP star helium shell flash convection on a 1536³ grid.
Here we see the central 0.2% of the simulation domain, convection cells as large as about a fifth of the entire convection zone are seen by this time.

Half of 3-D Domain

t = 400 min.

$FV_{H+He}$

Energy release from burning ingested hydrogen is shown as the dark blue and yellow flame.

Note the trains of small vortices containing entrained, stable gas being drawn down into the convection zone.

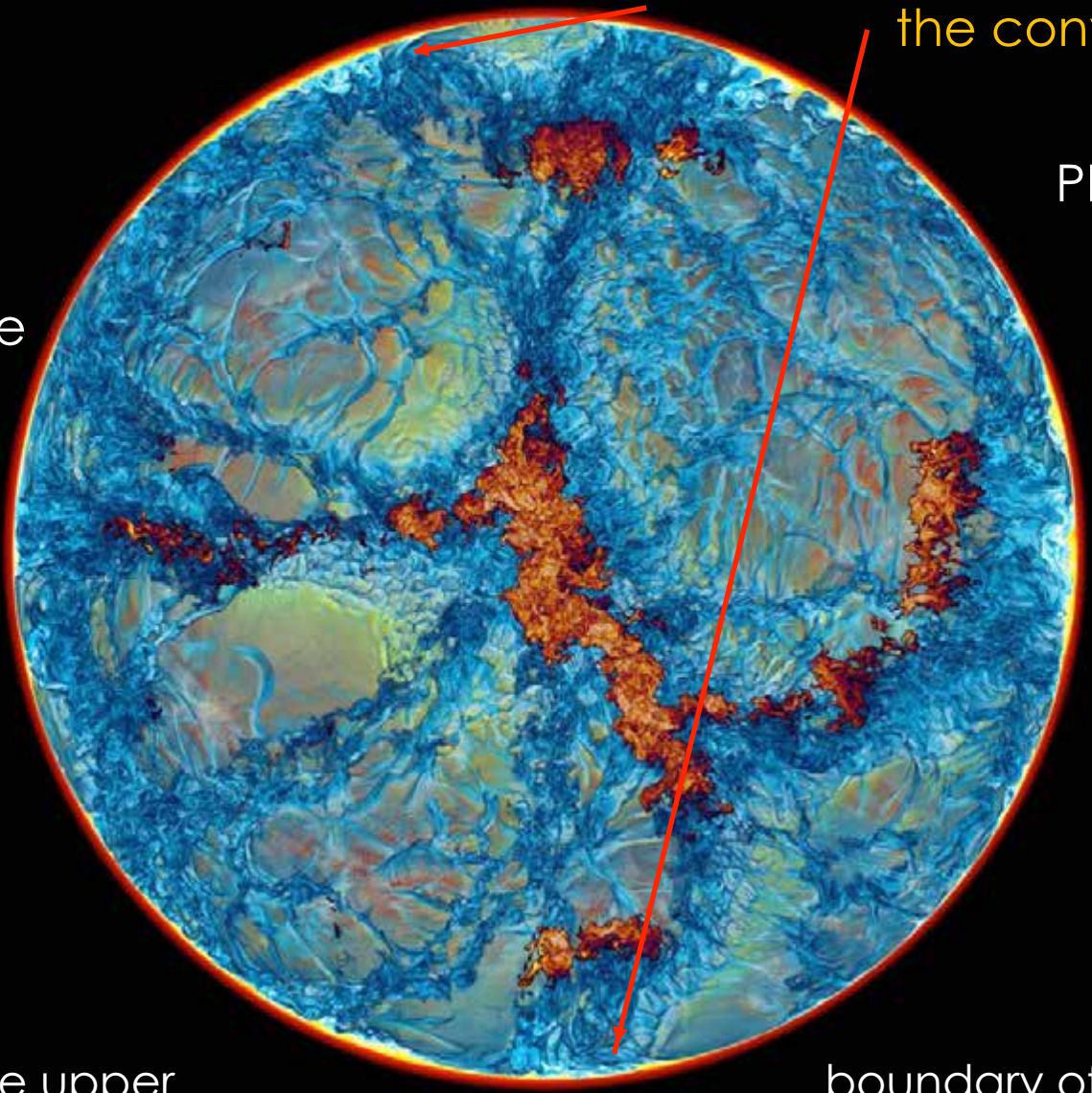

PPM simulation of VLTP star helium shell flash convection on a $1536^3$ grid.

Here we see the upper boundary of the convection zone above the helium burning shell, looking from the center of the star outward. The blue descending plumes trace out the convection cells

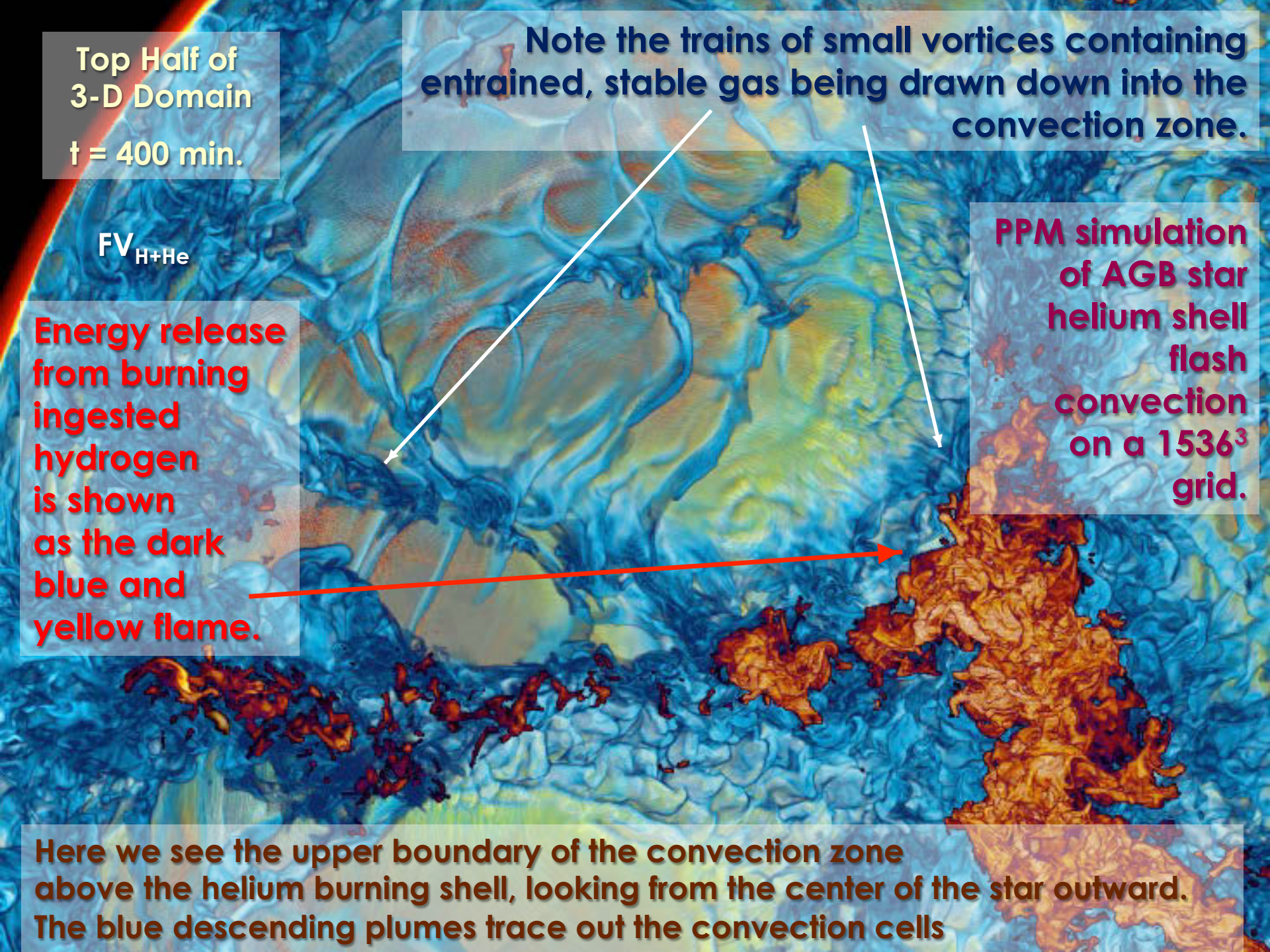
Top Half of 3-D Domain
t = 400 min.
$FV_{H+He}$
Note the trains of small vortices containing entrained, stable gas being drawn down into the convection zone.
PPM simulation of AGB star helium shell flash convection on a $1536^3$ grid.
Energy release from burning ingested hydrogen is shown as the dark blue and yellow flame.
Here we see the upper boundary of the convection zone above the helium burning shell, looking from the center of the star outward. The blue descending plumes trace out the convection cells

## Why is this simulation hard?

- Must include entire convection zone in 3-D grid.
- Flow Mach number between 0.02 and 0.035, increasing ultimately to 0.3 to 0.5
- Need several million time steps.
- Must carefully track H+He drawn down despite its greater buoyancy into the convection zone.
- Must compute reaction rate of $H+^{12}C$ which is highly sensitive to temperature.
- Must track $^{13}N$ that is formed for 10 minutes until decays to produce $^{13}C$
- Need to follow evolution for about 1500 minutes, with over 8 million time steps.

Falk Herwig convinced us that 3-D simulations were needed to understand the H-ingestion flash in metal-poor AGB stars.

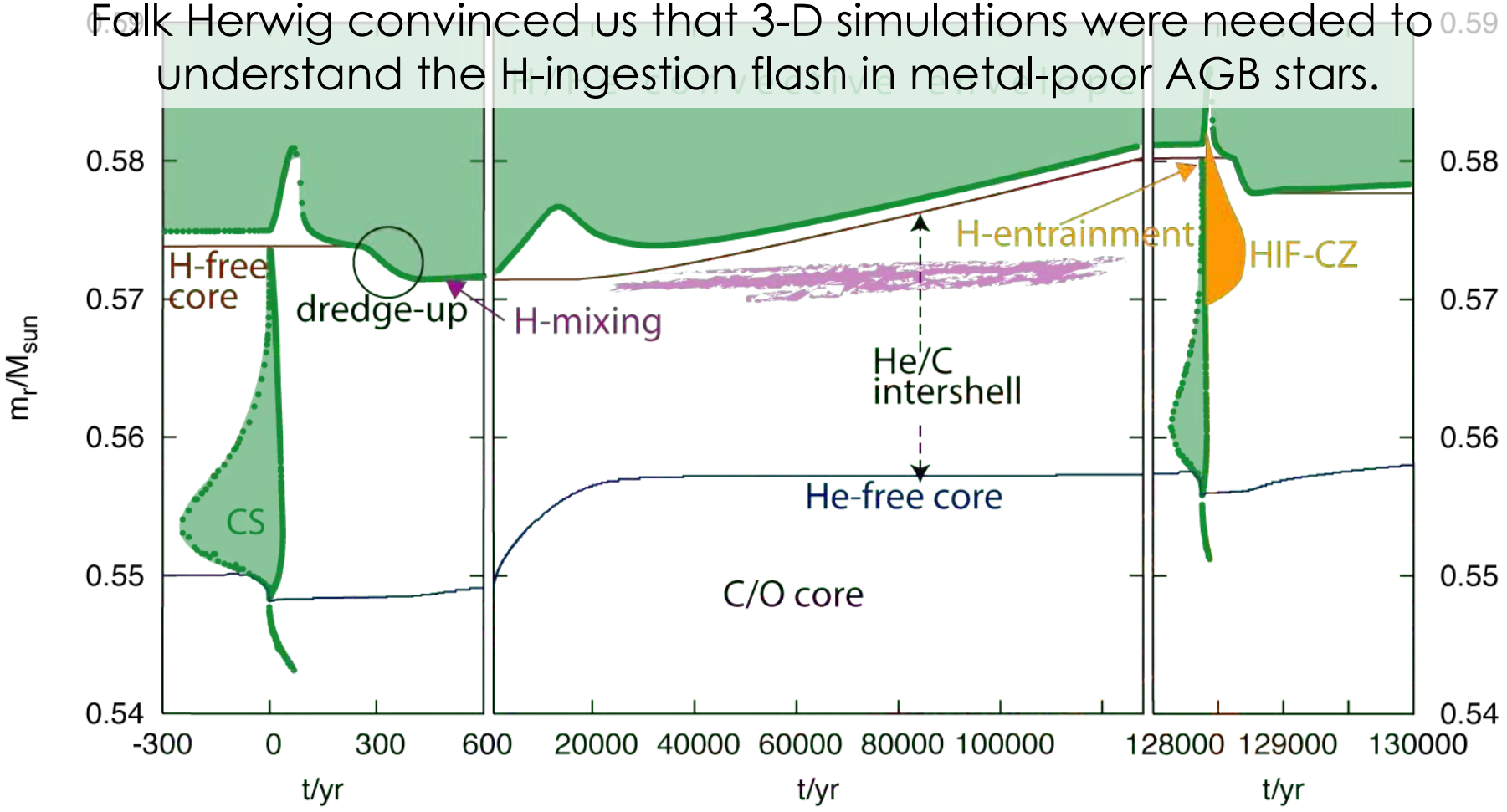


Time evolution of convective mixing and nuclear burning processes in He-shell flash AGB stars. Green regions indicate convectively unstable zones. CS is the He-shell flash convection zone. During and at the end of dredge-up, H-mixing (purple) into the C-rich intershell material can lead to formation of the n-source $^{13}C$ for the s-process (pink shaded region). H-entrainment into the CS leads to a H-ingestion flash convection zone (HIF-CZ), shown schematically in orange for the second He-flash. Adapted from Fig 3 in Herwig 2005.

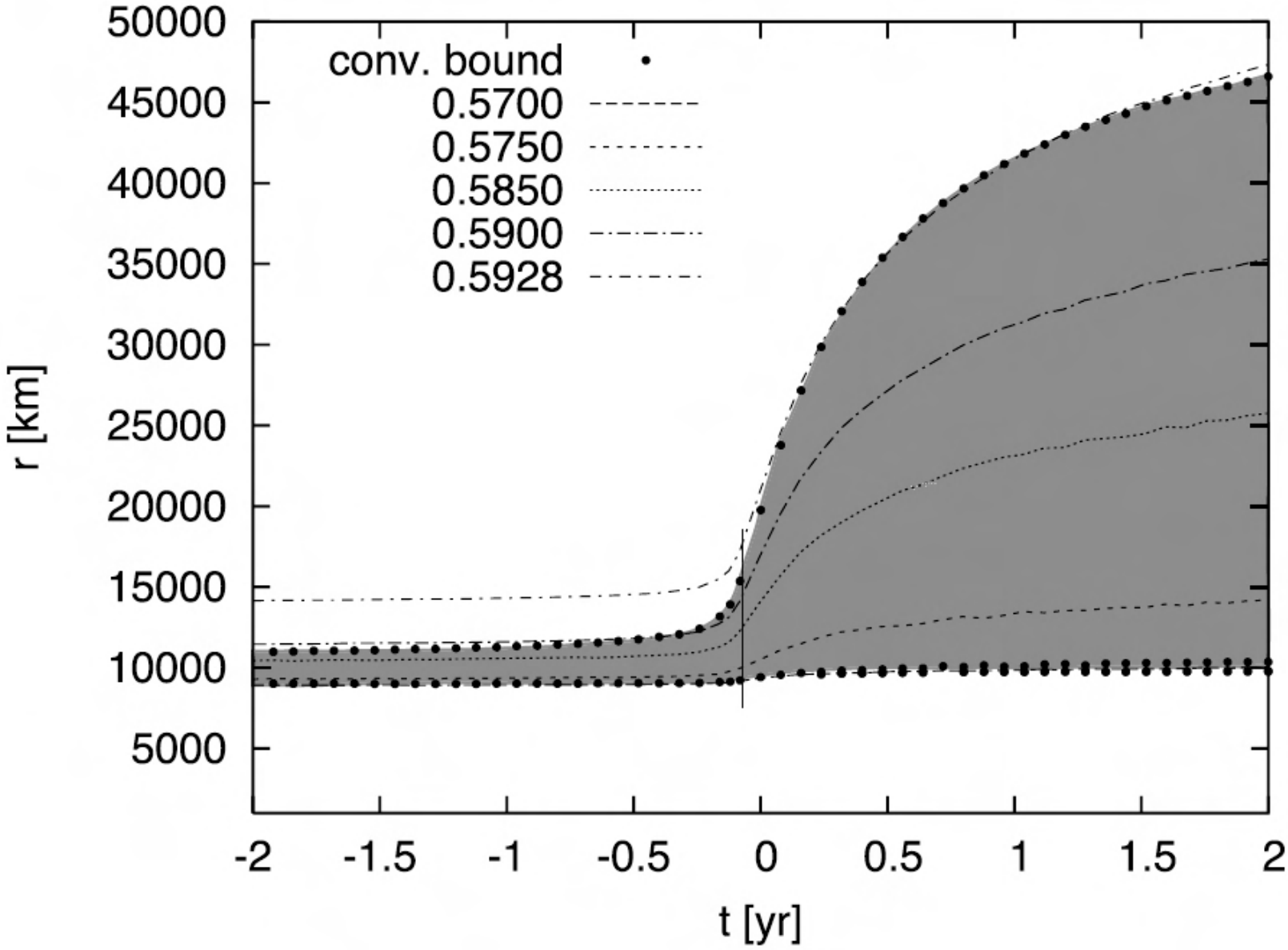


**Time evolution of the radial location of the He-shell flash convection zone based on the 1-D stellar evolution model of Herwig. Time is set to 0 at the peak of the He-burning luminosity. Dots represent individual time steps. Lagrangian lines at different mass fractions are shown. The convection zone grows both in radius and in mass fraction over the 2-year interval shown. Our simulation is performed at about time 0.2 yr on this slide.**

# *Nucleosynthesis in the First Stars:*

**Surely something must be easy about this:**

- **Can use a uniform Cartesian grid.**
- **One can use an explicit code.**
- **Very powerful computers are now available.**
  *Blue Waters enables grids of $1536^3$ @ 0.42 Pflop/s.*
- **The flow's modest Mach numbers allow simplified numerical methods to be used that run very fast.**
  *Messaging only in direction of pass,*
  *Trivial Riemann solver,*
  *No strong shock detection & treatment,*
  *No fluid viscosity, gamma-law, "easy" combustion.*

**One still must deal with the overall cost issue.**

**To use 32-bit arithmetic, we must subtract out the very strongly varying base state.**

# *Addressing the Cost Issue Algorithmically:*


**PPM for slow flow allows coarser grid:**

- Parabolae are just perfect for slow flow.
- Important not to be overzealous w monotonicity.
- PPM interpolates the cell interface value at one order higher formal accuracy than the scheme as a whole.
- Overall accuracy actually increases as Courant number decreases in this regime.

**PPB for gas-gas interfaces allows still coarser grid:**

- Built on Van Leer's Scheme VI. "Best" parabola.
- Delivers benefit only for advection, but that's what we need in this problem.
- PPB is as good as PPM advection (which is pretty good) with a mesh refined by a factor of 2 or 3 in each dimension and time. Extremely cost effective.

Illustration of the way PPB works in 1D.

We not only compute and retain the average value of the distribution in the new cell but also its shape via the best-fit parabola.

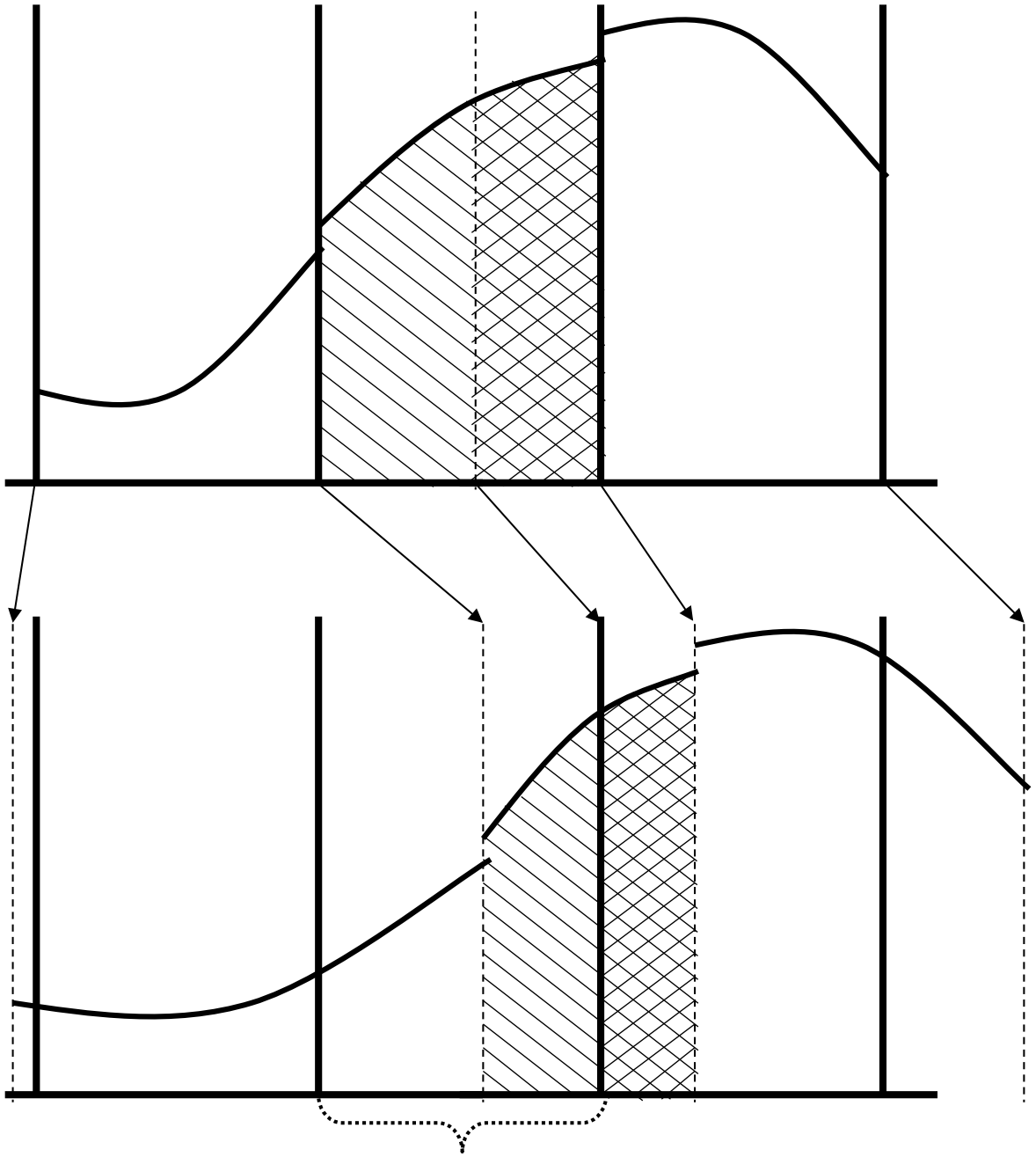

Even spectacular interpolation competence is not sufficient to recapture the shape of the new distribution.

We therefore find that PPB, using the best parabola, is immensely more accurate than PPM.

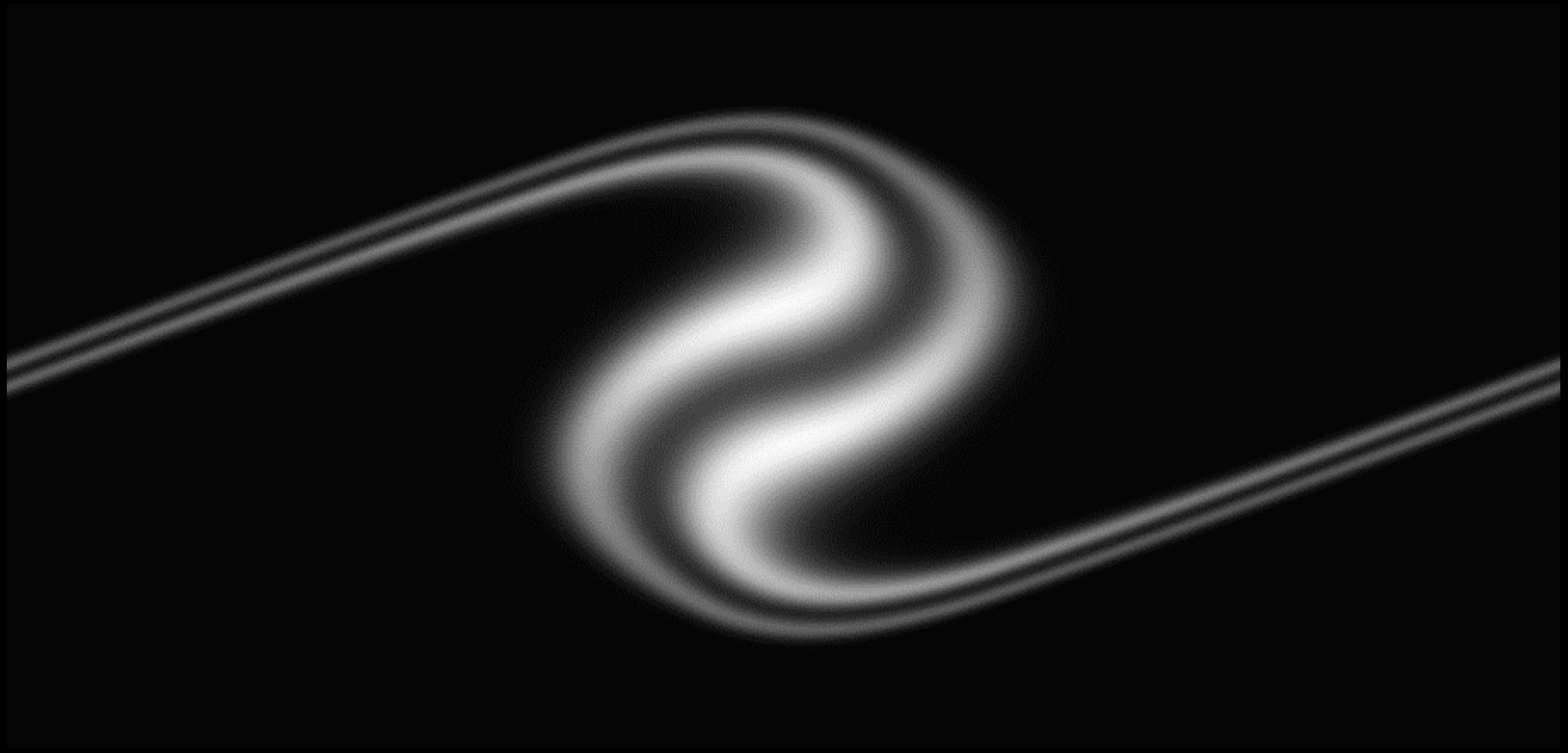

Result of the two-stream gravitational instability problem with the PPB scheme on a grid of $512^2$ cells.
This is the sort of flow that we need to follow accurately in convection and entrainment problems in stellar hydrodynamics.

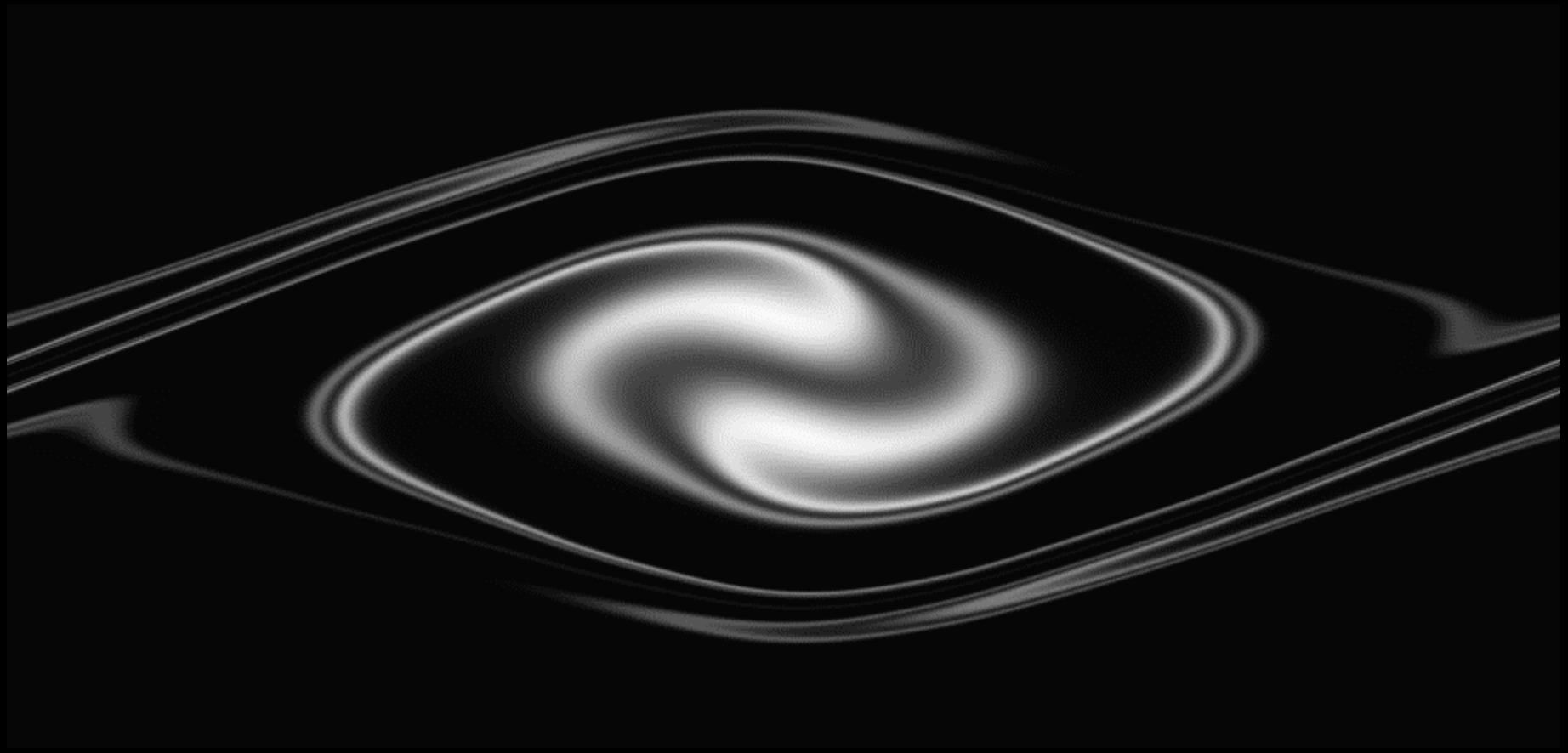

Result of the two-stream gravitational instability problem with the PPB scheme on a grid of $512^2$ cells.
This is the sort of flow that we need to follow accurately in convection and entrainment problems in stellar hydrodynamics.

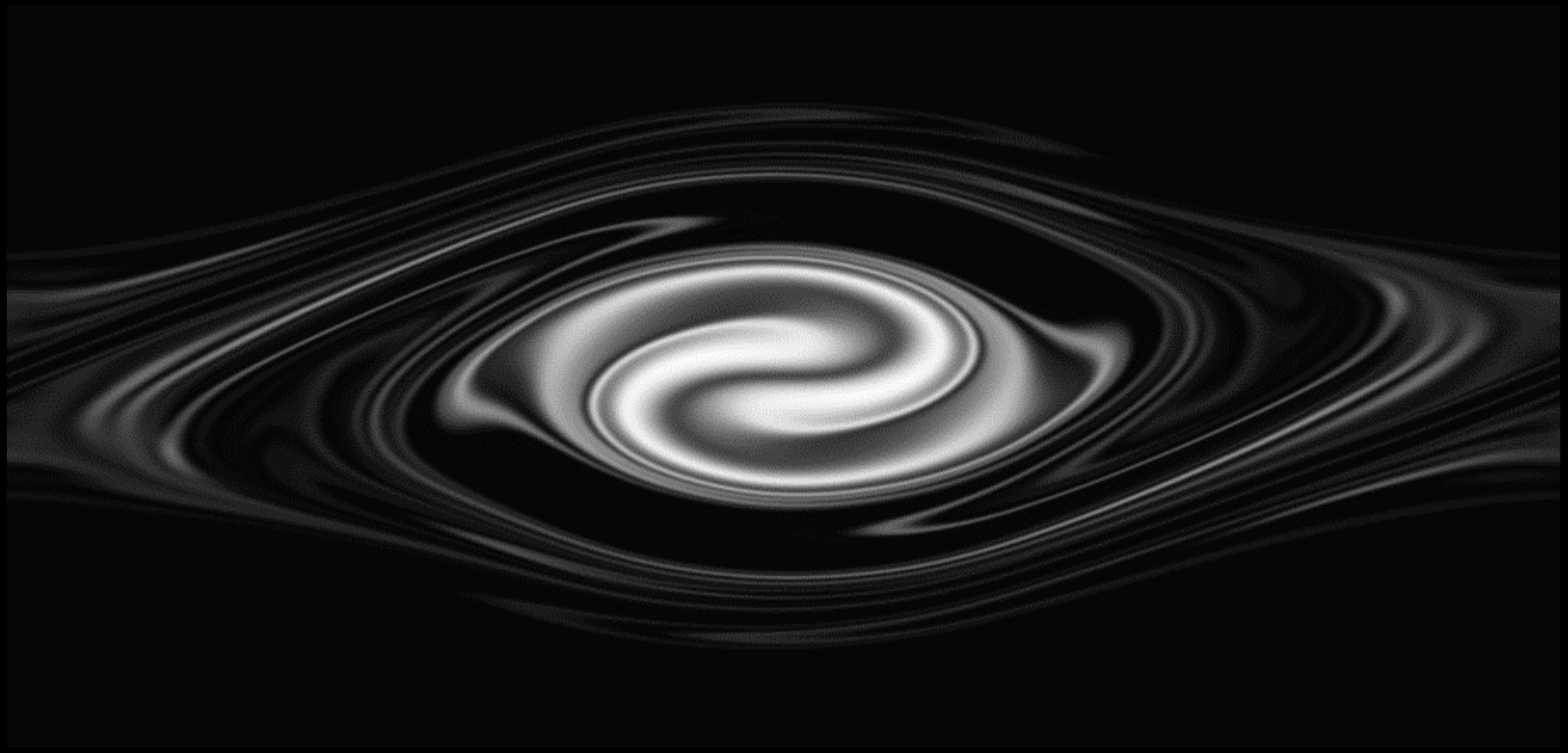

Result of the two-stream gravitational instability problem with the PPB scheme on a grid of $512^2$ cells.
This is the sort of flow that we need to follow accurately in convection and entrainment problems in stellar hydrodynamics.

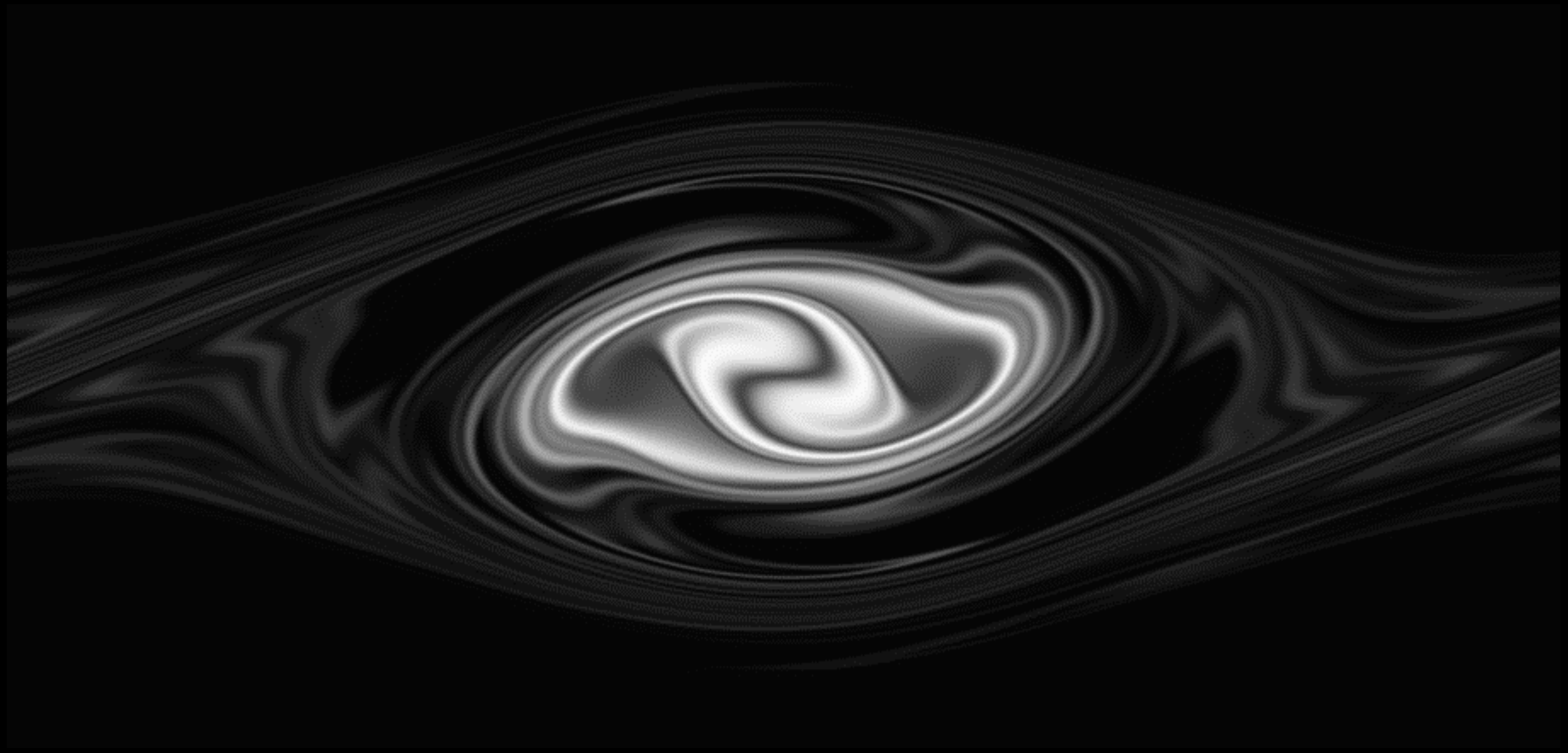

Result of the two-stream gravitational instability problem with the PPB scheme on a grid of $512^2$ cells.
This is the sort of flow that we need to follow accurately in convection and entrainment problems in stellar hydrodynamics.

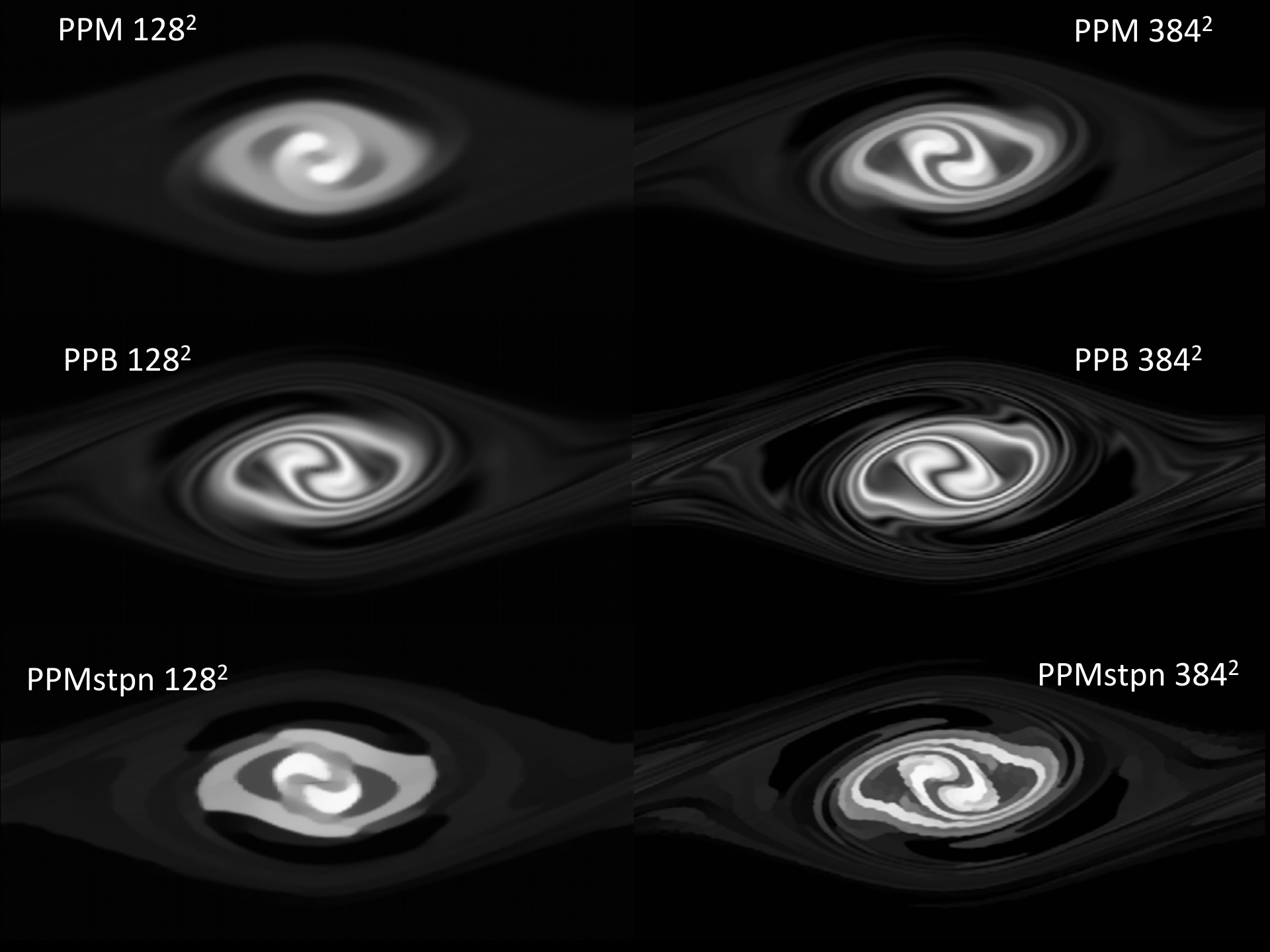
PPM $128^2$
PPM $384^2$
PPB $128^2$
PPB $384^2$
PPMstpn $128^2$
PPMstpn $384^2$

Result at time 15 of the gravitational two-stream instability problem. PPB $128^2$ grid.

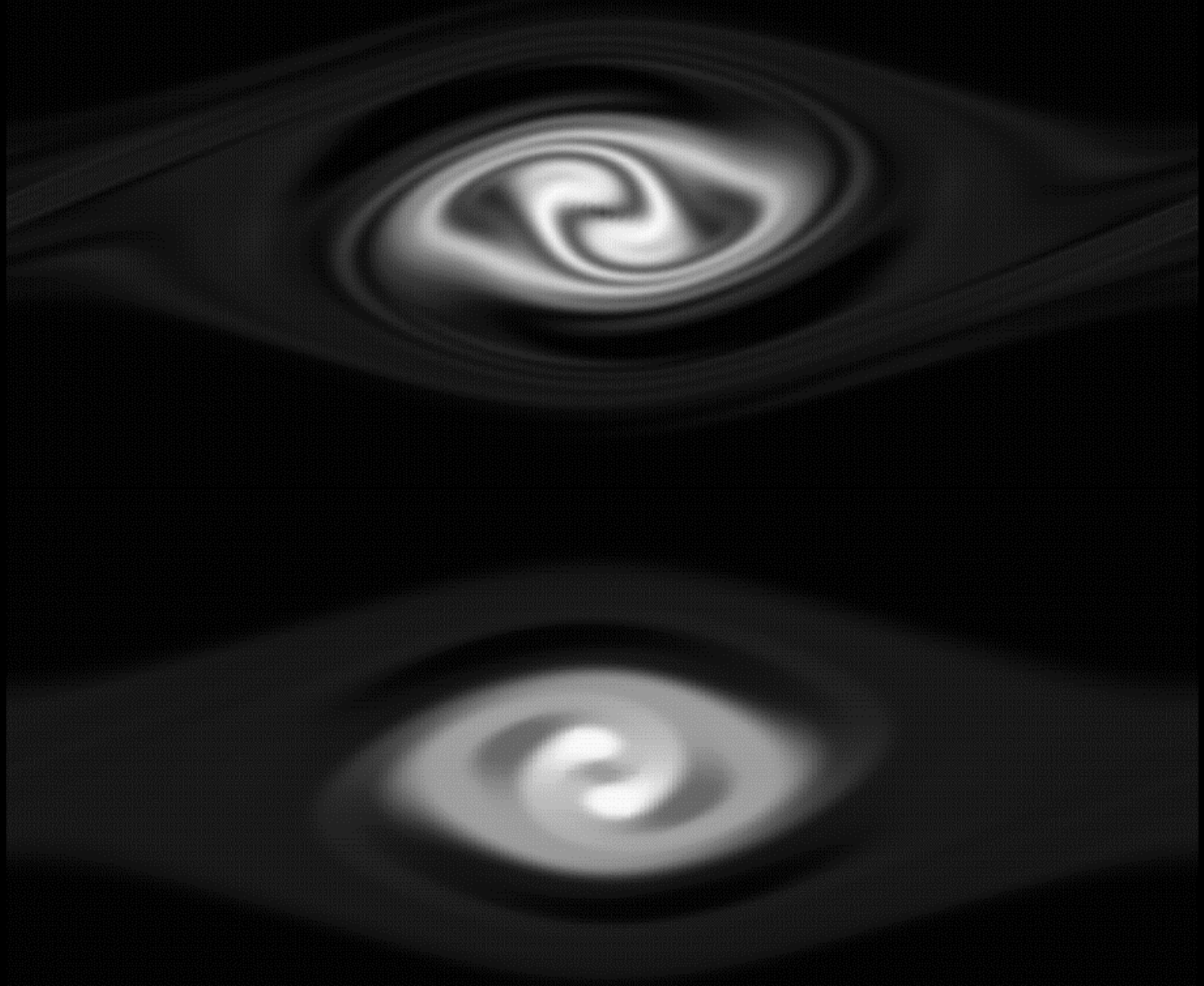

Result at time 15 of the gravitational two-stream instability problem. PPM $128^2$ grid.

Result at time 15 of the gravitational two-stream instability problem. PPB $128^2$ grid.

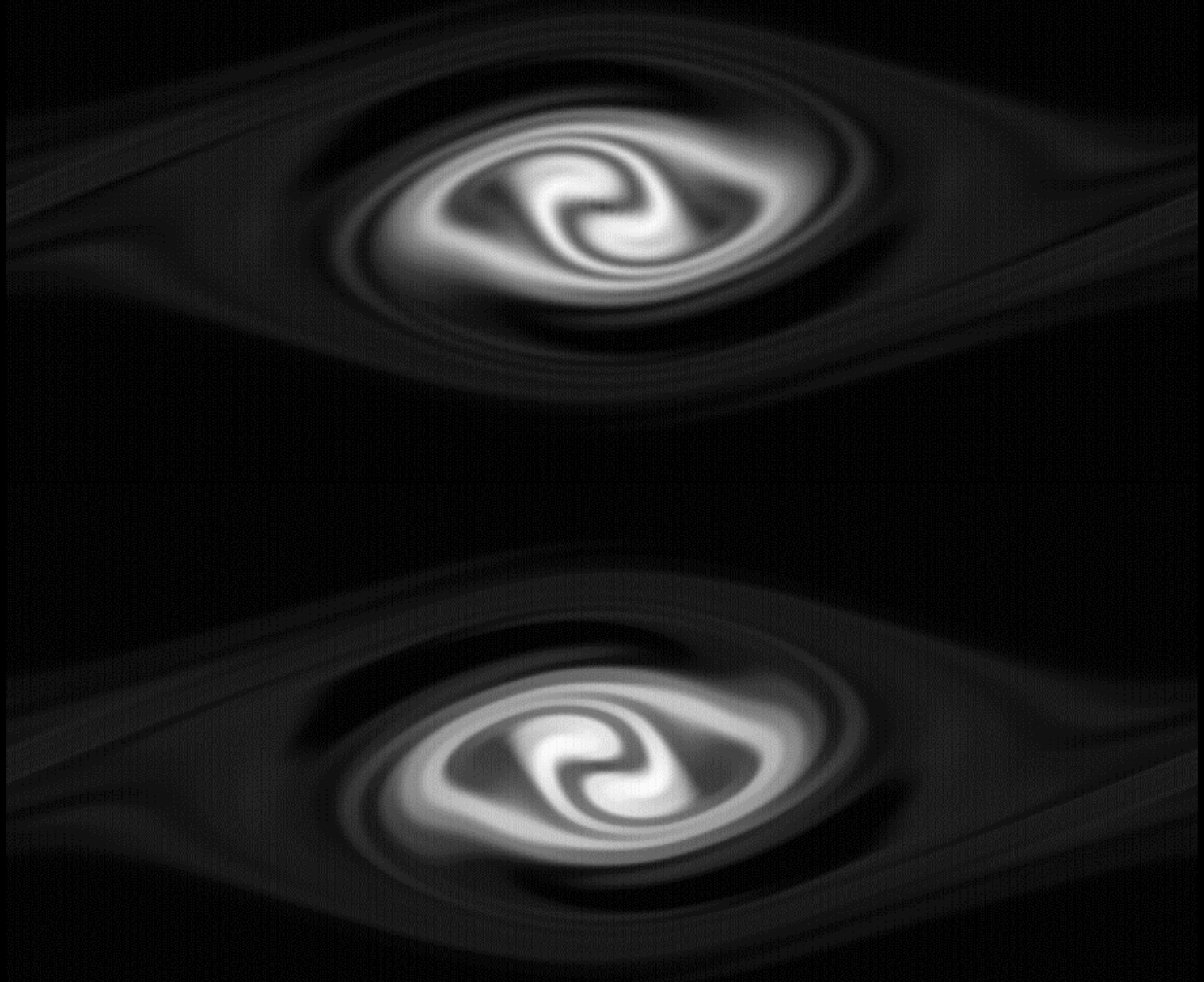

Result at time 15 of the gravitational two-stream instability problem. PPM $384^2$ grid.

Result at time 15 of the gravitational two-stream instability problem. PPB $128^2$ grid.

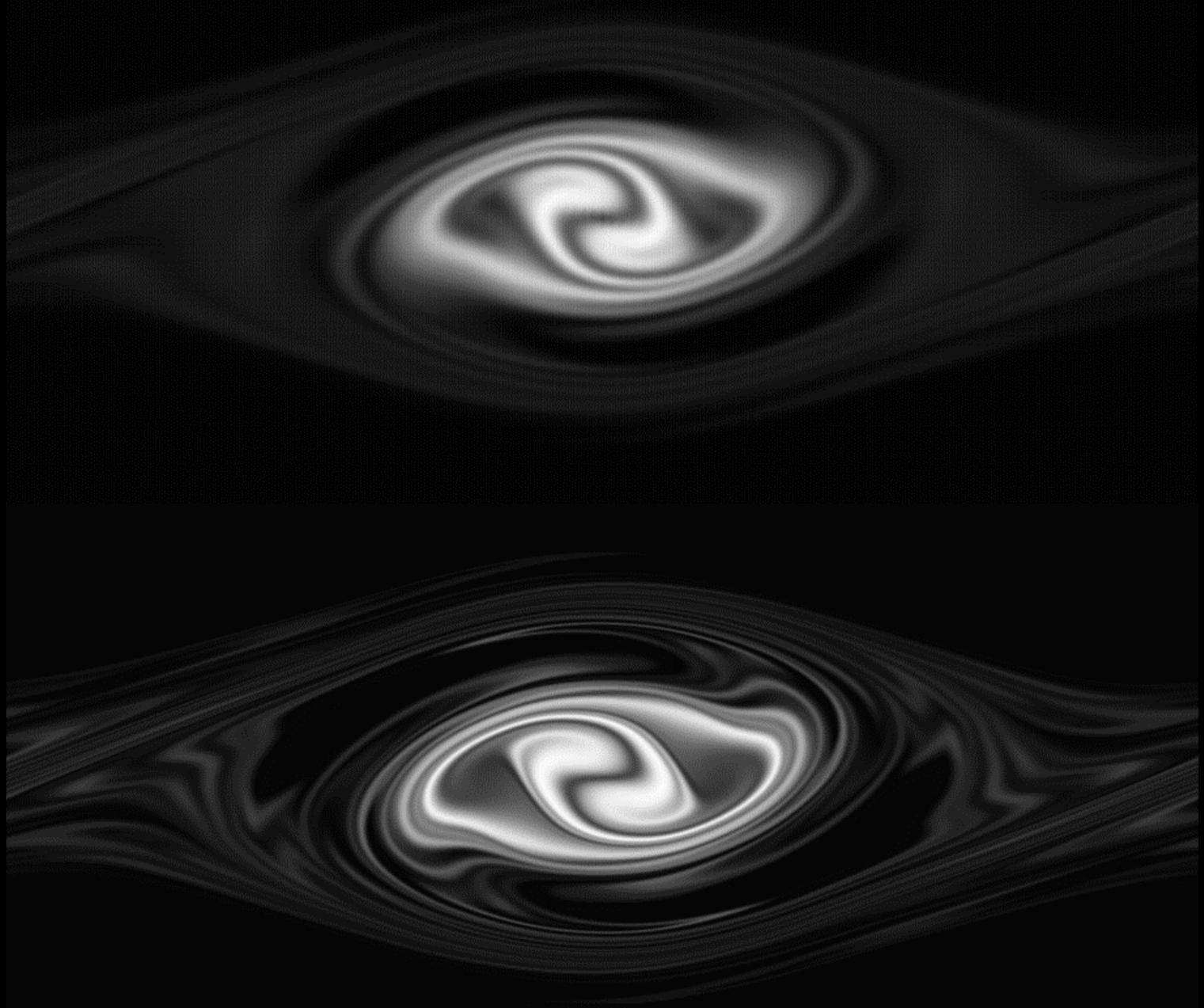

Result at time 15 of the gravitational two-stream instability problem. PPB $512^2$ grid.

# *Addressing the Cost Issue Structurally:*


**The code structure is distinct from its algorithms:**

- Good algorithm gives same accuracy for less computer time, usually by enabling use of a coarser grid.
- Good parallel implementation does same, by running same arithmetic faster and on more CPU cores.
- If on same equipment, your code runs a problem in 20 hours and mine runs it in 1, I get more done.
- But if your code only scales to 256 nodes, and mine scales to 25,000 nodes, I get 100 times as much done.
- These 2 factors are multiplicative, making for truly enormous differences in what we can accomplish.

**Our PPM code aggressively addresses both issues:**

- We run at 12% of peak on each node.
- And we can run at this rate on 22,000 nodes at once.

# *Addressing the Cost Issue Structurally:*


**Restructure code to operate on grid briquettes:**

- $m^3$ cells per briquette, with $m = 2$ or 4.
- Process briquettes in 1-D sequence in each 1-D pass.
- Prefetch 1 briquette ahead, and do entire computation in the on-chip cache in vector mode.
- Latest code does entire computation for 3 passes for grid block of $8^3$ briquettes within on-chip cache.
- Computational intensity is over 86 flops per word read or written, but of course not as good as LinPack.
- Performance is 10% to 12% of the peak performance of an entire node, even at scale & with all I/O costs included. This gets us to sustained 32-bit Pflop/s.

**Can others do this?**

- We have developed automated code translators.

We take every cell and chop it up into 64 cells, a briquette.

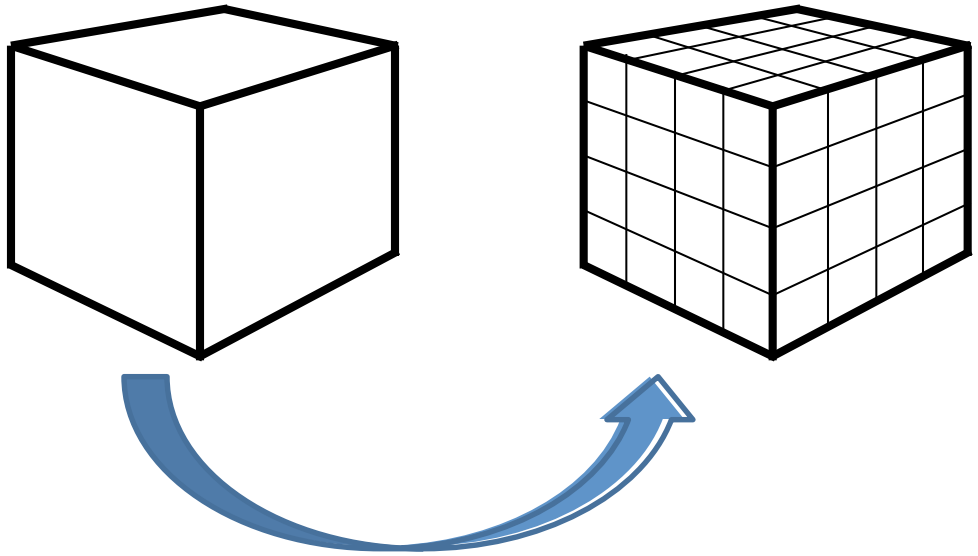

Computation on the resulting grid can exploit a SIMD engine.

The briquette is a data atom that can be very efficiently prefetched into cache.

MPI messaging exchanges ghost briquettes rather than ghost cells, messages are constructed as briquettes are updated, and all messaging is fully overlapped with computation.

Core of program is code for single briquette update.

In the on-chip cache workspace, we have many short segments of grid planes, each holding one variable and none > 5 planes.

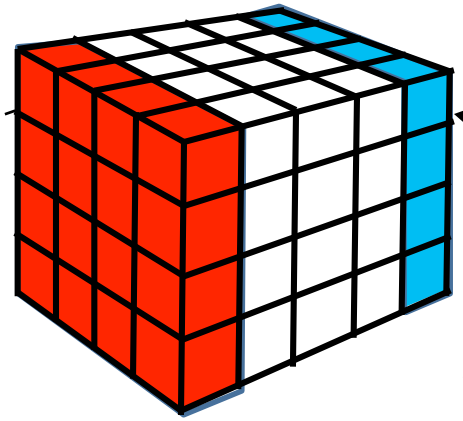

In the cache, we unpack arriving briquettes into our temporary segments, and we pack results into updated briquettes.

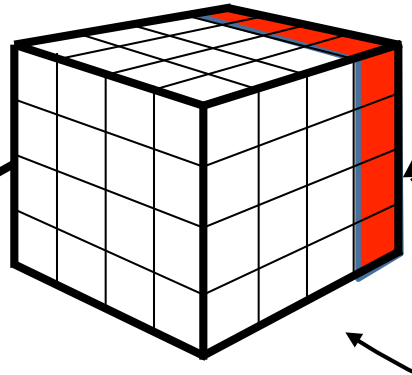

These briquettes are in transit between main memory and the cache.

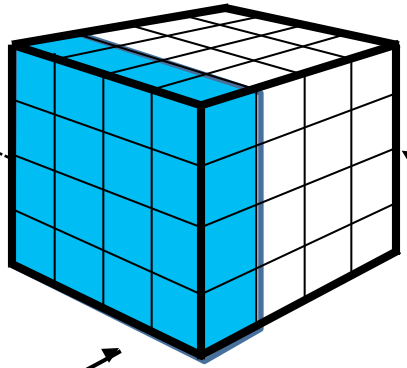

The computation proceeds along a sequence of briquettes at same grid level.

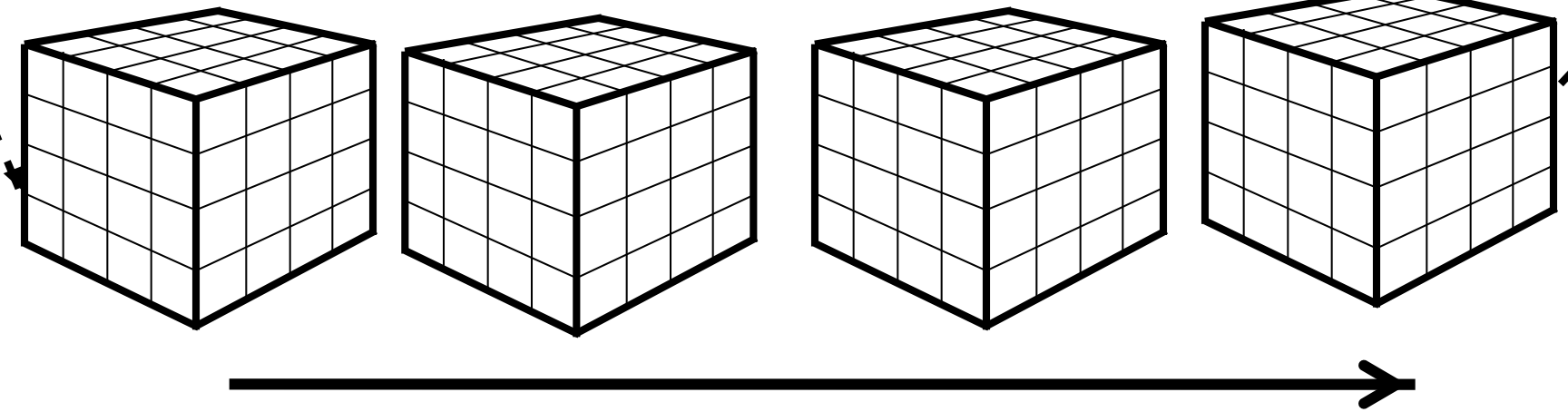

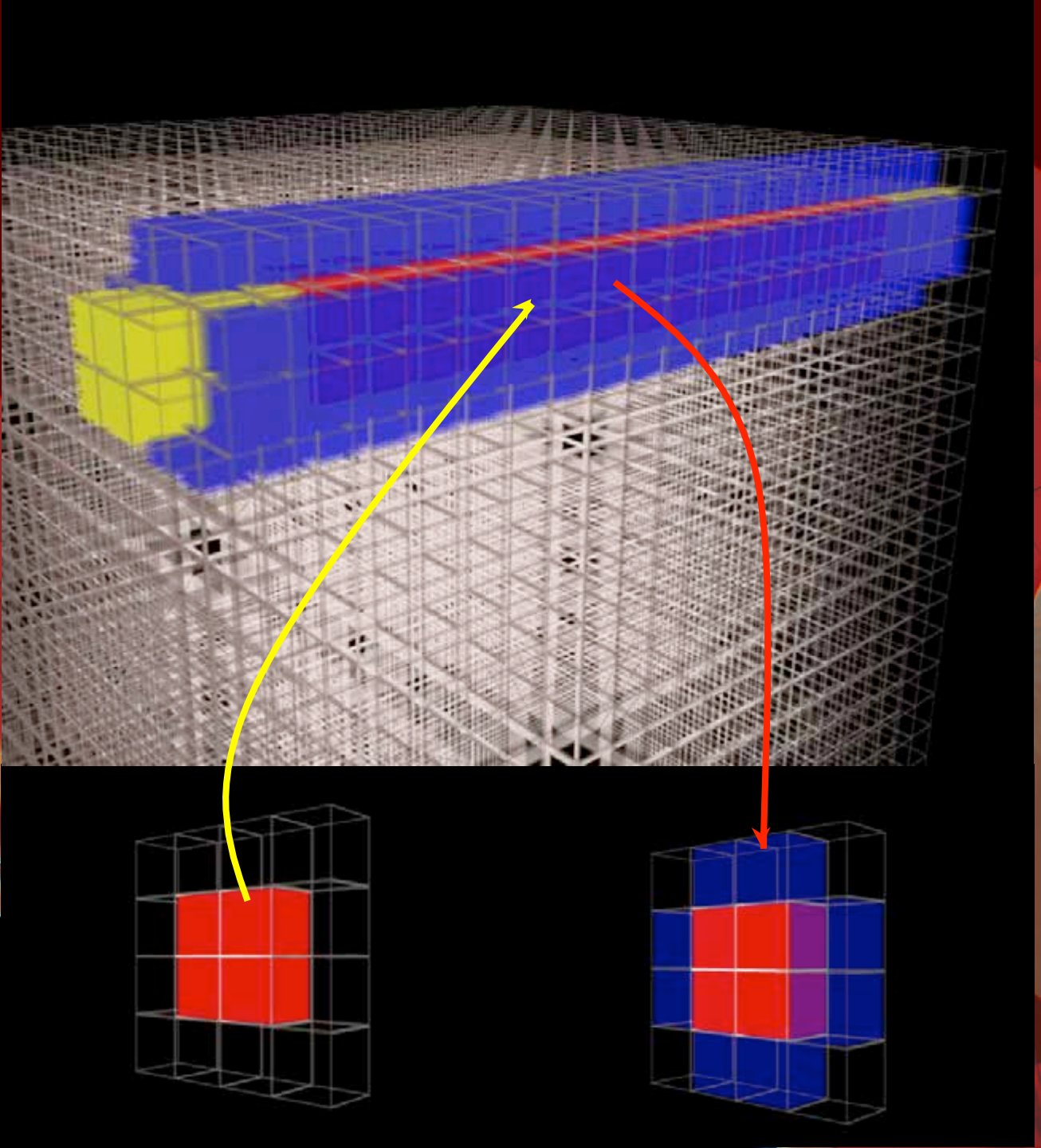

PPM difference stencil for high-speed flow suggests pipelined updates of grid pencils. Planes of 4 briquettes are extracted, updated, replaced.

Placement of 10 largest running jobs on the Gemini torus. Mon 27.01.2014 at 04:34:48 PM CST

| JOBID | USERID |
|---|---|
| 564751 | knox0043 |
| 565243 | lawrenz |
| 564004 | lawrenz |
| 565450 | harshith |
| 563257 | bstein |
| 564927 | yanxinl |
| 565368 | redwards |
| 565370 | redwards |
| 565456 | jejoong |
| 565163 | jejoong |

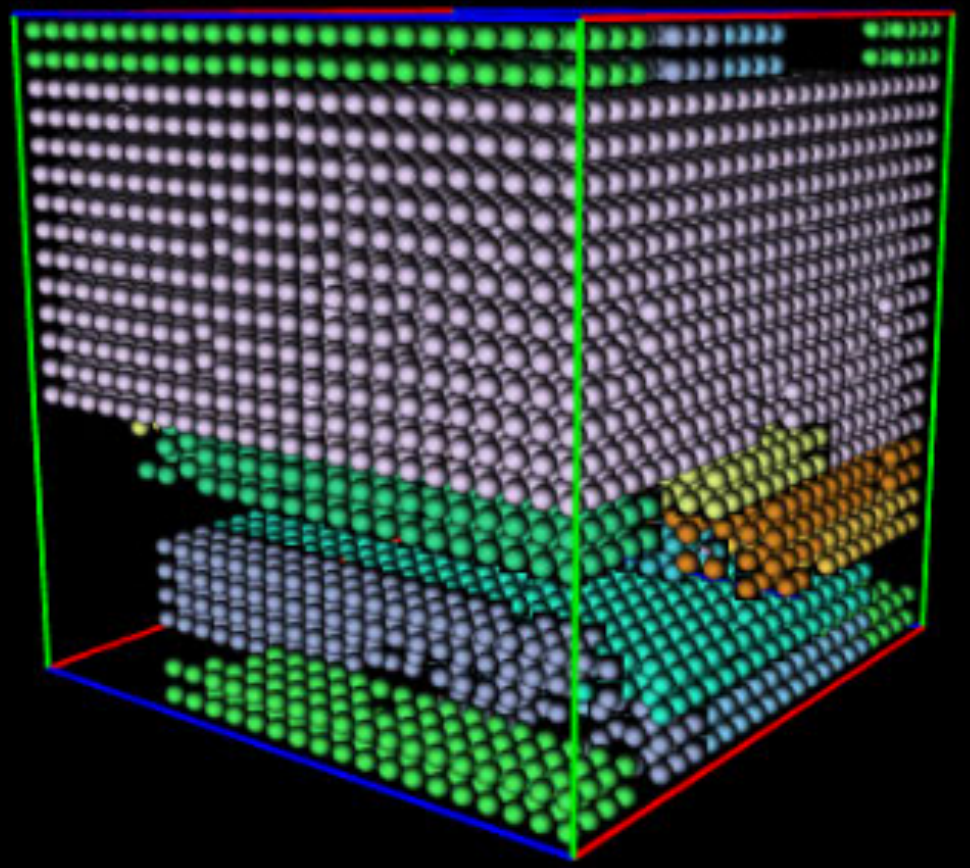

# *Addressing the Cost Issue Structurally:*


**Restructure code so that each MPI rank is multithreaded and all MPI messaging is completely overlapped with computation, so is NO WAITING:**

- **Entirely different set of code design considerations.**
- **Threads must share data, BUT ALMOST NEVER.**
- **Caching hardware will automate joint data accesses.**
- **Thread tasks MUST be self-scheduled.**
- **Thread barriers MUST be avoided like the plague.**
- **Redundant work of threads KILLS performance.**
- **Immensely faster *at scale* than pure MPI.**
- **Avoid redundant work by saving 20 KB workspace.**
- **Problem that took 2.5 months @ NCSA in 2003 is now done on 1/8 of Blue Waters in 10 min. 34 sec.**

**Can others do this?** ***This is not just about MY code.***

# *Unexpected Benefits of Restructuring:*


**Virtue is of course its own reward, but . . .**

- **Data context for 3 passes of 1-D update only 5.0 MB**
- **Fits into L3 cache!!**
- **Restart dump image for team of 64 workers is 1.6 GB**
- **Fits into team leader's main memory!!**
- **Restart dumps to team leader's /tmp RAM disk.**
- **Dumps will take NO TIME!**
- **If a node dies, overwhelmingly unlikely it is a leader.**
- **We can restart from leader dumps INSTANTLY.**
- **Leaders have so little to do that they could *render*.**
- **We could make multiple movies at NO COST.**
- **We could free up all those students to learn more useful aspects of scientific computing, *or even science*.**

**Can others do this? *This cannot be just about MY code.***

# Benefits for Machine Utilization:

Not only can we utilize a lot of the machine, but . . .

- We could compress or expand dynamically.
- Max of 32 MPI ranks per node.
- Min of 4 MPI ranks per node.
- Max of 8 threads per MPI rank.
- Min of 1 thread per MPI rank.
- 216 teams of 514 ranks each.
- Min of 3,470 nodes. Max of 27,756 nodes.
- Can stop on a dime: write out 1.6 GB to live DRAM memory of each of 216 team leaders in seconds.
- Move workers to any set of nodes with any desired number of threads per worker in a matter of seconds.
- Kill job, if not enough nodes available, in time for 216 team leaders to each write to disk 1.6 GB. < 3 min.

# *Interactive Supercomputing:*

**The code runs so fast that it could be interactive . . .**

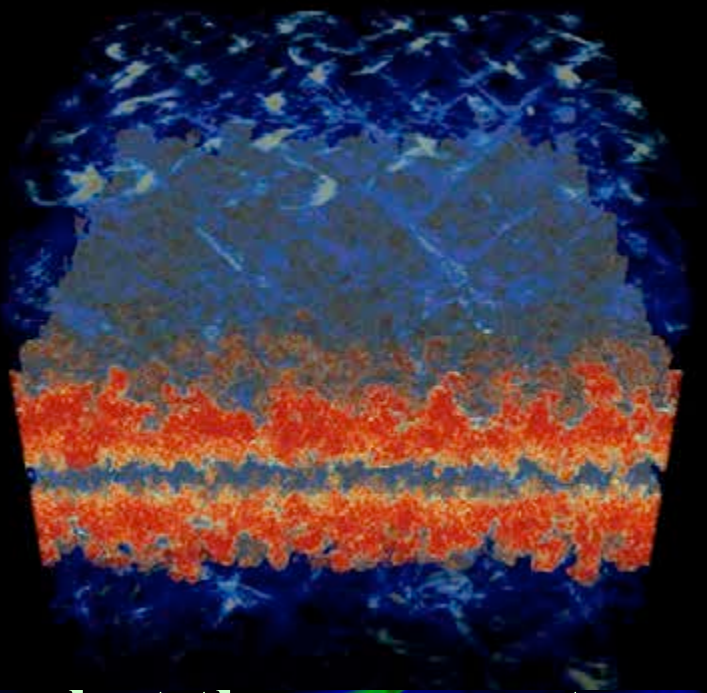

- **4 mins to set up problem.**
- **10.5 mins to run problem.**
- **20 dumps of 4 variables.**
- **Dump only 1 byte per grid cell.**
- **3 mins to reformat data.**
- **20 mins to build octree files.**
- **13 mins. To make 6 movies.**
- **3 mins to send them to UMN.**
- **Have the 13,824 workers render what they compute.**
- **Have the 216 team leaders composite these views.**
- **Send to UMN over Internet.**
- **Zoom and pan on PowerWall as simulation runs.**

***Full interactivity requires image rendering inside the code.***

|Vorticity|

4 frames from the movie.

Compress-ible mixing of krypton gas and air by Richtmyer-Meshkov, Rayleigh-Taylor, and Kelvin-Helmholtz instabilities.

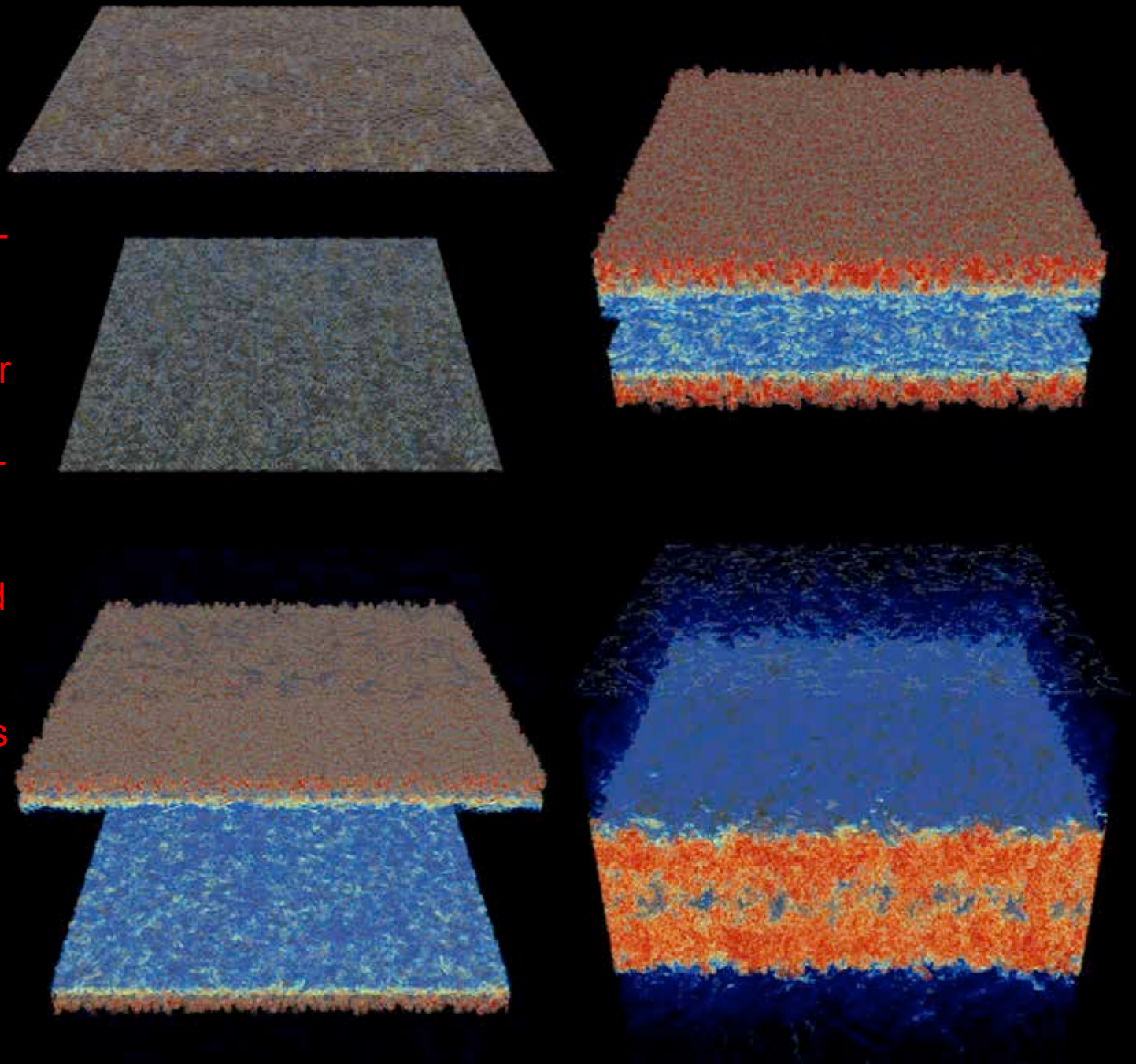

|Vorticity|

4 frames from the movie.

Compress-ible mixing of krypton gas and air by Richtmyer-Meshkov, Rayleigh-Taylor, and Kelvin-Helmholtz instabilities.

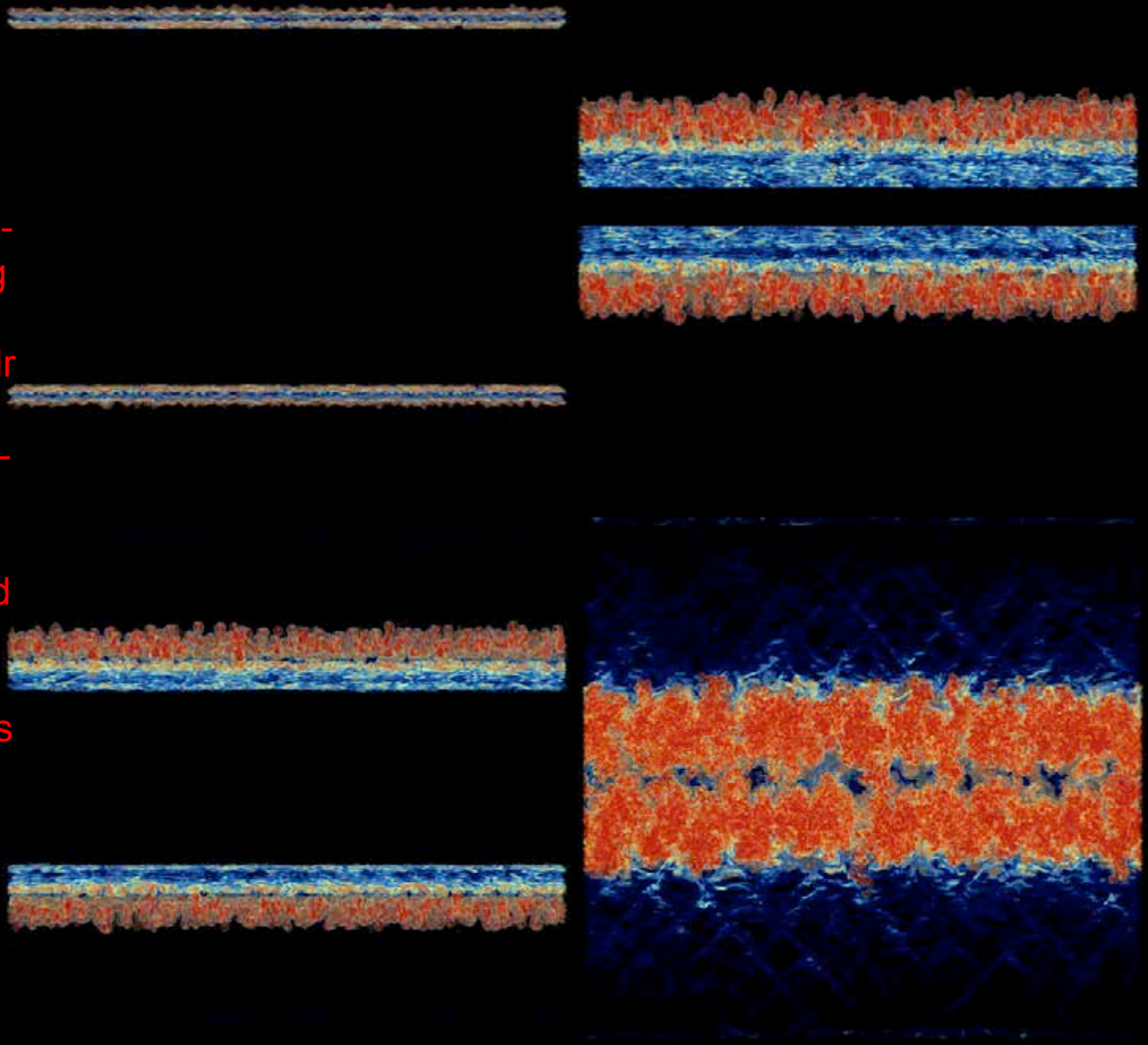

## *So, when we do all this, what do we get?*

**Simulate Sakurai's object, a "born again" AGB star, for about 20 hrs. with 5.7 million time steps at 0.42 Pflop/s (64-bit) sustained for 4 days on 443,232 cores on Blue Waters.**

**One dump of 4 variables every 3 minutes.**

*Our initial condition for the simulation of Sakurai's object in 3D was adapted from the 1-D model for this star from Herwig. The fit to the pressure and density distributions are quite good, but the resulting fit to the temperature distribution is slightly off in the bottom half of the convection zone. The importance of fitting the temperature closely is highest in the upper portion of the convection zone, where the burning of ingested hydrogen mostly takes place. In this region, our fit to the temperature distribution is very good.*

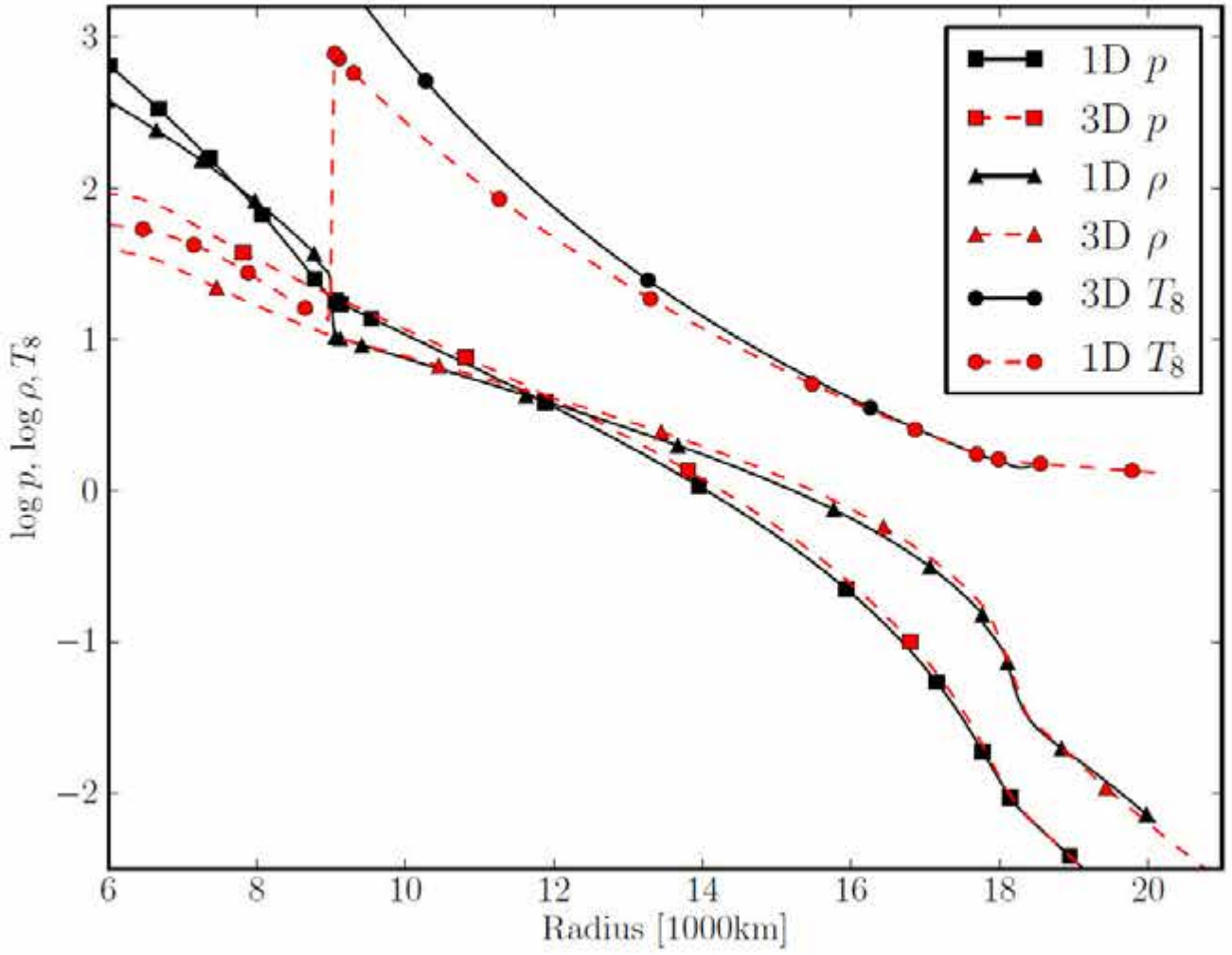


We find that the hydrogen ingestion does not extend below 14 to 15 Mm. Therefore in the region where ingested hydrogen burns our 3-D model tracks the structure of the 1-D model very closely.

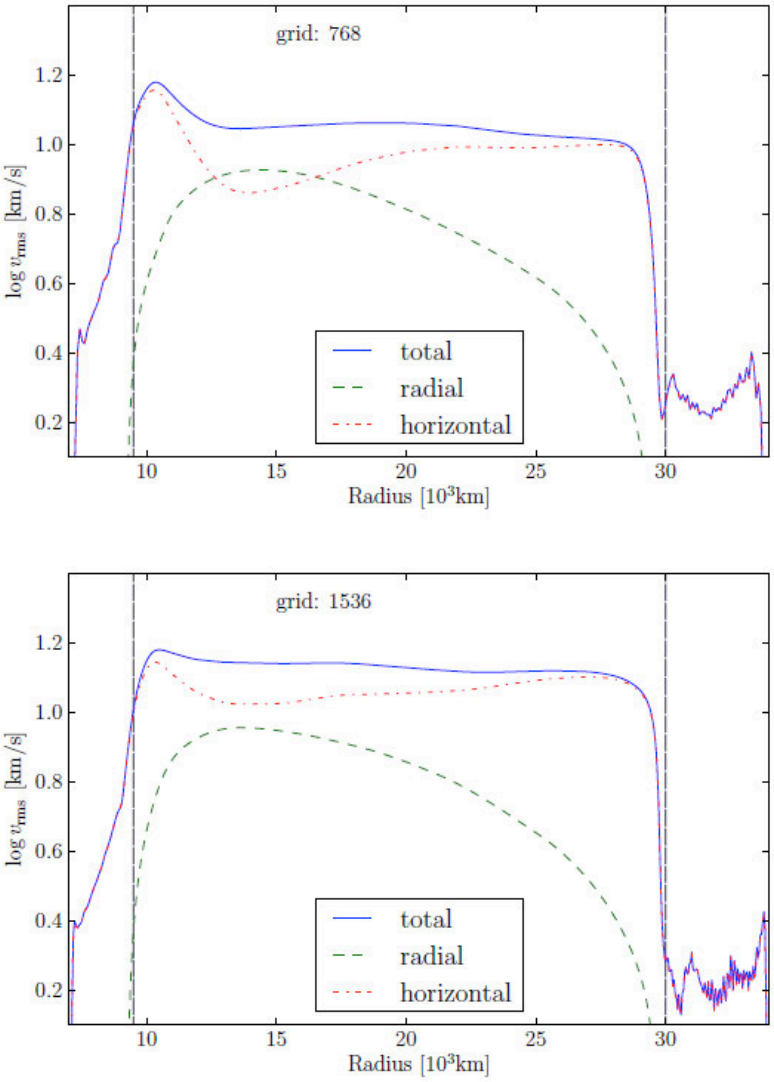


FIG. 8.— Logarithm of spherically averaged rms velocity, averaged from minute 400 to 430, for two resolutions. The dashed vertical lines are placed at the convective boundaries according to the initial setup.

Here we see the rms radial and horizontal velocity components, as well as the total rms velocity (blue) averaged over spherical surfaces in 2 simulations of entrainment without burning of the entrained gas. The agreement between runs on grids of $768^3$ and $1536^3$ cells is very good.

On both grids we see that the stiffness of the upper boundary of the helium shell flash convection zone forces the convecting gas to begin decelerating its vertical motion well before reaching this upper boundary. The rms velocity is not diminished; instead the velocity becomes predominantly horizontal. This produces very strong shear at the convective boundary, driving the Kelvin-Helmholtz instabilities that result in entrainment.

*In earlier work, we studied the entrainment of hydrogen-rich gas from above the convection zone without the complicating factor of feedback from burning of the ingested hydrogen. We observed that the entrainment rate appeared to converge at a grid resolution of about $1536^3$ cells. That is the grid resolution that we have used in our studies of Sakurai's object.*

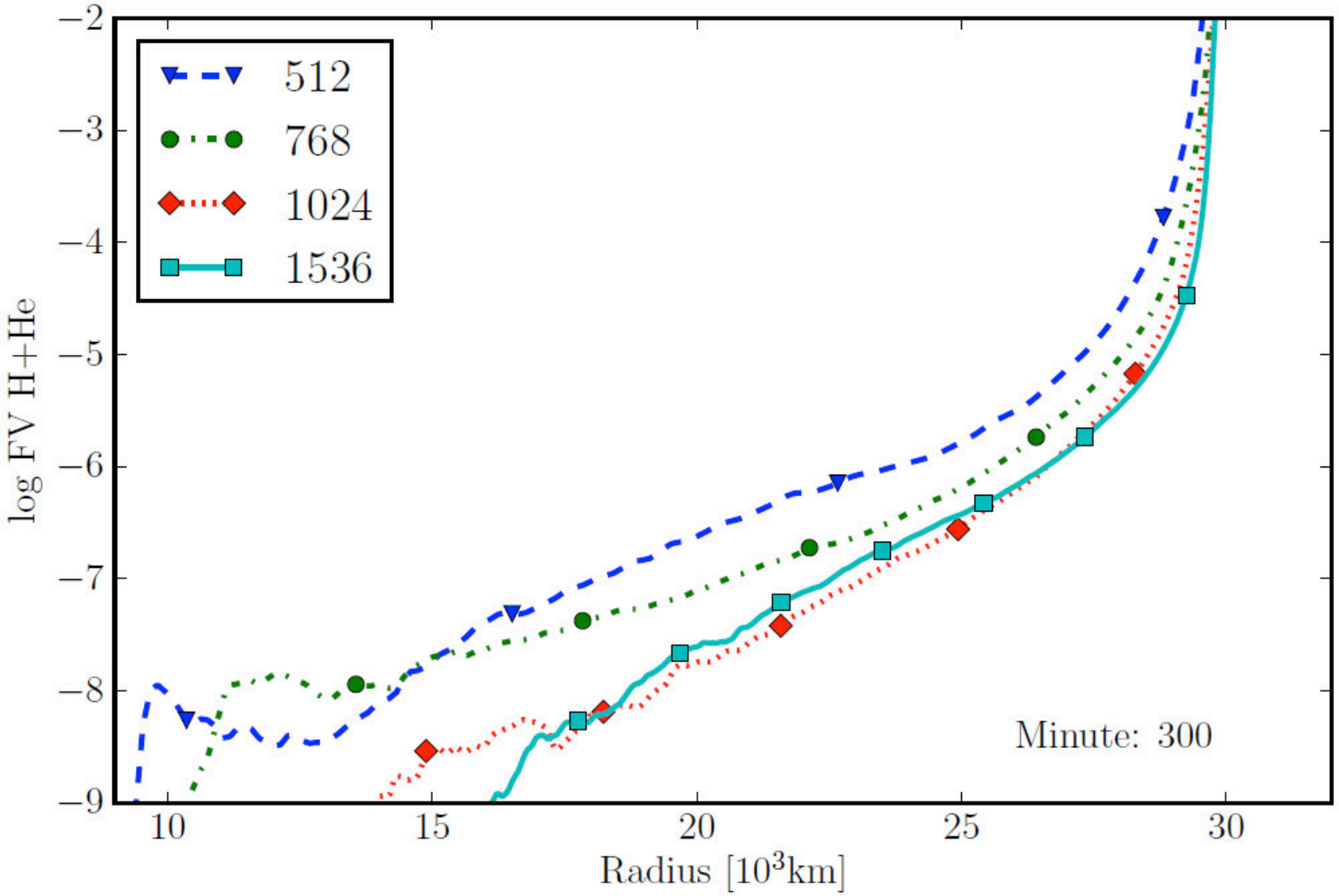

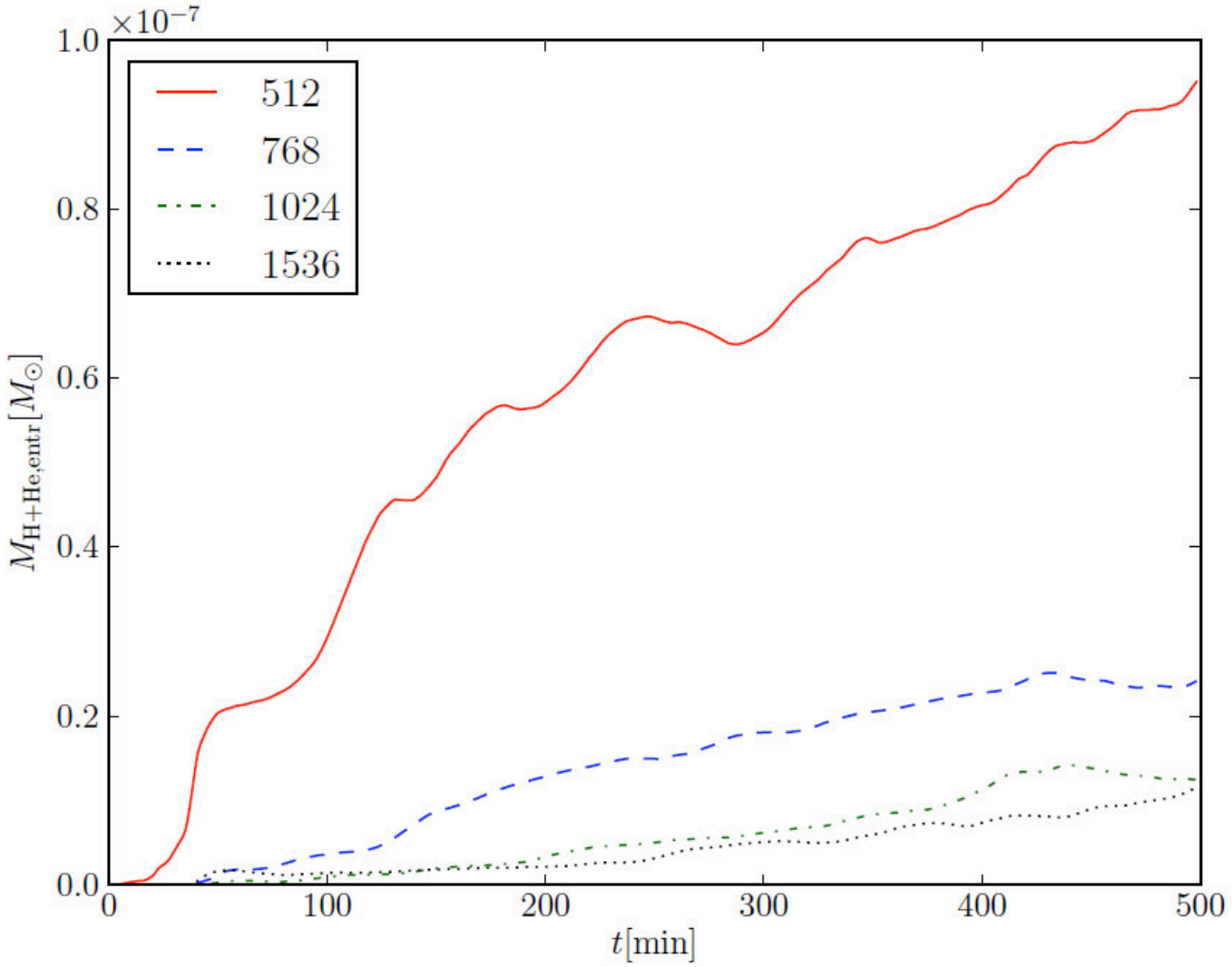


FIG. 13.— Entrained mass, integrated between the radial coordinates 10100km and 29200km, as a function of time. Simulations for different grid sized $n^3$ are shown. The number of grid points $n$ in one direction is shown in the legend.

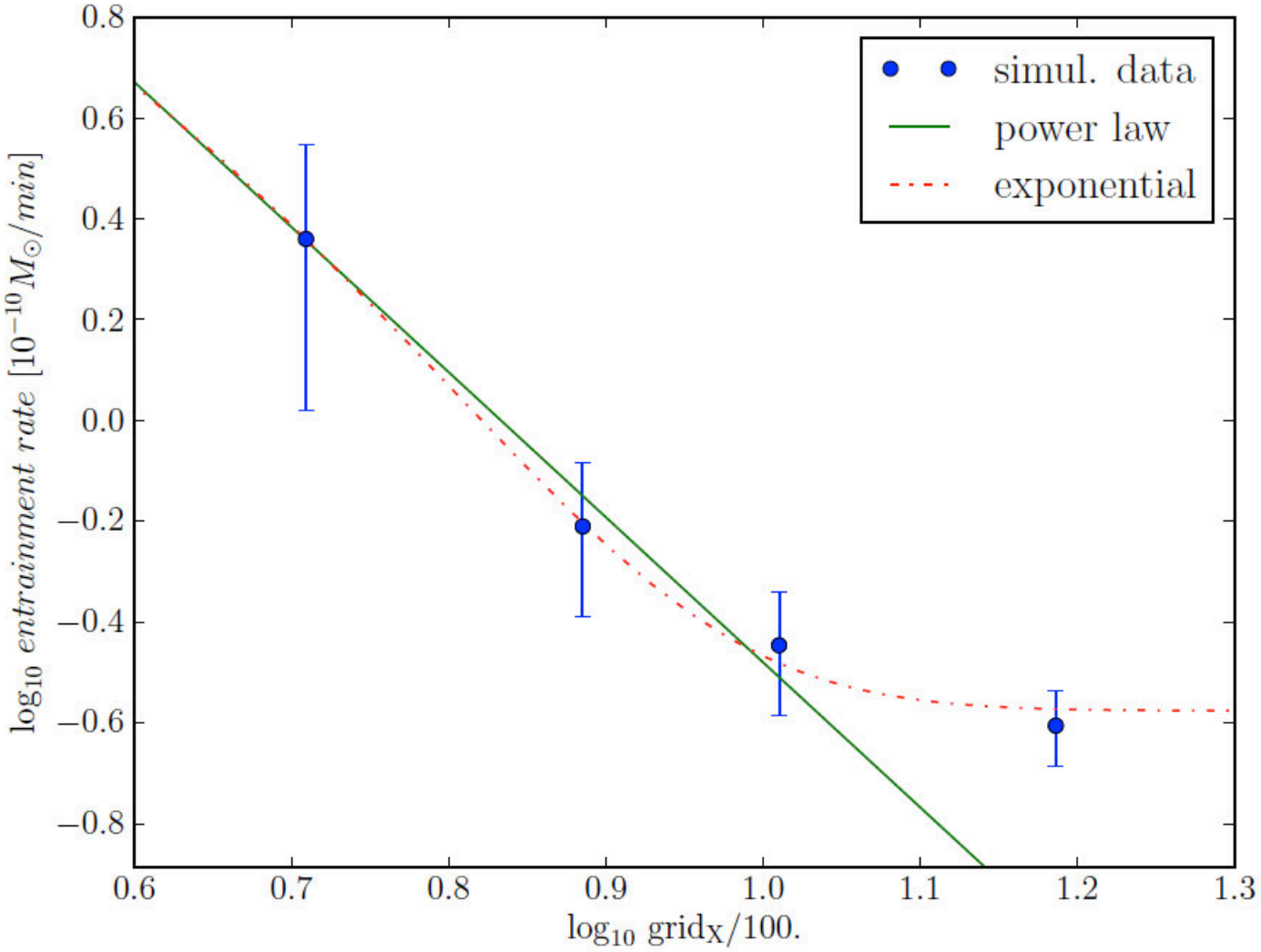


FIG. 14.— Logarithm of mean entrainment rates with error bars representing 99% confidence intervals (see text) as a function of grid size. The mean entrainment rates have been fitted with a power law and an exponential according to Eq. (6).

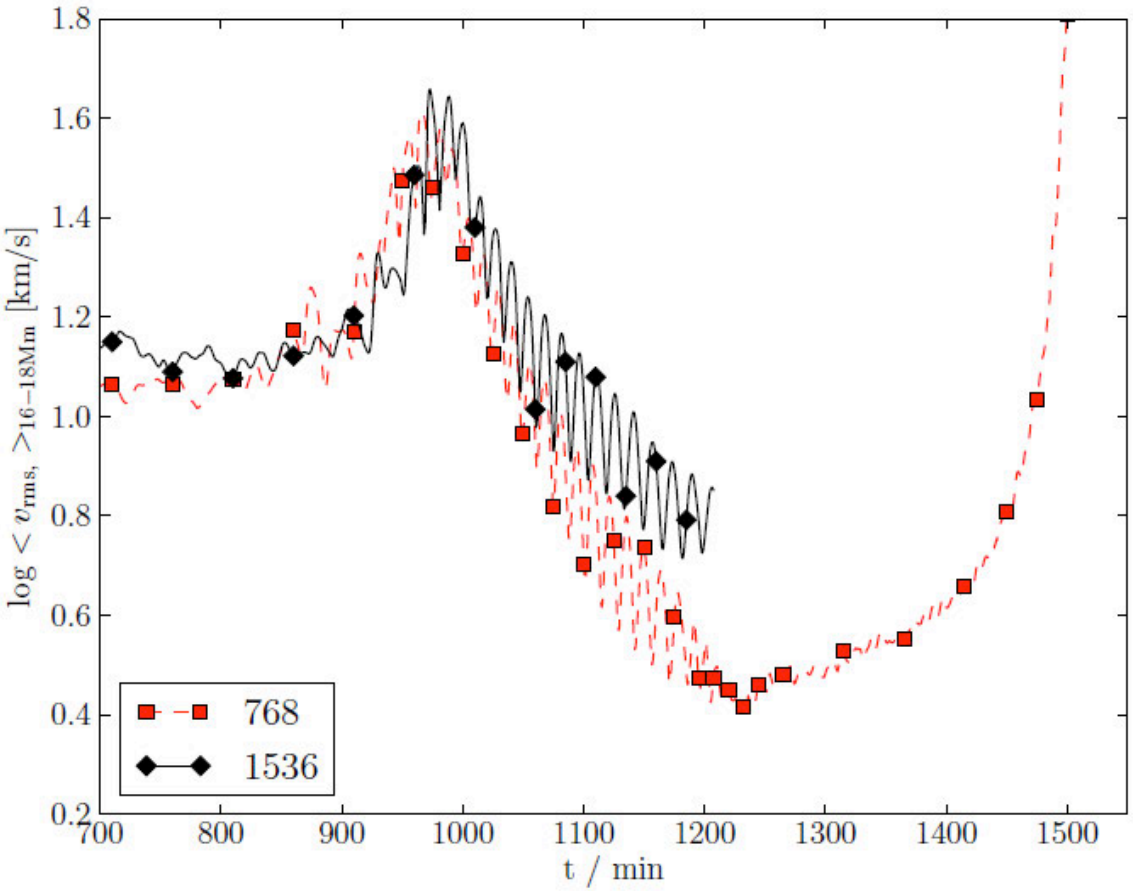


**Figure 1.** Top: Initial piecewise polytropic setup of 3-D simulation in comparison with the 1-D stellar evolution model for Sakurai's object at time $t_0$ (Fig. 2 Herwig et al. 2011). Shown are pressure $p$ and density $\rho$ in code units ($[p] = 10^{19}\mathrm{g\,cm^{-1}\,s^{-2}}$), $[\rho] = 10^{3}\mathrm{g\,cm^{-3}}$), and temperature ($[T] = 10^{8}\,\mathrm{K}$). Bottom: Spherically averaged rms velocity averaged over the top region of the convection zone from 16 to 18 $\times\ 10^{3}$km. The signature of a global oscillation is evident in these averaged velocities.

The spherically averaged rms velocity in the top region of the convection zone shows many oscillations in runs at both grid resolutions. These regular oscillations correspond to global sloshing motions of the gas in this region that result in greatly increased rates of hydrogen entrainment. This is a 1-D averaged signature of the GOSH.

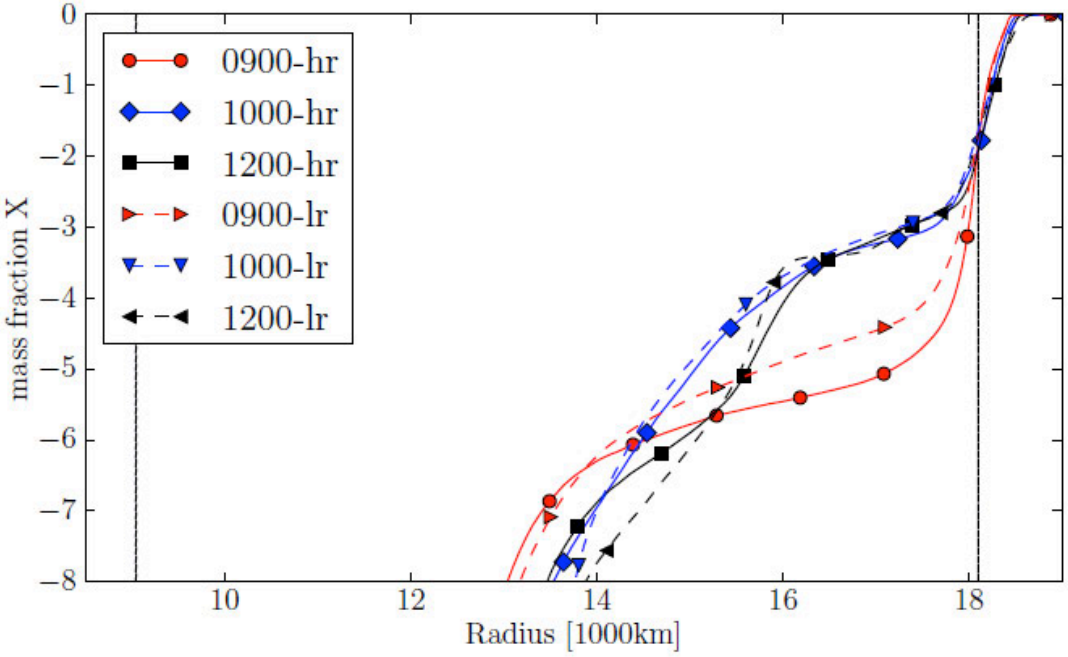


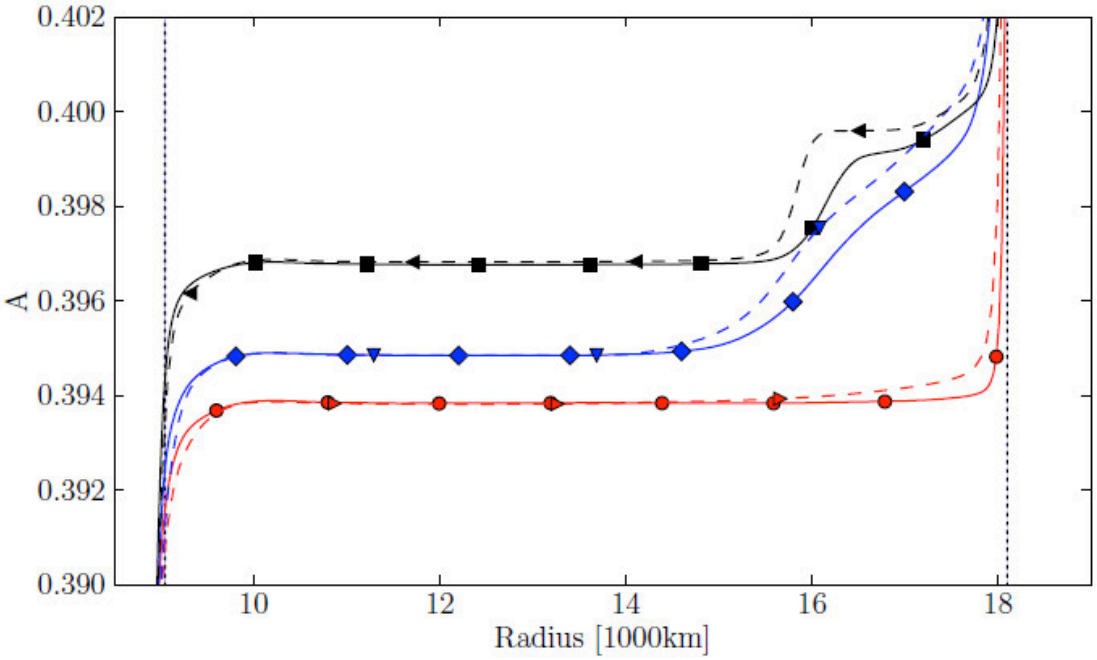


The radial distributions of spherically averaged concentrations (top panel) of entrained hydrogen-rich gas and of the adiabatic invariant $A = p / \rho^{\gamma}$ are plotted at different problem times for two runs on grids of $768^3$ and $1536^3$ cells. The ultimate emergence of a horizontal entropy shelf above 15.5 Mm indicates the formation of a new convection zone driven by burning of ingested hydrogen.

We also see that the hydrogen ingestion does not extend below 14 to 15 Mm. This is related to the time scale for the observed eruption (the rise time of the light curve) for Sakurai's object, which was only about 2 years, rather than about 200 that would result if the ingested hydrogen were to burn at 12 Mm instead of 14.

On the following slides, we show a volume rendered view of a hemisphere of the star. The degenerate carbon-oxygen core that will ultimately become a white dwarf after the outer layers of the star have been expelled is made transparent. Just above this dense core, helium burns in a shell at a radius of about 9 Mm (9000 km). Helium shell burning generates about 40 million solar luminosities, which has created the helium shell flash convection zone above the burning region. In this convection zone, we find a hydrogen-free mixture of mainly helium and carbon, the product of helium burning. We begin our simulation as the growing convection zone is just reaching the unprocessed, hydrogen-rich gas, now located at a radius of about 18.1 Mm.

We show concentrations of ingested hydrogen with logarithms to the base 10 ranging from -5.5 (dark blue), to -4.6 (light blue), -3.8 (white), -3.0 (yellow), and -1.8 (red). Pure hydrogen-rich gas above the convection zone, as well as pure convection zone gas, is made completely transparent. We skip over the first 200 minutes of the simulation, in which the flow, initialized from a 1-D stellar model, adjusts to the new degrees of freedom provided by our 3-D representation. We also note that we insert a perfectly reflecting, confining sphere as an outer boundary condition at a radius of 22.5 Mm. This outer boundary condition affects the tiny motions of the stably stratified gas above the convection zone, and our numerical experiments with this sort of problem indicate that the boundary condition we choose does have some effect upon the entrainment. Nevertheless, we cannot include the entire star in our grid, so we must do something at a bounding radius. In future work, we plan to move the bounding radius considerably further out, with a coarsened grid outside the domain of our present simulations. From the lack of distortion in the images that follow of the circular edge of the top of the convection zone in these views at 18 Mm, we may conclude that introducing our outer confining sphere at 22.5 Mm is not dramatically affecting the flow in the convection zone and the entrainment region, where we are most interested in the flow behavior. This is more clearly seen in visualizations of the vorticity in equatorial slices, which follow this sequence of hemisphere views. Only in the very brief, most violent hydrogen-burning episode is any substantial motion of the gas above the convection zone in evidence.

In the hemisphere views that follow, we can observe that the great radial depth of the convection zone has allowed very large convection cells to develop. In our hemisphere views, we typically see only 3 or 4 very large regions at the top of the convection zone where large-scale upwellings of relatively buoyant fluid spread out horizontally along the top of the convection zone. These horizontal flows create strong shear. Developing Kelvin-Helmholtz instabilities then create growing and breaking waves. In the images, these have the appearance of ripples which are most evident where the horizontal flows from neighboring convection cells collide. Along these collision regions, descending curtains of relatively less buoyant gas develop. This aspect of compressible convection is familiar from decades of investigations focused on convection in the sun. In this context, however, the descending curtains of cooler gas can drag downward with them small concentrations of entrained hydrogen-rich gas from above the convection zone, with profound effects upon the subsequent dynamics. The turbulent, swirling motions in the breaking Kelvin-Helmholtz waves causes mixing of this hydrogen-rich gas with the gas of the convection zone, making it more easily carried along with the descending flow despite its greater intrinsic buoyancy. This dynamics is best viewed in the animation from which the following sequence of images is taken. This animation can be found at www.lcse.umn.edu/MOVIES. The process of entraining this stably stratified gas from above the convection zone is difficult to simulate accurately, because it requires that sufficiently small-scale Kelvin-Helmholtz waves be resolved on the computational grid so that the numerical effects from the grid itself and from the method's numerical viscosity can become unimportant. Our best test that this criterion is met in our simulations is the evidence of convergence of the entrainment rate and of the spherically averaged radial profiles of important quantities, such as the entrained concentration and the rms velocities. We note that on the $1536^3$ grid where we observe this numerical convergence, the 0.5 Mm transition region from pure convection zone fluid to pure hydrogen-rich fluid, a property of the star rather than of our representation of it, is resolved by 11 grid cell widths. Using our PPB advection scheme, with its subcell resolution, this is enough to permit multiple complete swirls of entrained gas to be represented on our grid.

In the hemisphere views that follow, we have superposed volume renderings of the rate of energy release from the burning of ingested hydrogen. The burning region shows up very dark blue, where the energy release rate is smallest, and yellow and finally white where the energy release is greater. In some of these images, one sees a burning region sliced by our clipping plane through the equator of the star. Then it is evident that no burning occurs above about 13 to 14 Mm. One can clearly see descending curtains of gas containing entrained hydrogen that end in vigorous burning regions. The hydrogen burns by reacting with the carbon-12 that is abundant in the convection zone, and the product of this reaction is nitrogen-13 (plus energy of course, in the form of light). This reaction rate is highly dependent upon temperature. At a depth of around 12 to 12.5 Mm this reaction rate is so great that we can think of the hydrogen as burning before it can possibly be carried to greater depths. Therefore, hydrogen can accumulate only at larger radii. The energy release from burning ingested hydrogen can be seen to be highly localized. It is particularly concentrated in the small regions where descending gas curtains intersect. At the early times in the simulation, the concentration of hydrogen where it burns is not so high, and the back reaction of the flow to its energy release is minor. However, as the hydrogen ingestion proceeds, and an increasingly high abundance of hydrogen accumulates above about 15 Mm, it is clear form these images that the rate of hydrogen burning increases. Burning is still localized, but there are more local burning regions and these regions involve more intense energy release. Ultimately, this gradual increase in hydrogen burning causes positive feedback that increases the rate of entrainment by increasing the size of the horizontal velocities at the top of the convection zone. Now descending curtains of gas contain substantially higher hydrogen concentrations, and when they reach the appropriate depths and burn, they burn quite brightly. Hydrogen burning localized mainly to one small region and releasing substantial energy strongly disrupts the convection flow. It generates violent sloshing of the gas in the upper region of the convection zone that now contains higher concentrations of buoyant hydrogen-rich gas. This sloshing causes tremendously more powerful shear motions and greatly enhanced entrainment, as these images clearly show.

The powerful feedback between hydrogen burning and hydrogen ingestion produces a Global Oscillation of Shell Hydrogen ingestion (GOSH). We stress that this oscillatory behavior is global. We see hydrogen burning on one side of the star, followed immediately by a powerful updraft there from the enormous heat release, which forces the gas in the upper convection zone to rush violently toward the antipode, where the gas is forced downward and burns violently, setting the second half of the oscillation in motion.

Compared with the long, relatively quiet lead up to the GOSH, this burning and sloshing behavior is dramatic. One is tempted to call it explosive, yet it obviously is not. During the GOSH, it is clear that our reflecting, confining sphere at 22.5 Mm has an effect upon the flow. Nevertheless, there is no strong evidence from the behavior we see in this simulation that the star would explode. On the contrary, motions in the upper convection zone are much more violent than in the diffuse, stably stratified fluid just above it, as vorticity, radial velocity, and divergence of velocity images in equatorial slices make clear. The reason for this is the enormous strength of gravity above what is essentially a 0.6 solar mass white dwarf of radius 9 Mm. It has taken 40 million solar luminosities of energy over the course of about a year to this point to lift the fluid of the helium shell flash convection zone up so that the top of the convection zone is now located at 18.1 Mm. The GOSH lasts roughly an hour or two in comparison. If this oscillation were truly violent, its frequency would be given by the sound travel time around the star at about 18 Mm. Instead, the (1/20min) frequency of this global oscillation is much lower. It is given instead by the flow travel timescale, and the flow Mach numbers are significantly smaller, reaching Mach numbers of only around 1/3. There are no shocks, and we would certainly see them in our simulation if they were present.

We therefore see that the star does not explode, but this hydrogen ingestion flash has very significant effects. By the end of our simulation, a new convection zone is being established in the upper region of the helium shell flash convection zone. Also, the decay of the nitrogen-13 that is generated by burning hydrogen will produce carbon-13, which in turn reacts with helium at the high temperatures at the base of the convection zone to produce neutrons for nucleosynthesis.

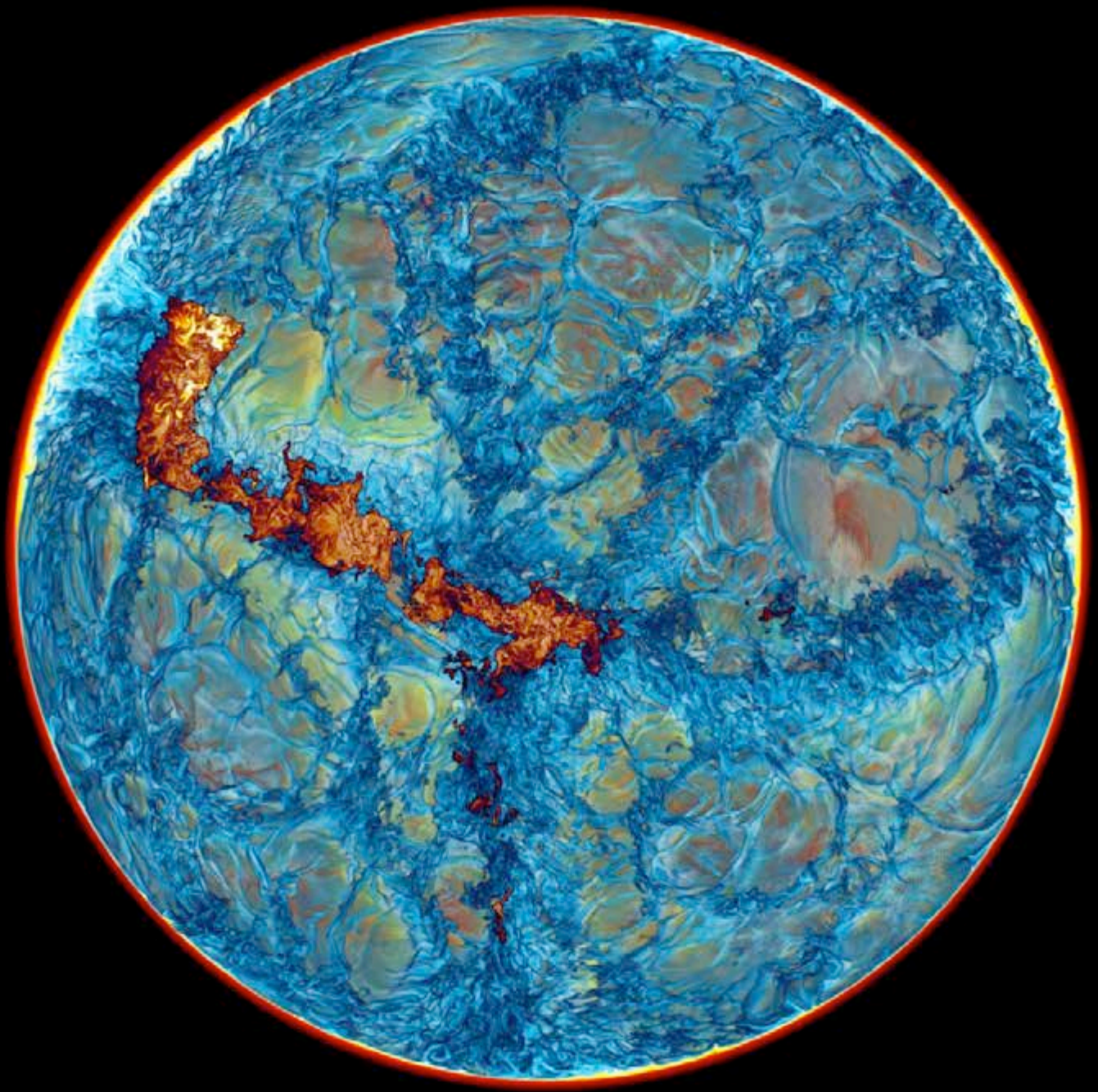

*Sakurai's Object H-ingestion simulation on Blue Waters machine in Jan., 2014, on a grid of $1536^3$ cells.*

*We see a hemisphere and make only mixtures of entrained hydrogen-rich gas with gas of the helium shell flash convection zone visible. The energy release rate from burning ingested H is shown in very dark blue, yellow, and white.*

*t = 200 min.*

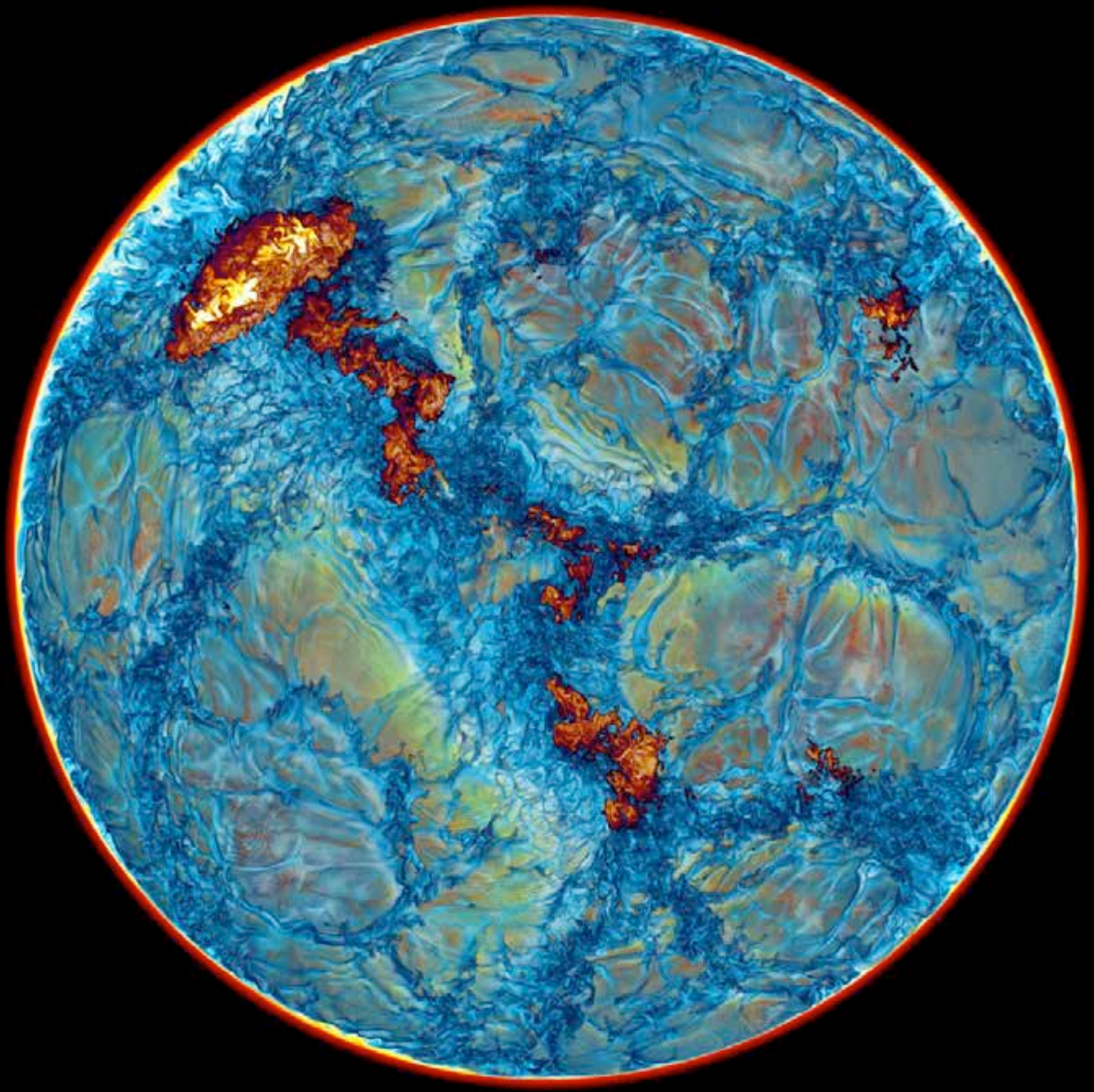

*Sakurai's Object H-ingestion simulation on Blue Waters machine in Jan., 2014, on a grid of $1536^3$ cells.*

Burning of ingested hydrogen is highly localized.

*t = 225 min.*

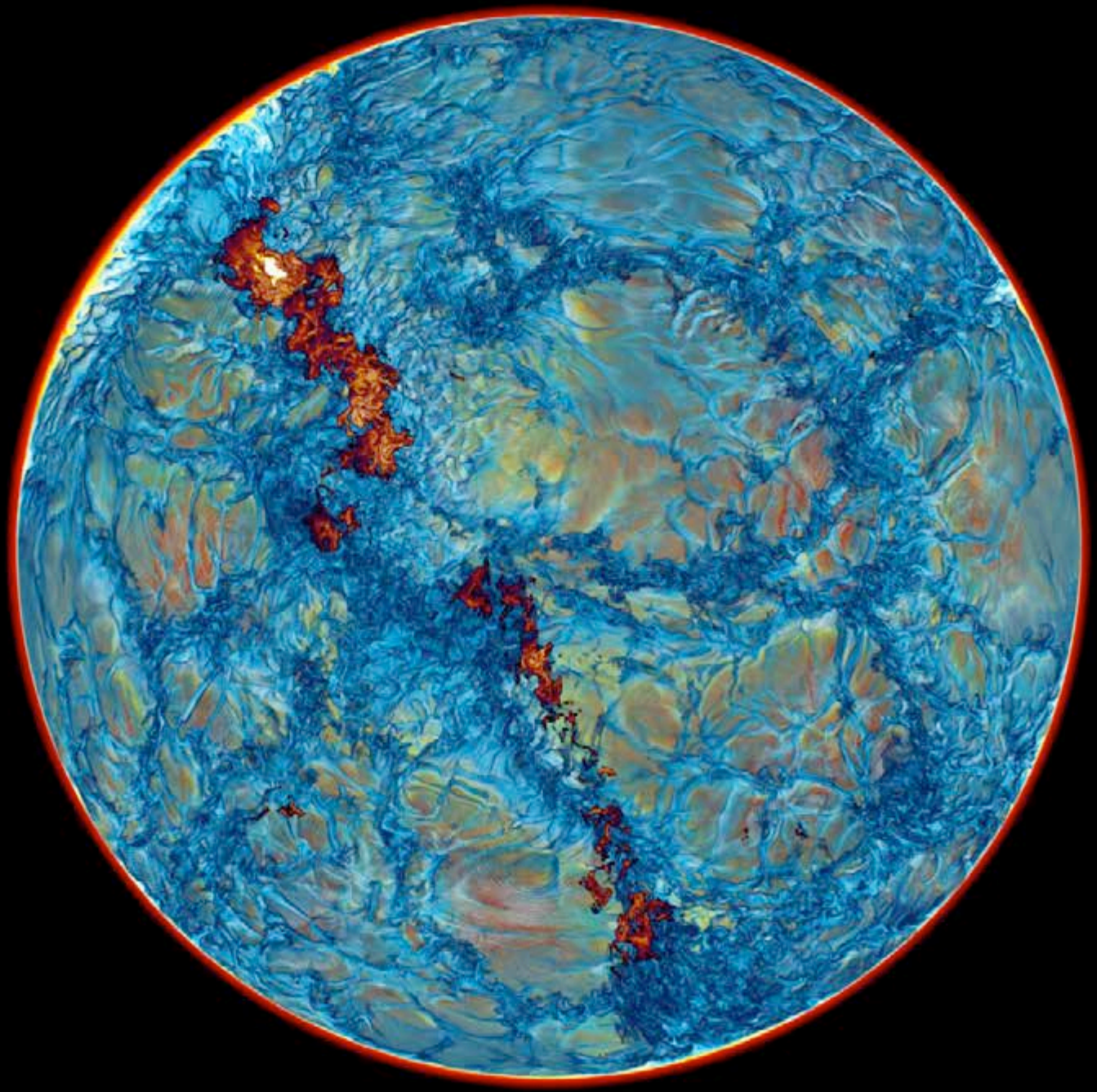

*Sakurai's Object H-ingestion simulation on Blue Waters machine in Jan., 2014, on a grid of $1536^3$ cells.*

*We see a hemisphere and make only mixtures of entrained hydrogen-rich gas with gas of the helium shell flash convection zone visible. The energy release rate from burning ingested H is shown in very dark blue, yellow, and white.*

*t = 250 min.*

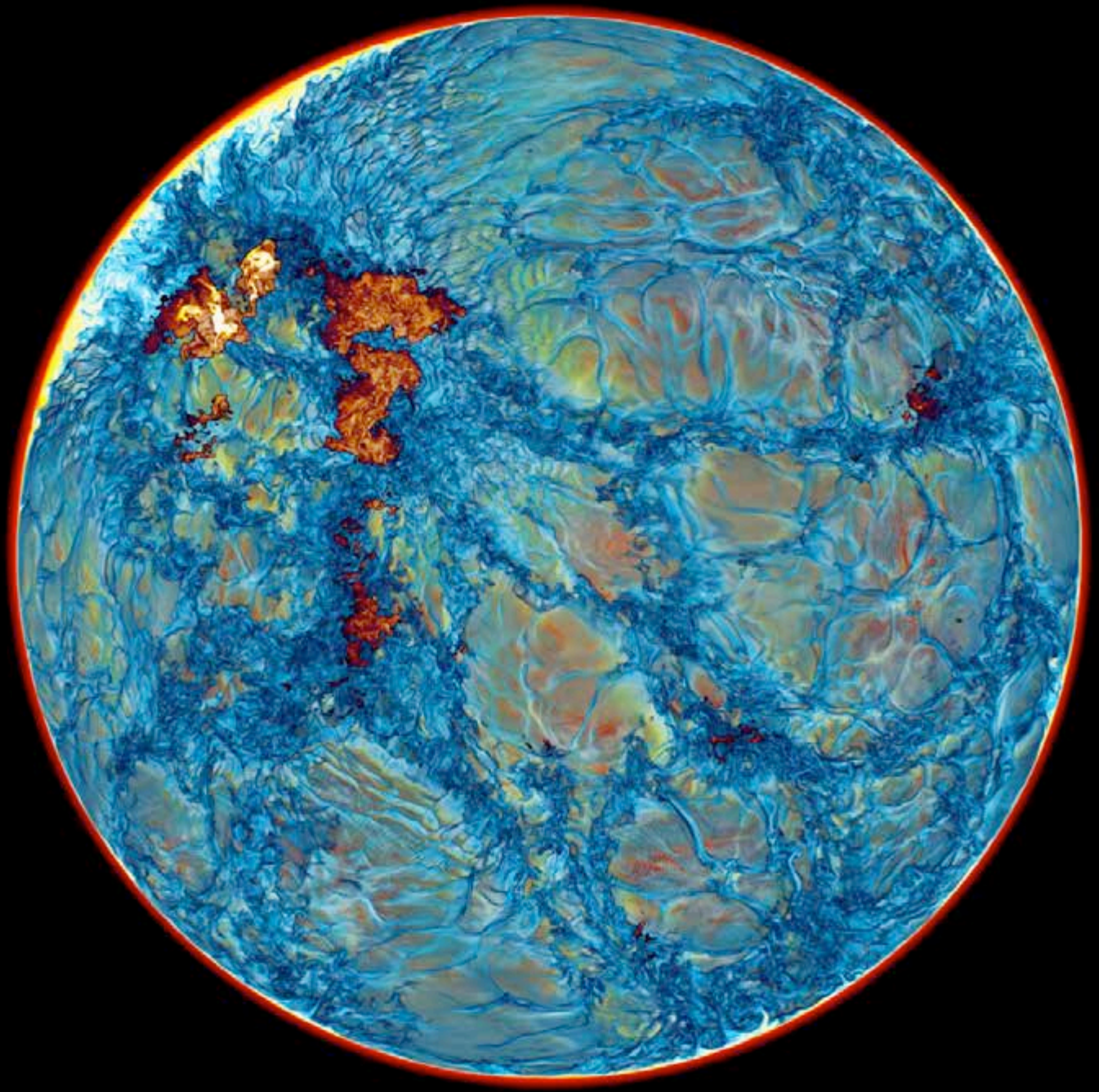

*Sakurai's Object H-ingestion simulation on Blue Waters machine in Jan., 2014, on a grid of $1536^3$ cells.*

Burning only at sufficient depth is very clear in this image.

*t = 275 min.*

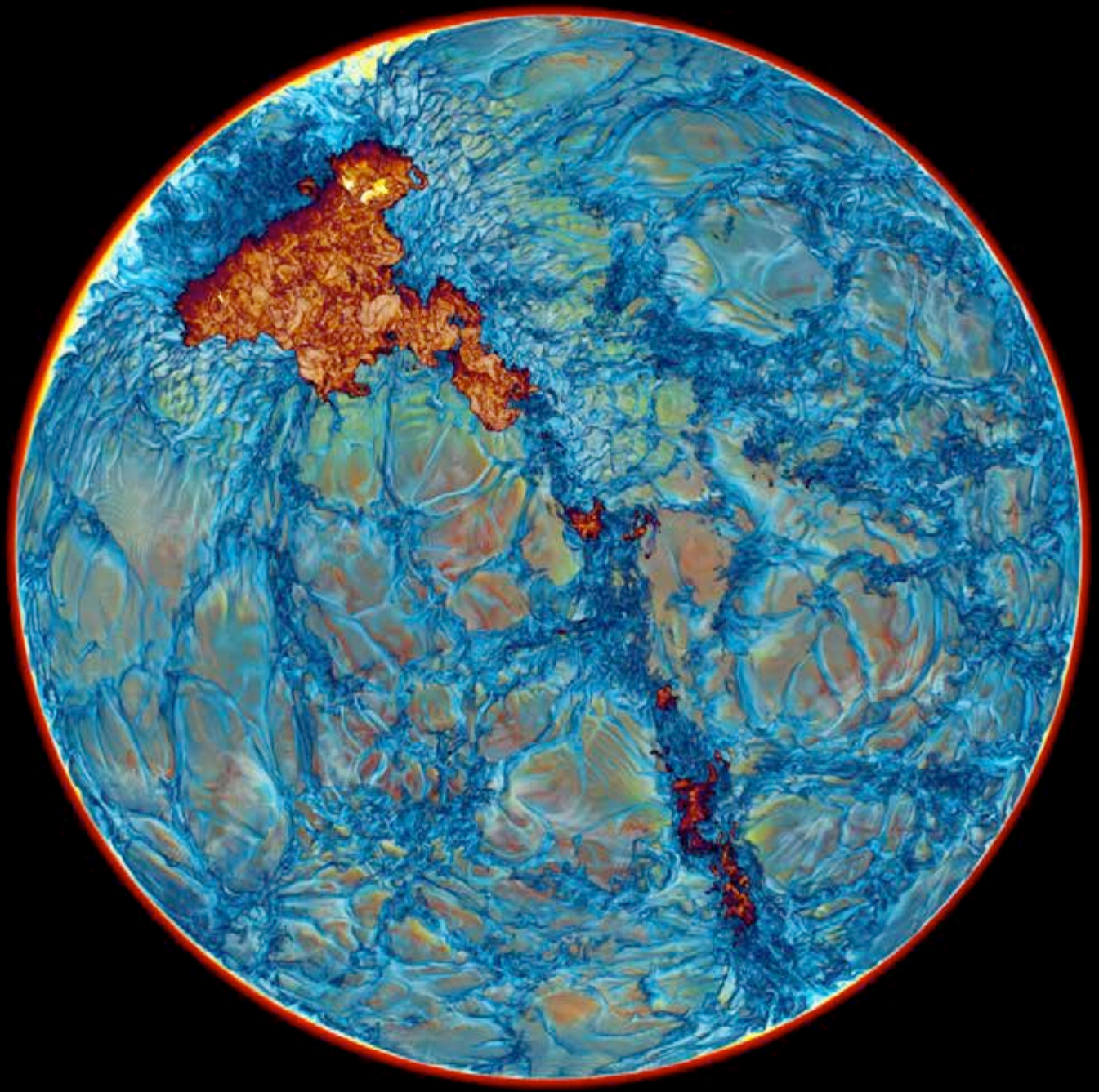

*Sakurai's Object H-ingestion simulation on Blue Waters machine in Jan., 2014, on a grid of $1536^3$ cells.*

*We see a hemisphere and make only mixtures of entrained hydrogen-rich gas with gas of the helium shell flash convection zone visible. The energy release rate from burning ingested H is shown in very dark blue, yellow, and white.*

*t = 300 min.*

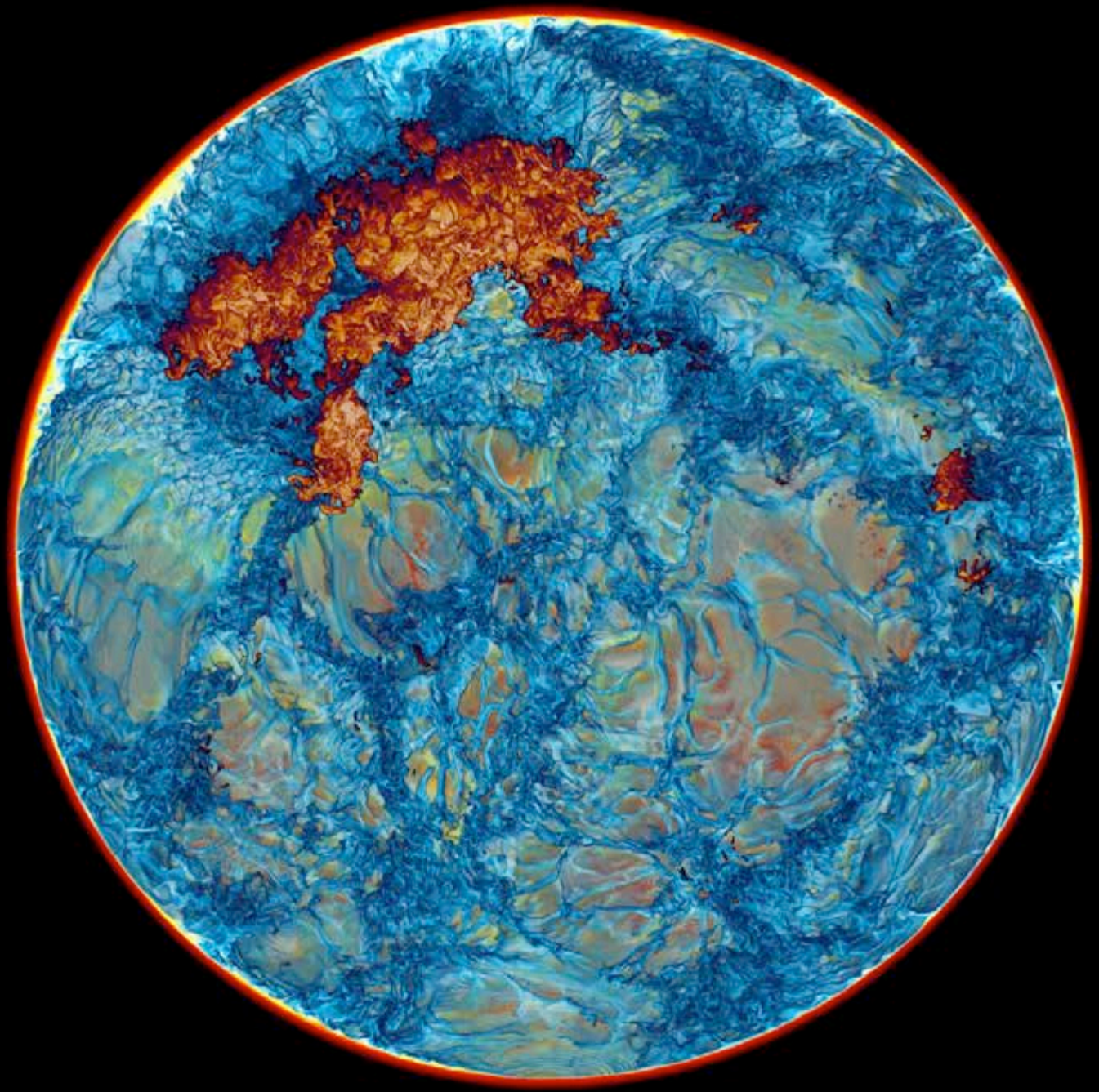

*Sakurai's Object H-ingestion simulation on Blue Waters machine in Jan., 2014, on a grid of $1536^3$ cells.*

Very gradually the concentration of ingested hyrogen builds up in the upper region of the convection zone.

*t = 325 min.*

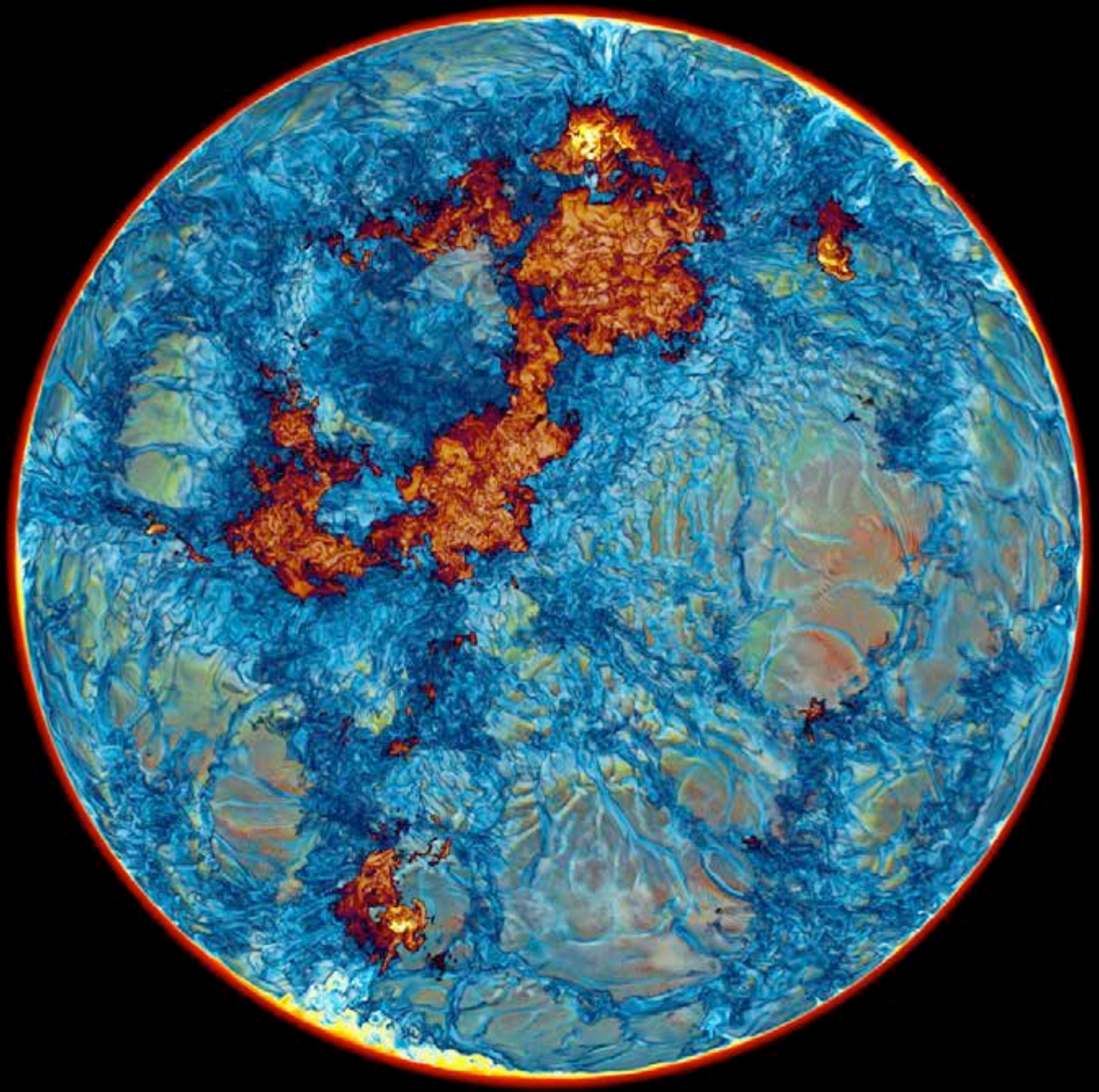

*Sakurai's Object H-ingestion simulation on Blue Waters machine in Jan., 2014, on a grid of $1536^3$ cells.*

*We see a hemisphere and make only mixtures of entrained hydrogen-rich gas with gas of the helium shell flash convection zone visible. The energy release rate from burning ingested H is shown in very dark blue, yellow, and white.*

*t = 350 min.*

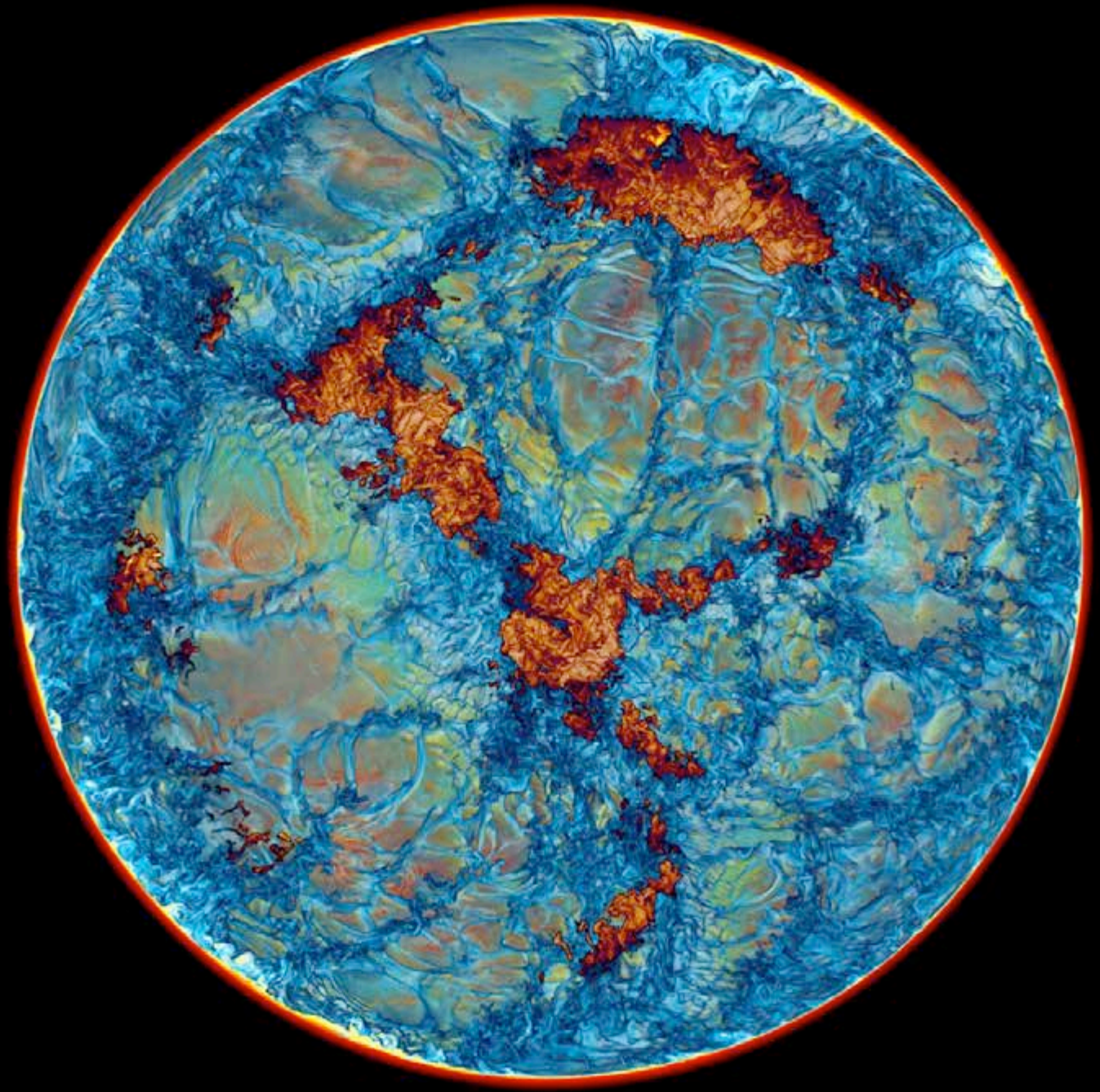

*Sakurai's Object H-ingestion simulation on Blue Waters machine in Jan., 2014, on a grid of $1536^3$ cells.*

*We see a hemisphere and make only mixtures of entrained hydrogen-rich gas with gas of the helium shell flash convection zone visible. The energy release rate from burning ingested H is shown in very dark blue, yellow, and white.*

*t = 375 min.*

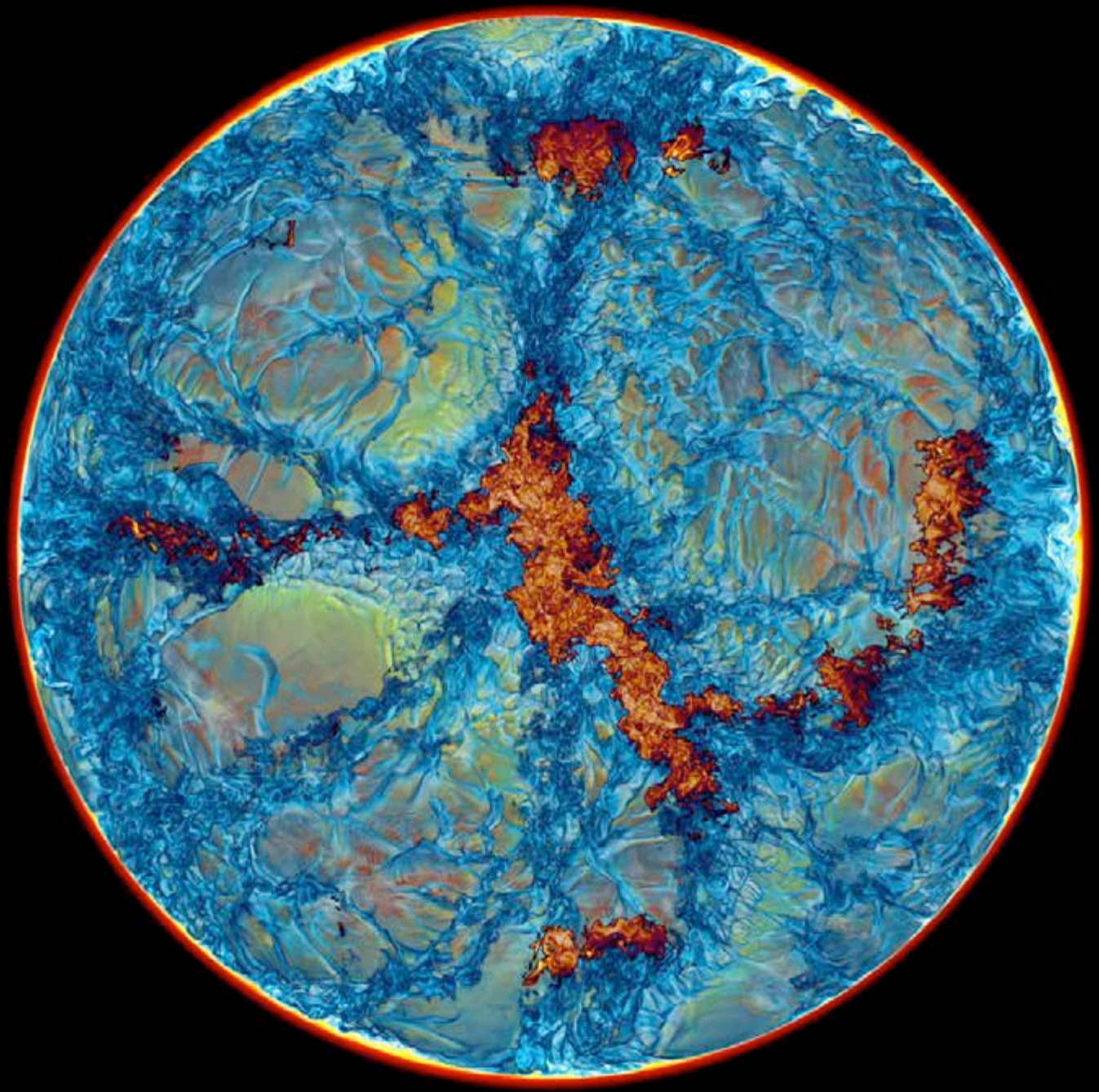

*Sakurai's Object H-ingestion simulation on Blue Waters machine in Jan., 2014, on a grid of $1536^3$ cells.*

*We see a hemisphere and make only mixtures of entrained hydrogen-rich gas with gas of the helium shell flash convection zone visible. The energy release rate from burning ingested H is shown in very dark blue, yellow, and white.*

*t = 400 min.*

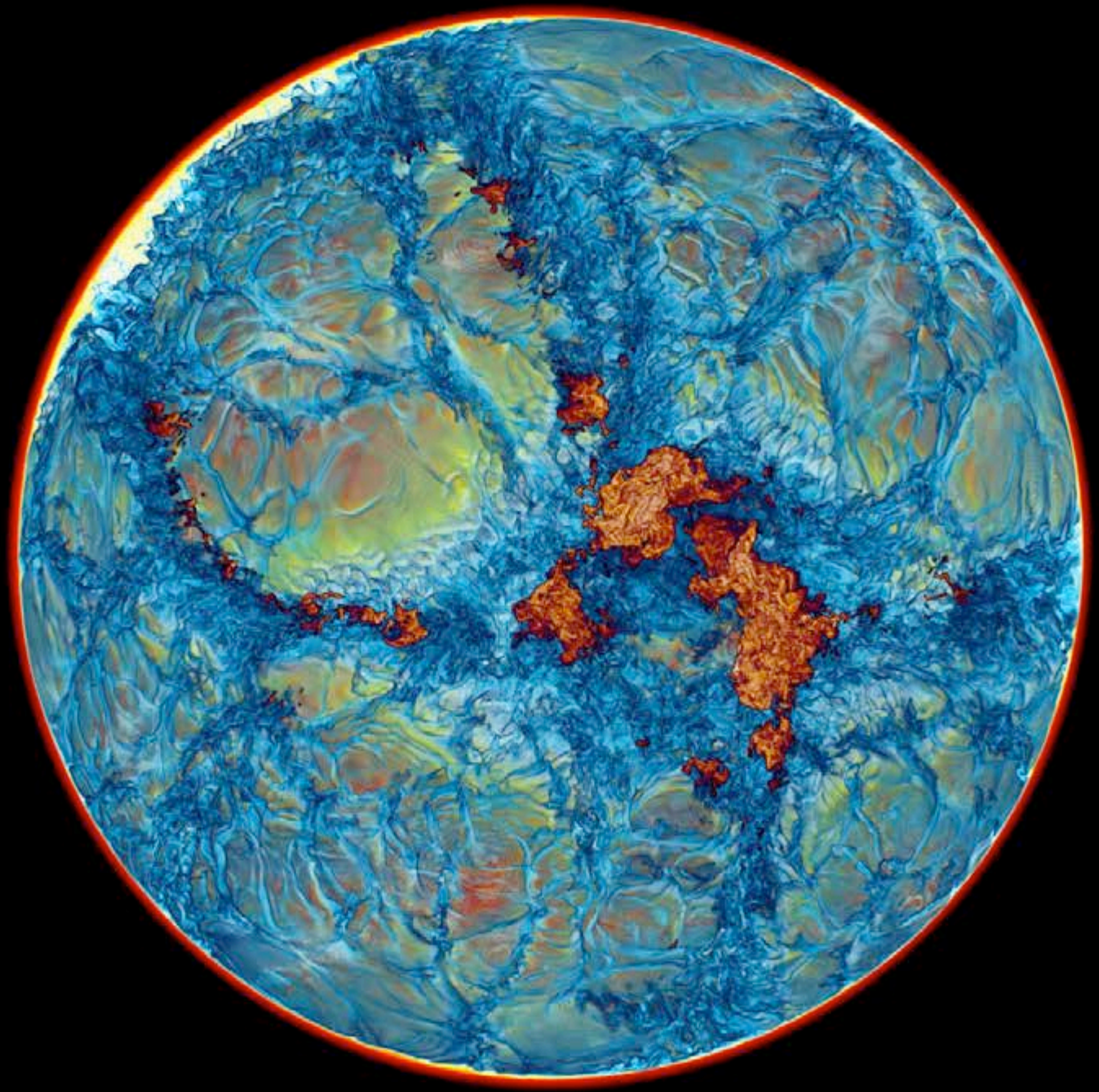

*Sakurai's Object H-ingestion simulation on Blue Waters machine in Jan., 2014, on a grid of $1536^3$ cells.*

Energy release from hydrogen burning is greatest in regions where multiple convection cells meet. Here curtains of descending gas intersect.

*t = 425 min.*

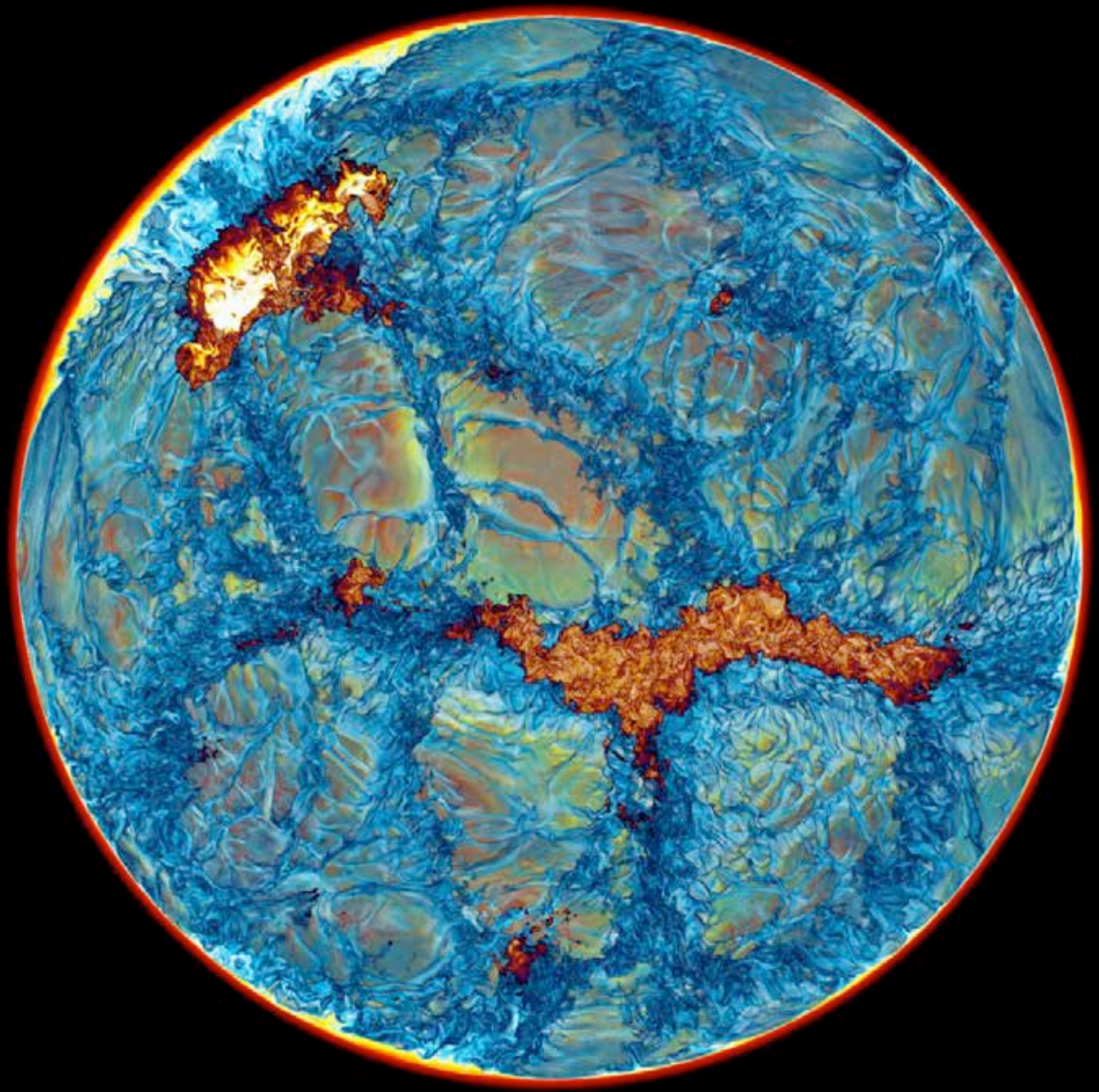

*Sakurai's Object H-ingestion simulation on Blue Waters machine in Jan., 2014, on a grid of $1536^3$ cells.*

*We see a hemisphere and make only mixtures of entrained hydrogen-rich gas with gas of the helium shell flash convection zone visible. The energy release rate from burning ingested H is shown in very dark blue, yellow, and white.*

*t = 450 min.*

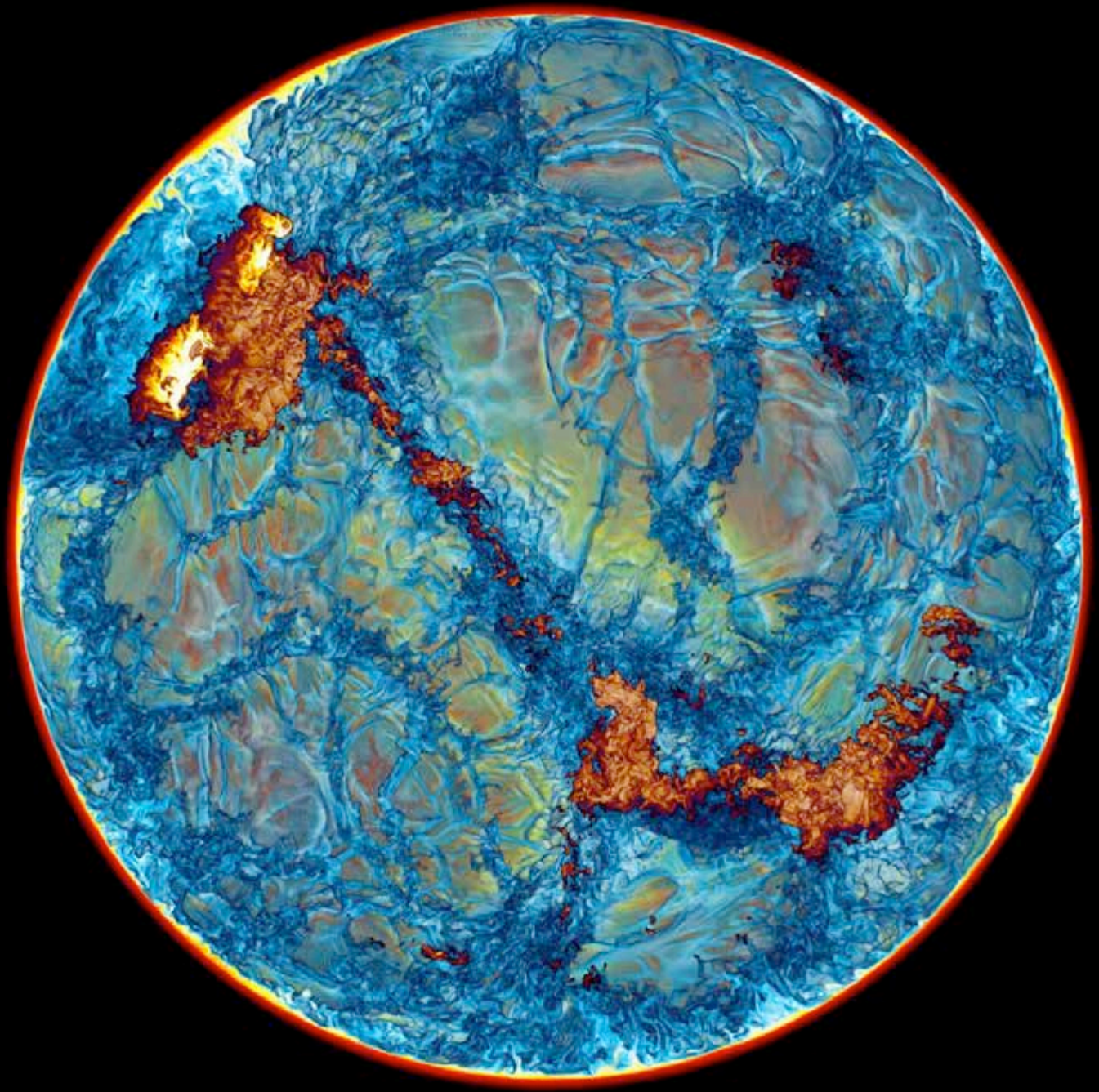

*Sakurai's Object H-ingestion simulation on Blue Waters machine in Jan., 2014, on a grid of $1536^3$ cells.*

*We see a hemisphere and make only mixtures of entrained hydrogen-rich gas with gas of the helium shell flash convection zone visible. The energy release rate from burning ingested H is shown in very dark blue, yellow, and white.*

*t = 475 min.*

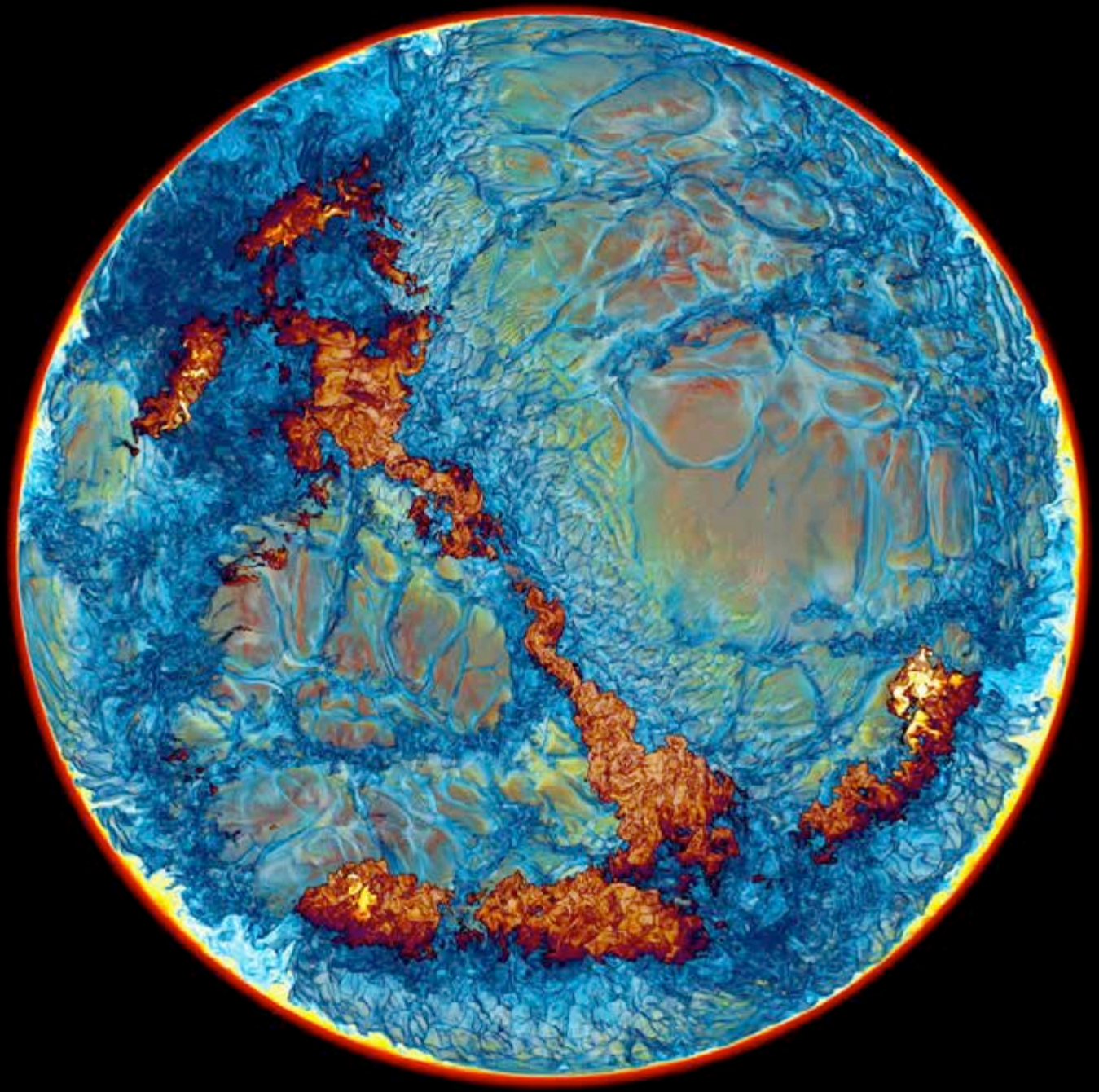

*Sakurai's Object H-ingestion simulation on Blue Waters machine in Jan., 2014, on a grid of $1536^3$ cells.*

*We see a hemisphere and make only mixtures of entrained hydrogen-rich gas with gas of the helium shell flash convection zone visible. The energy release rate from burning ingested H is shown in very dark blue, yellow, and white.*

*t = 500 min.*

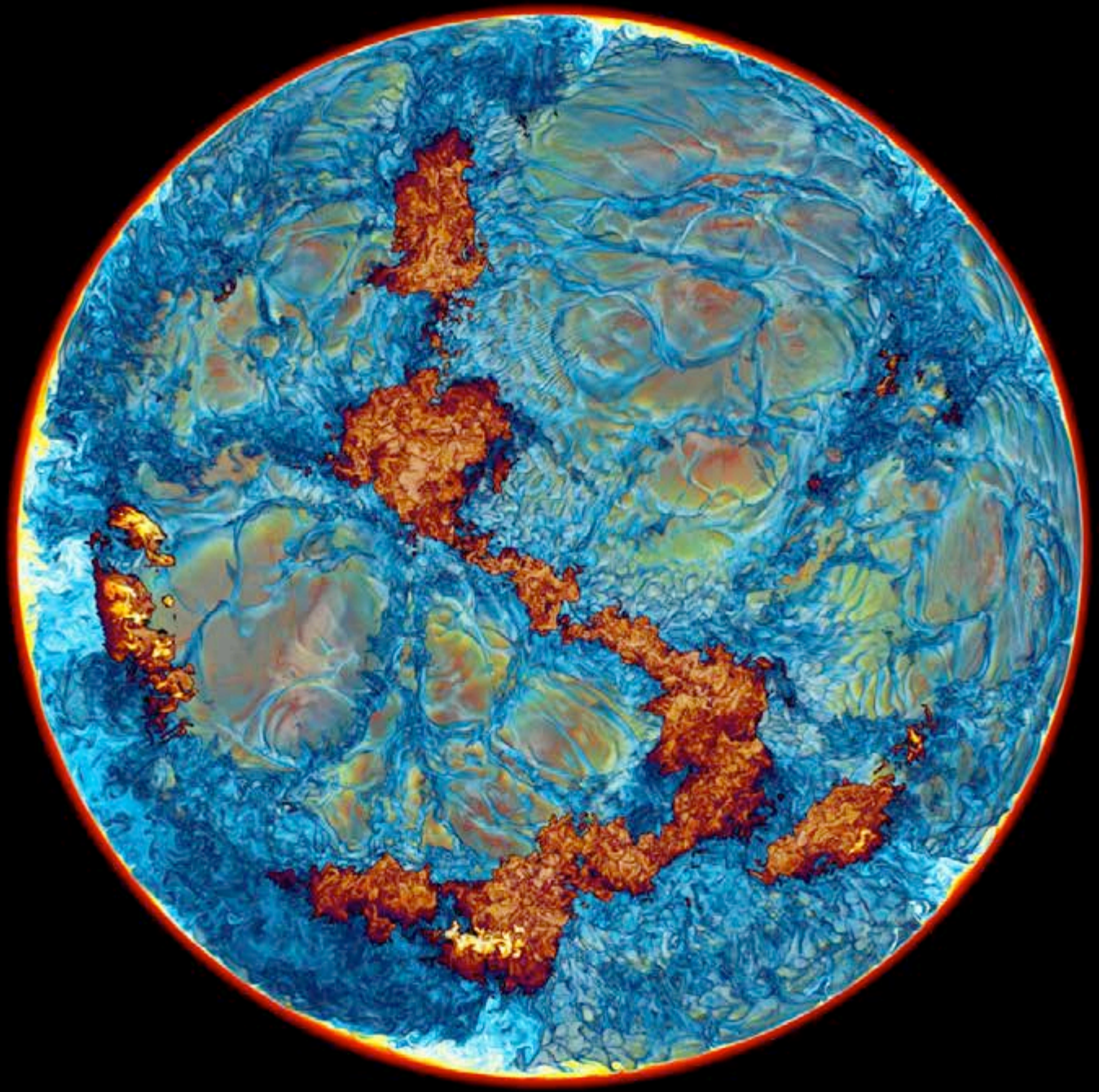

*Sakurai's Object H-ingestion simulation on Blue Waters machine in Jan., 2014, on a grid of $1536^3$ cells.*

*We see a hemisphere and make only mixtures of entrained hydrogen-rich gas with gas of the helium shell flash convection zone visible. The energy release rate from burning ingested H is shown in very dark blue, yellow, and white.*

*t = 525 min.*

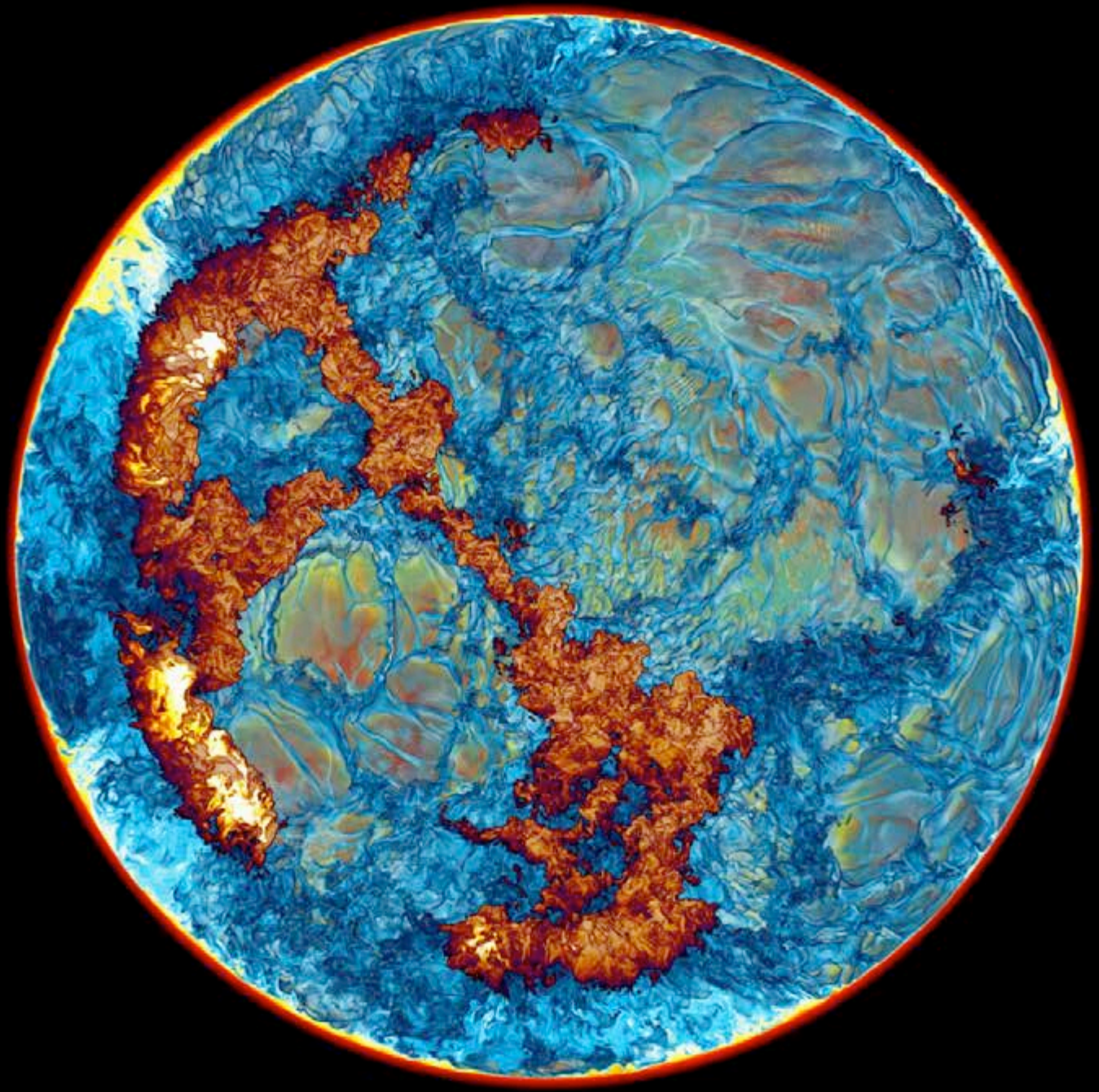

*Sakurai's Object H-ingestion simulation on Blue Waters machine in Jan., 2014, on a grid of $1536^3$ cells.*

*We see a hemisphere and make only mixtures of entrained hydrogen-rich gas with gas of the helium shell flash convection zone visible. The energy release rate from burning ingested H is shown in very dark blue, yellow, and white.*

*t = 550 min.*

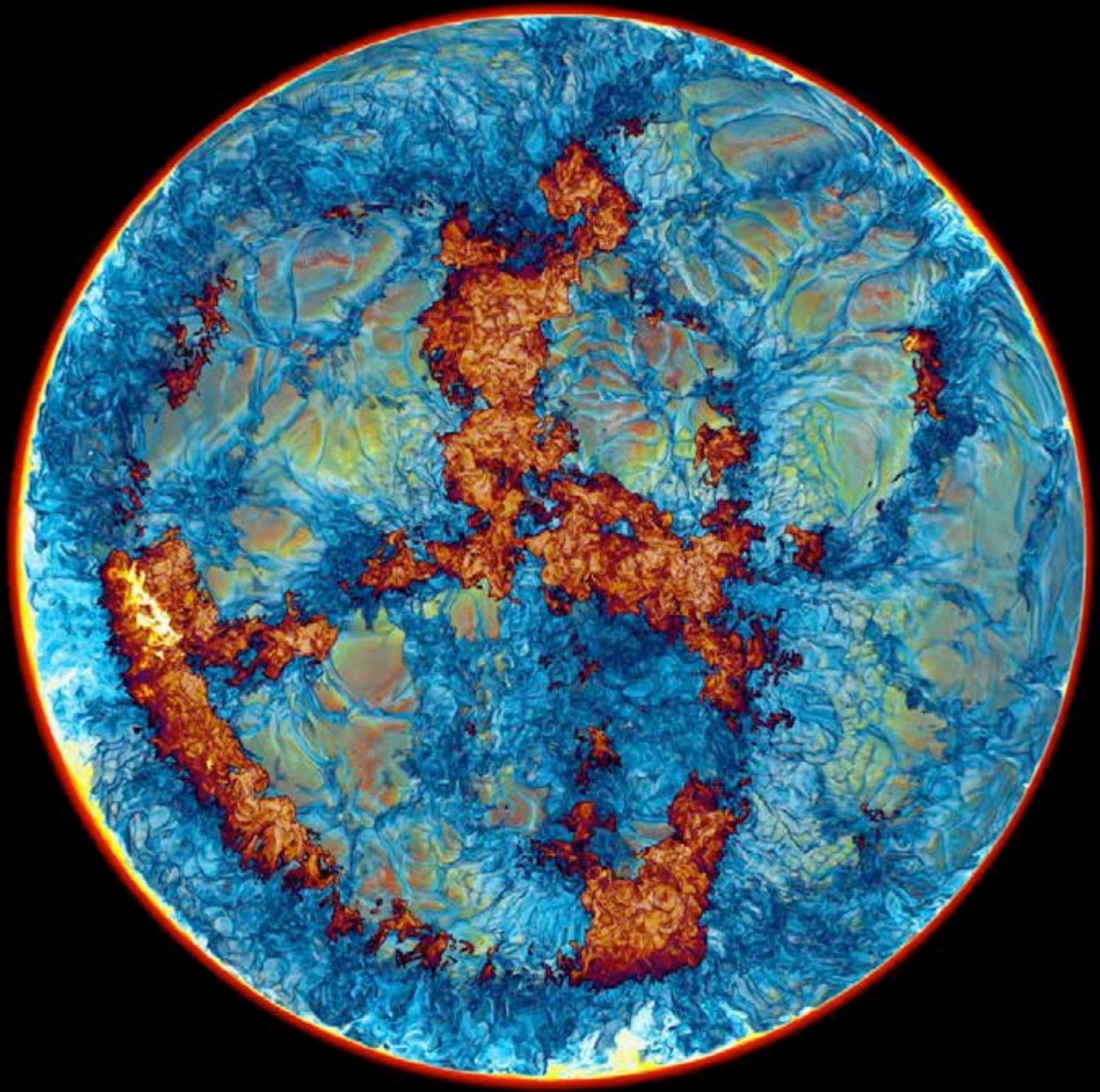

*Sakurai's Object H-ingestion simulation on Blue Waters machine in Jan., 2014, on a grid of $1536^3$ cells.*

Very gradually the concentration of ingested hydrogen builds up in the upper region of the convection zone.

*t = 575 min.*

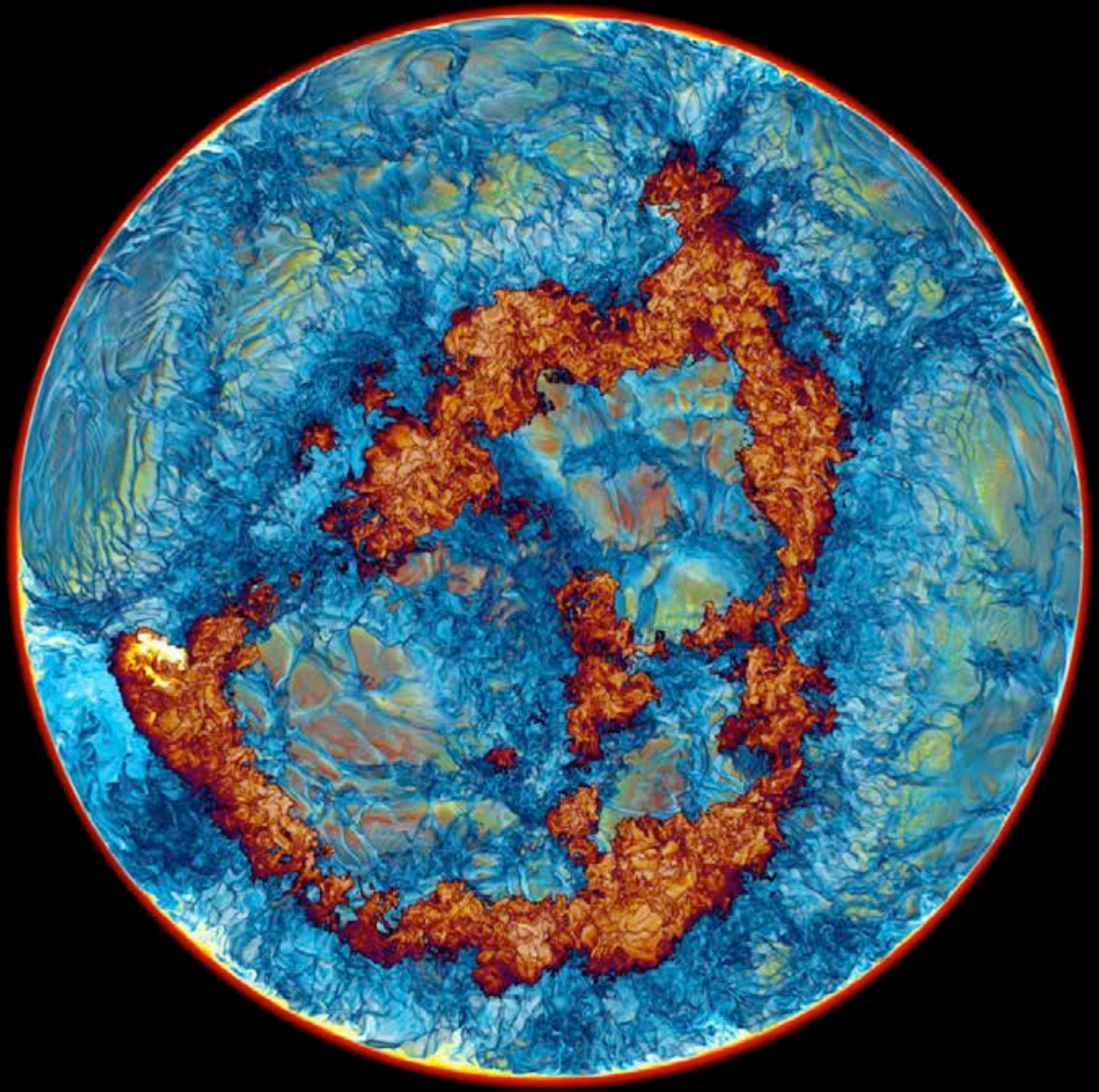

*Sakurai's Object H-ingestion simulation on Blue Waters machine in Jan., 2014, on a grid of $1536^3$ cells.*

*We see a hemisphere and make only mixtures of entrained hydrogen-rich gas with gas of the helium shell flash convection zone visible. The energy release rate from burning ingested H is shown in very dark blue, yellow, and white.*

*t = 600 min.*

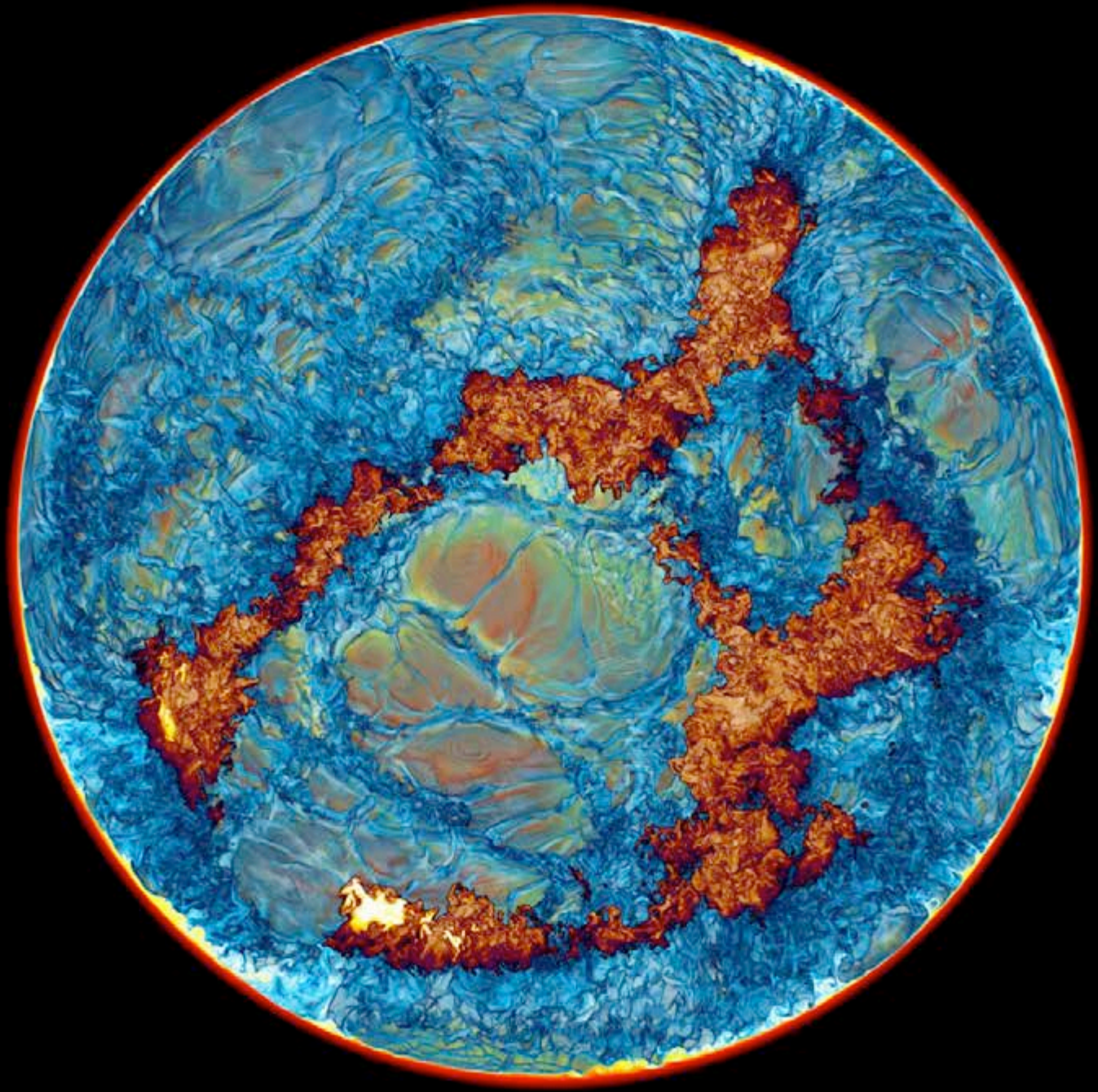

*Sakurai's Object H-ingestion simulation on Blue Waters machine in Jan., 2014, on a grid of $1536^3$ cells.*

*We see a hemisphere and make only mixtures of entrained hydrogen-rich gas with gas of the helium shell flash convection zone visible. The energy release rate from burning ingested H is shown in very dark blue, yellow, and white.*

*t = 625 min.*

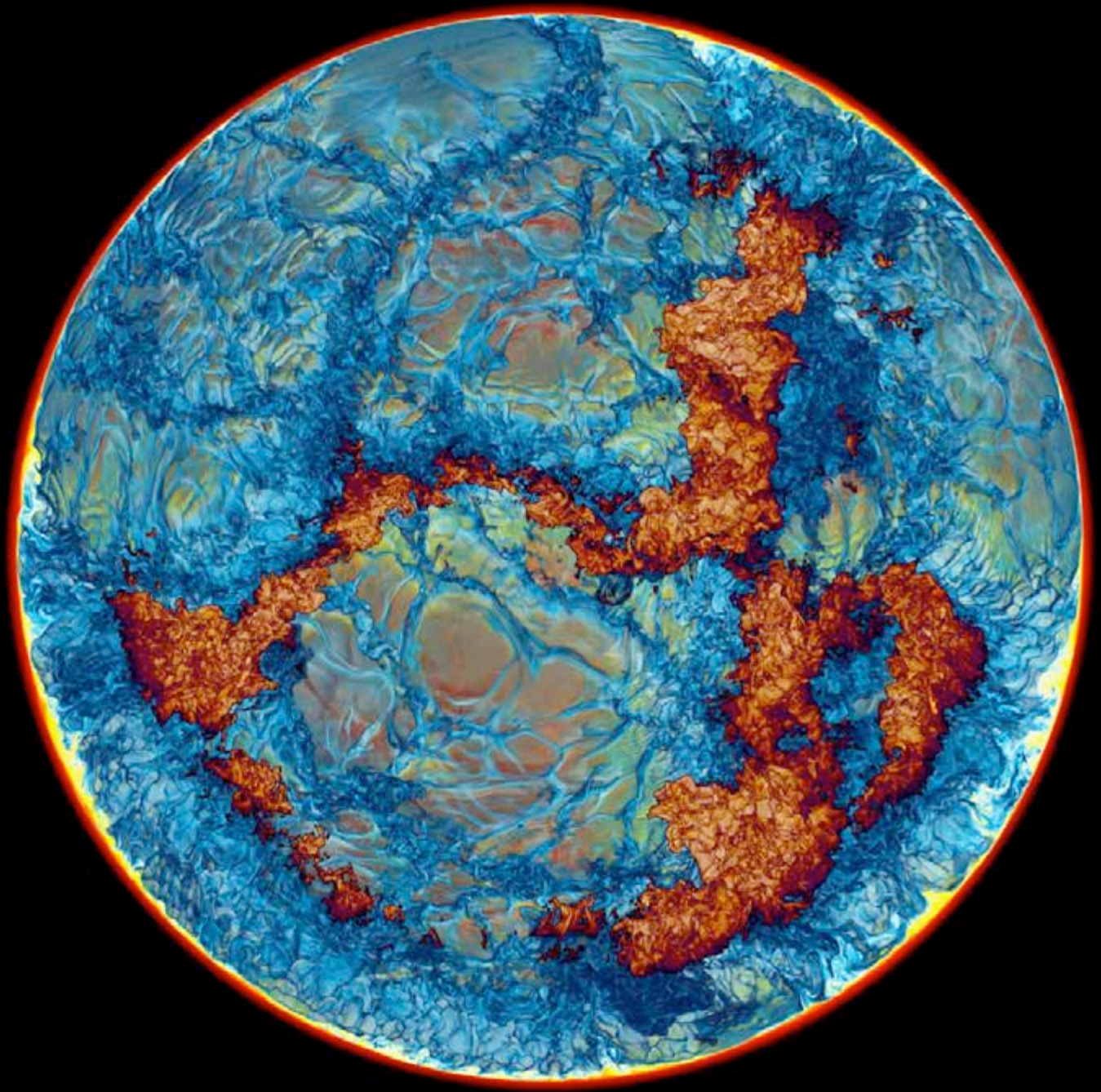

*Sakurai's Object H-ingestion simulation on Blue Waters machine in Jan., 2014, on a grid of $1536^3$ cells.*

Burning is now occurring at a larger number of locations at the same time.

*t = 650 min.*

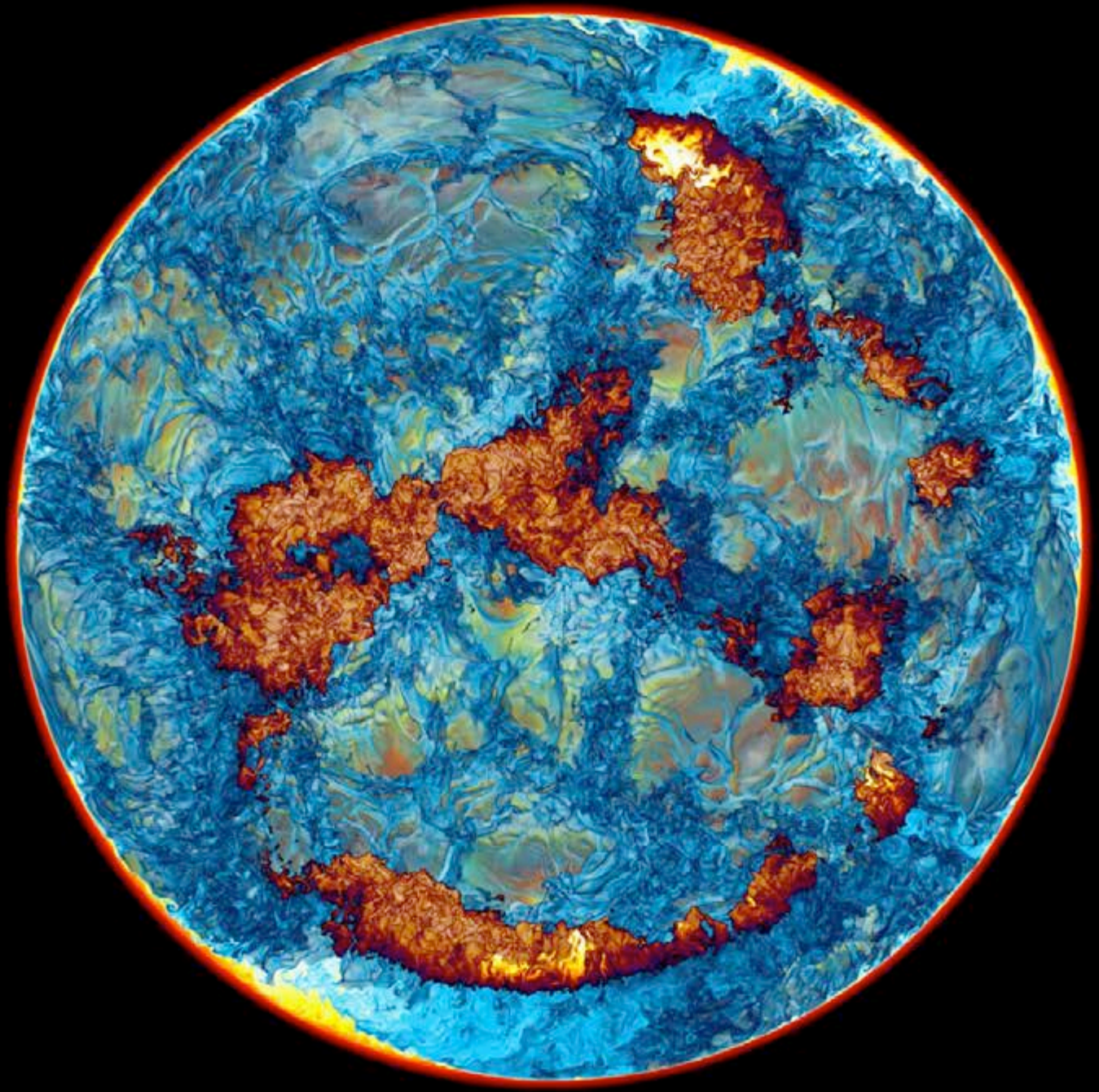

*Sakurai's Object H-ingestion simulation on Blue Waters machine in Jan., 2014, on a grid of $1536^3$ cells.*

*We see a hemisphere and make only mixtures of entrained hydrogen-rich gas with gas of the helium shell flash convection zone visible. The energy release rate from burning ingested H is shown in very dark blue, yellow, and white.*

*t = 675 min.*

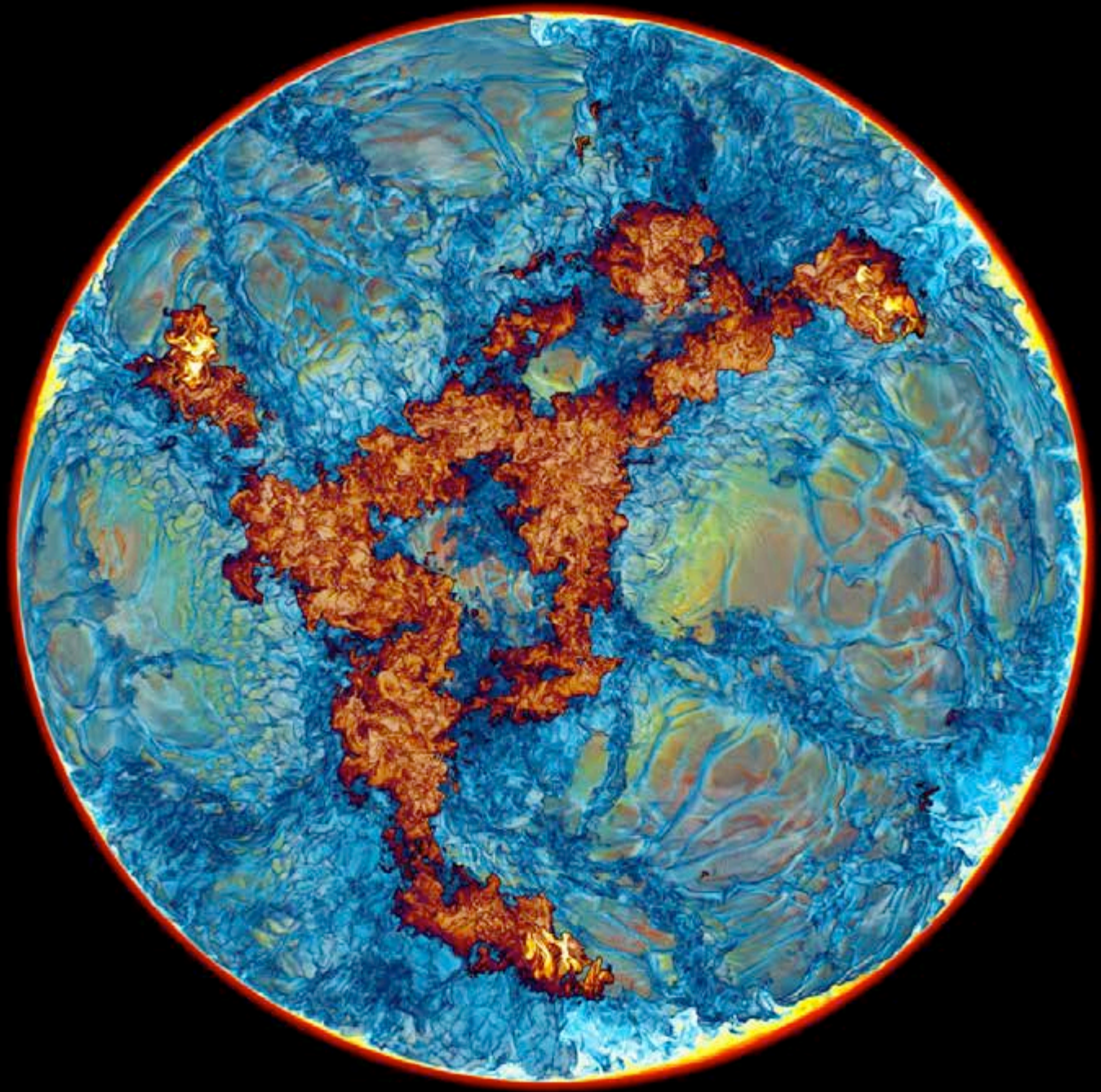

*Sakurai's Object H-ingestion simulation on Blue Waters machine in Jan., 2014, on a grid of $1536^3$ cells.*

*We see a hemisphere and make only mixtures of entrained hydrogen-rich gas with gas of the helium shell flash convection zone visible. The energy release rate from burning ingested H is shown in very dark blue, yellow, and white.*

*t = 700 min.*

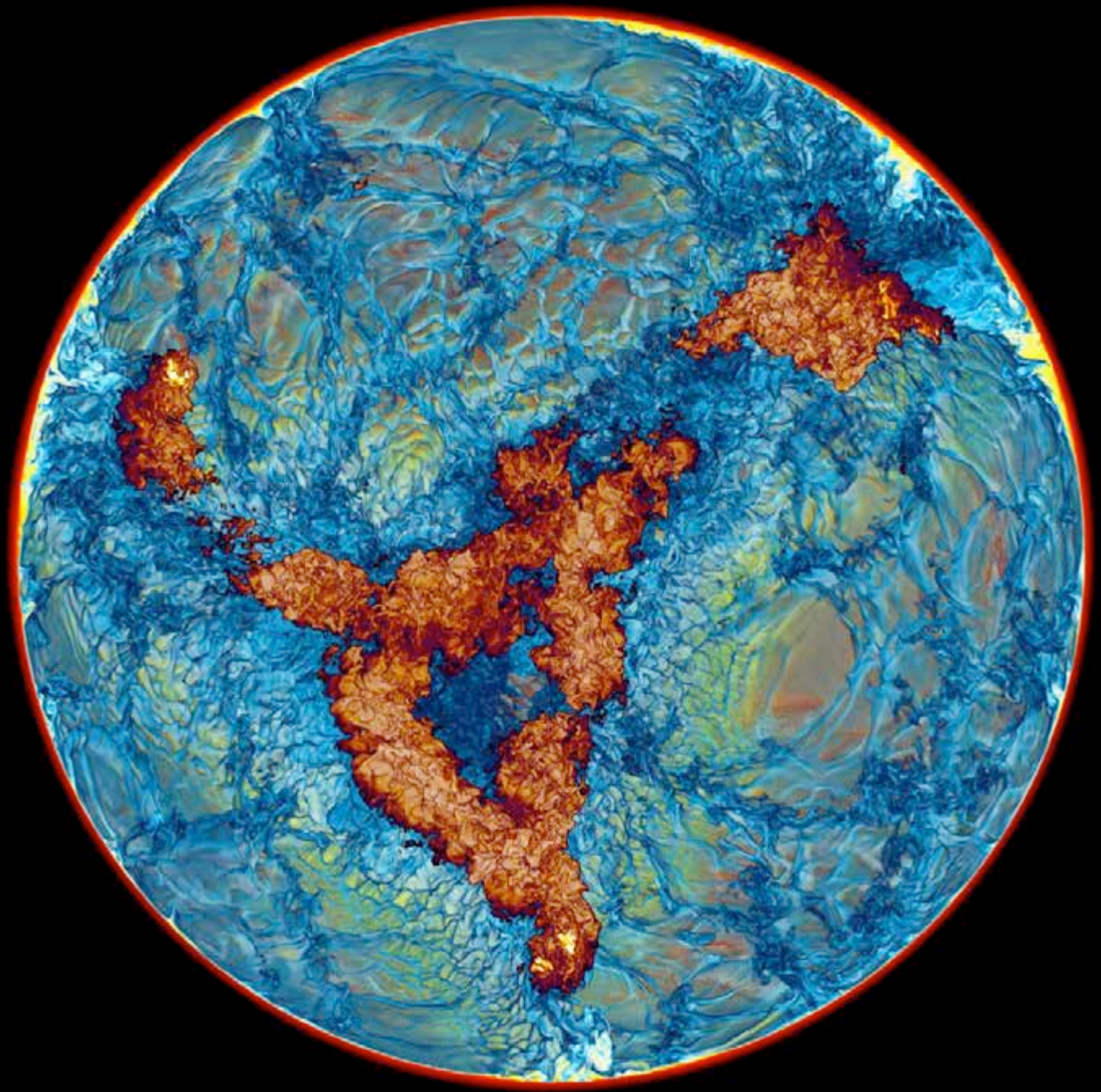

*Sakurai's Object H-ingestion simulation on Blue Waters machine in Jan., 2014, on a grid of $1536^3$ cells.*

*We see a hemisphere and make only mixtures of entrained hydrogen-rich gas with gas of the helium shell flash convection zone visible. The energy release rate from burning ingested H is shown in very dark blue, yellow, and white.*

*t = 725 min.*

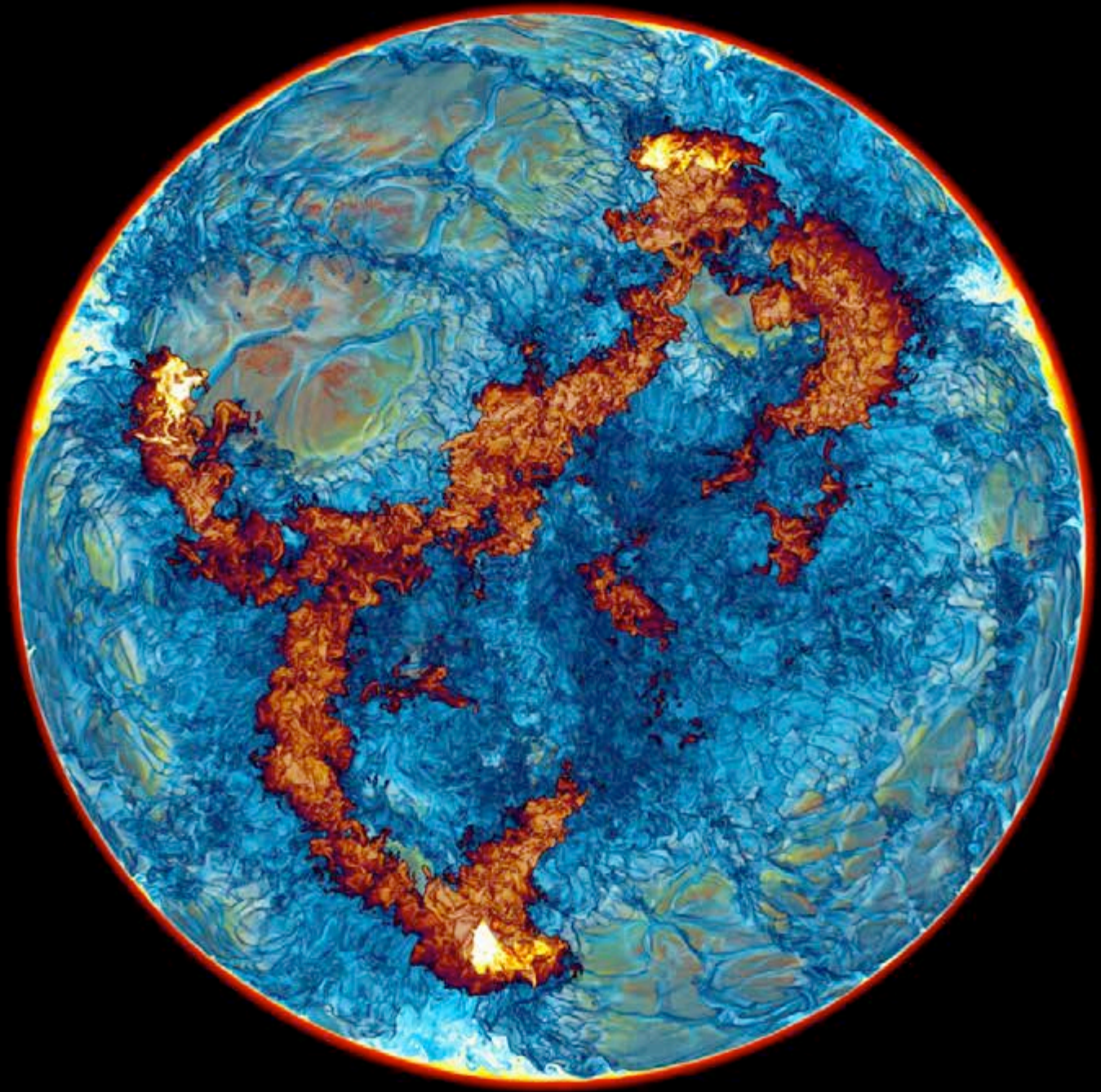

*Sakurai's Object H-ingestion simulation on Blue Waters machine in Jan., 2014, on a grid of $1536^3$ cells.*

*We see a hemisphere and make only mixtures of entrained hydrogen-rich gas with gas of the helium shell flash convection zone visible. The energy release rate from burning ingested H is shown in very dark blue, yellow, and white.*

*t = 750 min.*

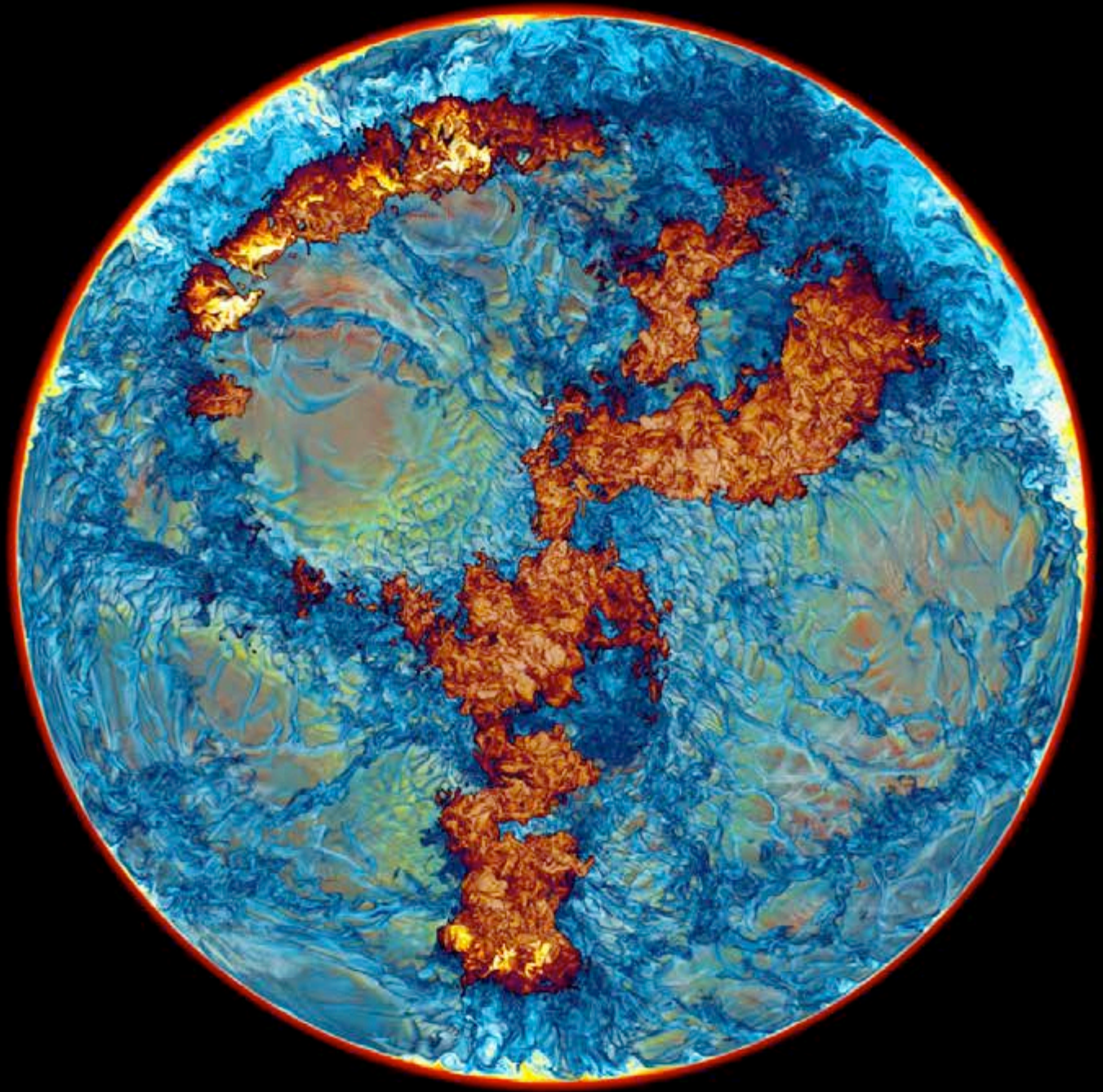

*Sakurai's Object H-ingestion simulation on Blue Waters machine in Jan., 2014, on a grid of $1536^3$ cells.*

*We see a hemisphere and make only mixtures of entrained hydrogen-rich gas with gas of the helium shell flash convection zone visible. The energy release rate from burning ingested H is shown in very dark blue, yellow, and white.*

*t = 775 min.*

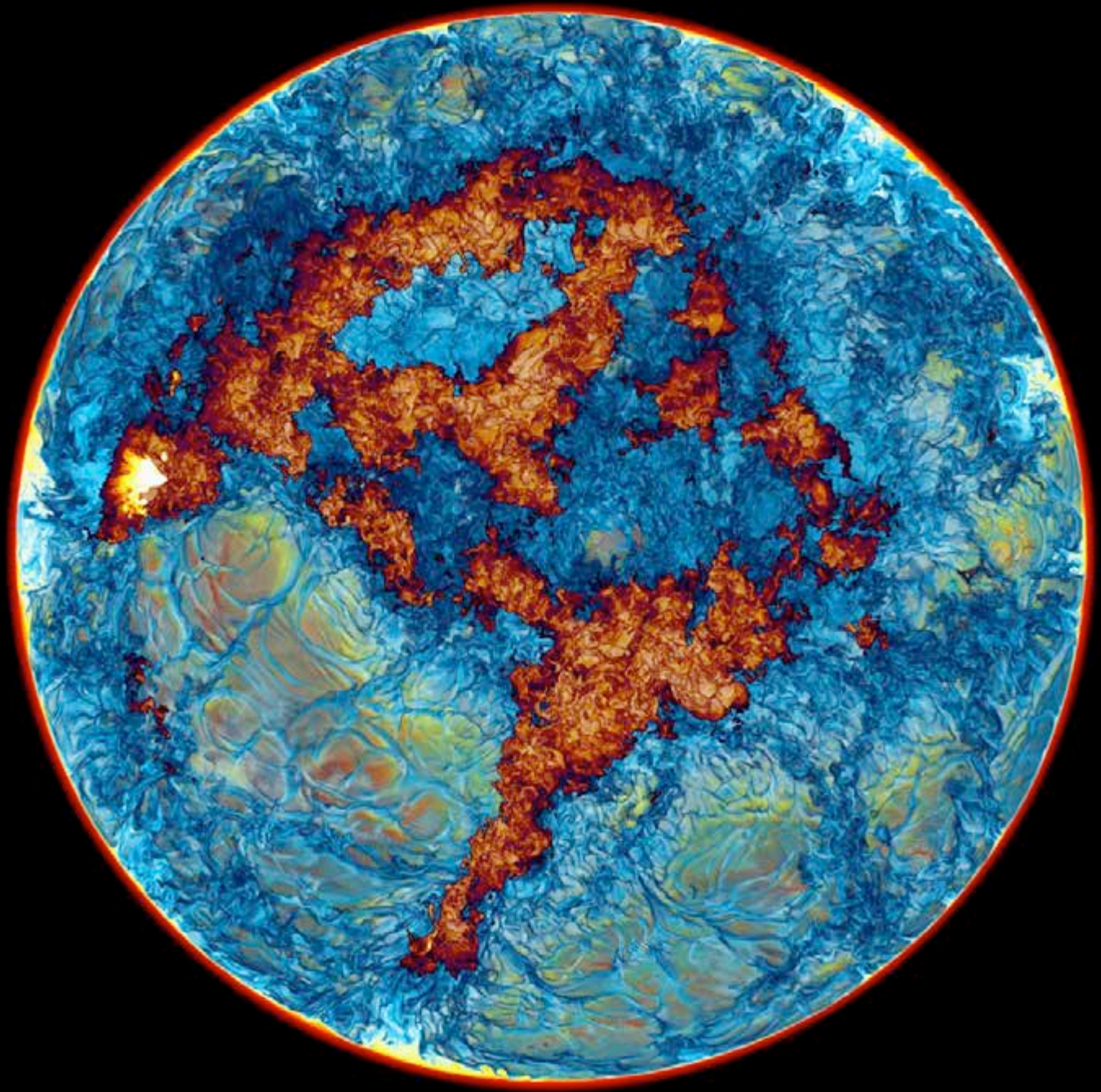

*Sakurai's Object H-ingestion simulation on Blue Waters machine in Jan., 2014, on a grid of $1536^3$ cells.*

*We see a hemisphere and make only mixtures of entrained hydrogen-rich gas with gas of the helium shell flash convection zone visible. The energy release rate from burning ingested H is shown in very dark blue, yellow, and white.*

*t = 800 min.*

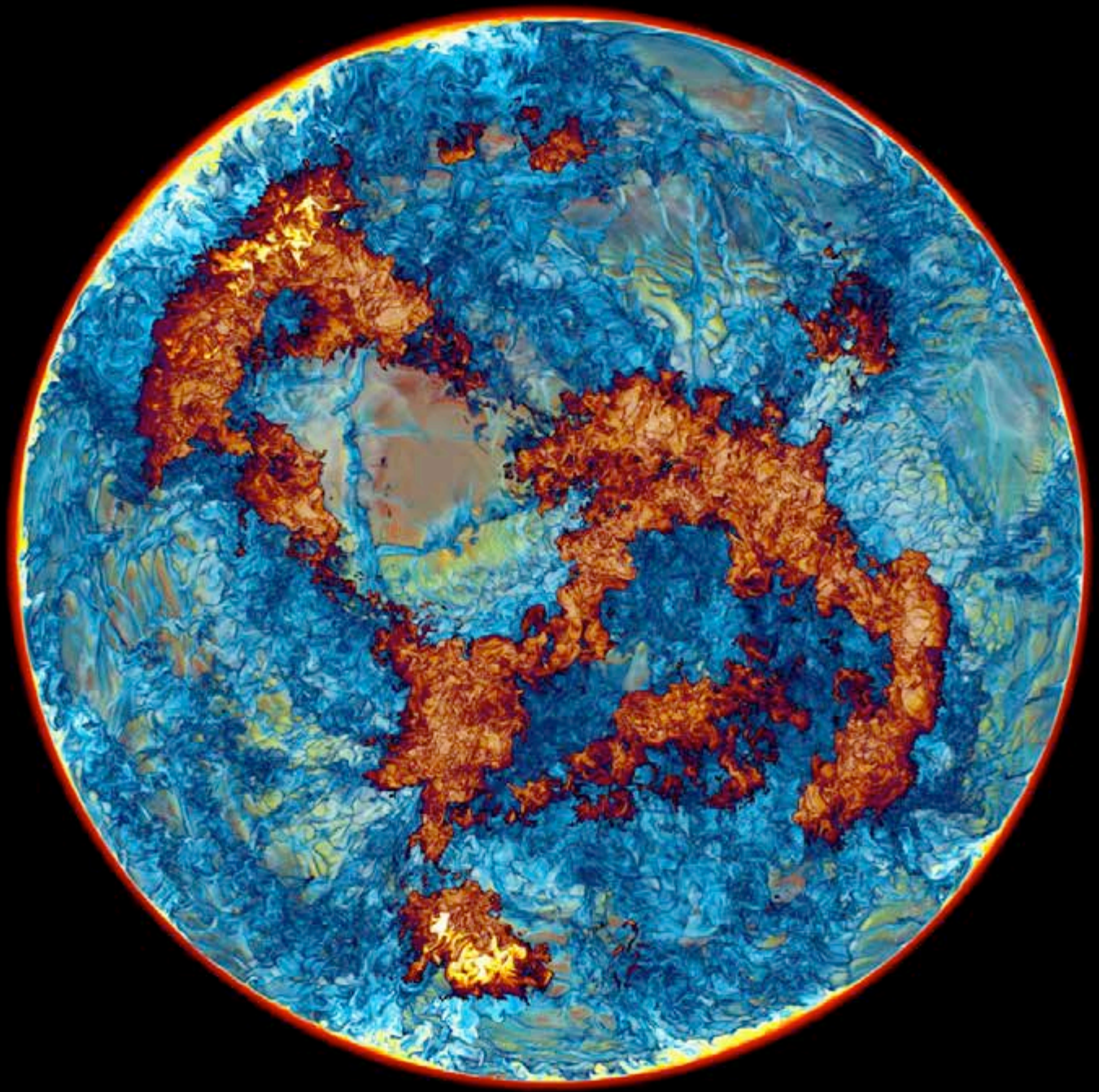

*Sakurai's Object H-ingestion simulation on Blue Waters machine in Jan., 2014, on a grid of $1536^3$ cells.*

*We see a hemisphere and make only mixtures of entrained hydrogen-rich gas with gas of the helium shell flash convection zone visible. The energy release rate from burning ingested H is shown in very dark blue, yellow, and white.*

*t = 825 min.*

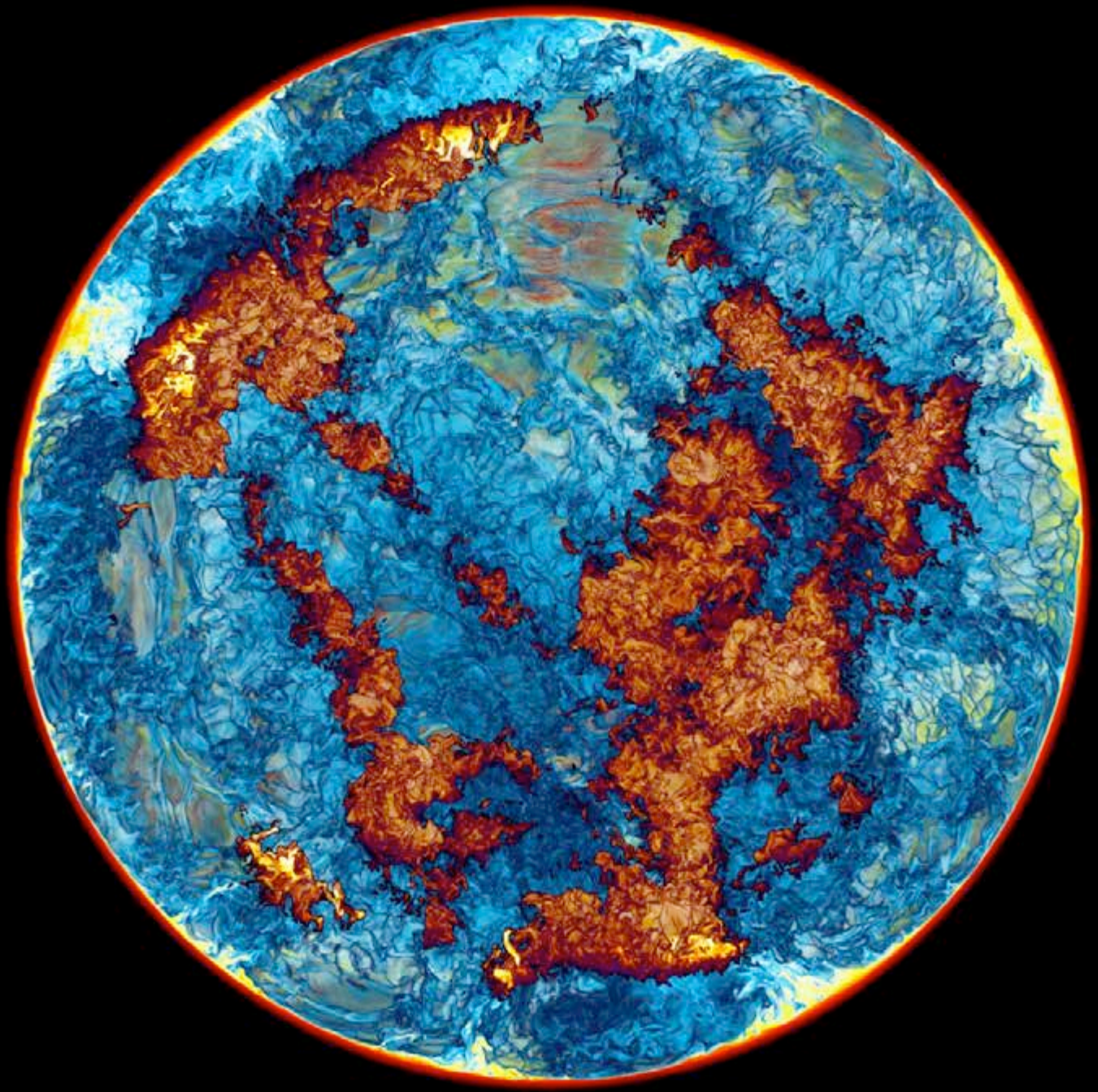

*Sakurai's Object H-ingestion simulation on Blue Waters machine in Jan., 2014, on a grid of $1536^3$ cells.*

*We see a hemisphere and make only mixtures of entrained hydrogen-rich gas with gas of the helium shell flash convection zone visible. The energy release rate from burning ingested H is shown in very dark blue, yellow, and white.*

*t = 850 min.*

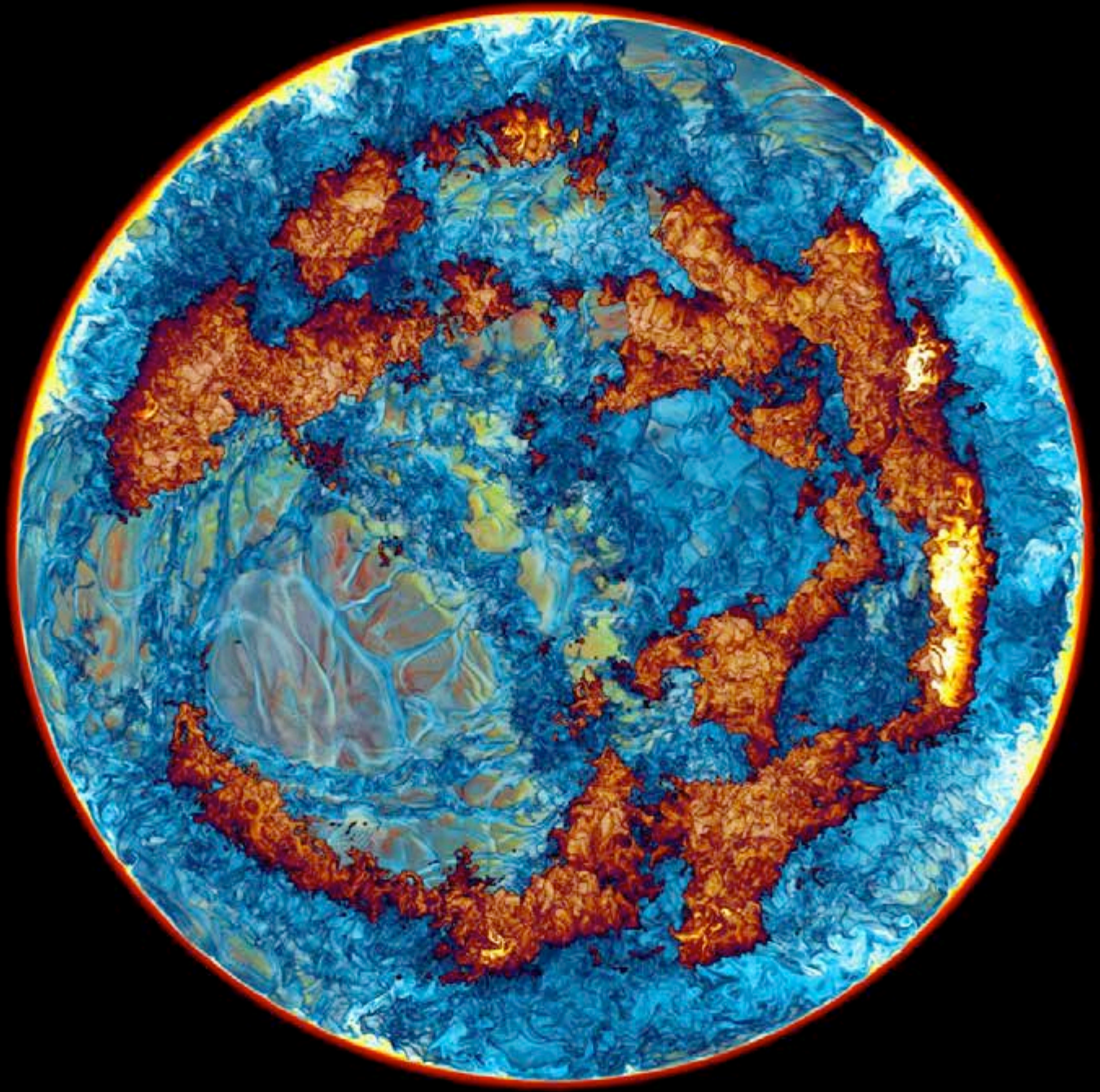

*Sakurai's Object H-ingestion simulation on Blue Waters machine in Jan., 2014, on a grid of $1536^3$ cells.*

*We see a hemisphere and make only mixtures of entrained hydrogen-rich gas with gas of the helium shell flash convection zone visible. The energy release rate from burning ingested H is shown in very dark blue, yellow, and white.*

*t = 875 min.*

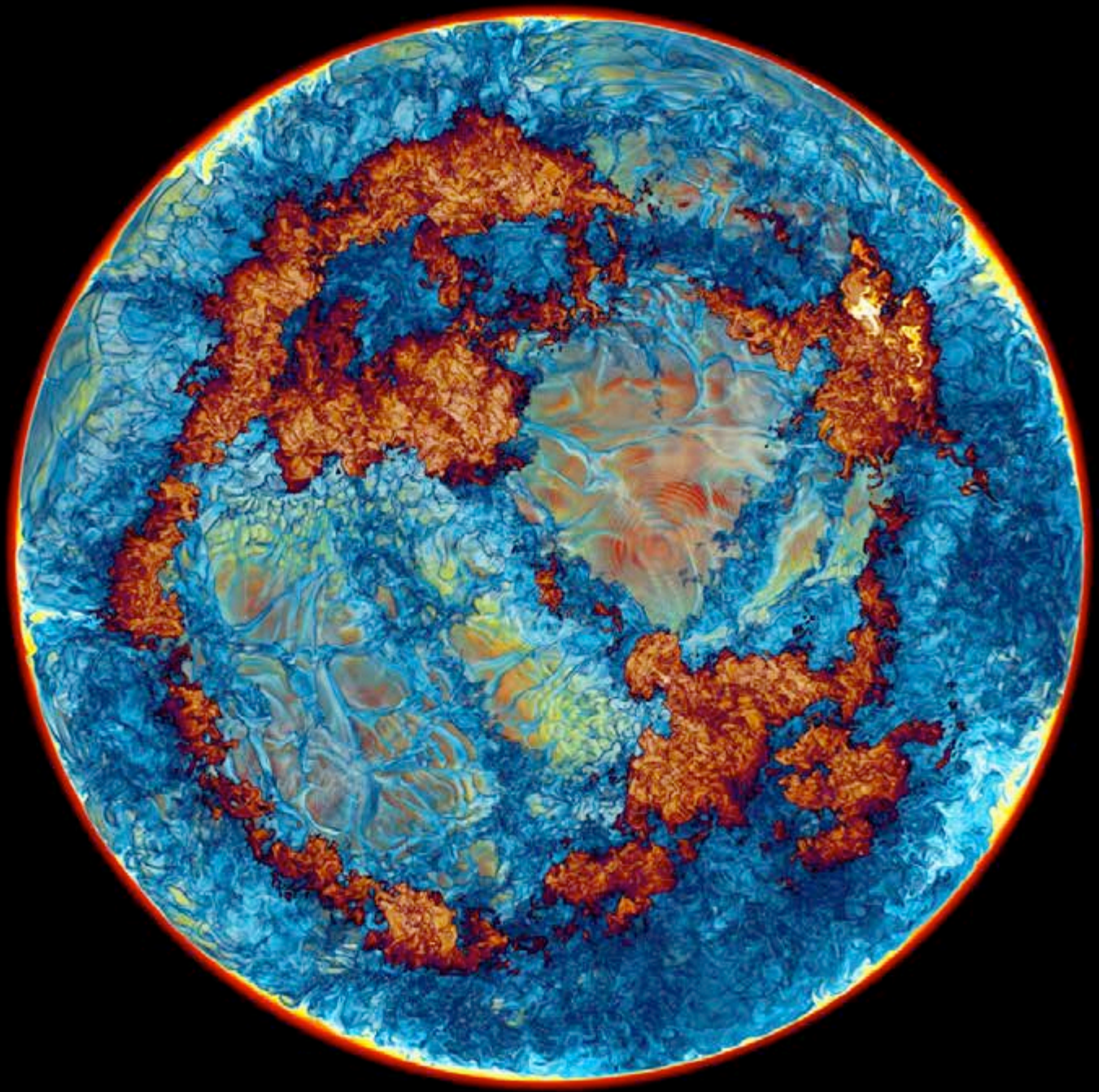

*Sakurai's Object H-ingestion simulation on Blue Waters machine in Jan., 2014, on a grid of $1536^3$ cells.*

*We see a hemisphere and make only mixtures of entrained hydrogen-rich gas with gas of the helium shell flash convection zone visible. The energy release rate from burning ingested H is shown in very dark blue, yellow, and white.*

*t = 900 min.*

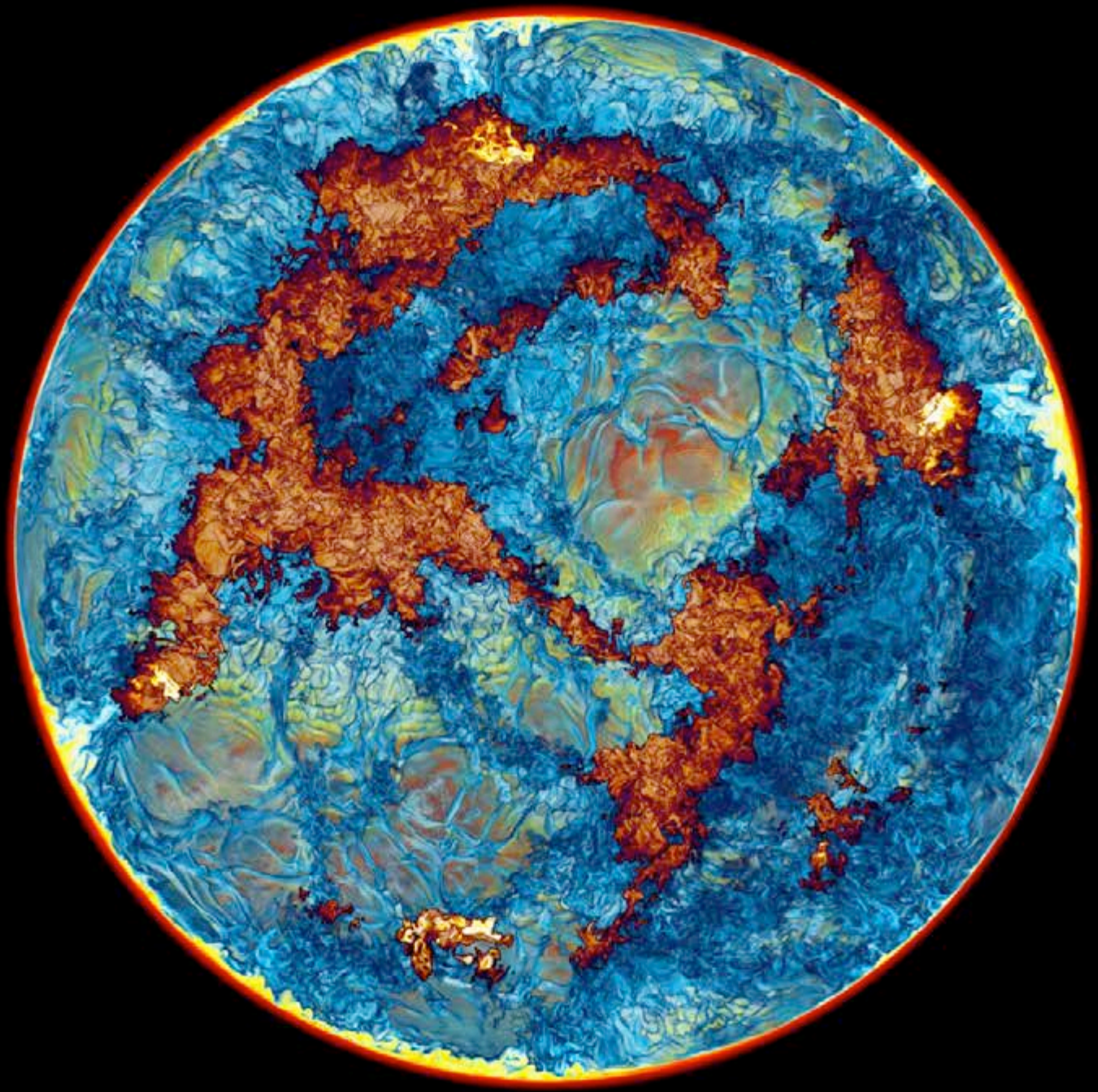

*Sakurai's Object H-ingestion simulation on Blue Waters machine in Jan., 2014, on a grid of $1536^3$ cells.*

The accumulation of ingested hydrogen in the upper convection region is becoming increasingly noticeable.

*t = 925 min.*

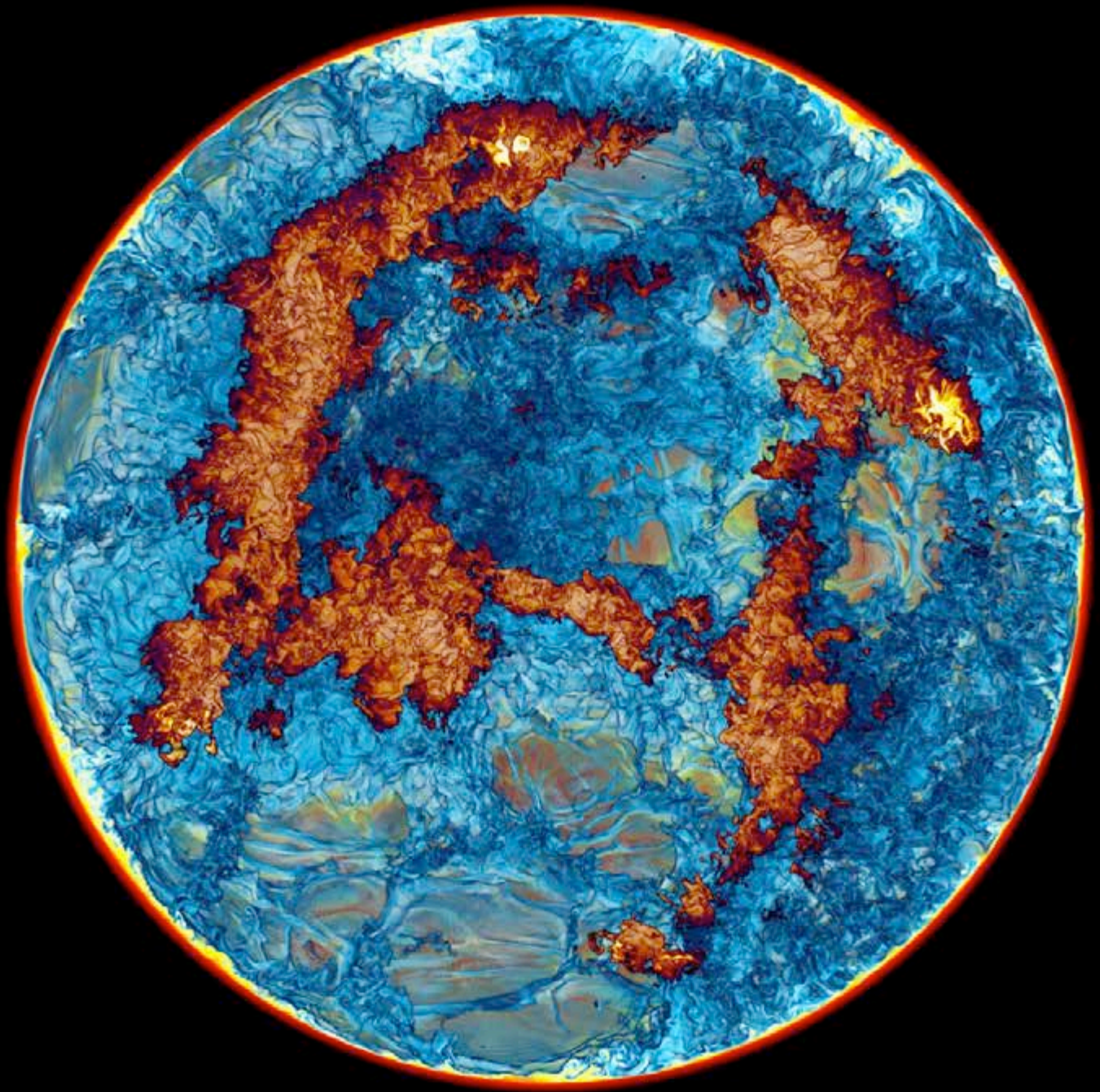

*Sakurai's Object H-ingestion simulation on Blue Waters machine in Jan., 2014, on a grid of $1536^3$ cells.*

*We see a hemisphere and make only mixtures of entrained hydrogen-rich gas with gas of the helium shell flash convection zone visible. The energy release rate from burning ingested H is shown in very dark blue, yellow, and white.*

*t = 950 min.*

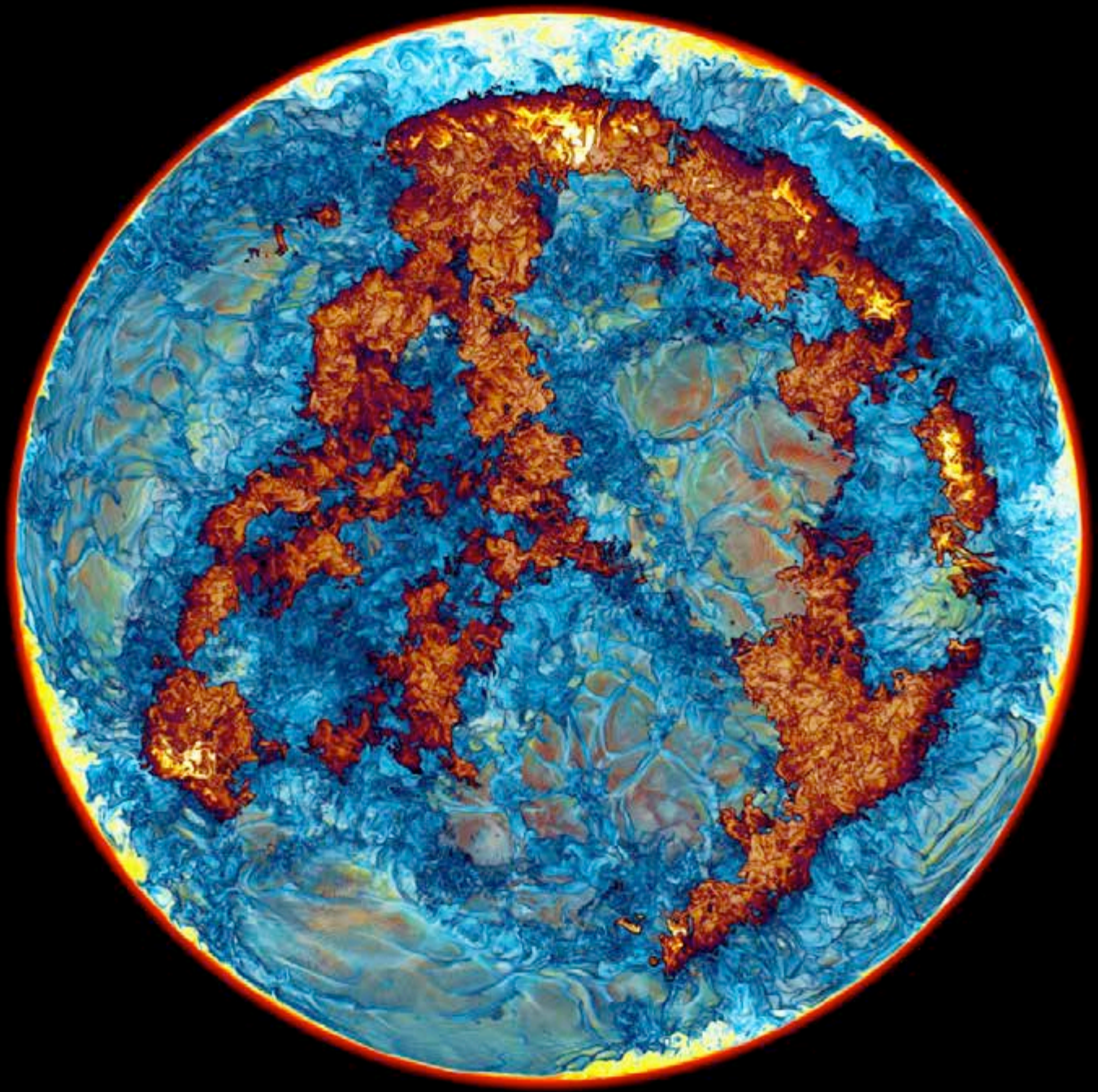

*Sakurai's Object H-ingestion simulation on Blue Waters machine in Jan., 2014, on a grid of $1536^3$ cells.*

*We see a hemisphere and make only mixtures of entrained hydrogen-rich gas with gas of the helium shell flash convection zone visible. The energy release rate from burning ingested H is shown in very dark blue, yellow, and white.*

*t = 975 min.*

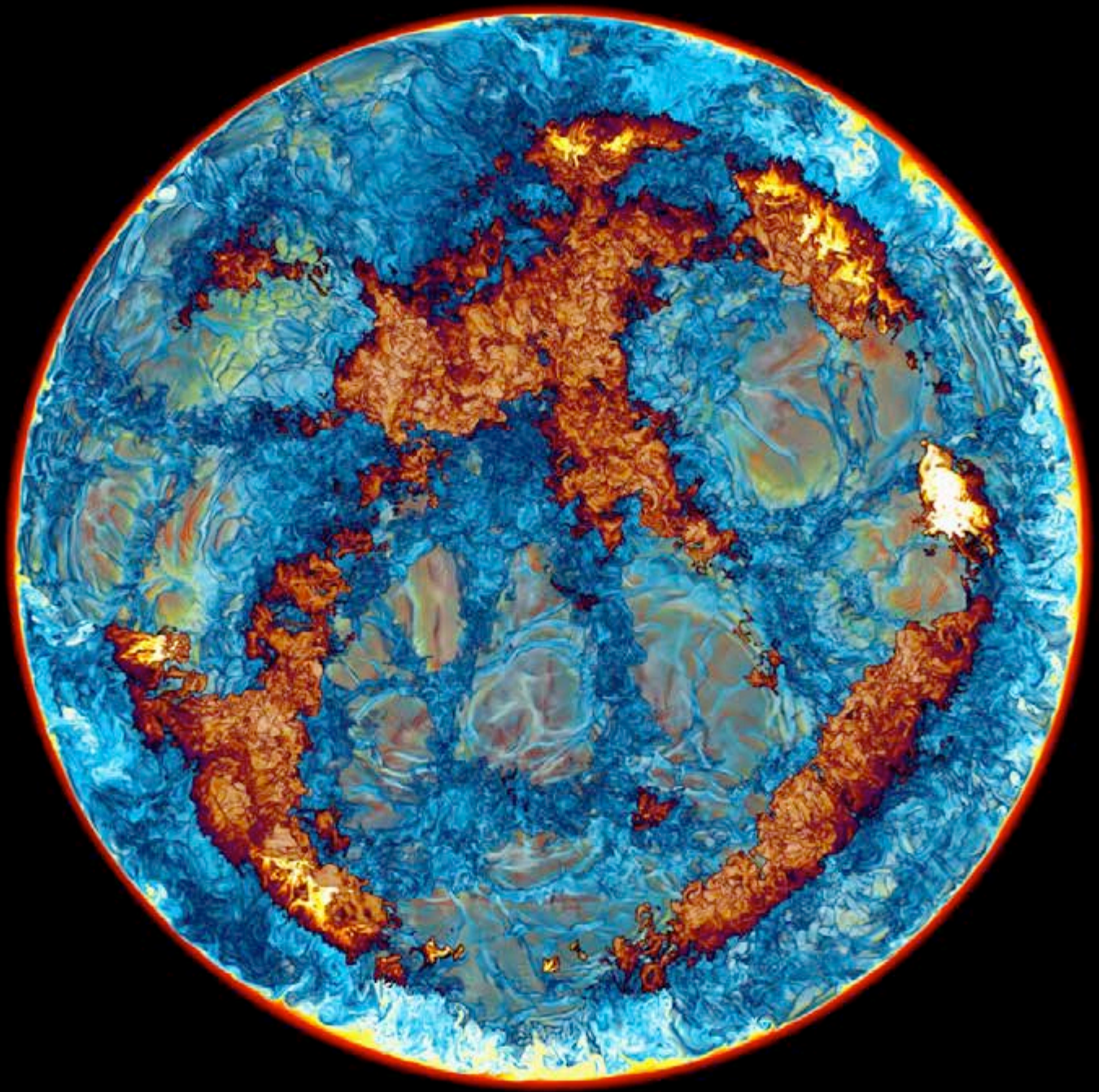

*Sakurai's Object H-ingestion simulation on Blue Waters machine in Jan., 2014, on a grid of $1536^3$ cells.*

*We see a hemisphere and make only mixtures of entrained hydrogen-rich gas with gas of the helium shell flash convection zone visible. The energy release rate from burning ingested H is shown in very dark blue, yellow, and white.*

*t = 1000 min.*

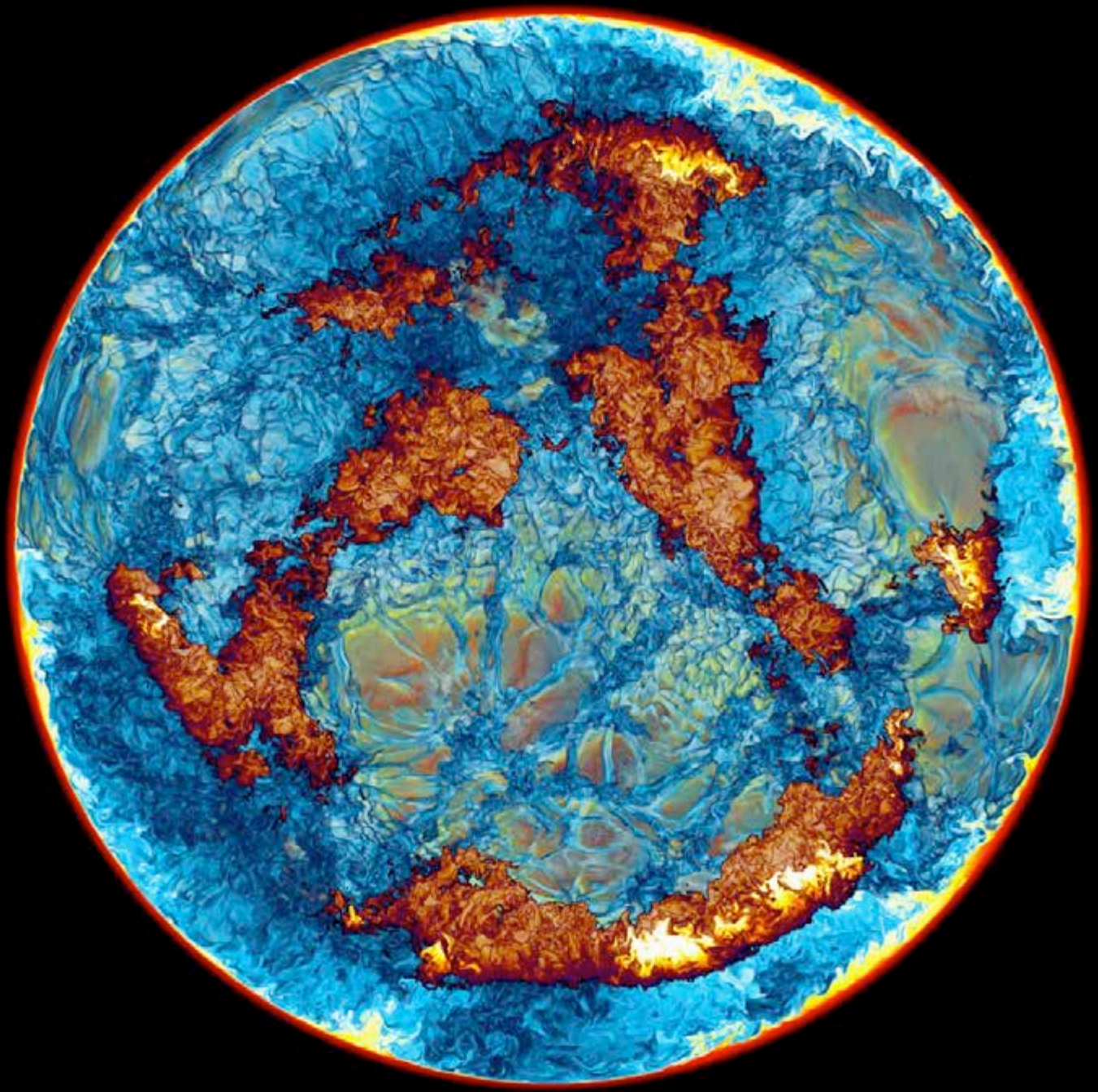

*Sakurai's Object H-ingestion simulation on Blue Waters machine in Jan., 2014, on a grid of $1536^3$ cells.*

*We see a hemisphere and make only mixtures of entrained hydrogen-rich gas with gas of the helium shell flash convection zone visible. The energy release rate from burning ingested H is shown in very dark blue, yellow, and white.*

*t = 1025 min.*

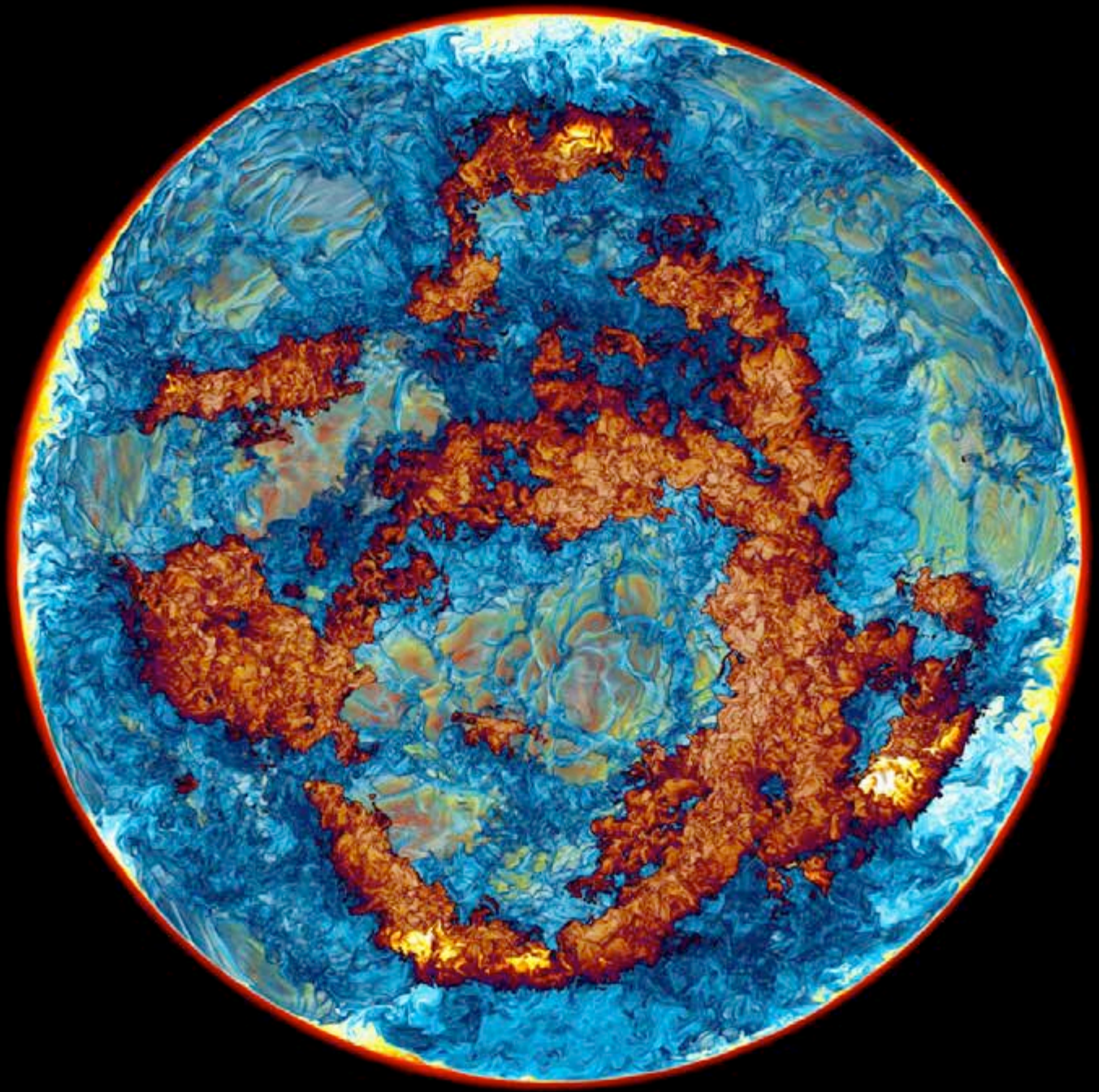

*Sakurai's Object H-ingestion simulation on Blue Waters machine in Jan., 2014, on a grid of $1536^3$ cells.*

*We see a hemisphere and make only mixtures of entrained hydrogen-rich gas with gas of the helium shell flash convection zone visible. The energy release rate from burning ingested H is shown in very dark blue, yellow, and white.*

*t = 1050 min.*

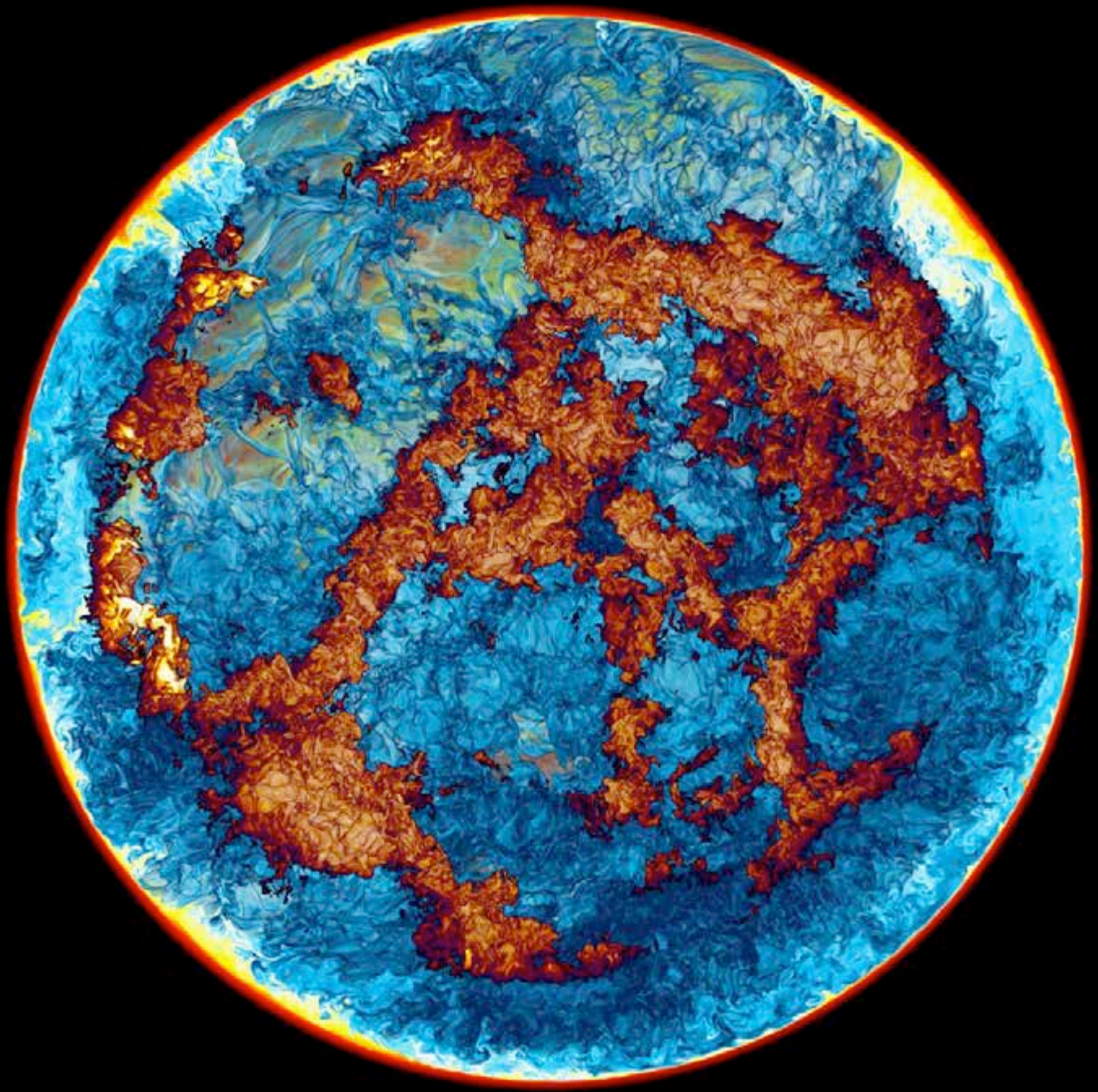

*Sakurai's Object H-ingestion simulation on Blue Waters machine in Jan., 2014, on a grid of $1536^3$ cells.*

Regions of higher hydrogen concentration (yellow and red) can now be seen descending into the upper region from the top of the convection zone.

*t = 1075 min.*

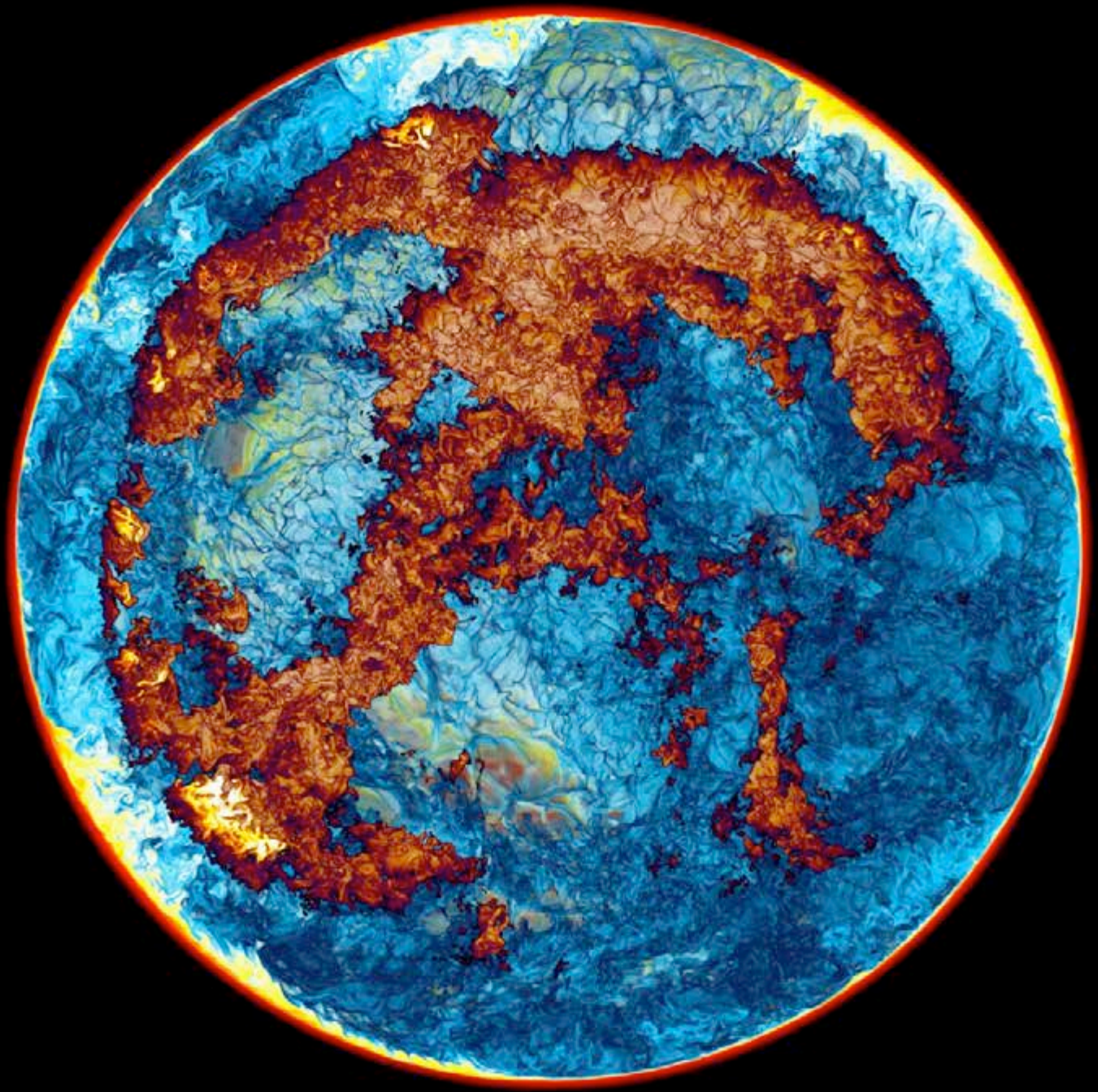

*Sakurai's Object H-ingestion simulation on Blue Waters machine in Jan., 2014, on a grid of $1536^3$ cells.*

*We see a hemisphere and make only mixtures of entrained hydrogen-rich gas with gas of the helium shell flash convection zone visible. The energy release rate from burning ingested H is shown in very dark blue, yellow, and white.*

*t = 1088 min.*

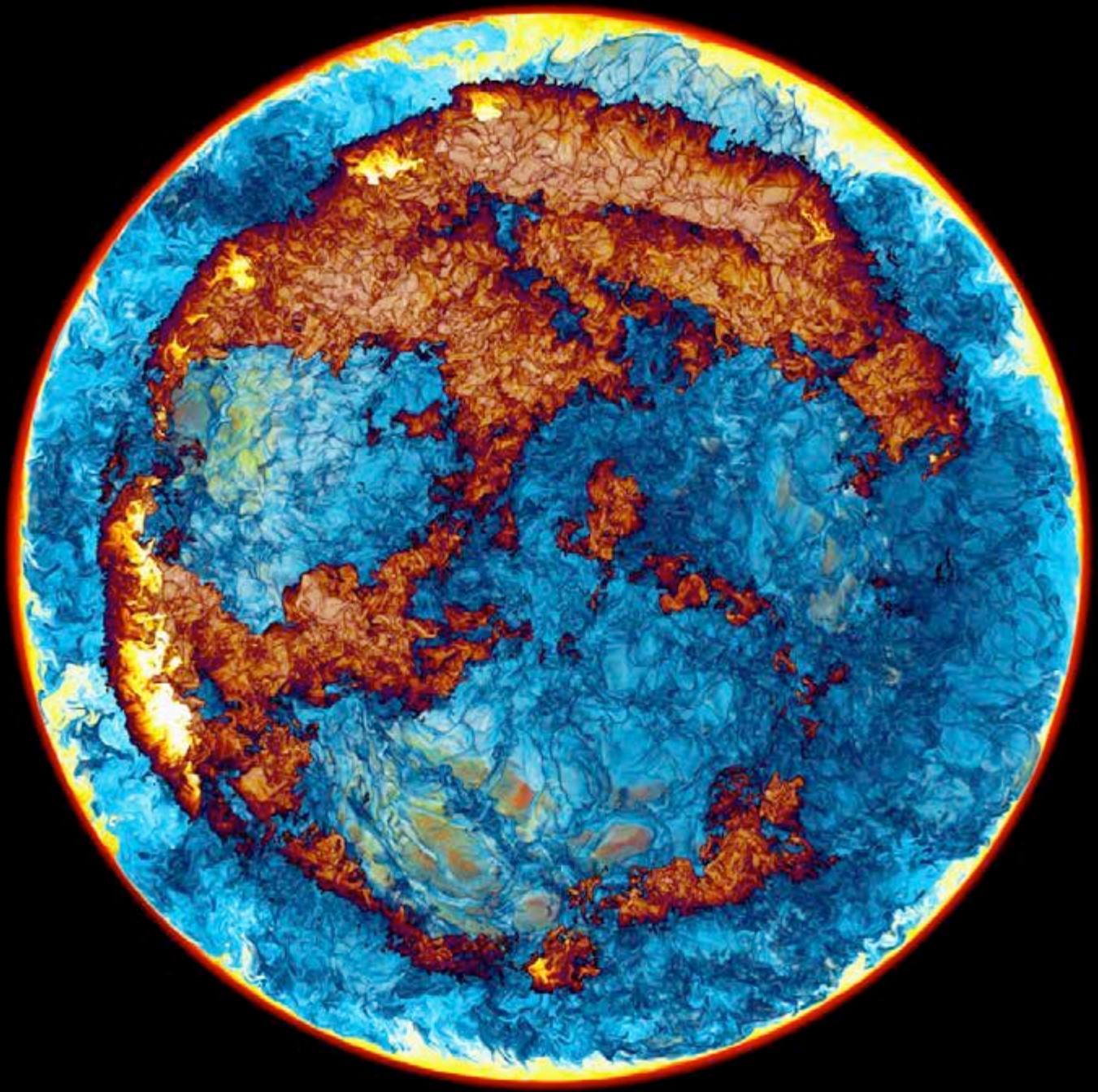

*Sakurai's Object H-ingestion simulation on Blue Waters machine in Jan., 2014, on a grid of $1536^3$ cells.*

*We see a hemisphere and make only mixtures of entrained hydrogen-rich gas with gas of the helium shell flash convection zone visible. The energy release rate from burning ingested H is shown in very dark blue, yellow, and white.*

*t = 1100 min.*

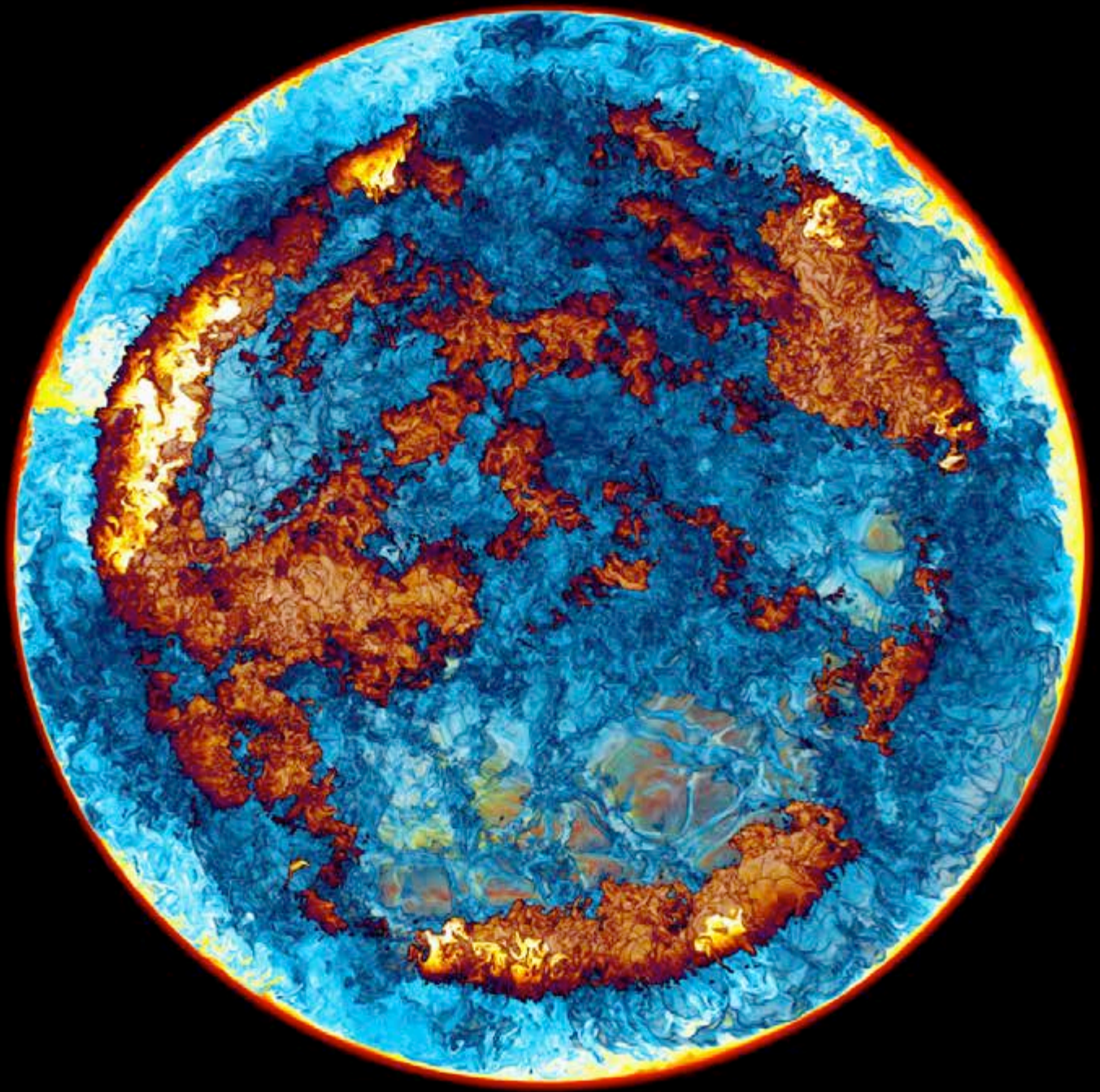

*Sakurai's Object H-ingestion simulation on Blue Waters machine in Jan., 2014, on a grid of $1536^3$ cells.*

*We see a hemisphere and make only mixtures of entrained hydrogen-rich gas with gas of the helium shell flash convection zone visible. The energy release rate from burning ingested H is shown in very dark blue, yellow, and white.*

*t = 1112 min.*

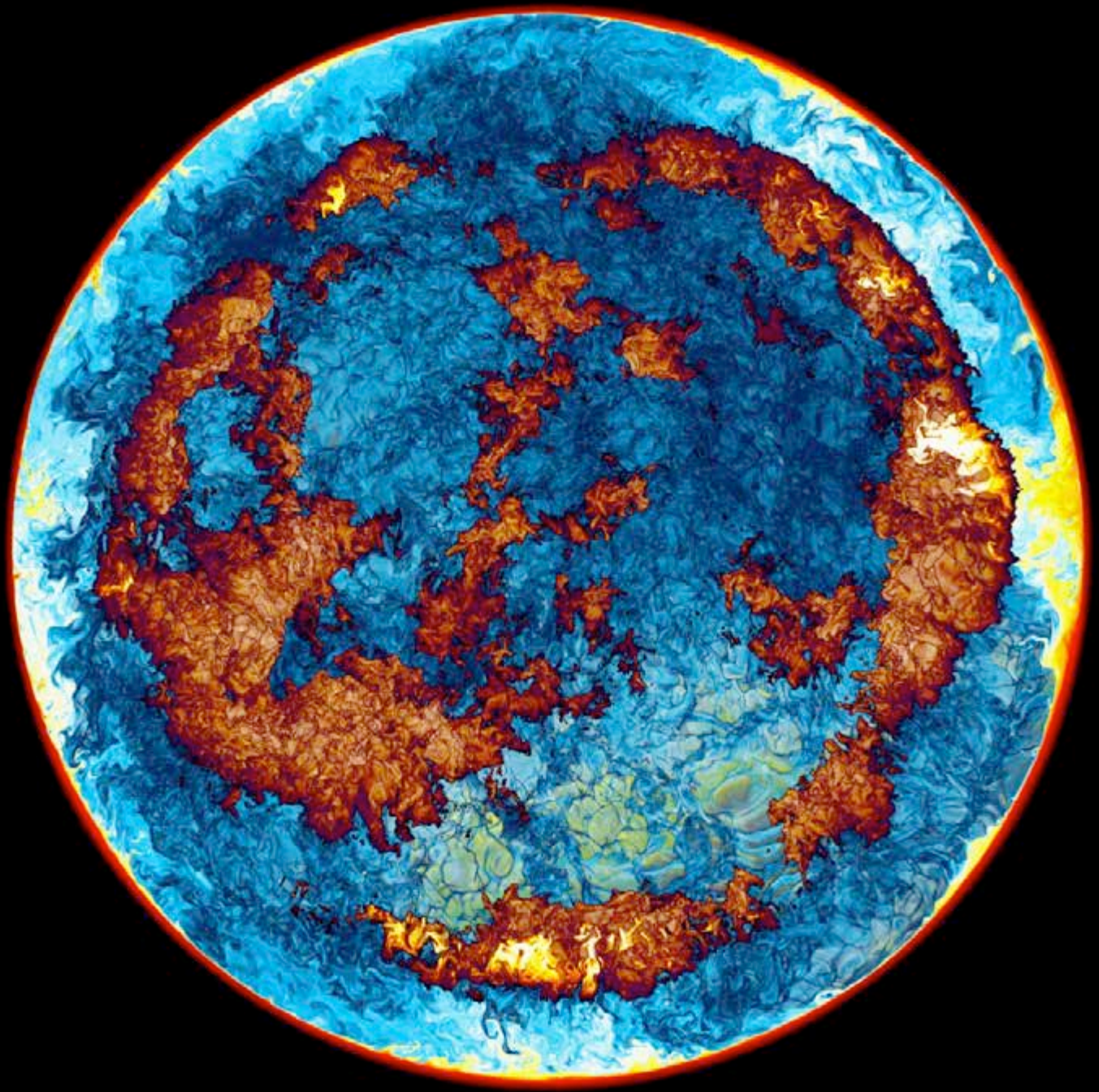

*Sakurai's Object H-ingestion simulation on Blue Waters machine in Jan., 2014, on a grid of $1536^3$ cells.*

The high average concentration of ingested hydrogen in the upper part of the convection zone is now unmistak-able.

*t = 1125 min.*

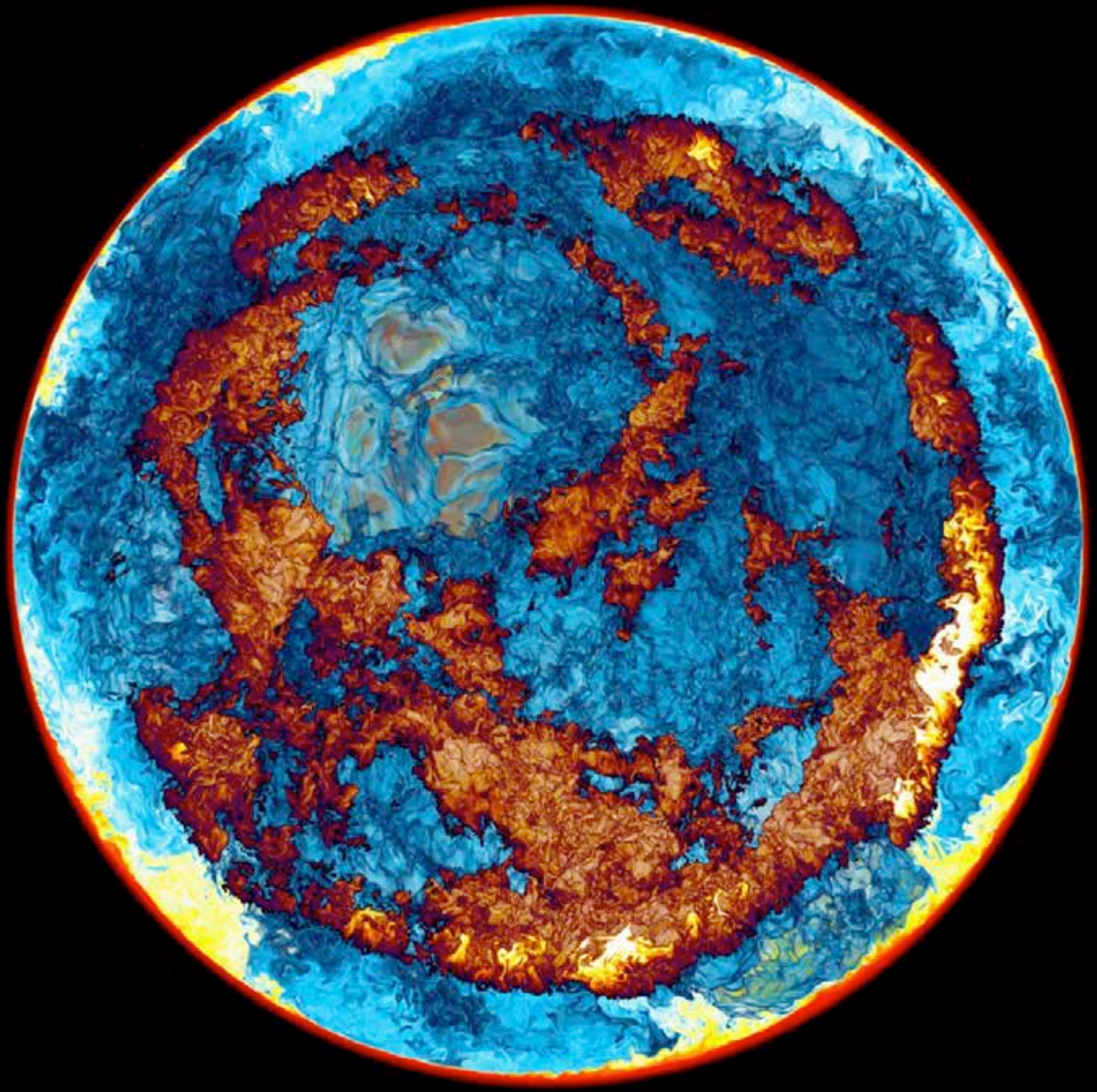

*Sakurai's Object H-ingestion simulation on Blue Waters machine in Jan., 2014, on a grid of $1536^3$ cells.*

*We see a hemisphere and make only mixtures of entrained hydrogen-rich gas with gas of the helium shell flash convection zone visible. The energy release rate from burning ingested H is shown in very dark blue, yellow, and white.*

*t = 1138 min.*

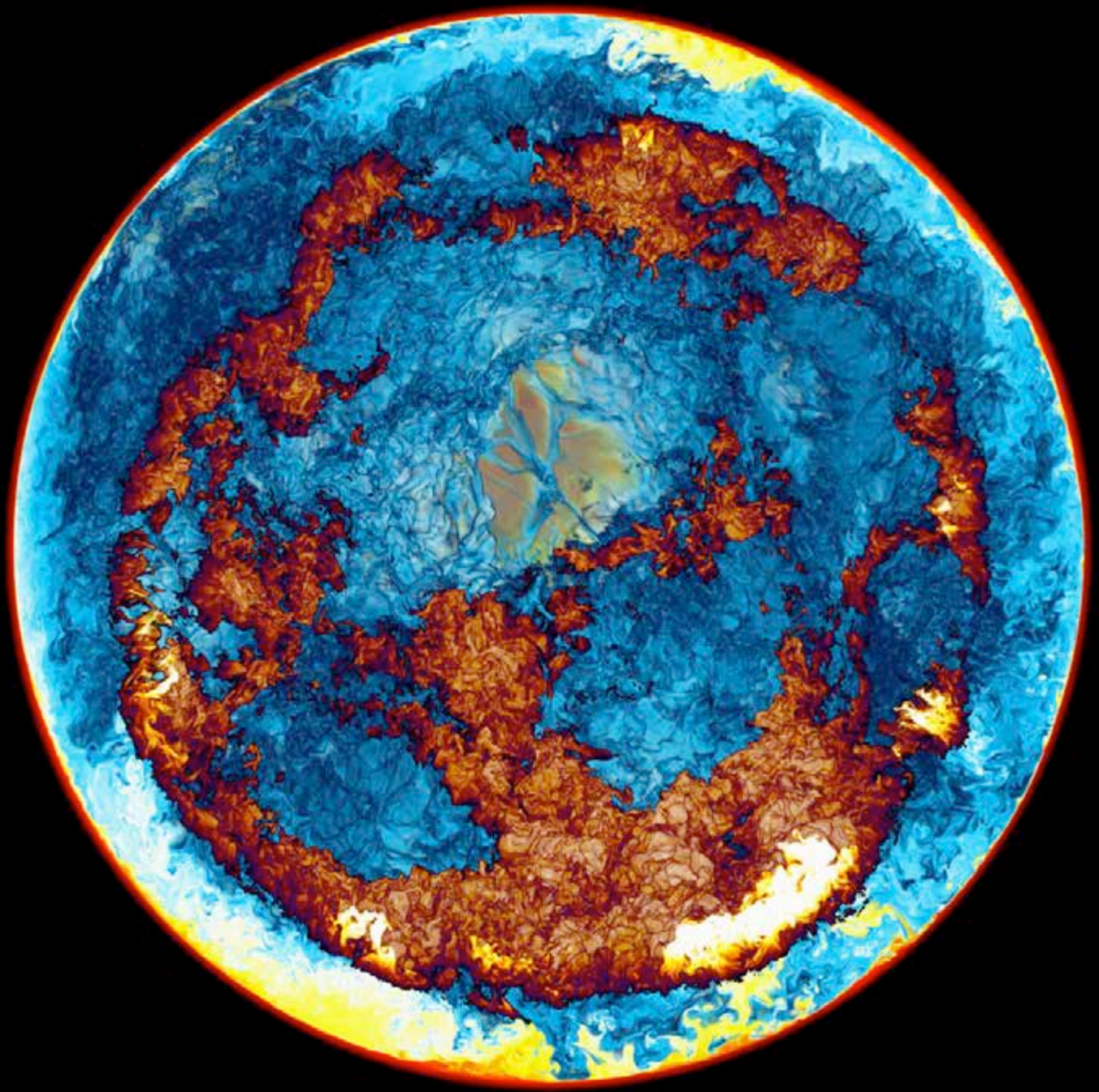

*Sakurai's Object H-ingestion simulation on Blue Waters machine in Jan., 2014, on a grid of $1536^3$ cells.*

The very strong energy release at the bottom-right produces a violent updraft there, which sets off a Global Oscillation of Shell Hydrogen ingestion (GOSH), unmistakable in the next few images.

*t = 1150 min.*

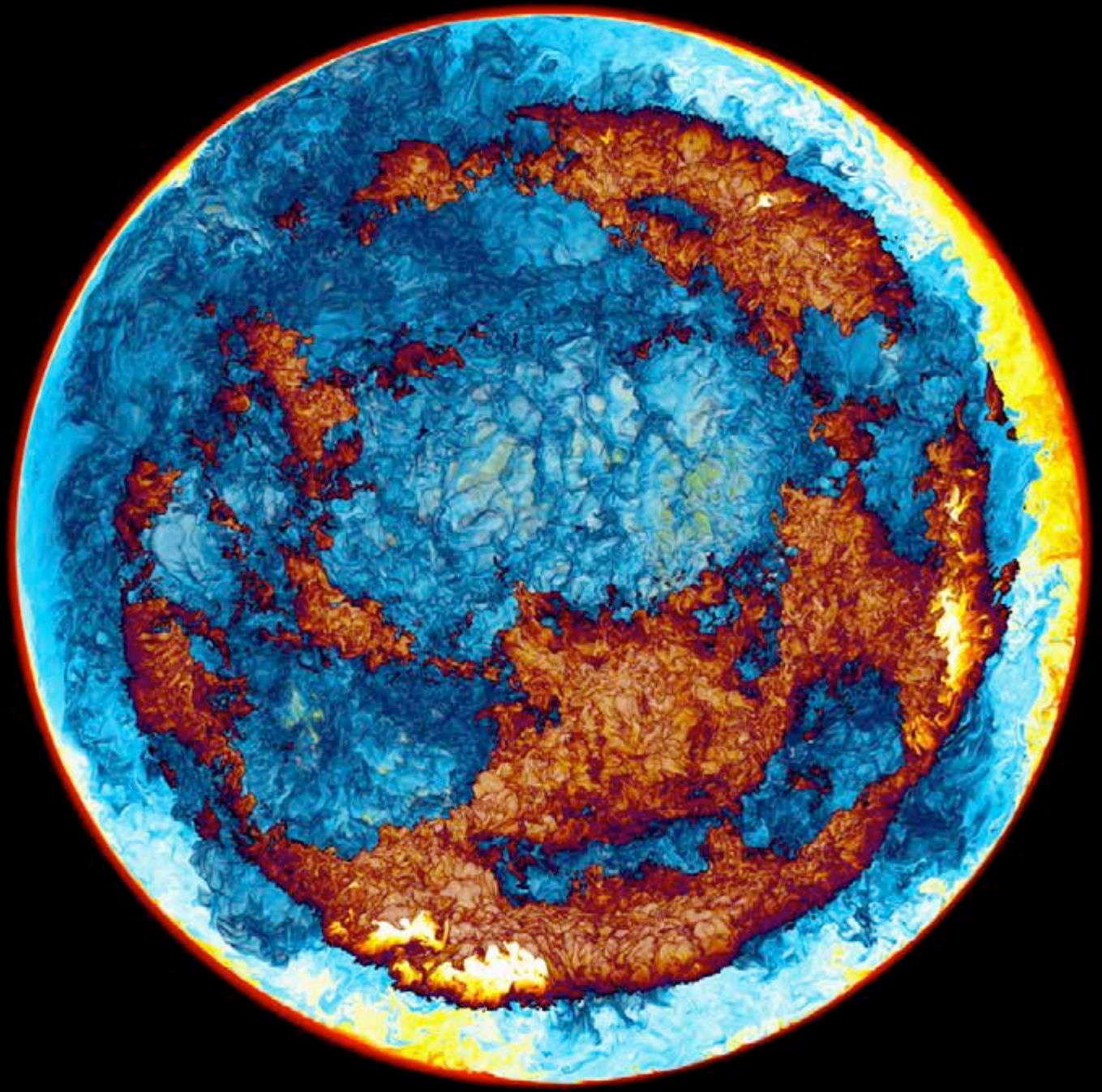

*Sakurai's Object H-ingestion simulation on Blue Waters machine in Jan., 2014, on a grid of $1536^3$ cells.*

The regions of most powerful energy release are moving outward as a wave from the earlier site at the bottom right.

*t = 1162 min.*

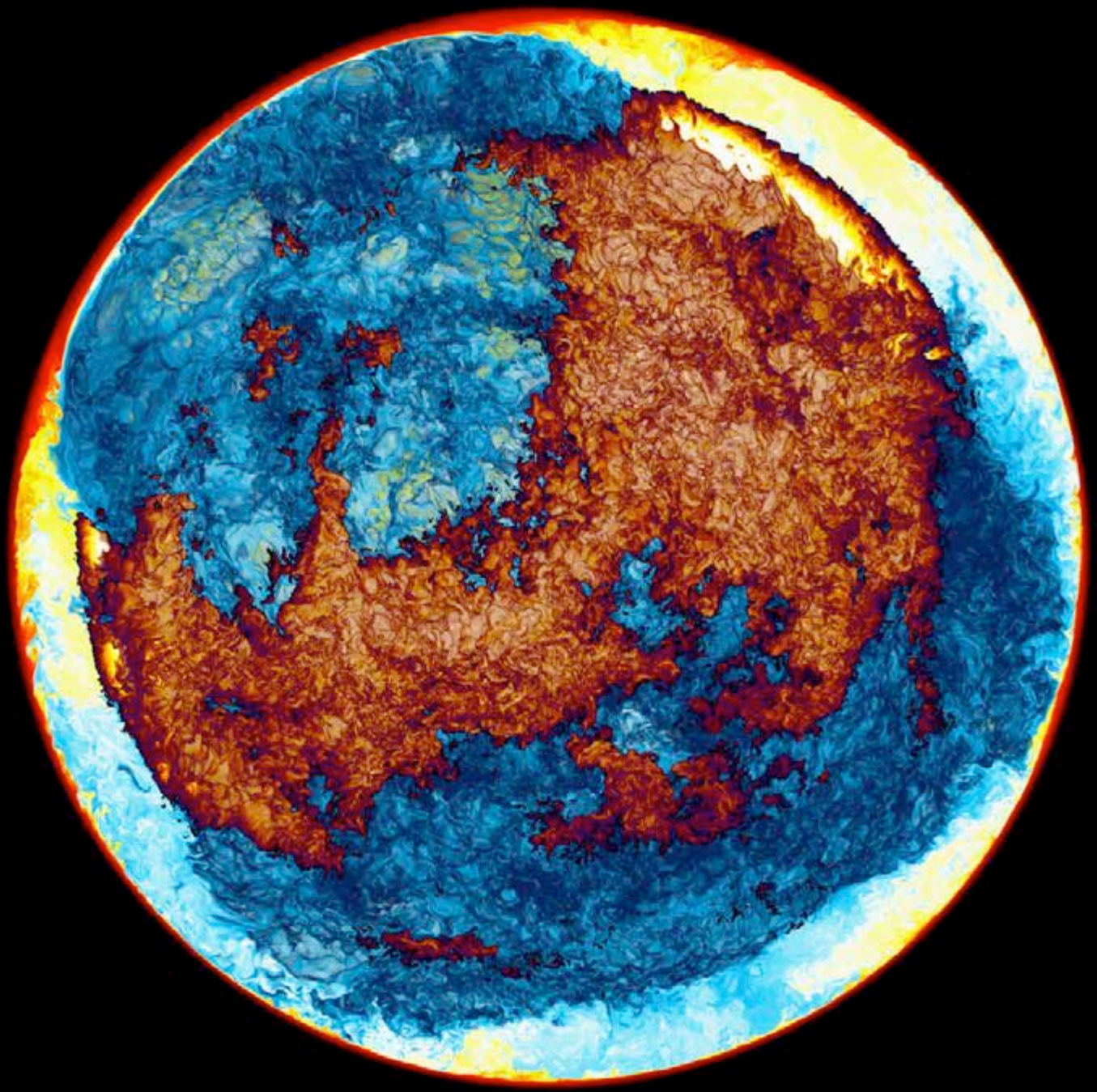

*Sakurai's Object H-ingestion simulation on Blue Waters machine in Jan., 2014, on a grid of $1536^3$ cells.*

As the front where hydrogen burns most rapidly advances, it drives ahead of it a ring of violent hydrogen ingestion, visible here in cross section. The averaged entrainment rate has jumped up from its early level by about 2 orders of magnitude.

*t = 1175 min.*

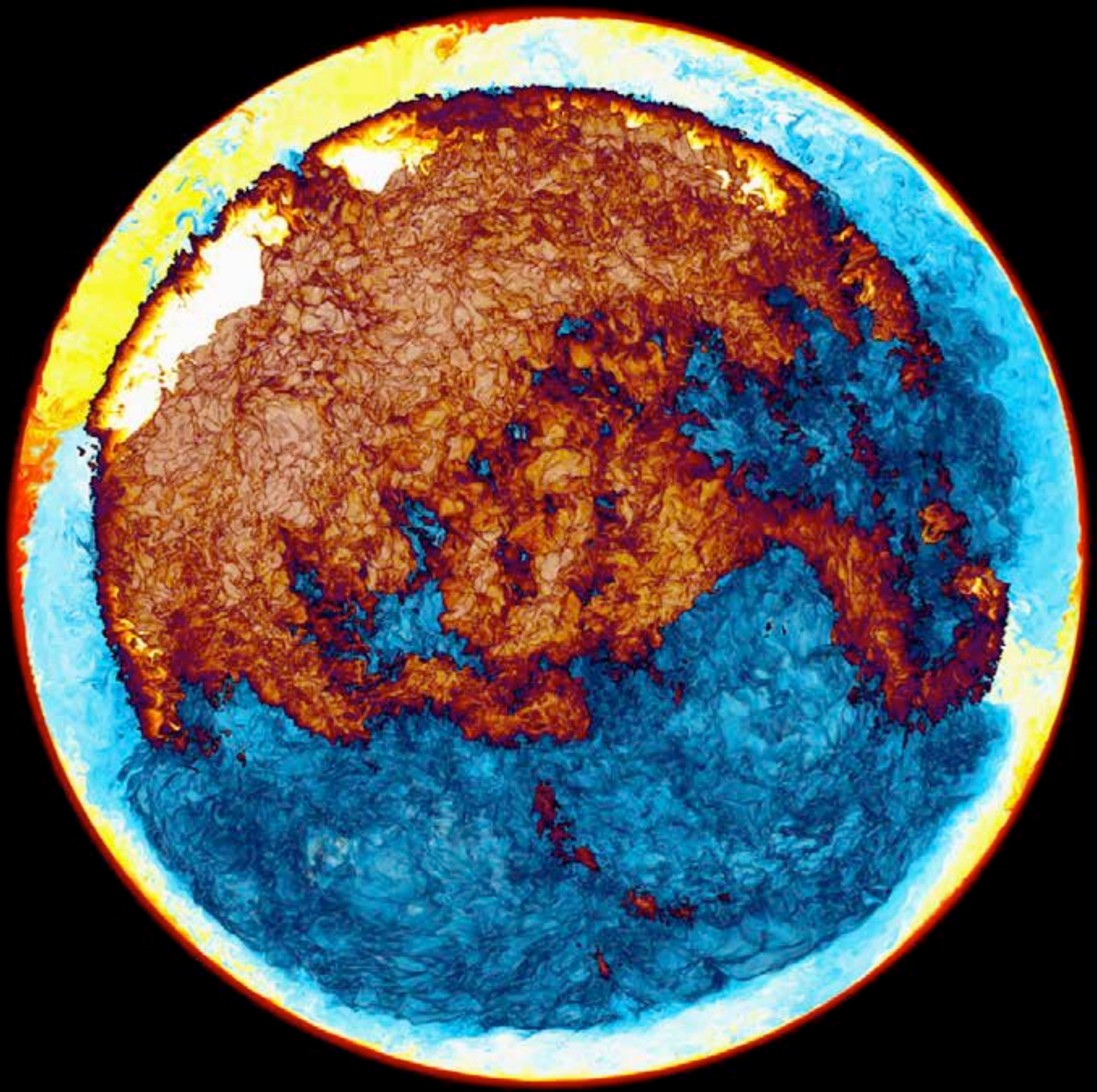

*Sakurai's Object H-ingestion simulation on Blue Waters machine in Jan., 2014, on a grid of $1536^3$ cells.*

The burning front has now reached the antipode, where violent, localized energy release drives the oscillation back to its original site.

*t = 1188 min.*

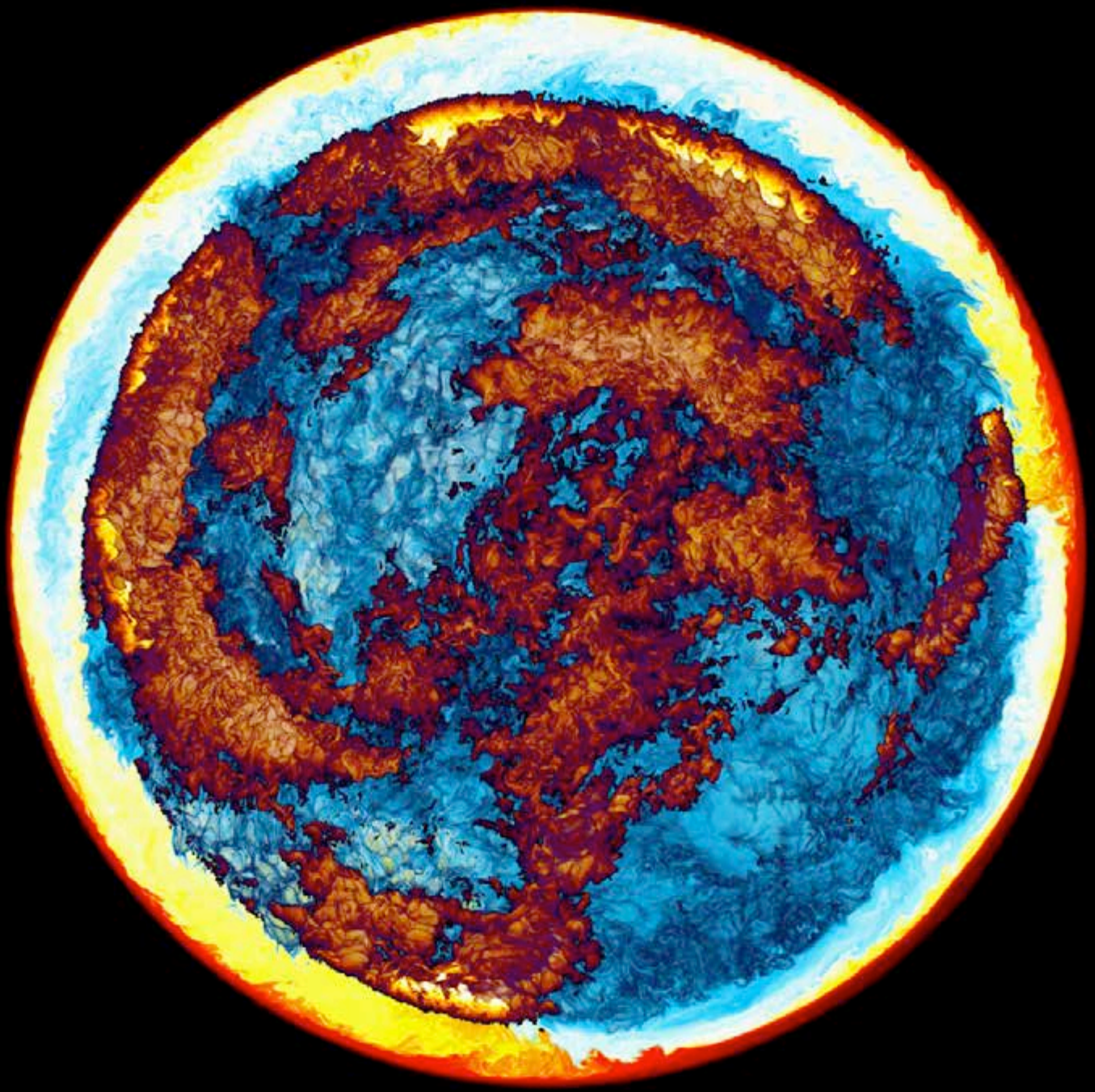

*Sakurai's Object H-ingestion simulation on Blue Waters machine in Jan., 2014, on a grid of $1536^3$ cells.*

The GOSH is indeed global. This flow has a 1-D average, but it is by no means a 1-D phenomenon. Blue Waters makes it possible to see the GOSH in its full 3-D complexity.

*t = 1200 min.*

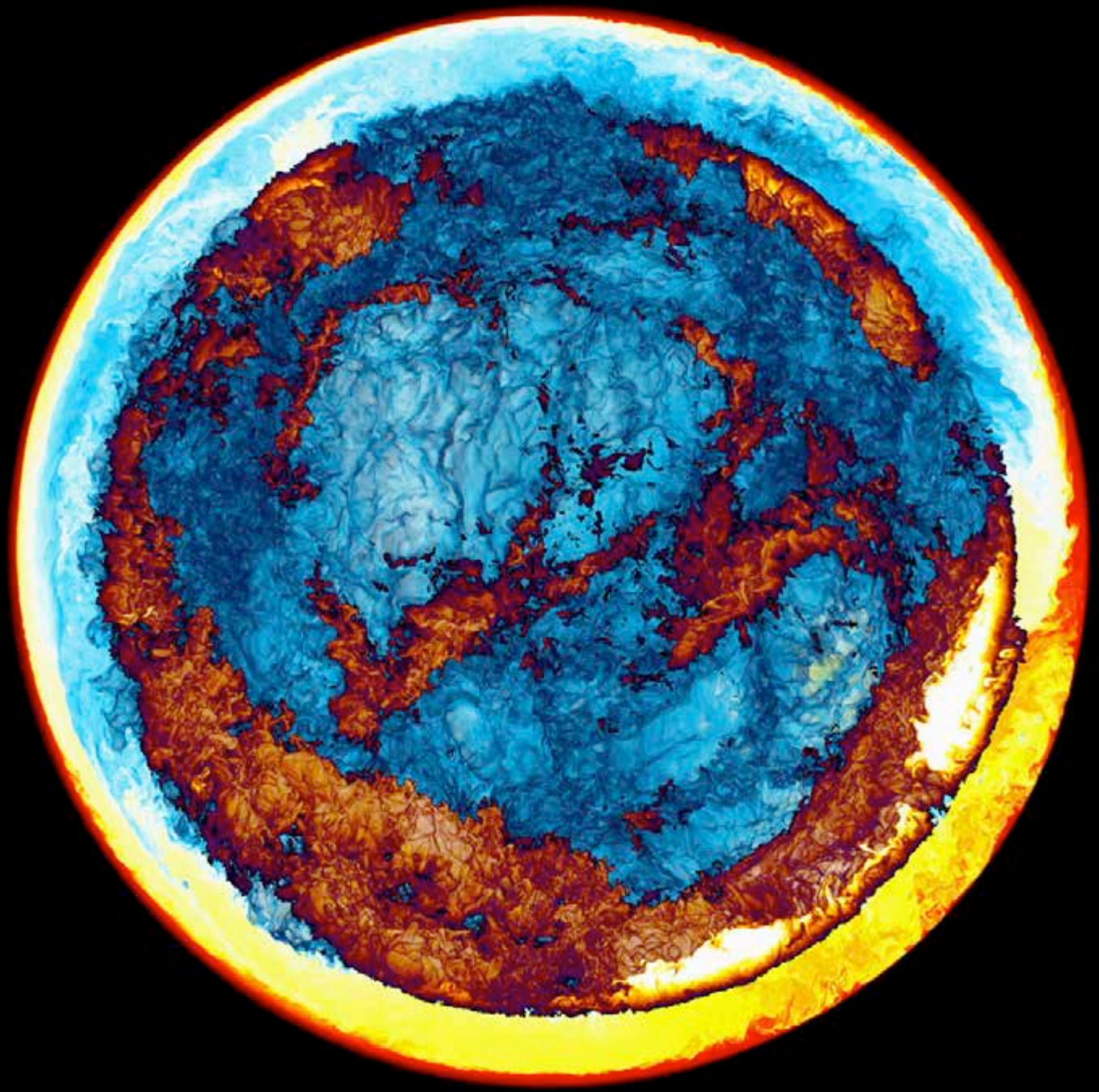

*Sakurai's Object H-ingestion simulation on Blue Waters machine in Jan., 2014, on a grid of $1536^3$ cells.*

Once the GOSH quiets down, after about a day in the life of this star, we can be well justified in carrying our description of the star forward with a 1-D stellar evolution code, suitably modified.

*t = 1212 min.*

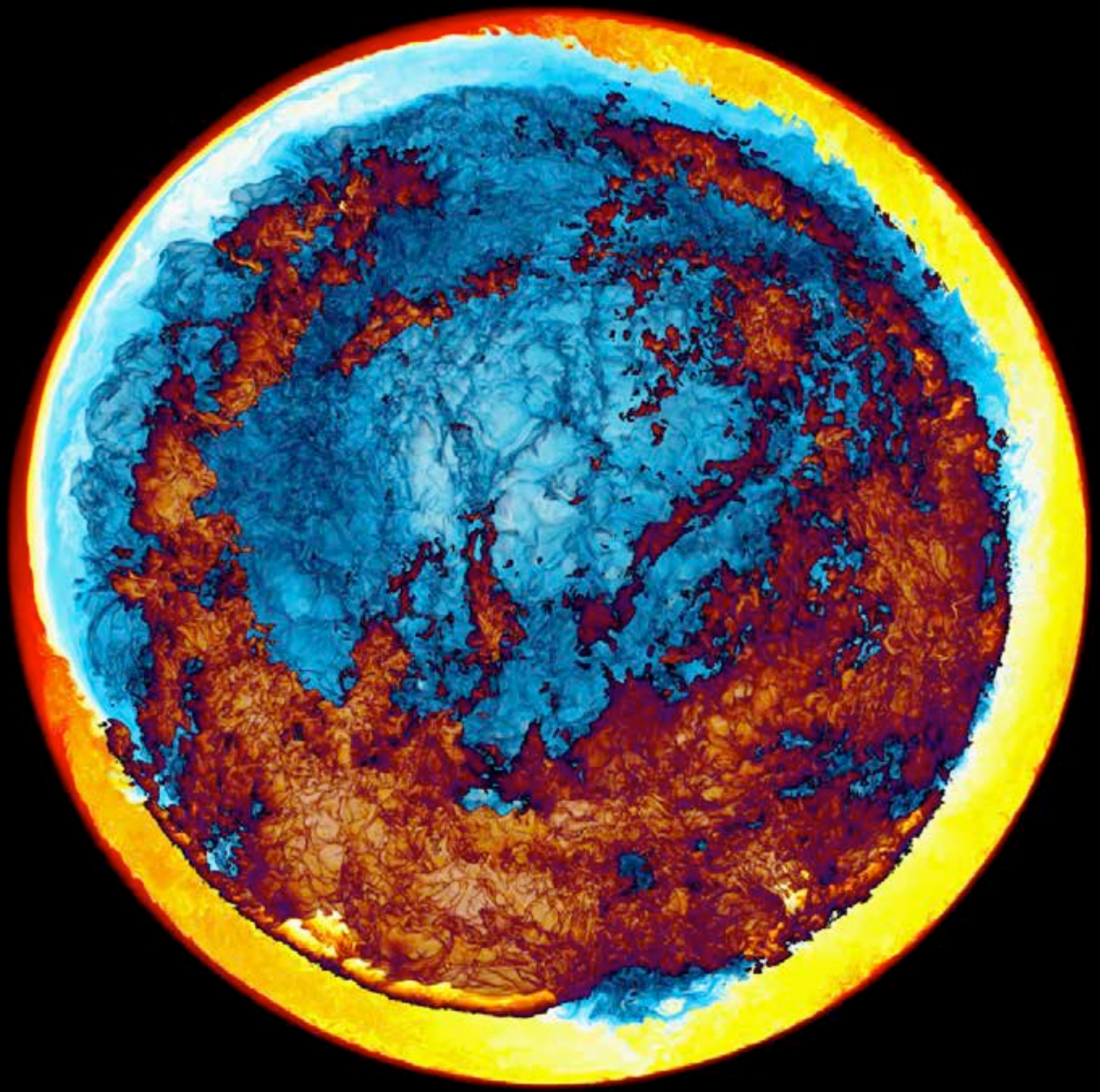

*Sakurai's Object H-ingestion simulation on Blue Waters machine in Jan., 2014, on a grid of $1536^3$ cells.*

*We see a hemisphere and make only mixtures of entrained hydrogen-rich gas with gas of the helium shell flash convection zone visible. The energy release rate from burning ingested H is shown in very dark blue, yellow, and white.*

*t = 1225 min.*

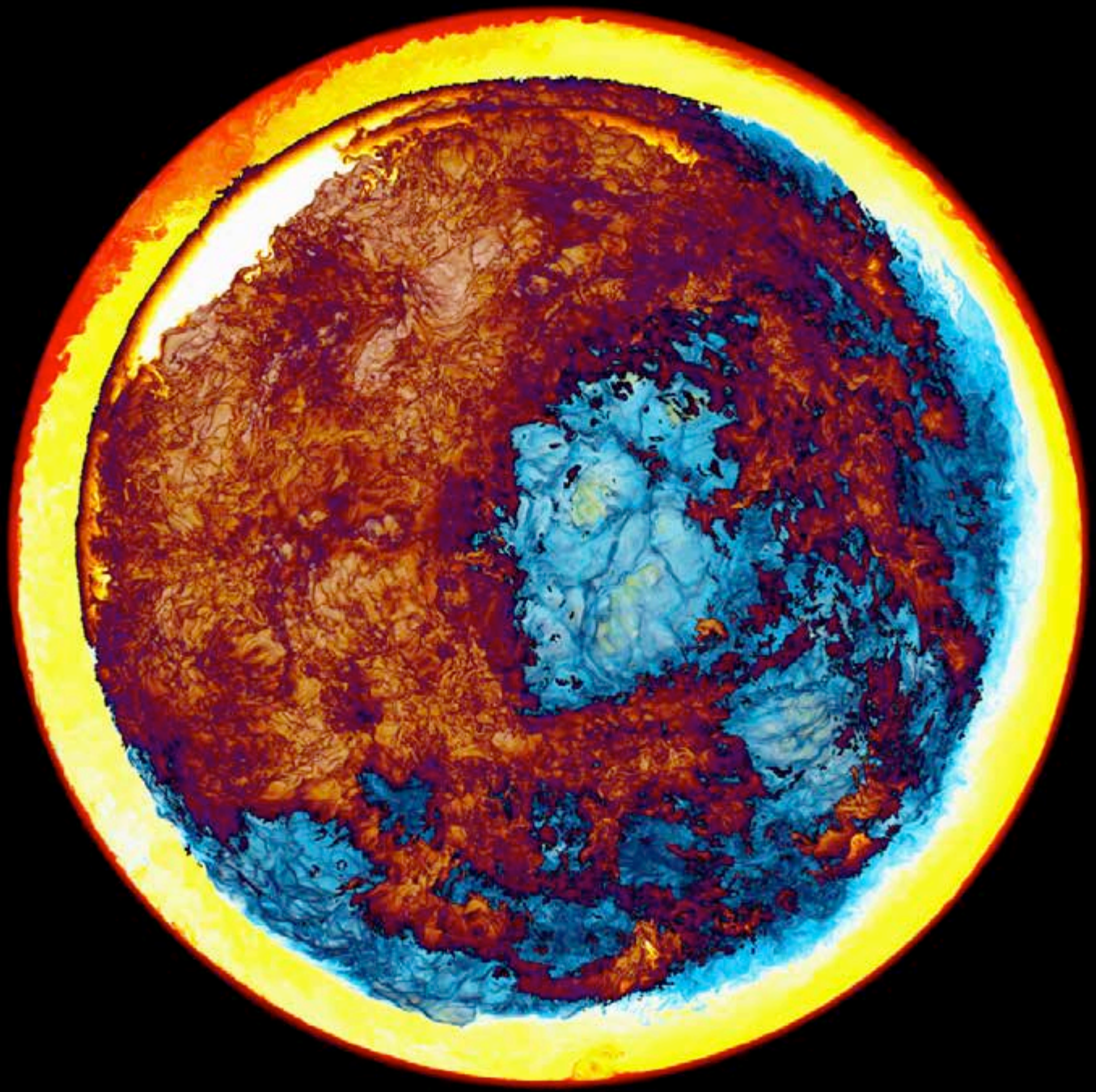

*Sakurai's Object H-ingestion simulation on Blue Waters machine in Jan., 2014, on a grid of $1536^3$ cells.*

*We see a hemisphere and make only mixtures of entrained hydrogen-rich gas with gas of the helium shell flash convection zone visible. The energy release rate from burning ingested H is shown in very dark blue, yellow, and white.*

*t = 1238 min.*

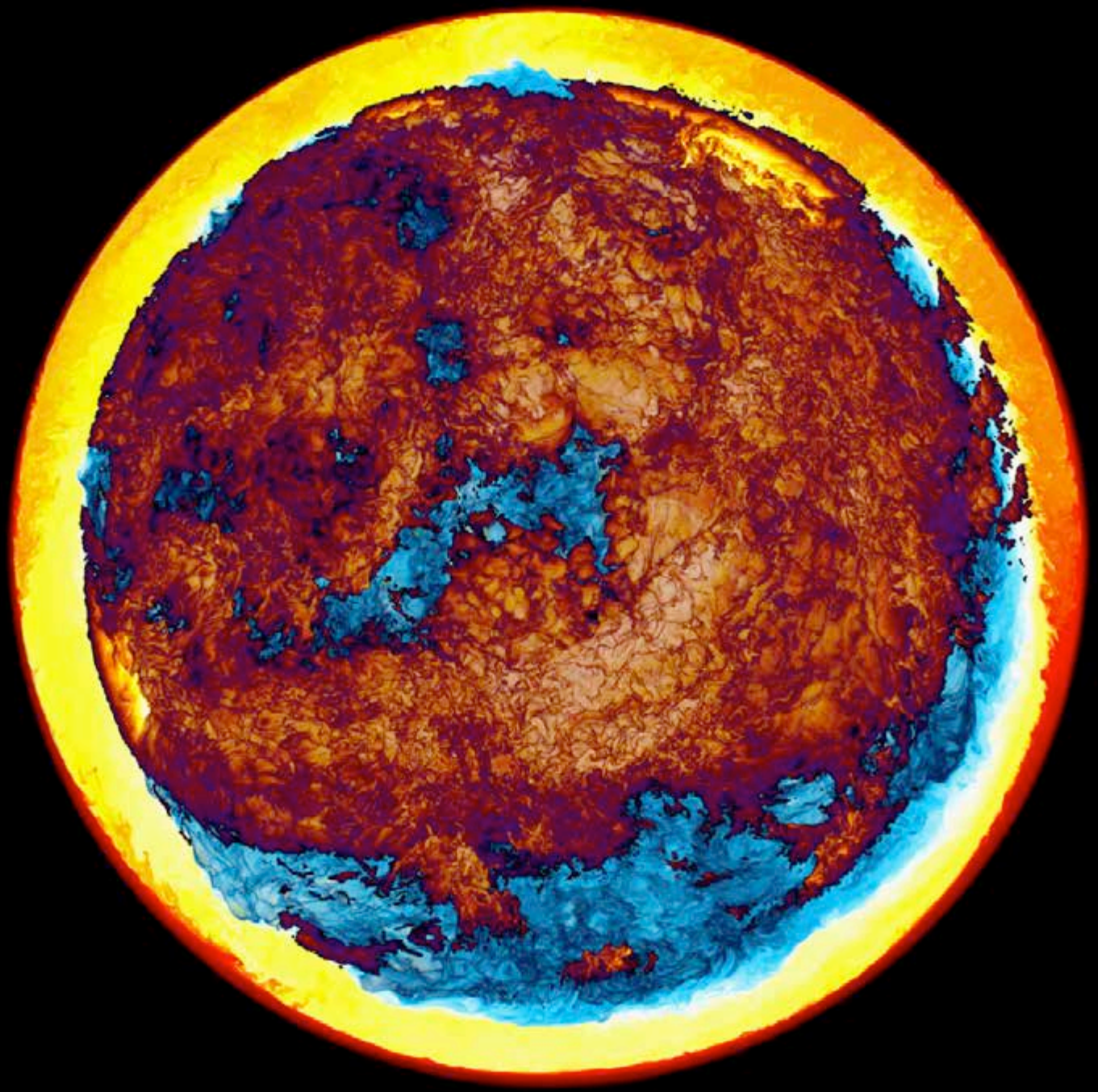

*Sakurai's Object H-ingestion simulation on Blue Waters machine in Jan., 2014, on a grid of $1536^3$ cells.*

*We see a hemisphere and make only mixtures of entrained hydrogen-rich gas with gas of the helium shell flash convection zone visible. The energy release rate from burning ingested H is shown in very dark blue, yellow, and white.*

*t = 1250 min.*

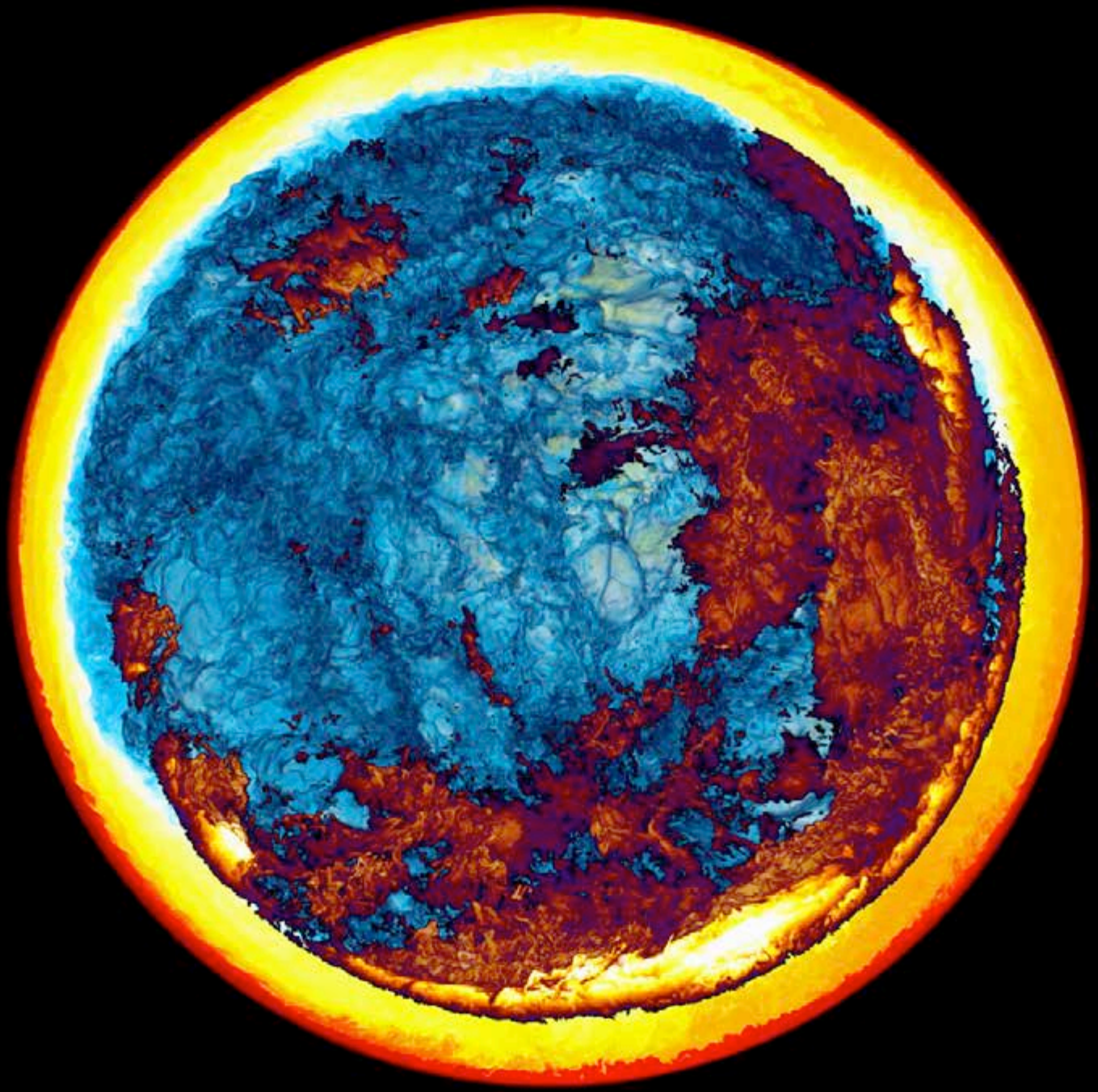

*Sakurai's Object H-ingestion simulation on Blue Waters machine in Jan., 2014, on a grid of $1536^3$ cells.*

*We see a hemisphere and make only mixtures of entrained hydrogen-rich gas with gas of the helium shell flash convection zone visible. The energy release rate from burning ingested H is shown in very dark blue, yellow, and white.*

*t = 1262 min.*

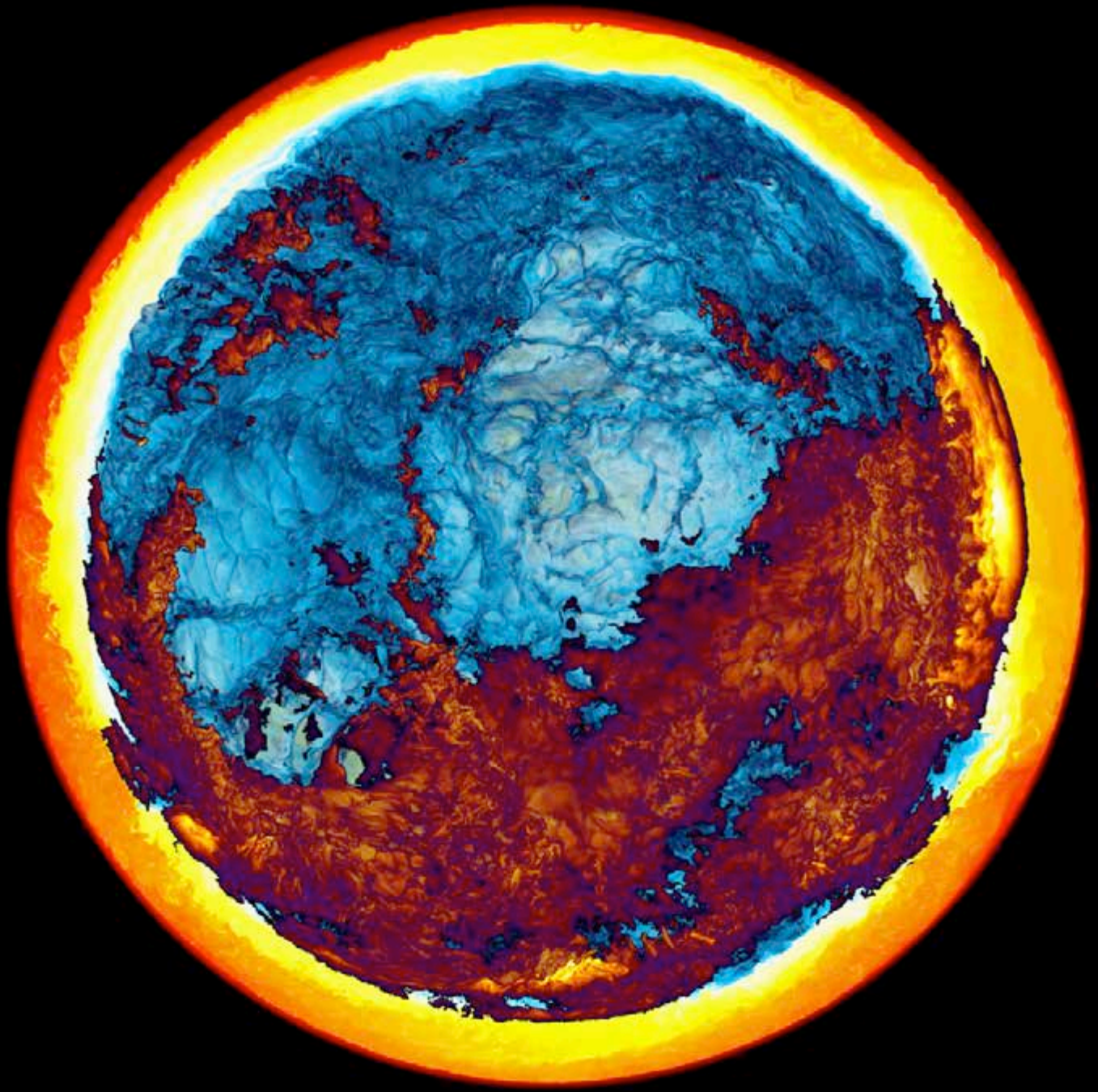

*Sakurai's Object H-ingestion simulation on Blue Waters machine in Jan., 2014, on a grid of $1536^3$ cells.*

*We see a hemisphere and make only mixtures of entrained hydrogen-rich gas with gas of the helium shell flash convection zone visible. The energy release rate from burning ingested H is shown in very dark blue, yellow, and white.*

*t = 1275 min.*

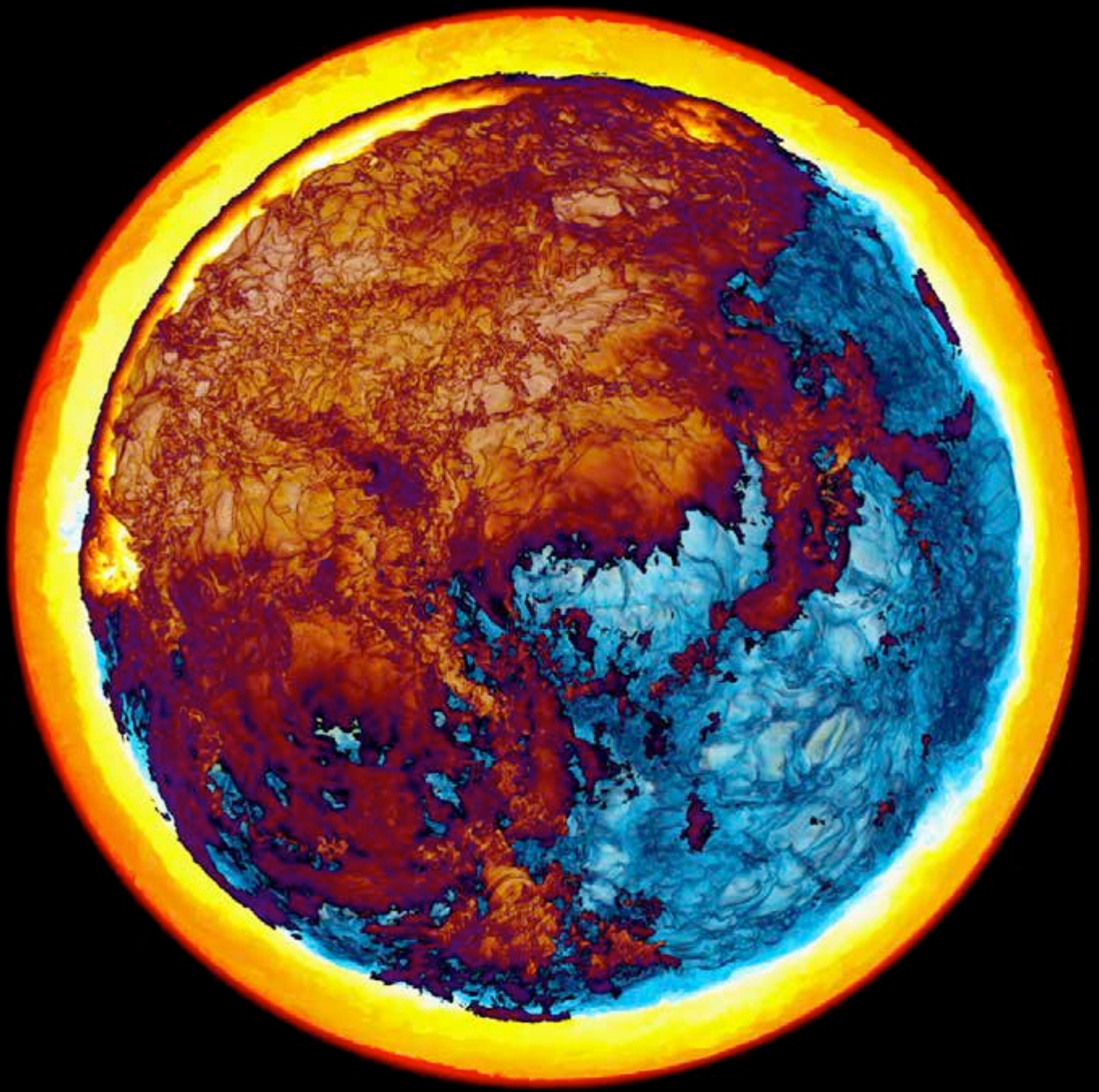

*Sakurai's Object H-ingestion simulation on Blue Waters machine in Jan., 2014, on a grid of $1536^3$ cells.*

The GOSH has resulted in greatly enhanced hydrogen entrainment. The much greater H concentration near the original top of the convection zone now cannot be overlooked.

*t = 1288 min.*

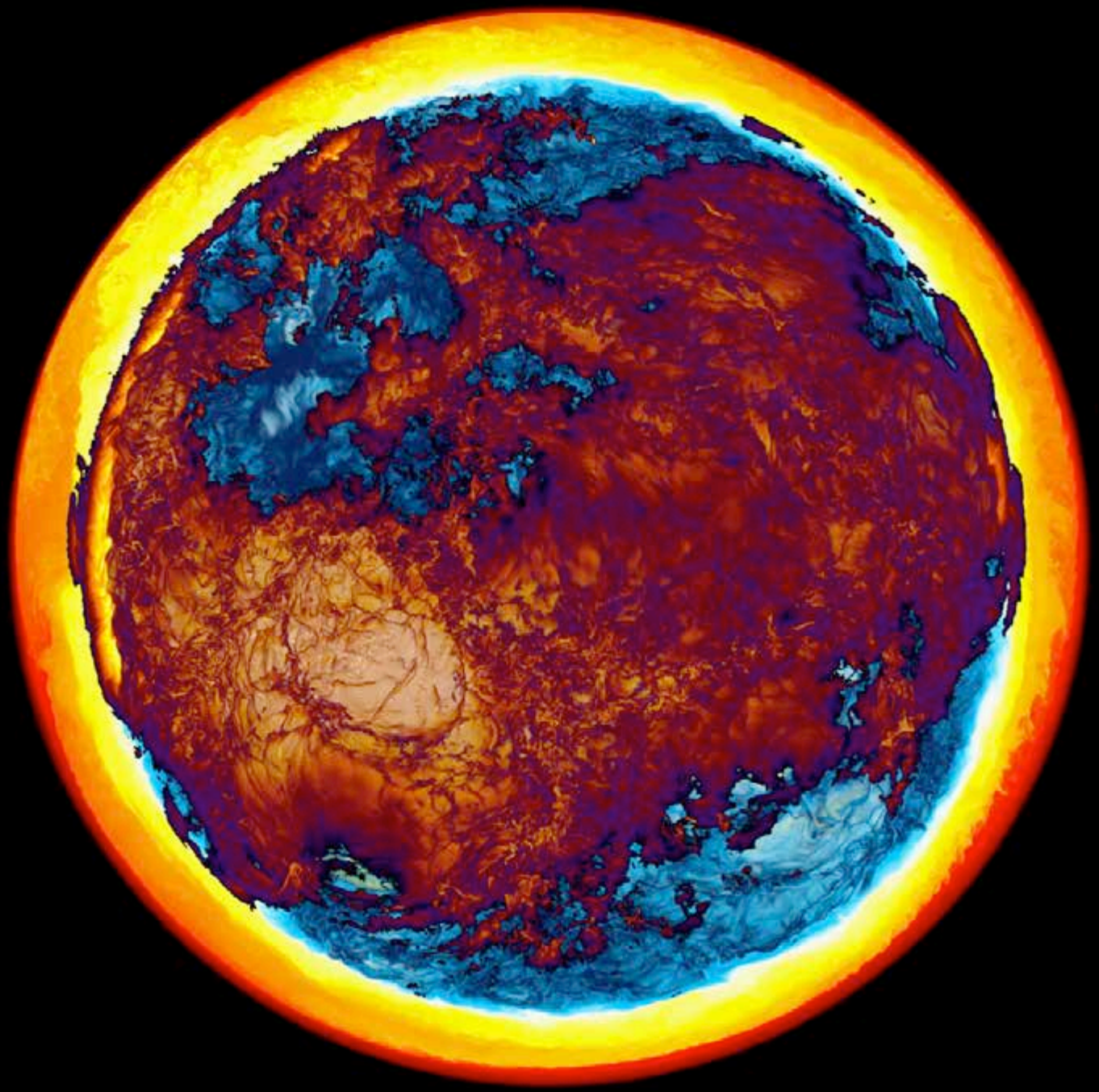

*Sakurai's Object H-ingestion simulation on Blue Waters machine in Jan., 2014, on a grid of $1536^3$ cells.*

Ultimately, we expect a new convection zone to form, driven by burning of H at the base of the shell of ingested H that we see in this image. We do see this in lower resolution runs, but have yet to complete this one.

*t = 1300 min.*

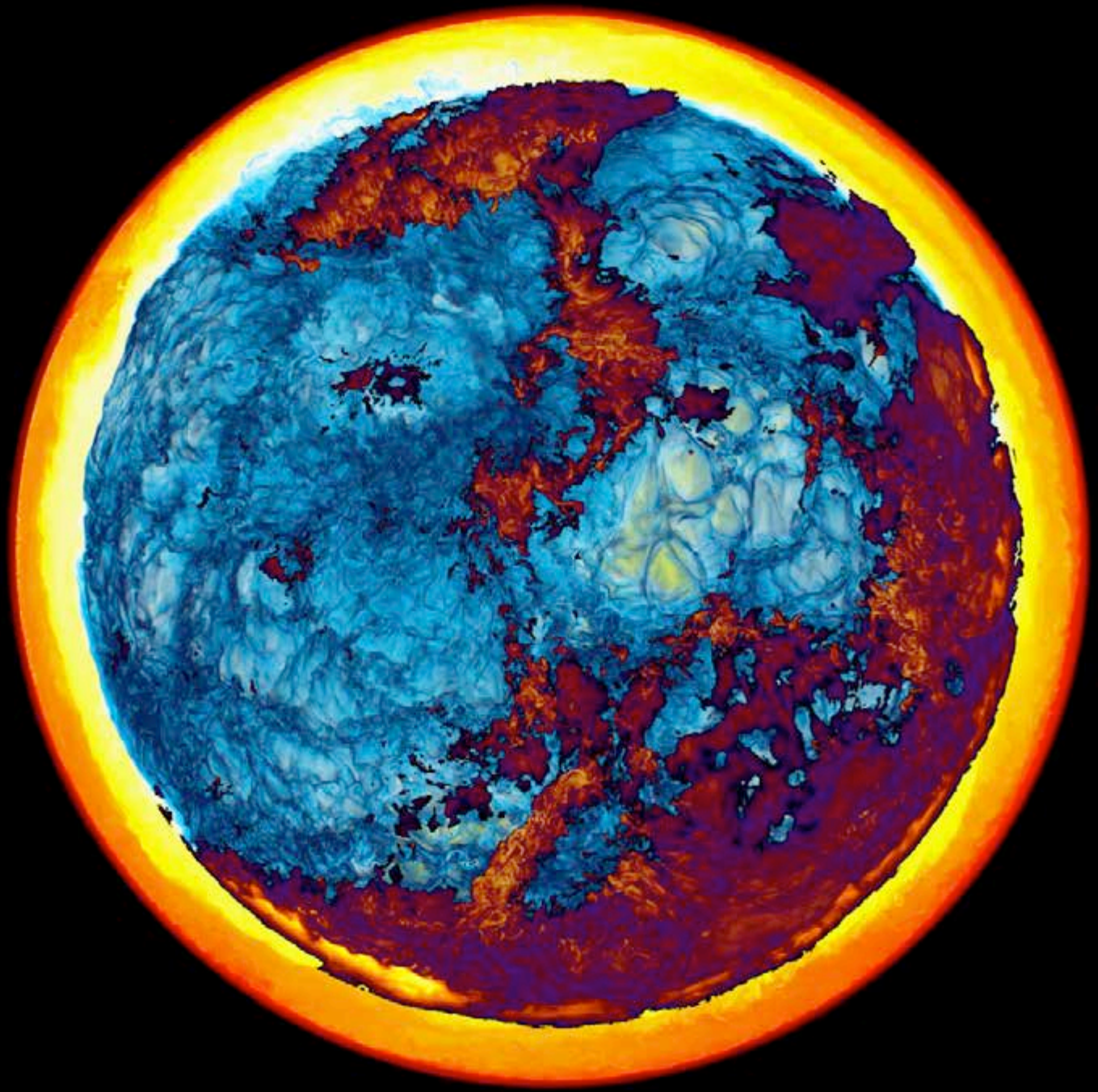

*Sakurai's Object H-ingestion simulation on Blue Waters machine in Jan., 2014, on a grid of $1536^3$ cells.*

*We see a hemisphere and make only mixtures of entrained hydrogen-rich gas with gas of the helium shell flash convection zone visible. The energy release rate from burning ingested H is shown in very dark blue, yellow, and white.*

*t = 1312 min.*

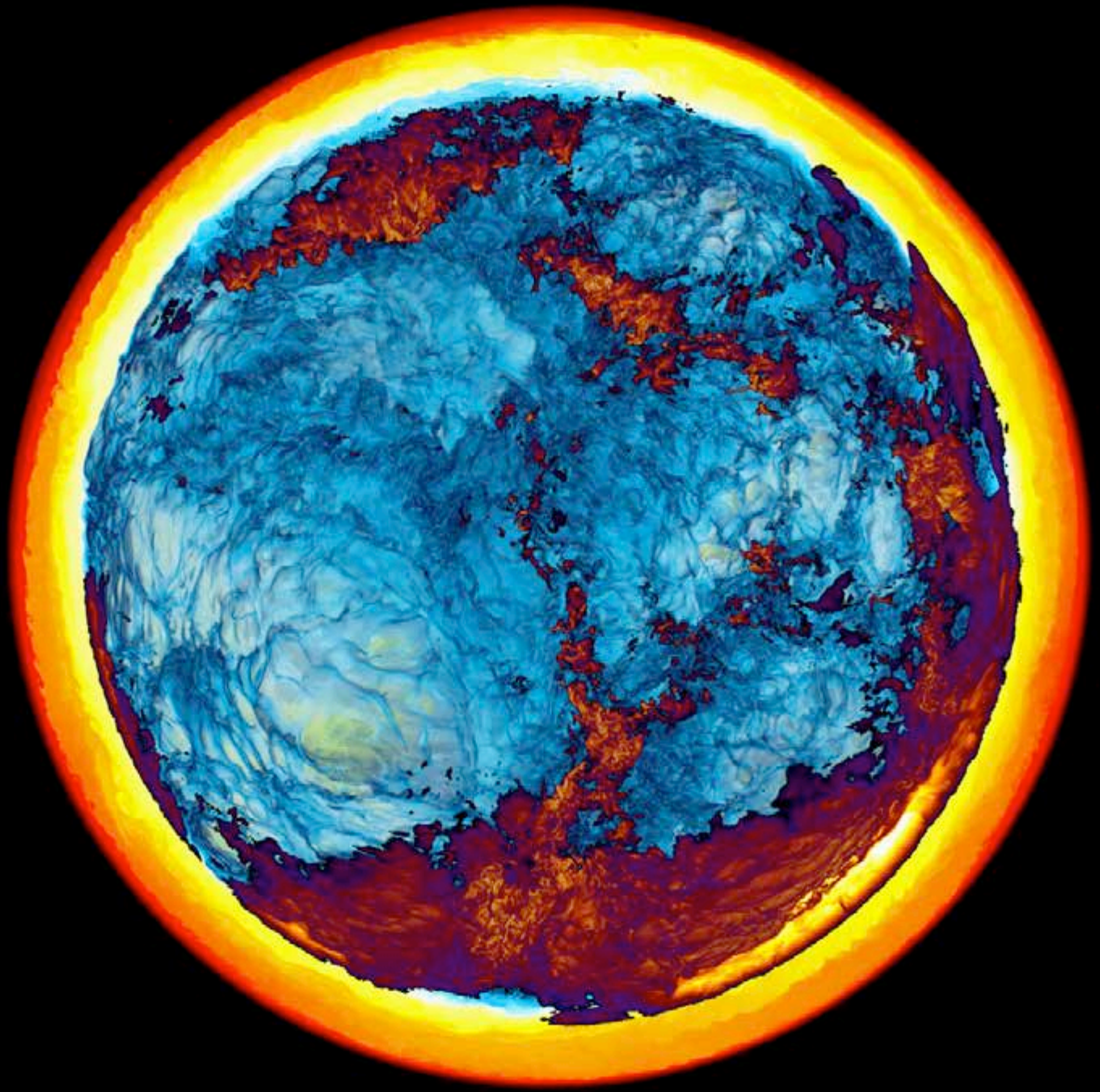

*Sakurai's Object H-ingestion simulation on Blue Waters machine in Jan., 2014, on a grid of $1536^3$ cells.*

*We see a hemisphere and make only mixtures of entrained hydrogen-rich gas with gas of the helium shell flash convection zone visible. The energy release rate from burning ingested H is shown in very dark blue, yellow, and white.*

*t = 1325 min.*

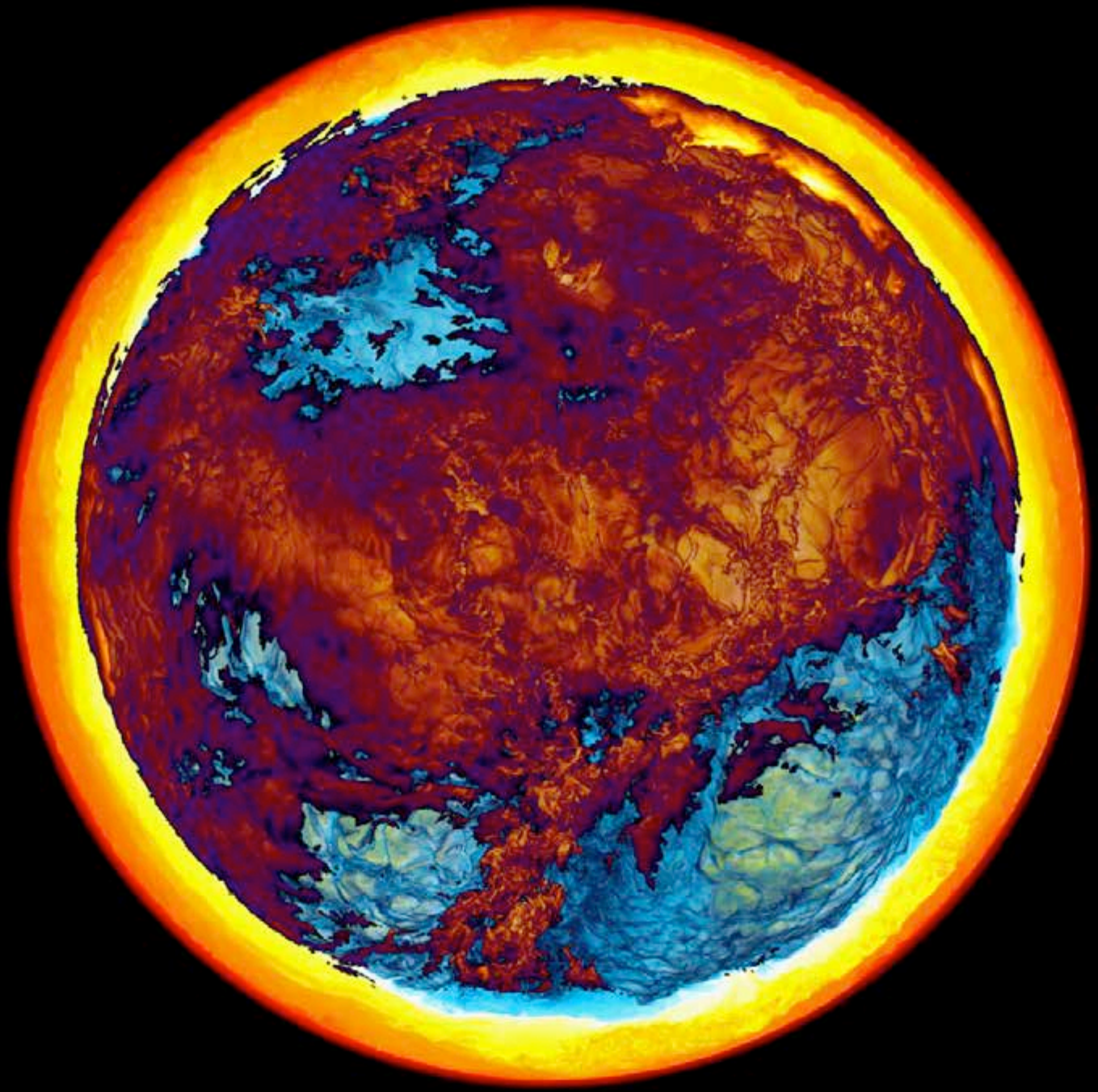

*Sakurai's Object H-ingestion simulation on Blue Waters machine in Jan., 2014, on a grid of $1536^3$ cells.*

*We see a hemisphere and make only mixtures of entrained hydrogen-rich gas with gas of the helium shell flash convection zone visible. The energy release rate from burning ingested H is shown in very dark blue, yellow, and white.*

*t = 1338 min.*

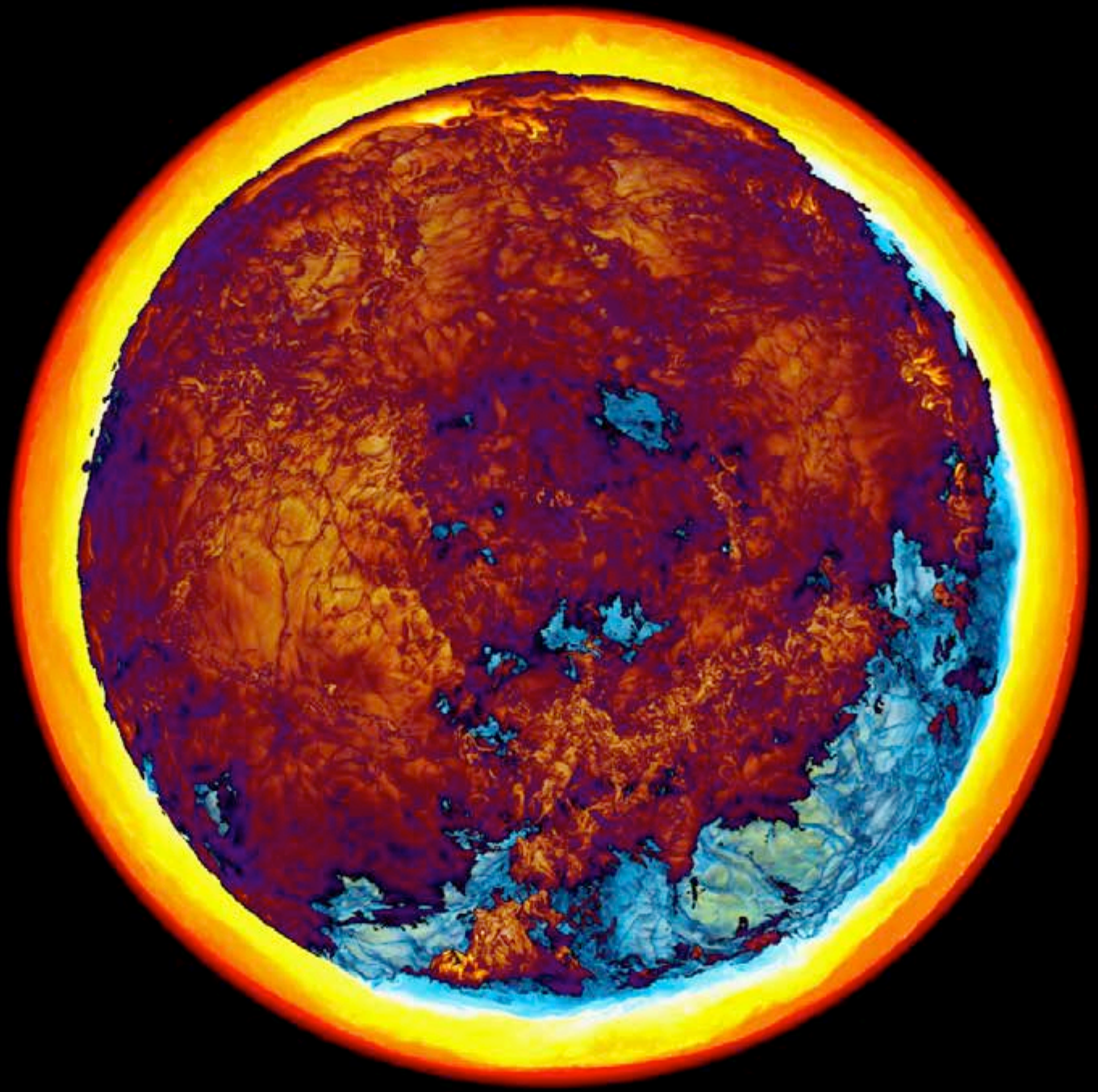

*Sakurai's Object H-ingestion simulation on Blue Waters machine in Jan., 2014, on a grid of $1536^3$ cells.*

*We see a hemisphere and make only mixtures of entrained hydrogen-rich gas with gas of the helium shell flash convection zone visible. The energy release rate from burning ingested H is shown in very dark blue, yellow, and white.*

*t = 1350 min.*

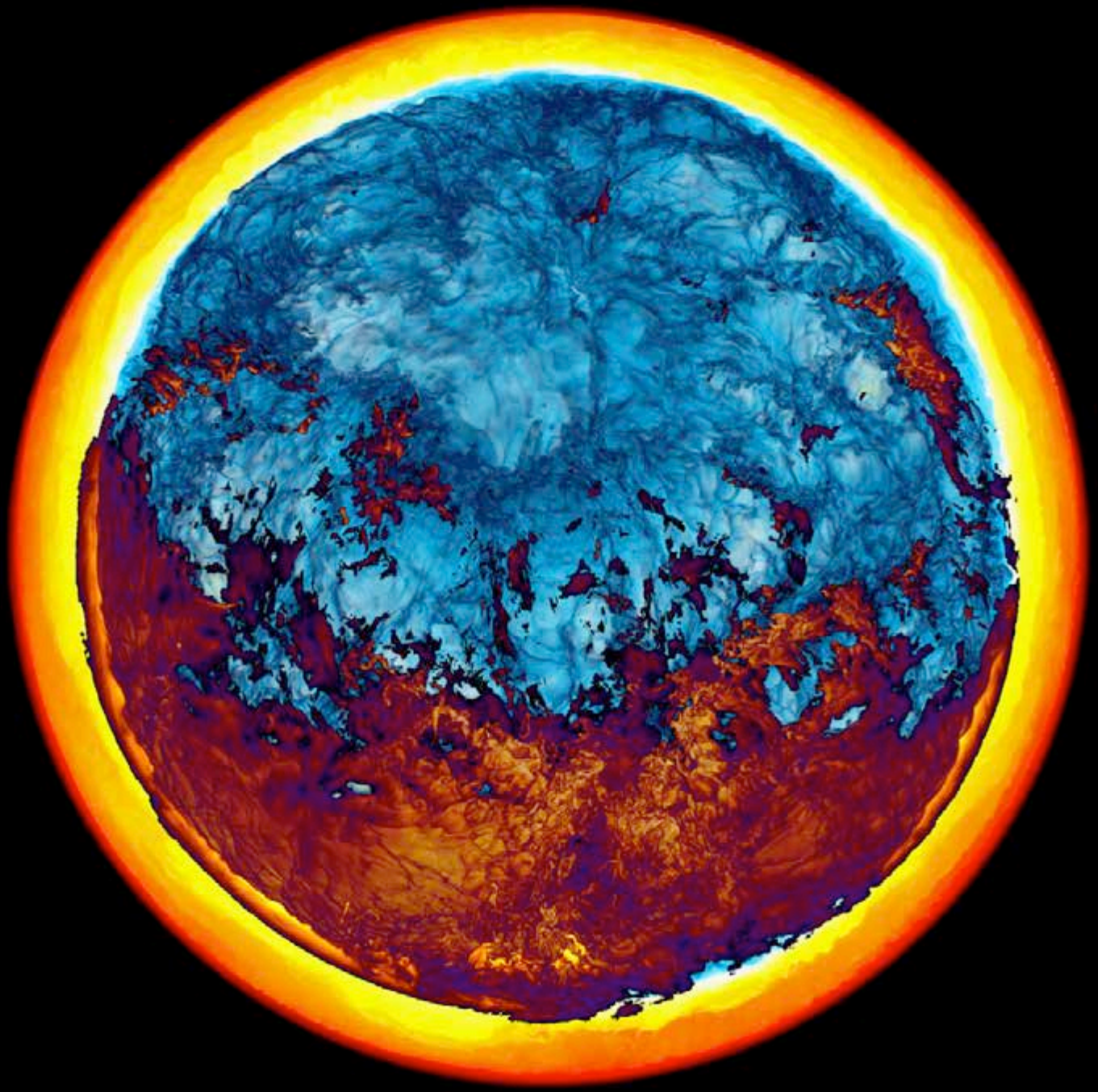

*Sakurai's Object H-ingestion simulation on Blue Waters machine in Jan., 2014, on a grid of $1536^3$ cells.*

*We see a hemisphere and make only mixtures of entrained hydrogen-rich gas with gas of the helium shell flash convection zone visible. The energy release rate from burning ingested H is shown in very dark blue, yellow, and white.*

*t = 1362 min.*

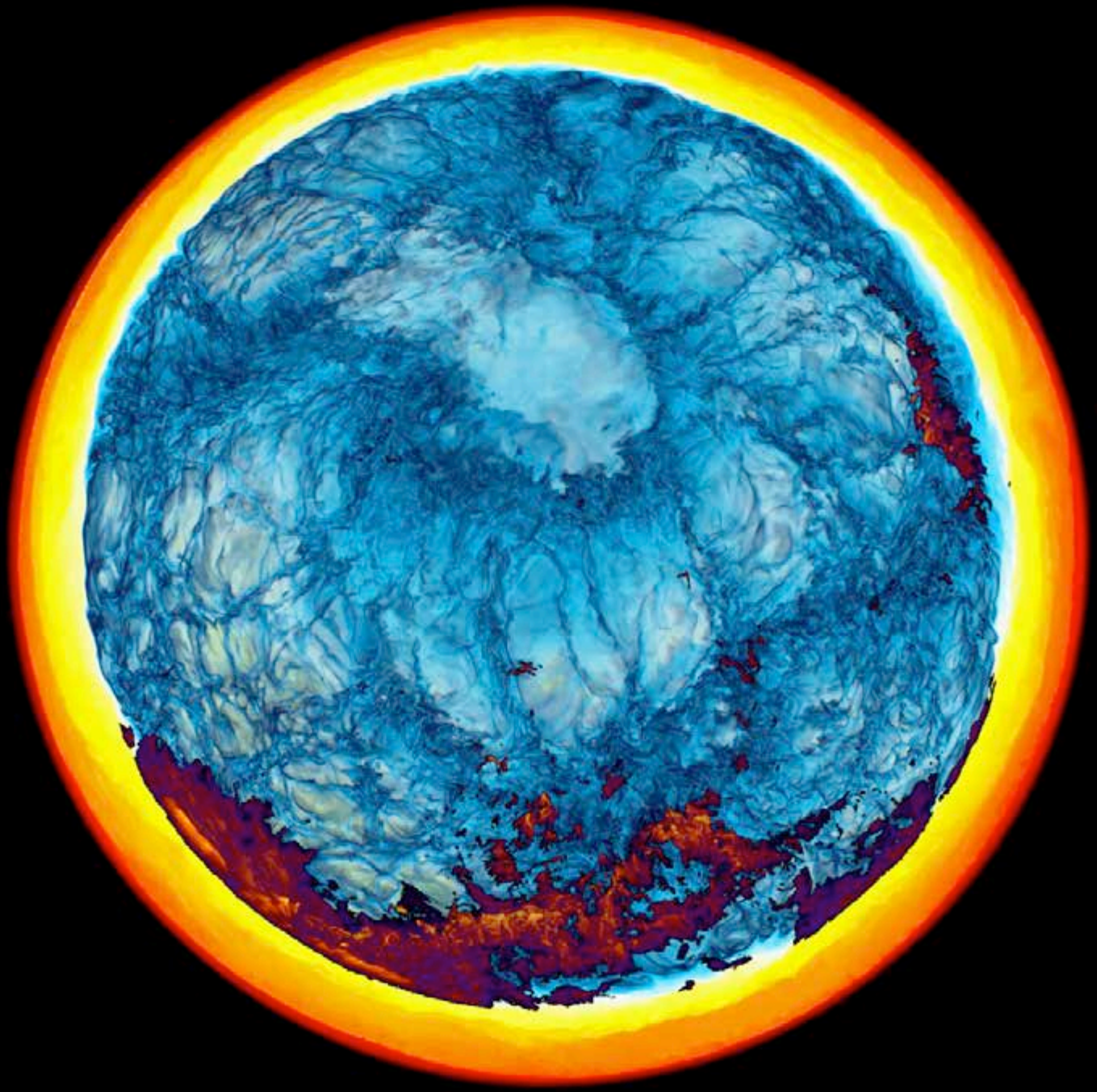

*Sakurai's Object H-ingestion simulation on Blue Waters machine in Jan., 2014, on a grid of $1536^3$ cells.*

*We see a hemisphere and make only mixtures of entrained hydrogen-rich gas with gas of the helium shell flash convection zone visible. The energy release rate from burning ingested H is shown in very dark blue, yellow, and white.*

*t = 1375 min.*

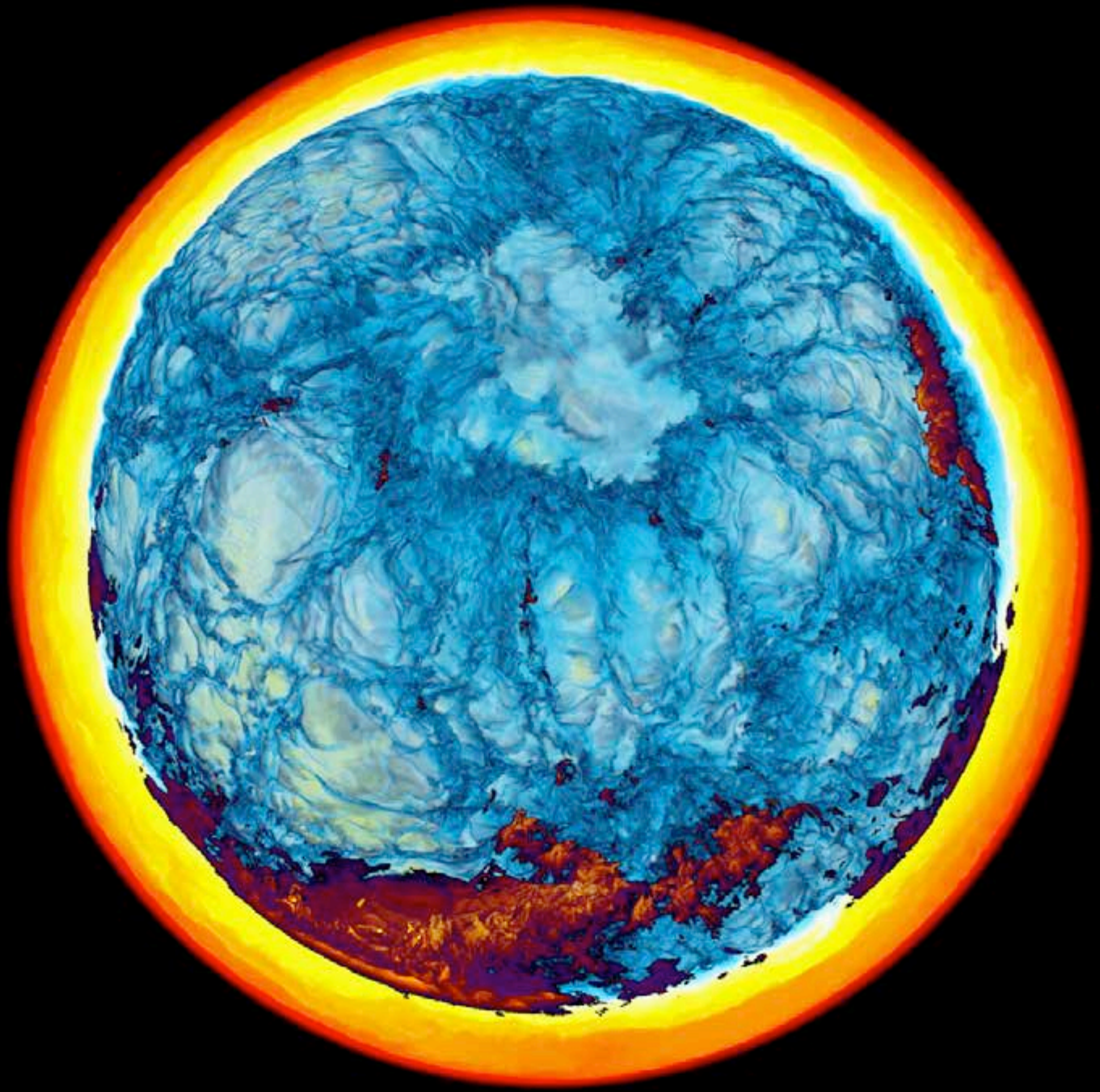

*Sakurai's Object H-ingestion simulation on Blue Waters machine in Jan., 2014, on a grid of $1536^3$ cells.*

*We see a hemisphere and make only mixtures of entrained hydrogen-rich gas with gas of the helium shell flash convection zone visible. The energy release rate from burning ingested H is shown in very dark blue, yellow, and white.*

*t = 1388 min.*

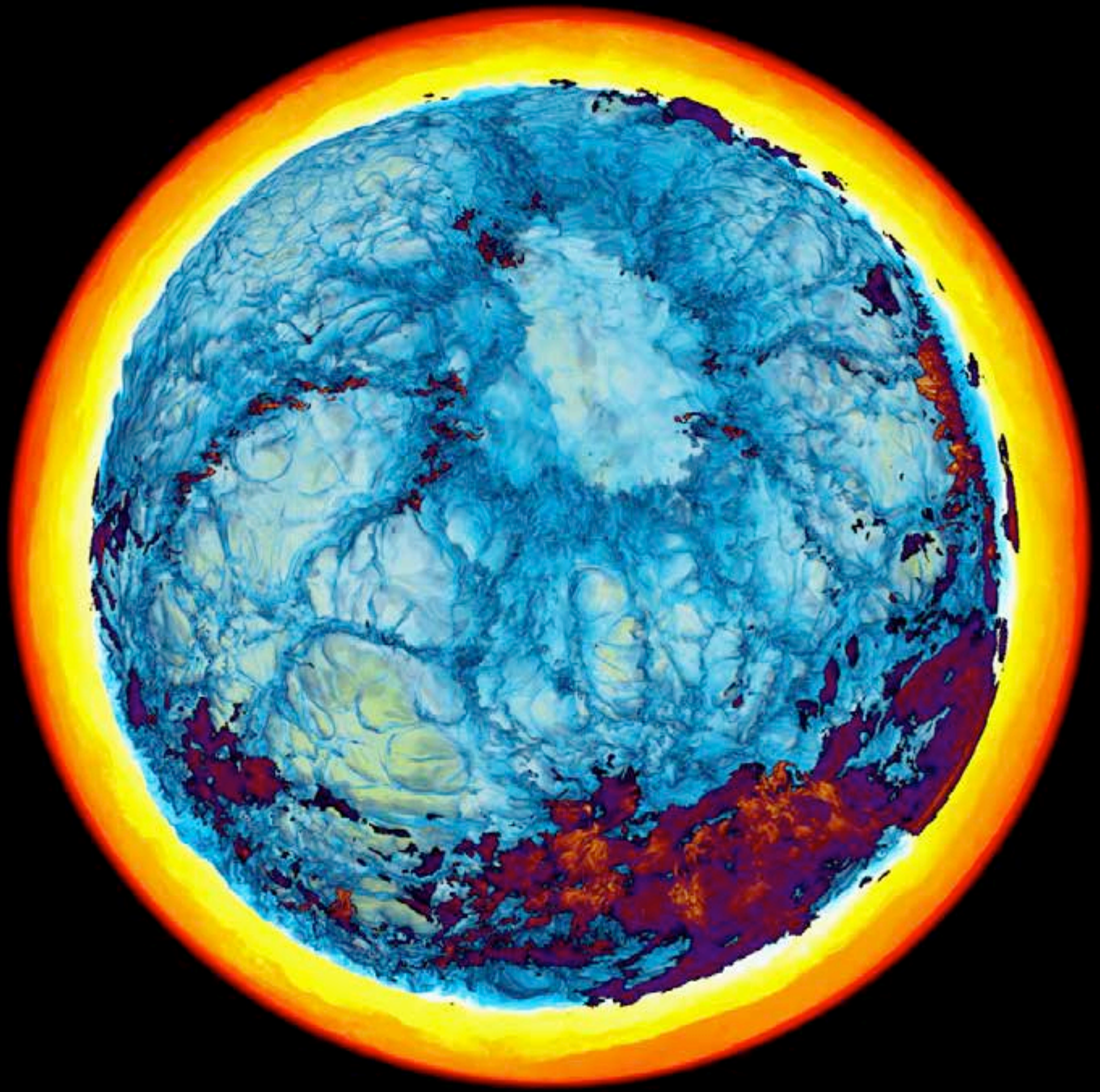

*Sakurai's Object H-ingestion simulation on Blue Waters machine in Jan., 2014, on a grid of $1536^3$ cells.*

*We see a hemisphere and make only mixtures of entrained hydrogen-rich gas with gas of the helium shell flash convection zone visible. The energy release rate from burning ingested H is shown in very dark blue, yellow, and white.*

*t = 1400 min.*

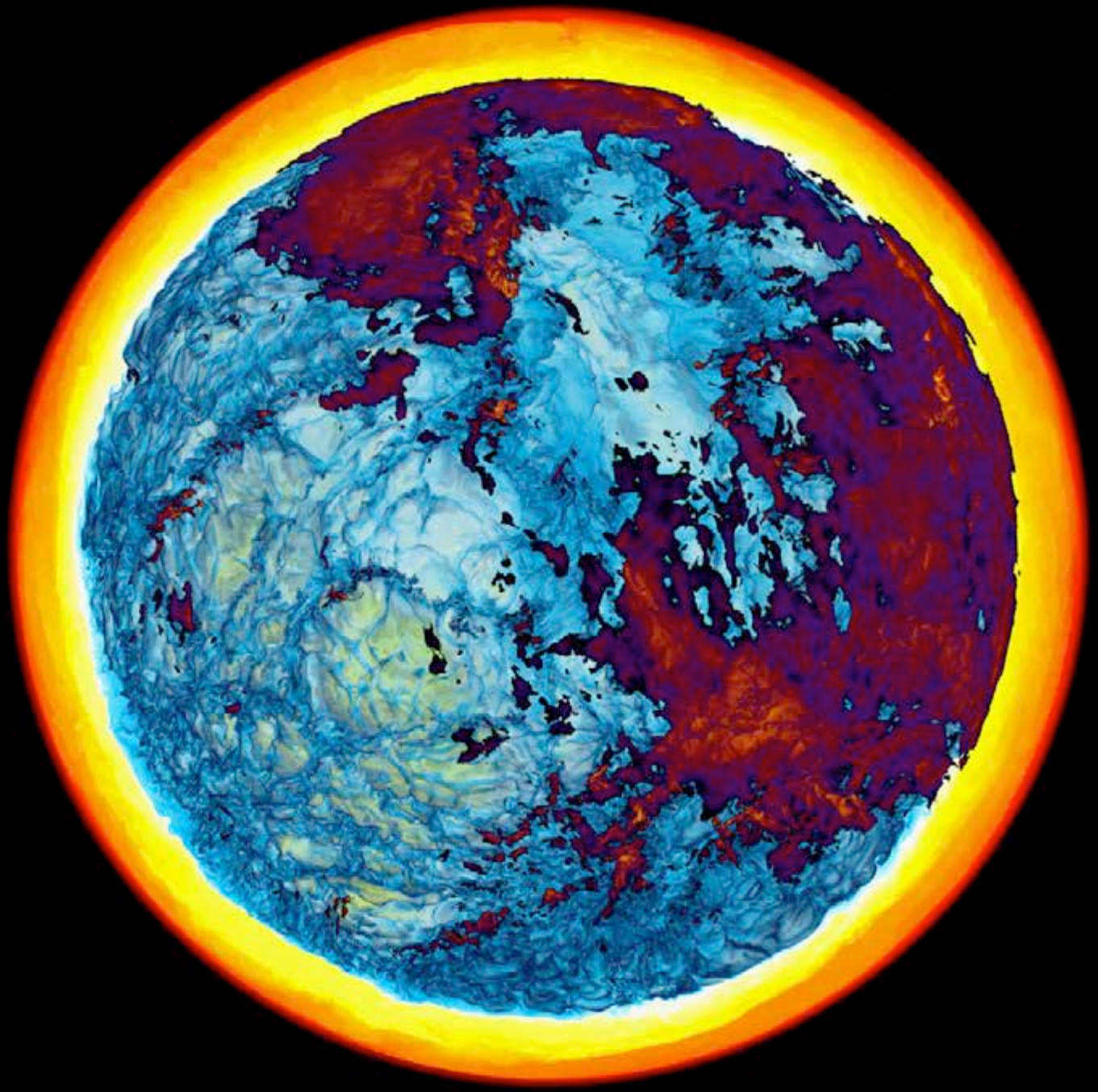

*Sakurai's Object H-ingestion simulation on Blue Waters machine in Jan., 2014, on a grid of $1536^3$ cells.*

*We see a hemisphere and make only mixtures of entrained hydrogen-rich gas with gas of the helium shell flash convection zone visible. The energy release rate from burning ingested H is shown in very dark blue, yellow, and white.*

*t = 1412 min.*

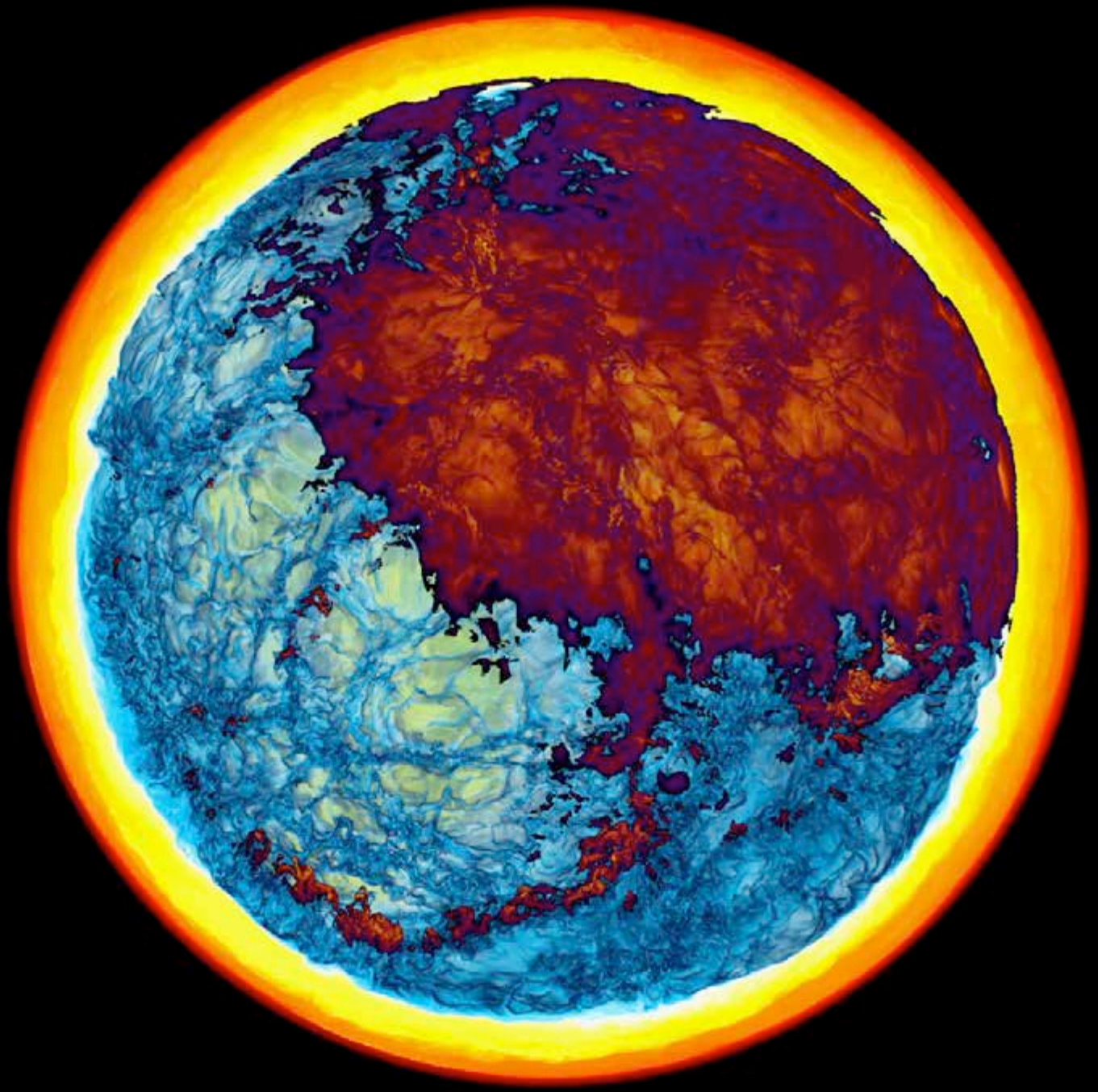

*Sakurai's Object H-ingestion simulation on Blue Waters machine in Jan., 2014, on a grid of $1536^3$ cells.*

*We see a hemisphere and make only mixtures of entrained hydrogen-rich gas with gas of the helium shell flash convection zone visible. The energy release rate from burning ingested H is shown in very dark blue, yellow, and white.*

*t = 1425 min.*

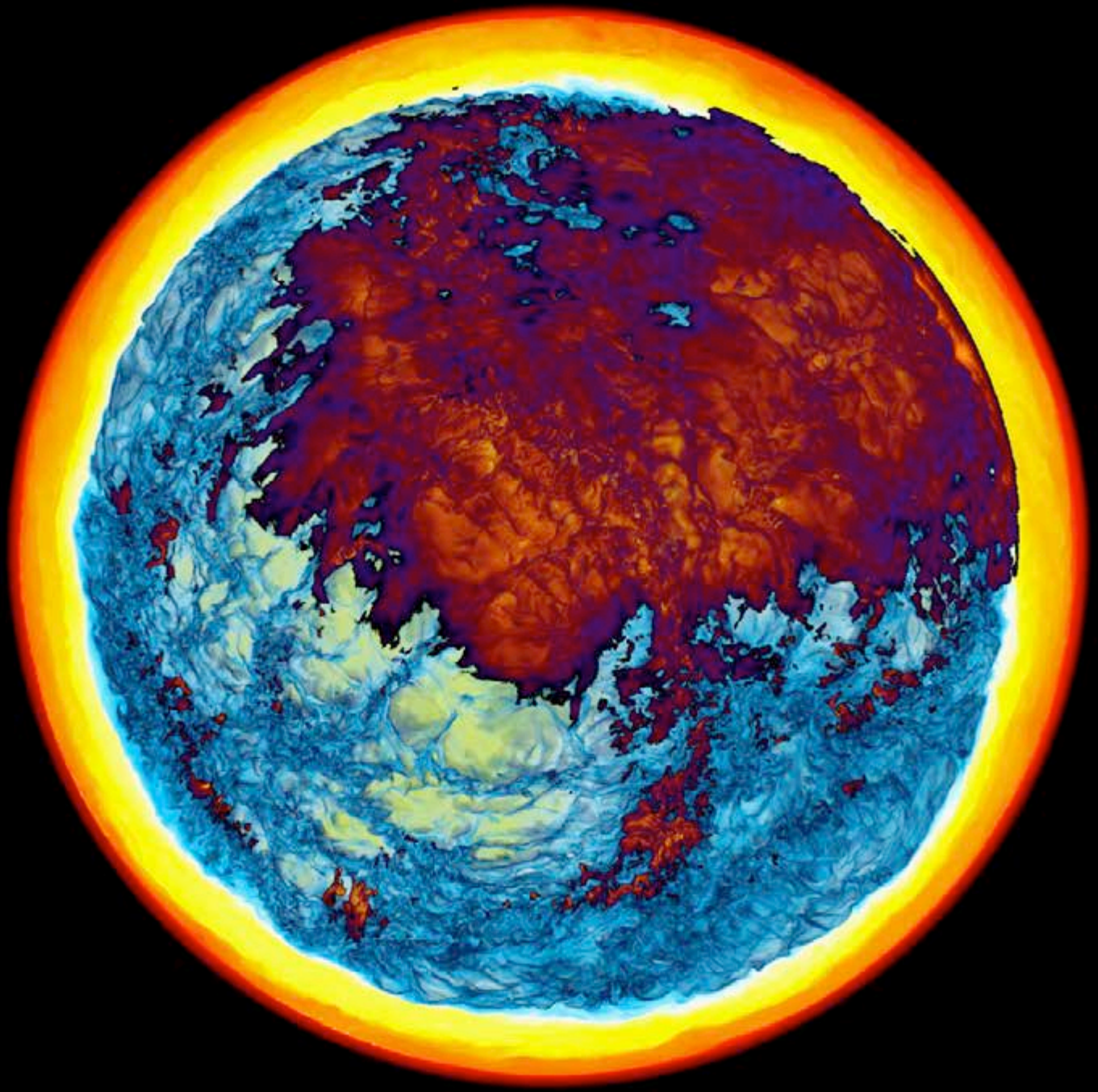

*Sakurai's Object H-ingestion simulation on Blue Waters machine in Jan., 2014, on a grid of $1536^3$ cells.*

*We see a hemisphere and make only mixtures of entrained hydrogen-rich gas with gas of the helium shell flash convection zone visible. The energy release rate from burning ingested H is shown in very dark blue, yellow, and white.*

*t = 1438 min.*

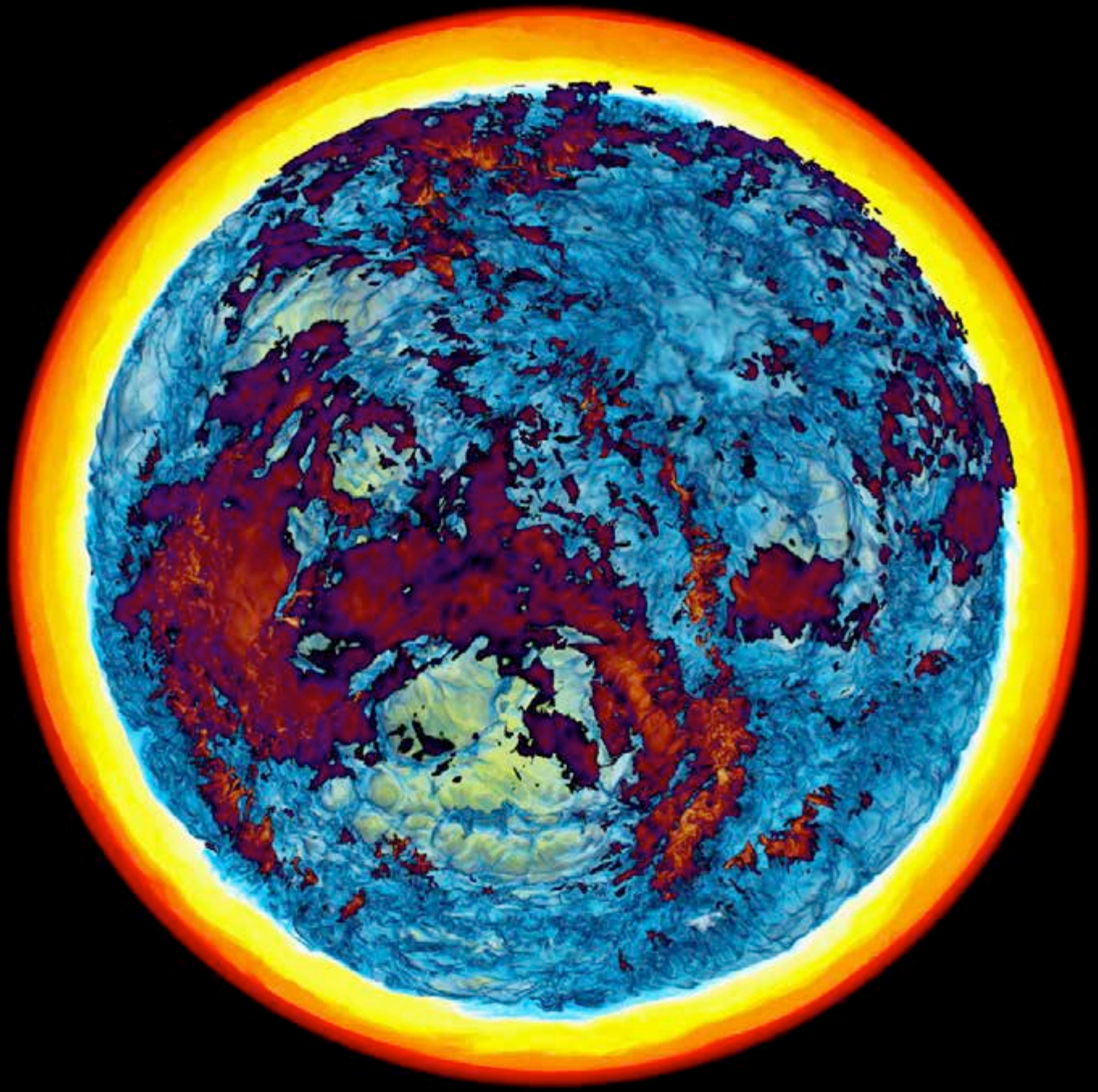

*Sakurai's Object H-ingestion simulation on Blue Waters machine in Jan., 2014, on a grid of $1536^3$ cells.*

*We see a hemisphere and make only mixtures of entrained hydrogen-rich gas with gas of the helium shell flash convection zone visible. The energy release rate from burning ingested H is shown in very dark blue, yellow, and white.*

*t = 1450 min.*

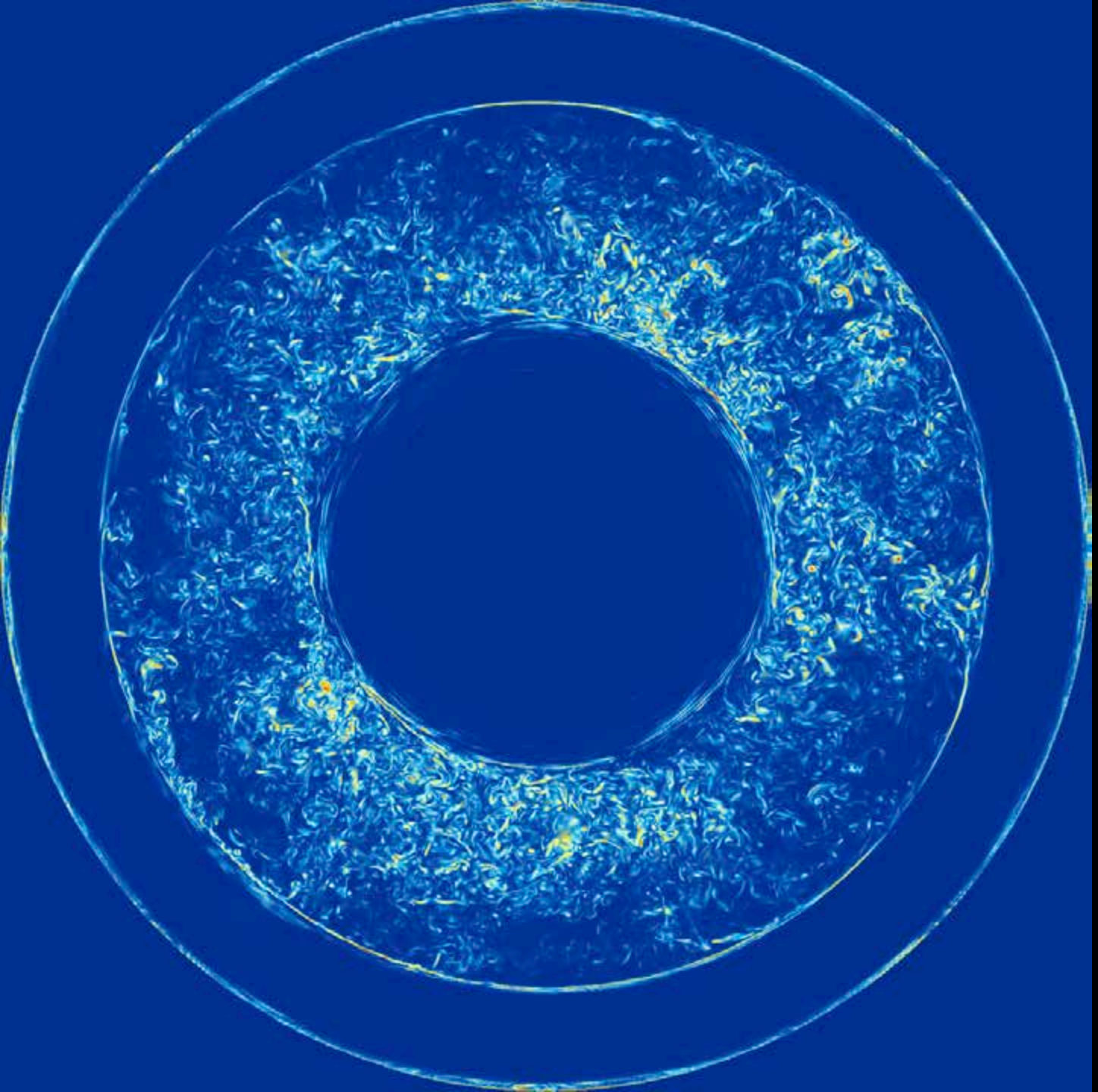

*These images of the magnitude of the vorticity show the flow field in a slice through the middle of the equator that is 1% of the domain's thickness.*

*Sakurai's Object H-ingestion simulation on Blue Waters machine in Jan., 2014, on a grid of $1536^3$ cells.*

*We look down the Y axis from Y = 1.5 using rho7lut with opacity 32*

*t = 270 min.*

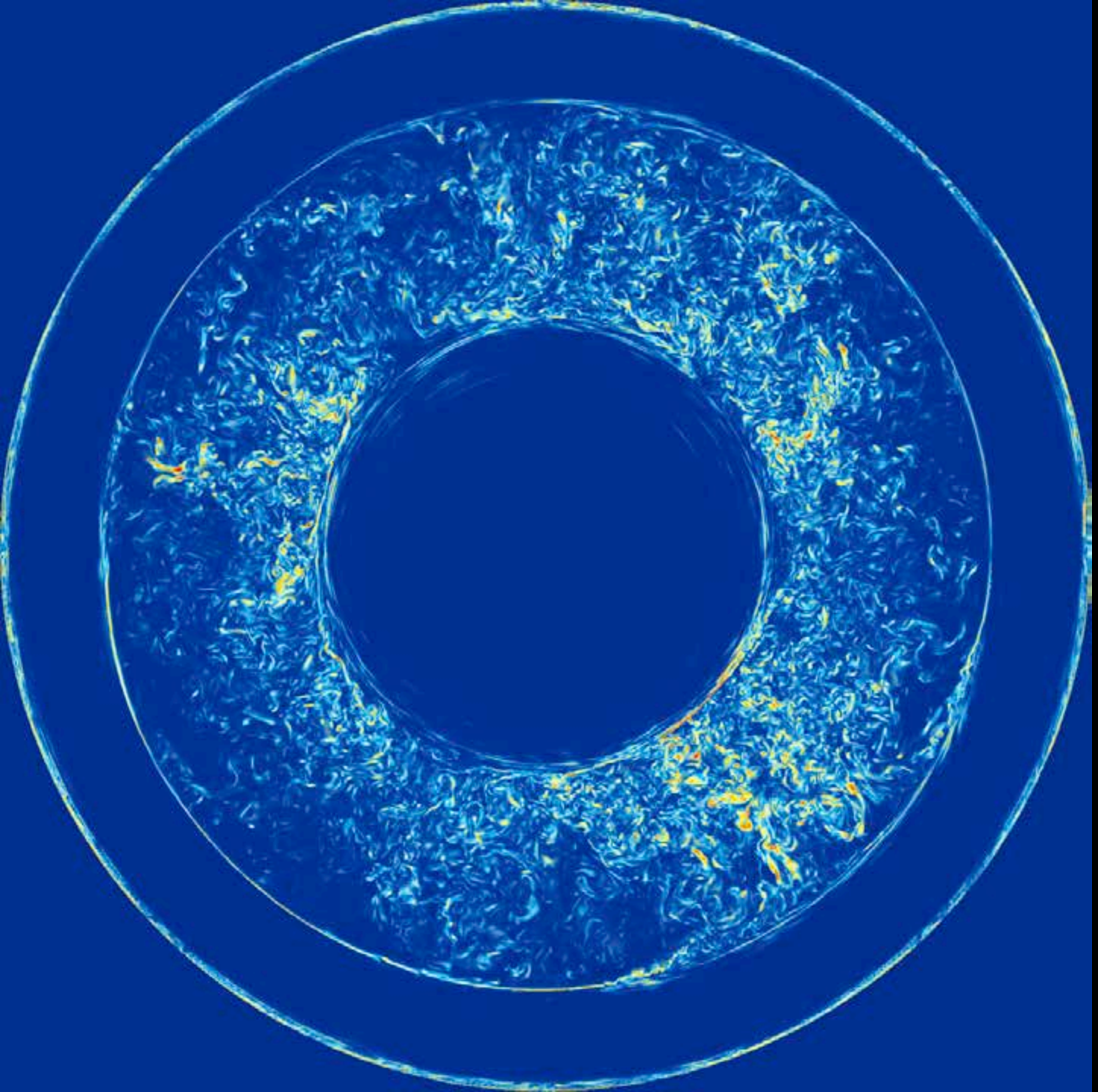

*These images of the magnitude of the vorticity show the flow field in a slice through the middle of the equator that is 1% of the domain's thickness.*

*Sakurai's Object H-ingestion simulation on Blue Waters machine in Jan., 2014, on a grid of $1536^3$ cells.*

*We look down the Y axis from Y = 1.5 using rho7lut with opacity 32*

*t = 400 min.*

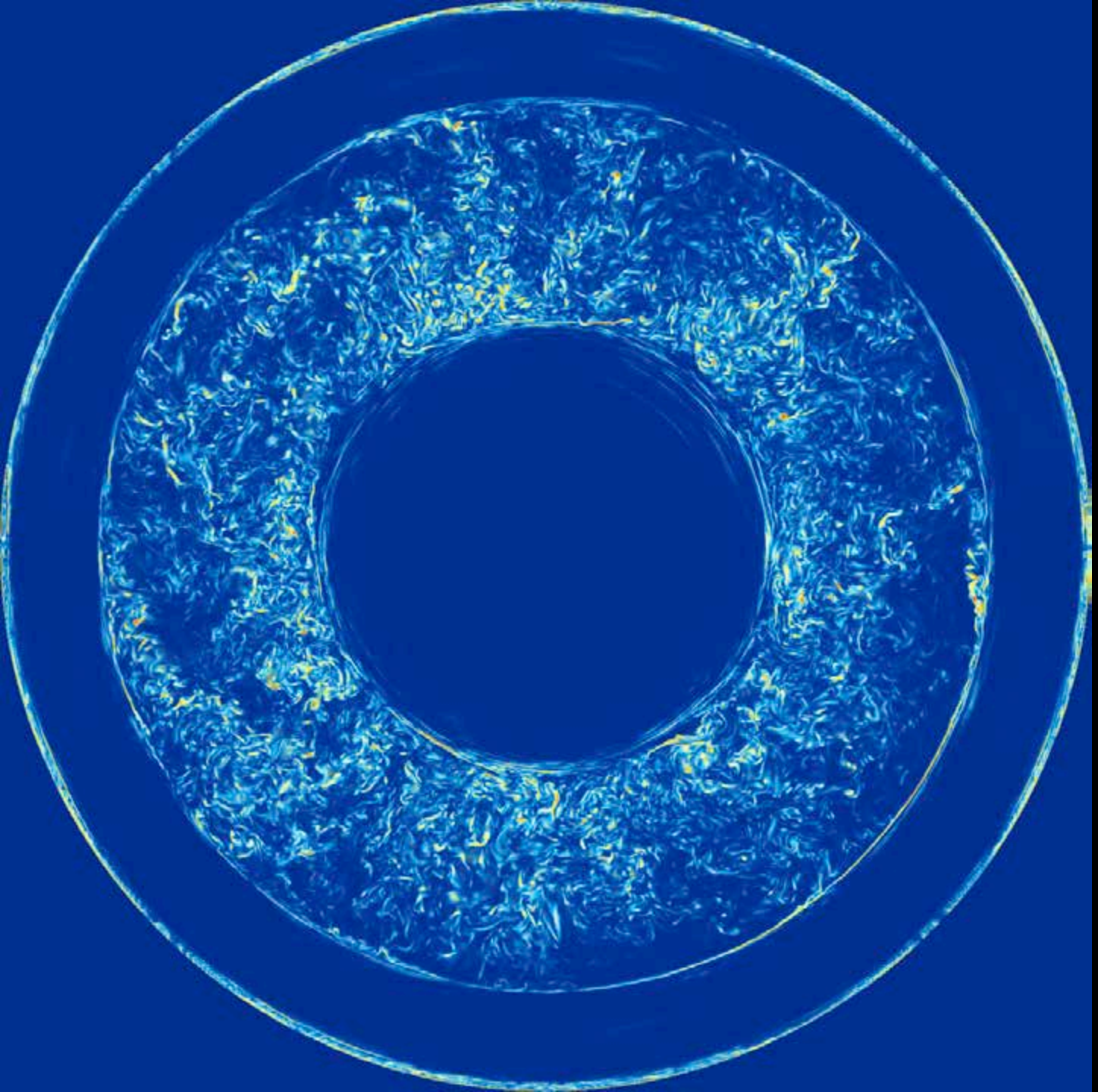

*These images of the magnitude of the vorticity show the flow field in a slice through the middle of the equator that is 1% of the domain's thickness.*

*Sakurai's Object H-ingestion simulation on Blue Waters machine in Jan., 2014, on a grid of $1536^3$ cells.*

*We look down the Y axis from Y = 1.5 using rho7lut with opacity 32*

*t = 540 min.*

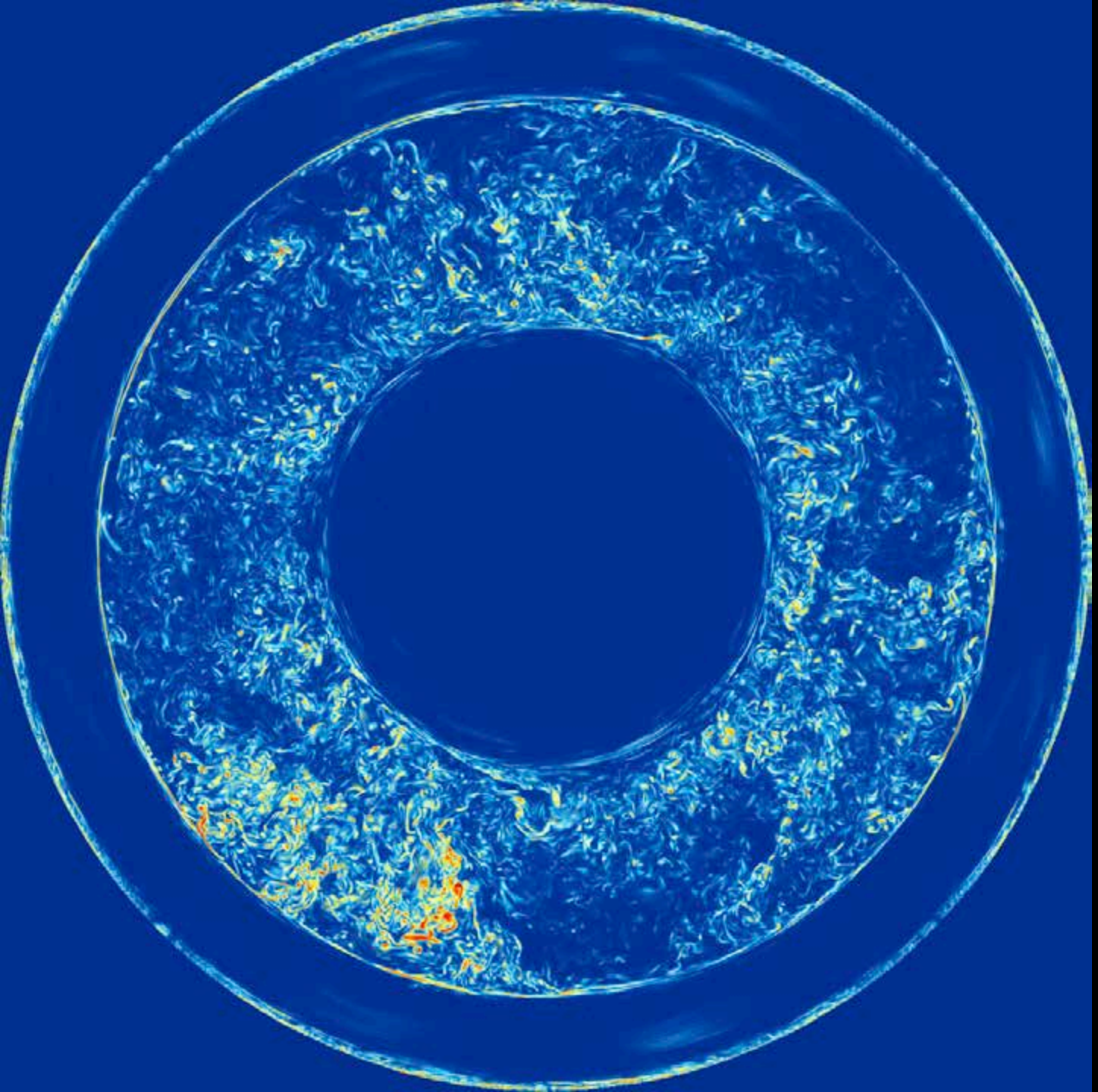

*These images of the magnitude of the vorticity show the flow field in a slice through the middle of the equator that is 1% of the domain's thickness.*

*Sakurai's Object H-ingestion simulation on Blue Waters machine in Jan., 2014, on a grid of $1536^3$ cells.*

*We look down the Y axis from Y = 1.5 using rho7lut with opacity 32*

*t = 925 min.*

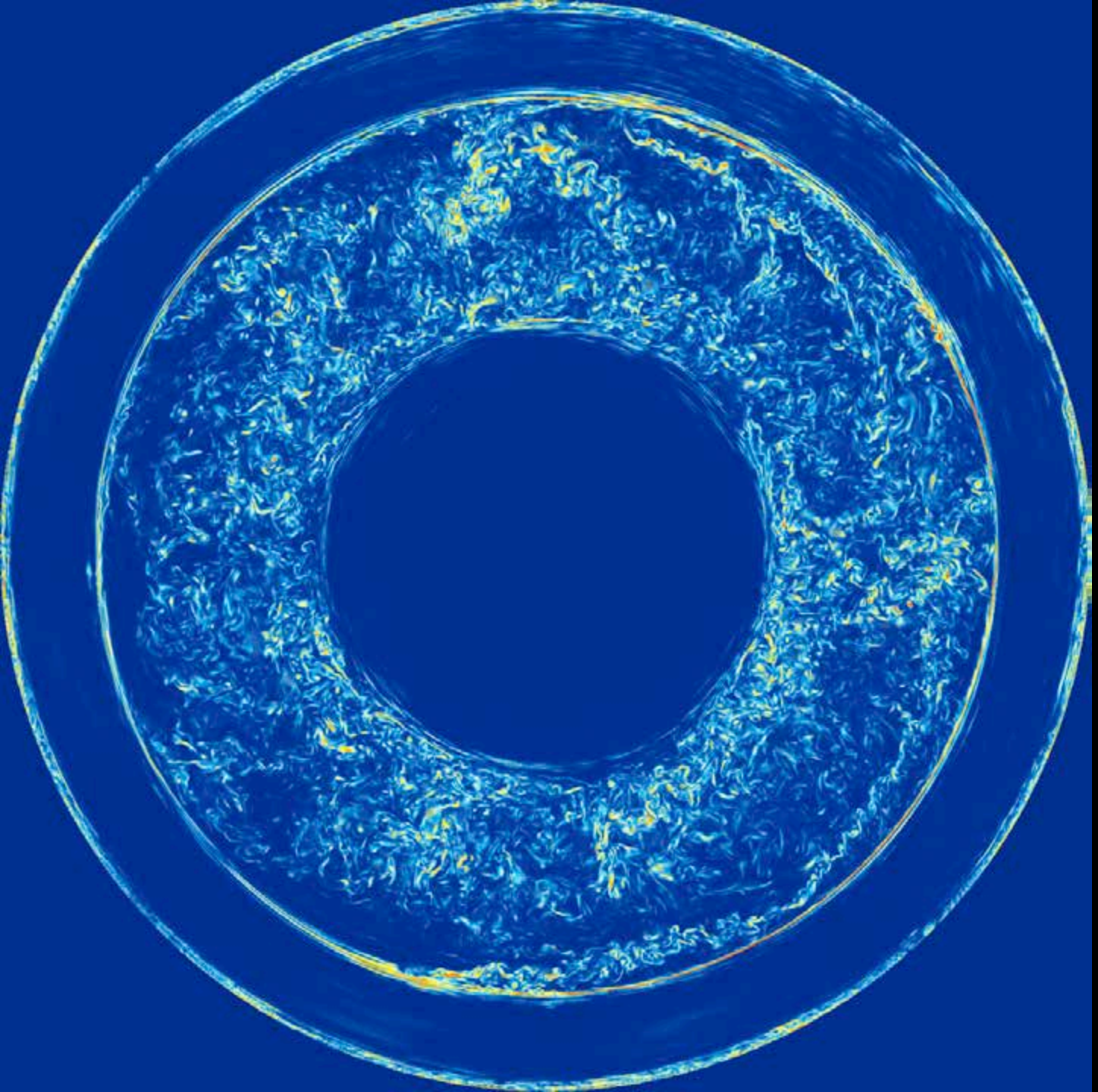

*These images of the magnitude of the vorticity show the flow field in a slice through the middle of the equator that is 1% of the domain's thickness.*

*Sakurai's Object H-ingestion simulation on Blue Waters machine in Jan., 2014, on a grid of $1536^3$ cells.*

*We look down the Y axis from Y = 1.5 using rho7lut with opacity 32*

*t = 948 min.*

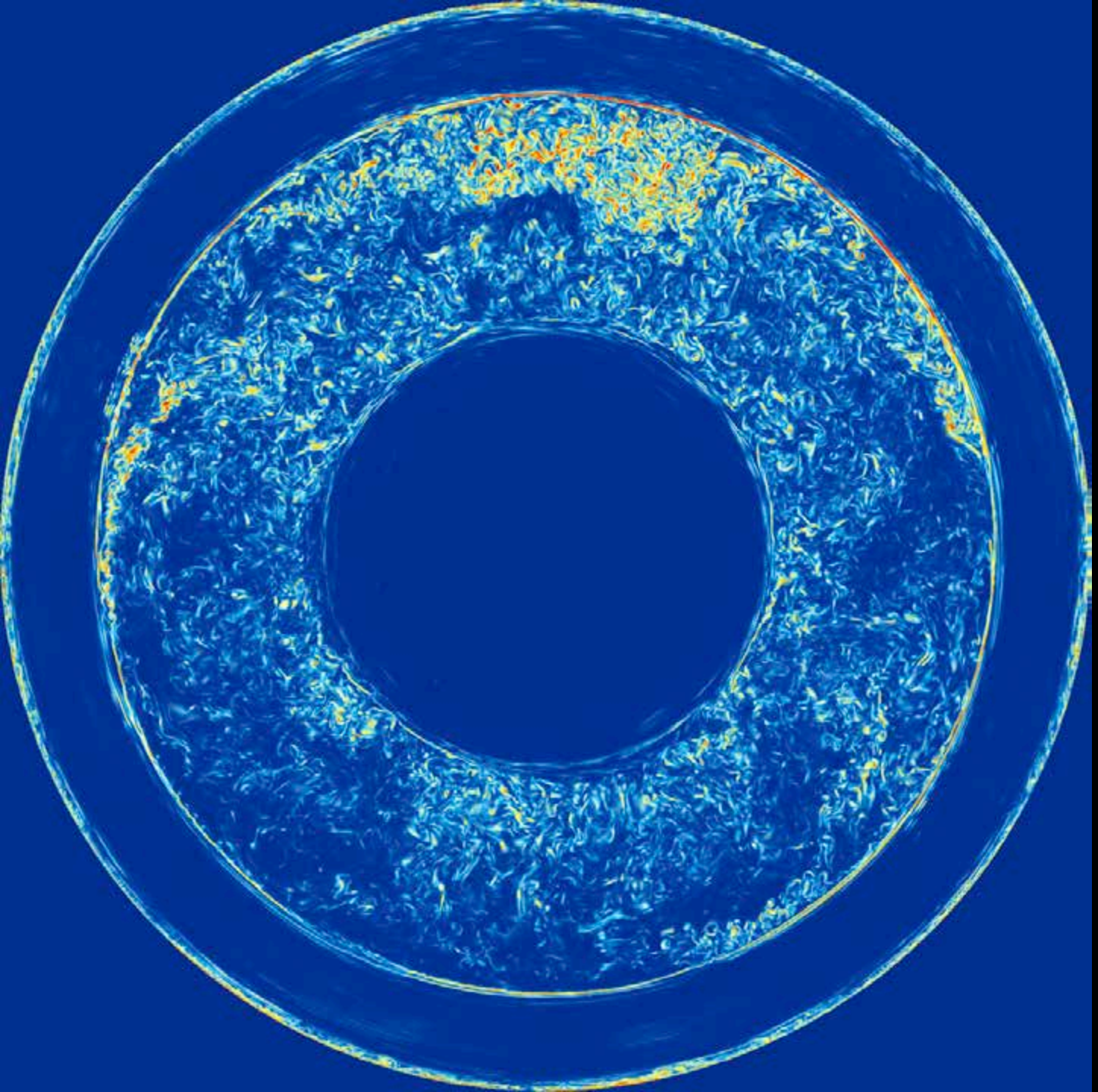

*These images of the magnitude of the vorticity show the flow field in a slice through the middle of the equator that is 1% of the domain's thickness.*

*Sakurai's Object H-ingestion simulation on Blue Waters machine in Jan., 2014, on a grid of $1536^3$ cells.*

*We look down the Y axis from Y = 1.5 using rho7lut with opacity 32*

*t = 956 min.*

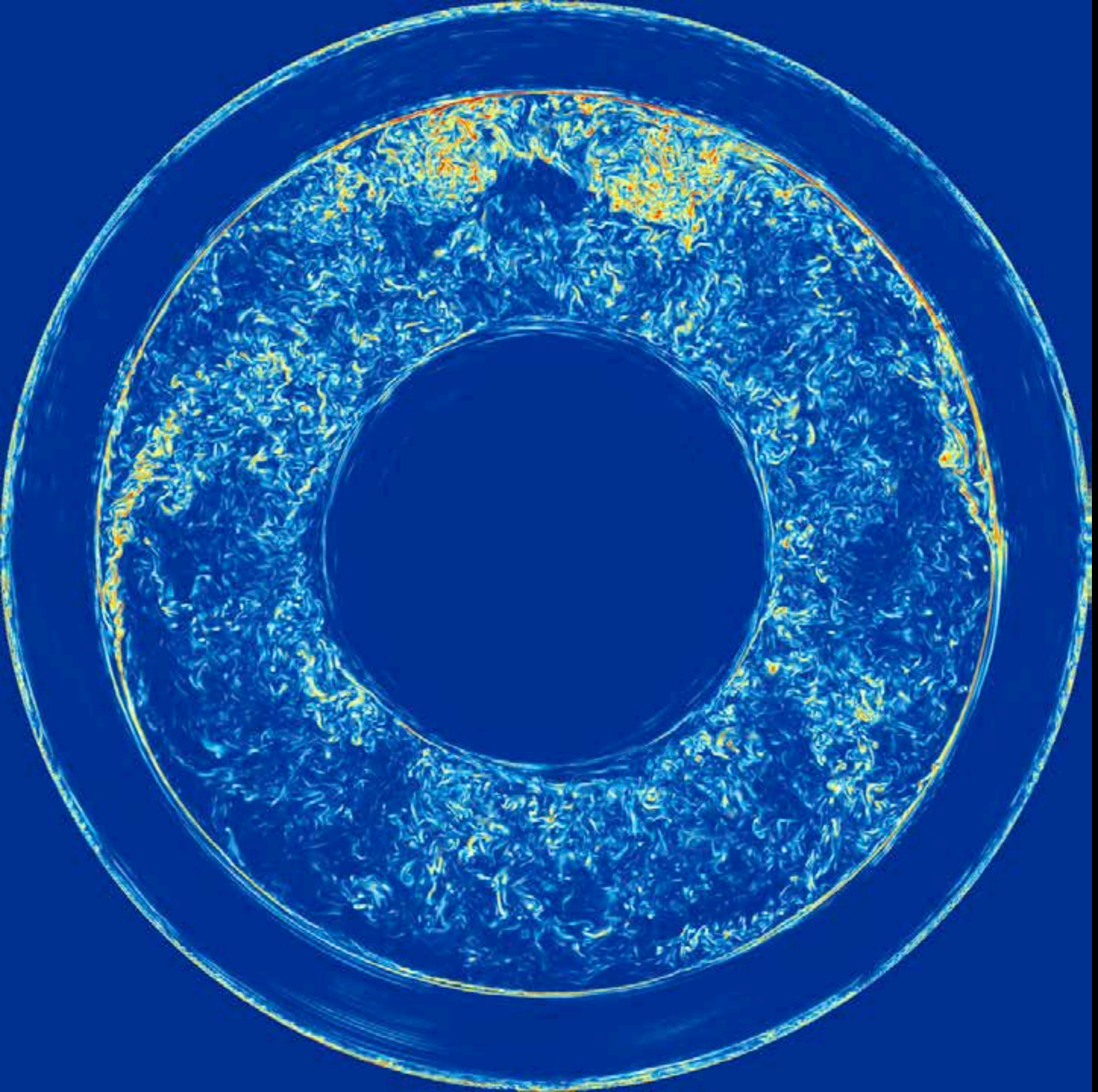

*These images of the magnitude of the vorticity show the flow field in a slice through the middle of the equator that is 1% of the domain's thickness.*

*Sakurai's Object H-ingestion simulation on Blue Waters machine in Jan., 2014, on a grid of $1536^3$ cells.*

*We look down the Y axis from Y = 1.5 using rho7lut with opacity 32*

*t = 957 min.*

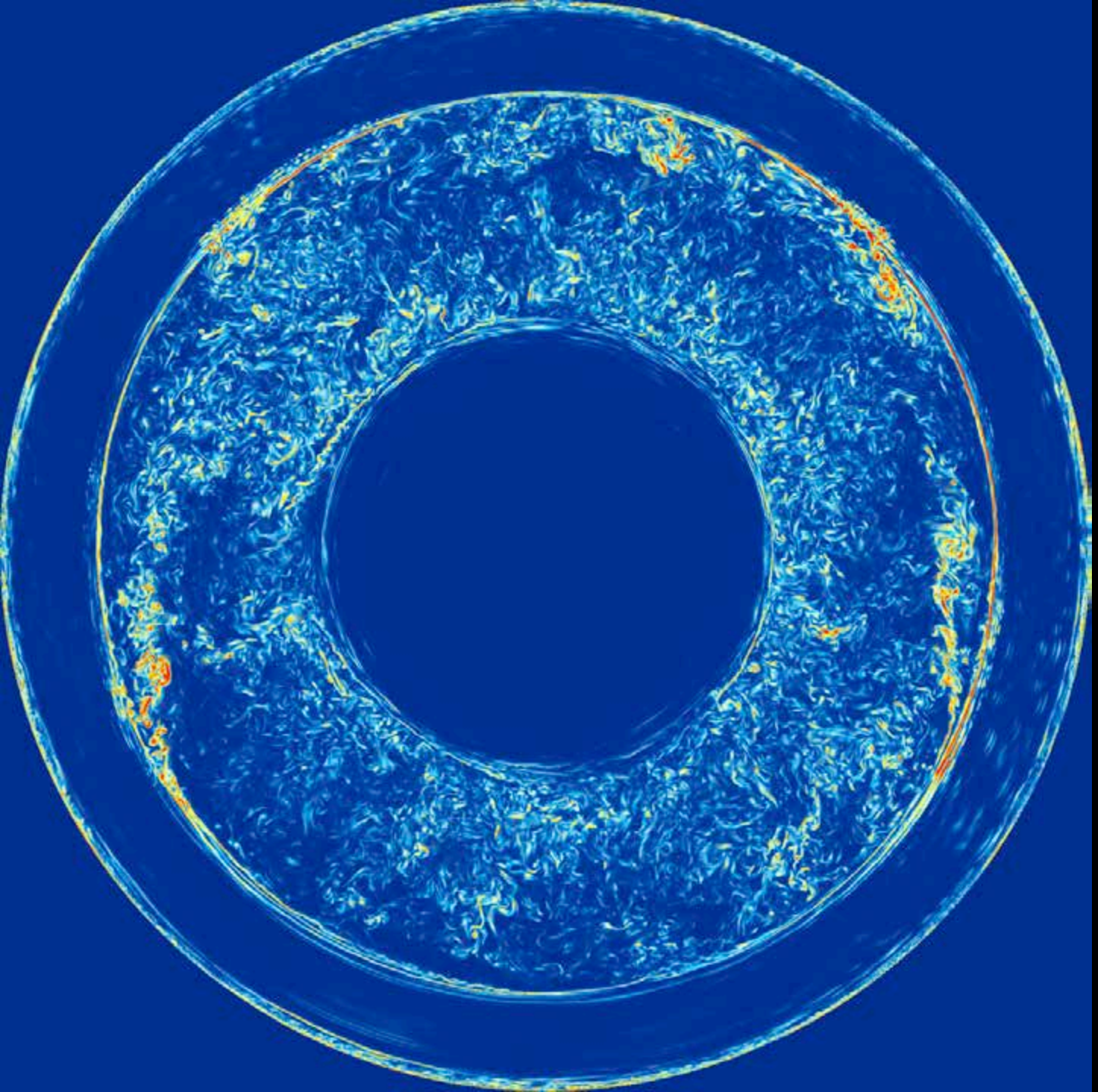

*These images of the magnitude of the vorticity show the flow field in a slice through the middle of the equator that is 1% of the domain's thickness.*

*Sakurai's Object H-ingestion simulation on Blue Waters machine in Jan., 2014, on a grid of $1536^3$ cells.*

*We look down the Y axis from Y = 1.5 using rho7lut with opacity 32*

*t = 960 min.*

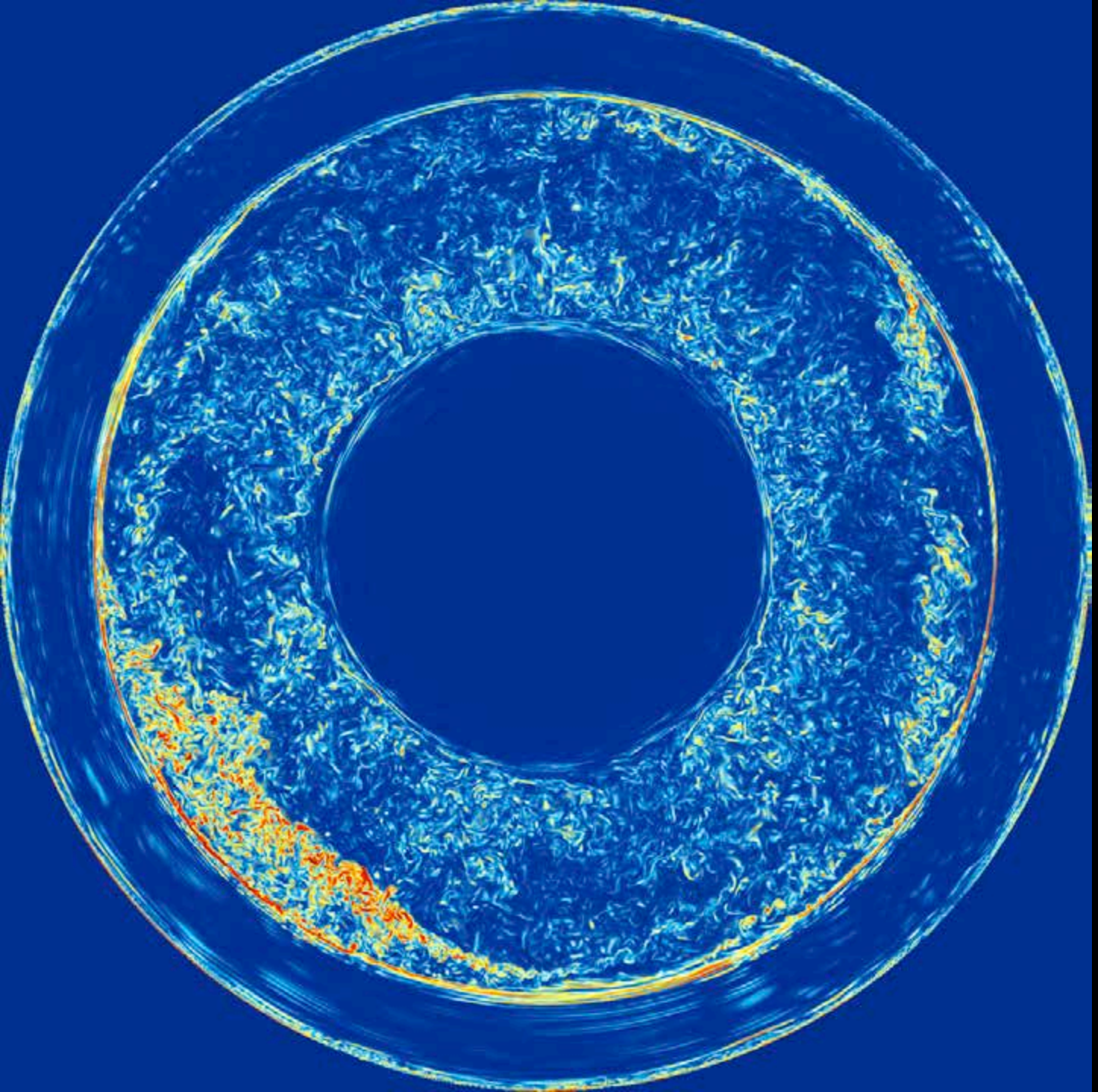

*These images of the magnitude of the vorticity show the flow field in a slice through the middle of the equator that is 1% of the domain's thickness.*

*Sakurai's Object H-ingestion simulation on Blue Waters machine in Jan., 2014, on a grid of $1536^3$ cells.*

*We look down the Y axis from Y = 1.5 using rho7lut with opacity 32*

*t = 963 min.*

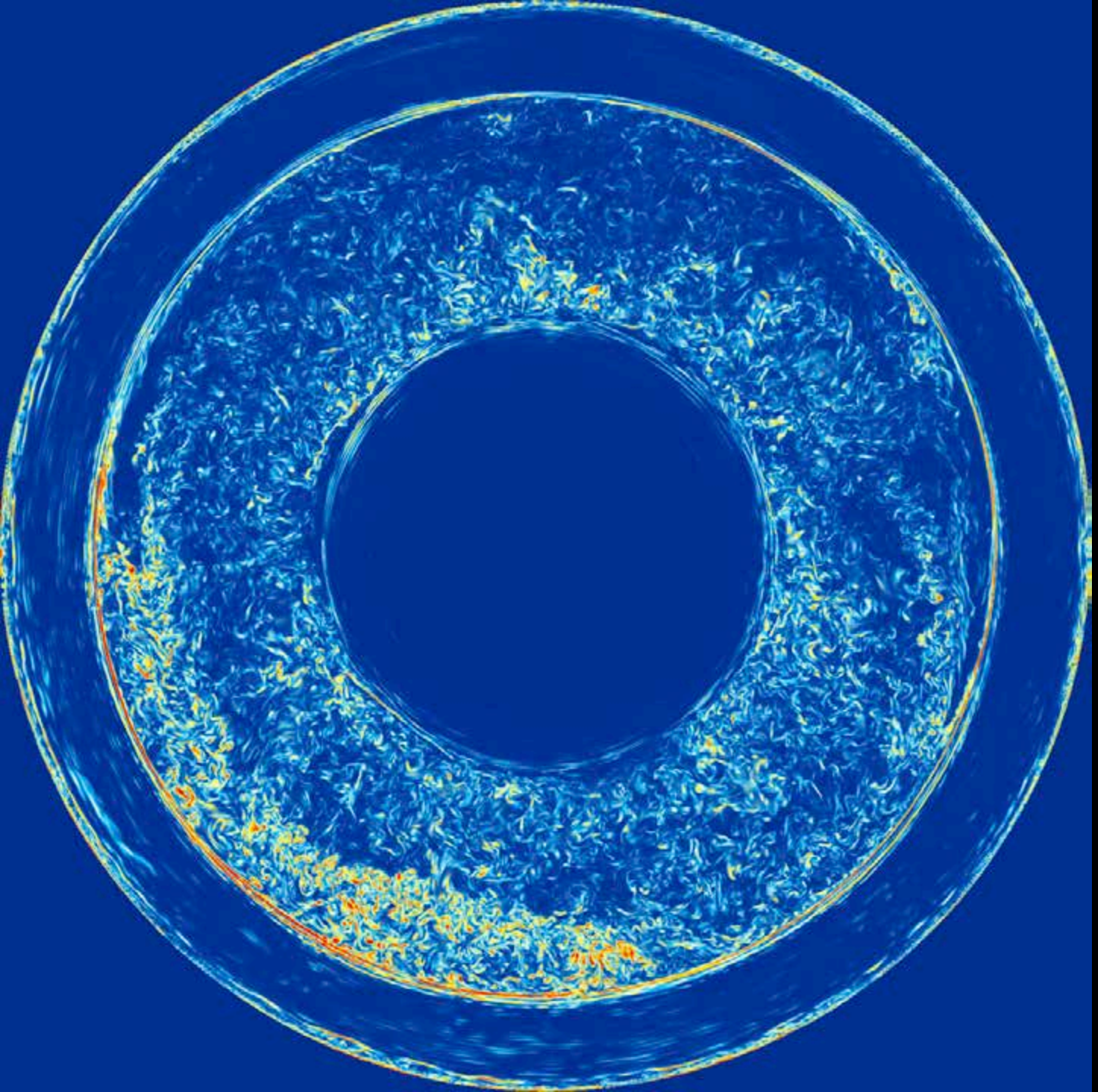

*These images of the magnitude of the vorticity show the flow field in a slice through the middle of the equator that is 1% of the domain's thickness.*

*Sakurai's Object H-ingestion simulation on Blue Waters machine in Jan., 2014, on a grid of $1536^3$ cells.*

*We look down the Y axis from Y = 1.5 using rho7lut with opacity 32*

*t = 966 min.*

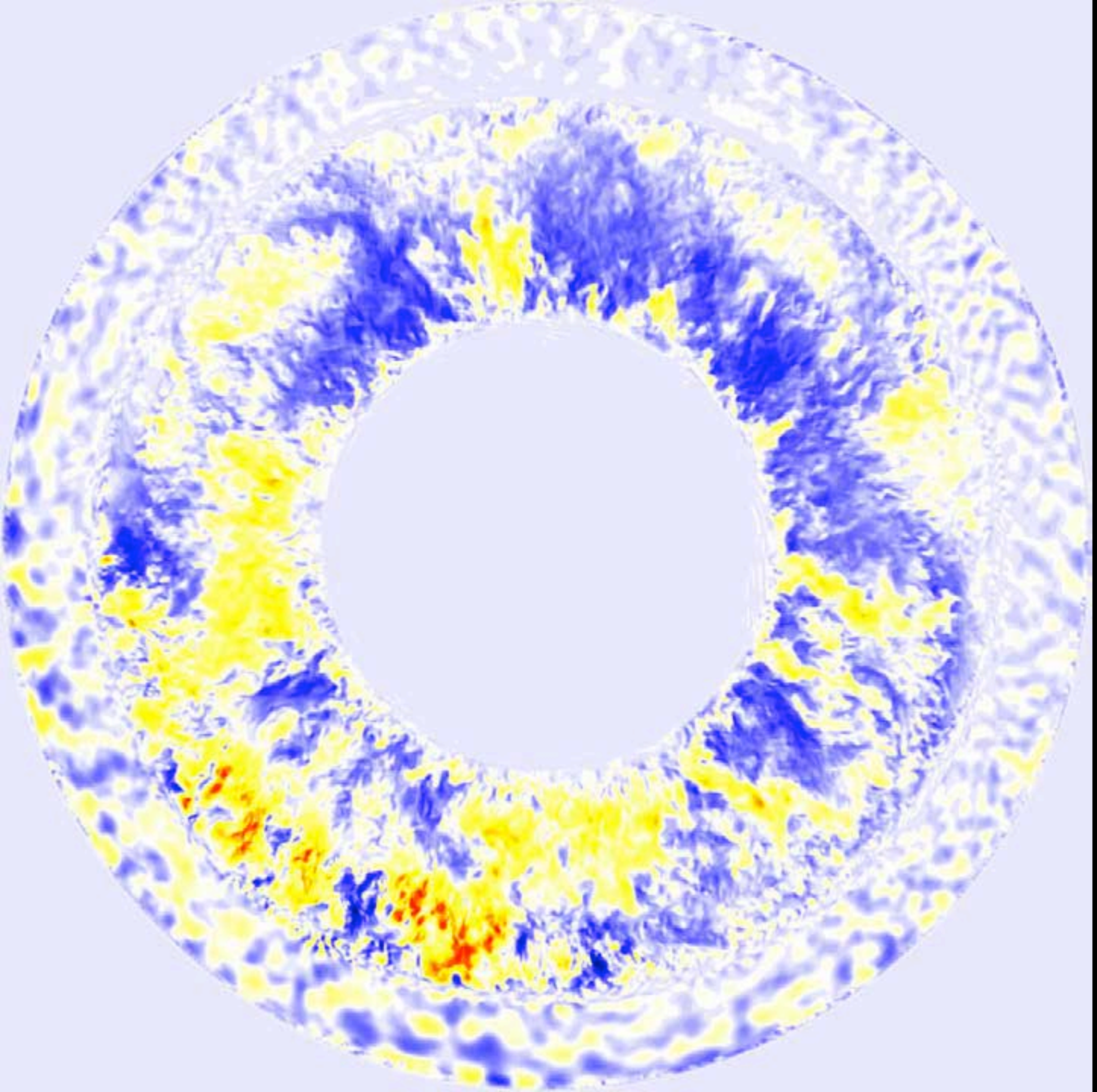

*These images of the radial component of velocity show the flow field in a slice through the middle of the equator that is 1% of the domain's thickness.*

*Sakurai's Object H-ingestion simulation on Blue Waters machine in Jan., 2014, on a grid of $1536^3$ cells.*

*We look down the Y axis from Y = 1.5 using rho7lut with opacity 32*

*t = 966 min.*

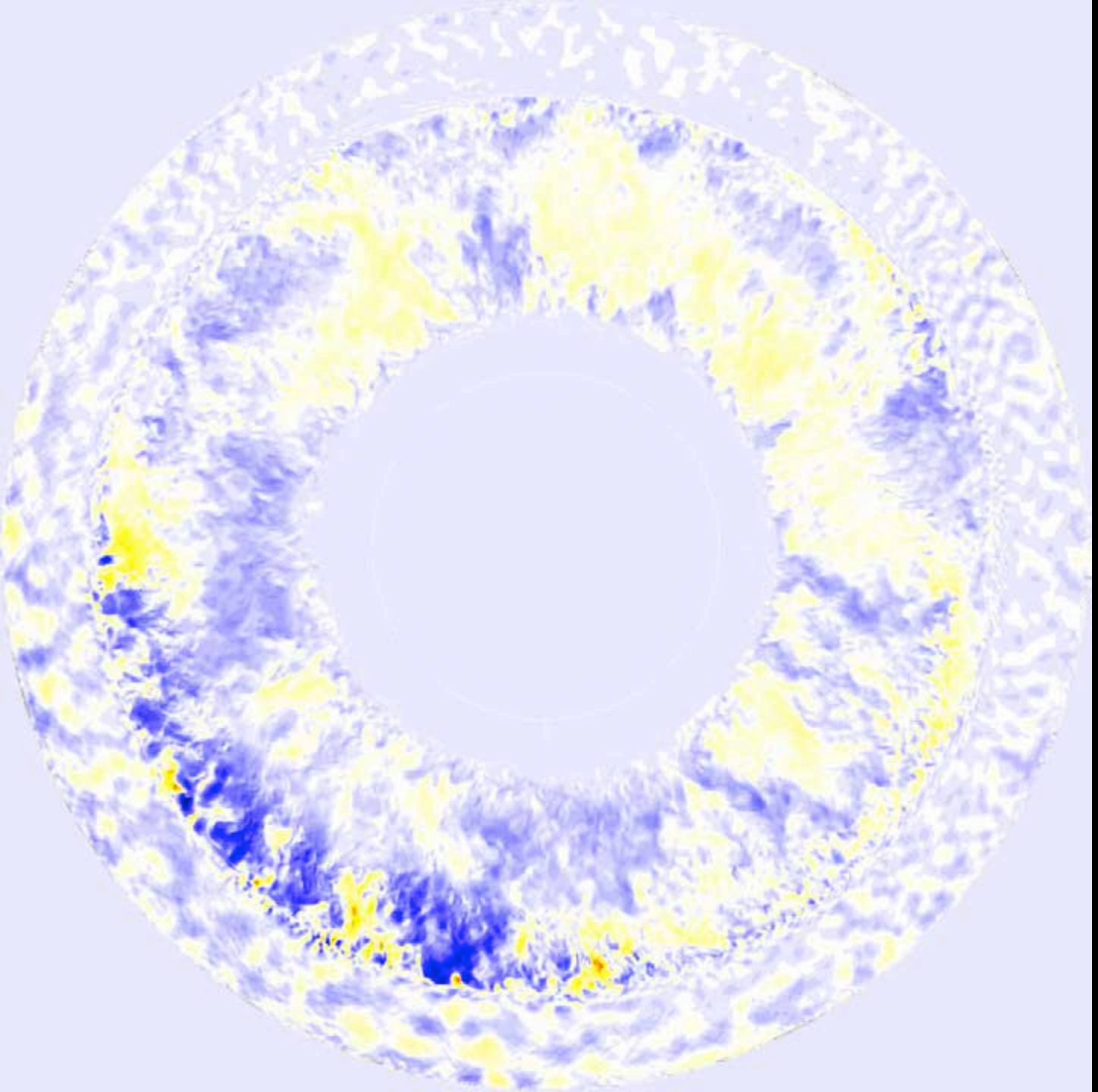

*These images of the divergence of velocity show the flow field in a slice through the middle of the equator that is 1% of the domain's thickness.*

*Sakurai's Object H-ingestion simulation on Blue Waters machine in Jan., 2014, on a grid of $1536^3$ cells.*

*We look down the Y axis from Y = 1.5 using rho7lut with opacity 32*

*t = 966 min.*

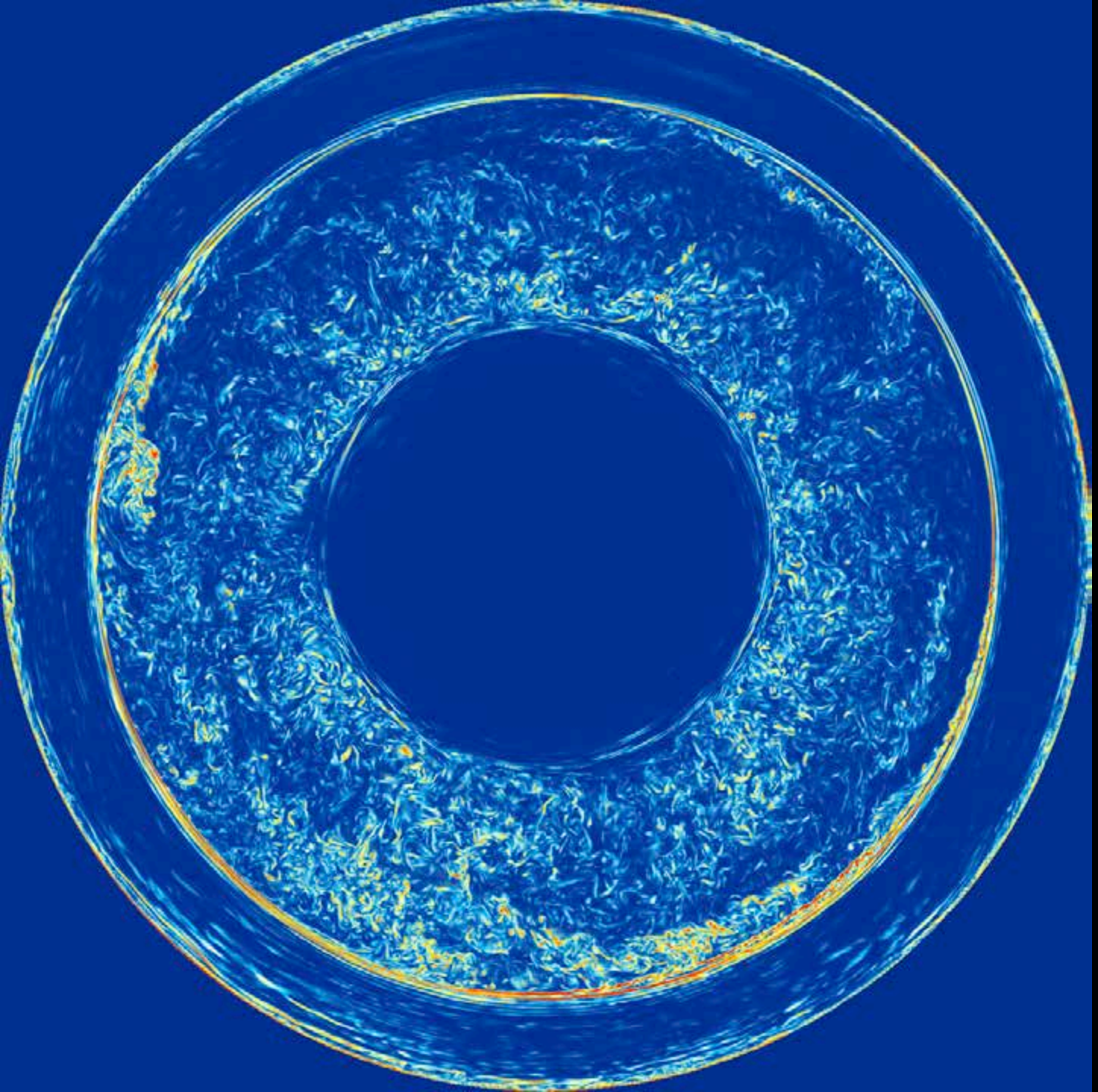

*These images of the magnitude of the vorticity show the flow field in a slice through the middle of the equator that is 1% of the domain's thickness.*

*Sakurai's Object H-ingestion simulation on Blue Waters machine in Jan., 2014, on a grid of $1536^3$ cells.*

*We look down the Y axis from Y = 1.5 using rho7lut with opacity 32*

*t = 970 min.*

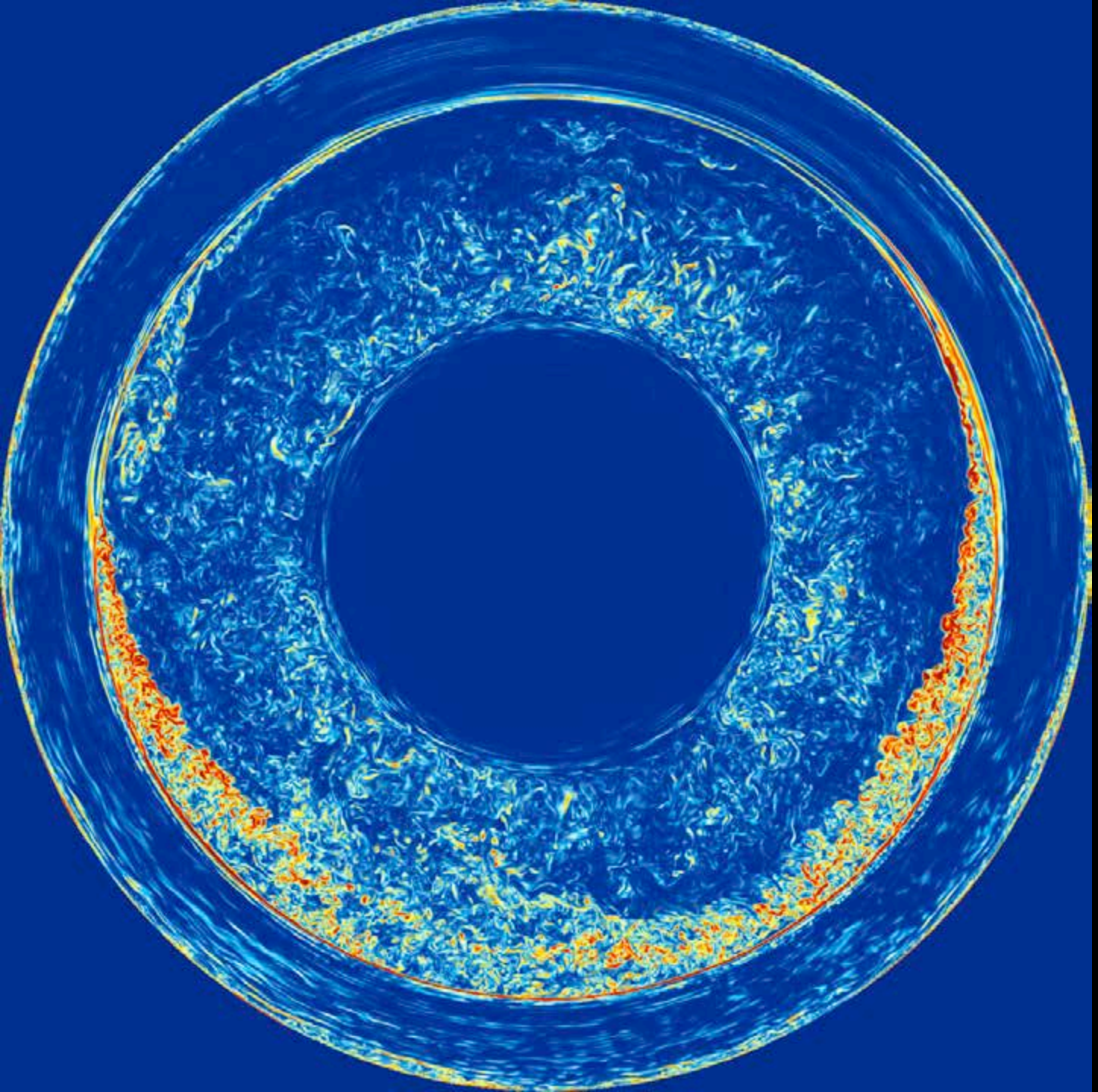

*These images of the magnitude of the vorticity show the flow field in a slice through the middle of the equator that is 1% of the domain's thickness.*

*Sakurai's Object H-ingestion simulation on Blue Waters machine in Jan., 2014, on a grid of $1536^3$ cells.*

*We look down the Y axis from Y = 1.5 using rho7lut with opacity 32*

*t = 973 min.*

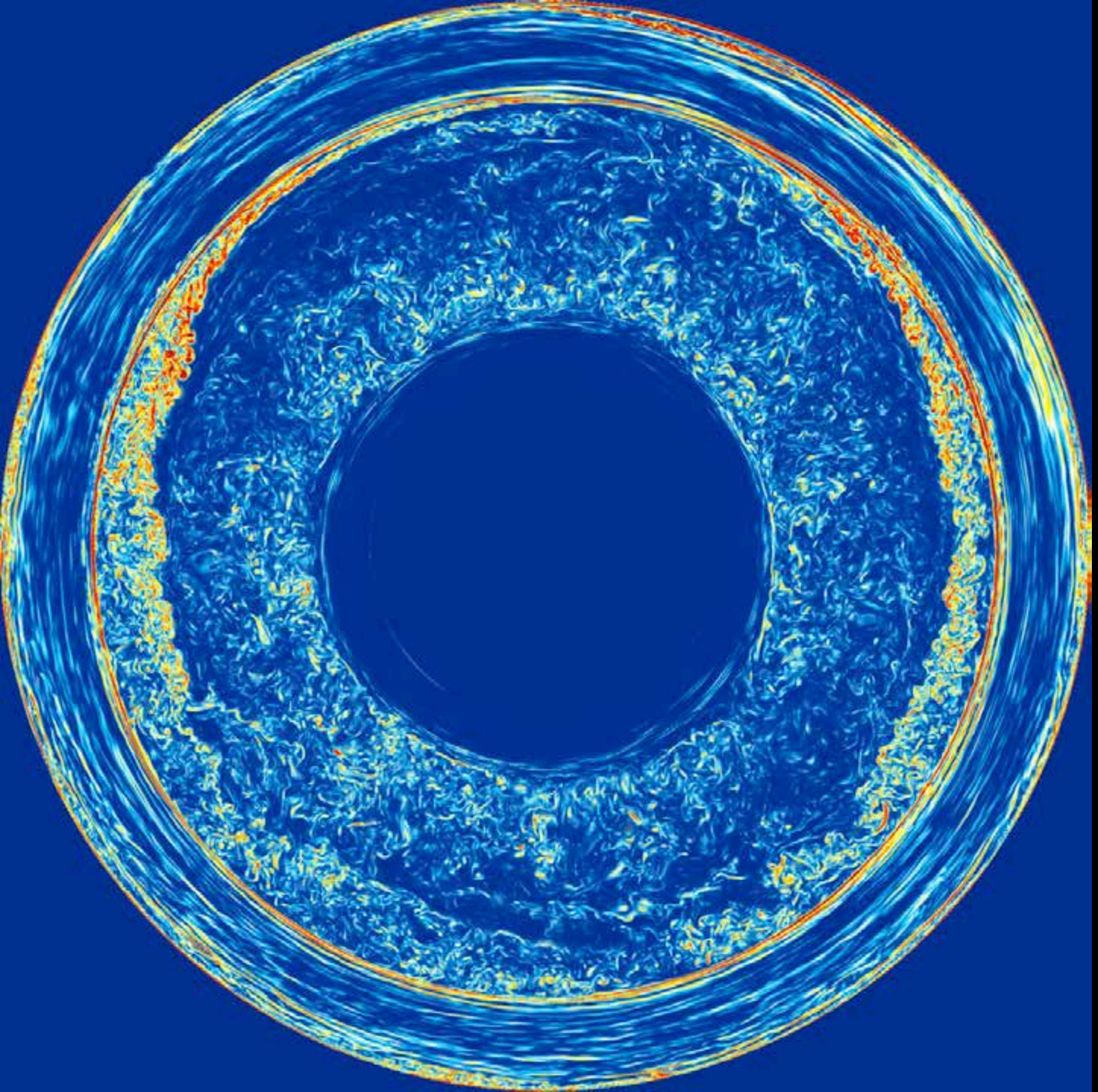

*These images of the magnitude of the vorticity show the flow field in a slice through the middle of the equator that is 1% of the domain's thickness.*

*Sakurai's Object H-ingestion simulation on Blue Waters machine in Jan., 2014, on a grid of $1536^3$ cells.*

*We look down the Y axis from Y = 1.5 using rho7lut with opacity 32*

*t = 1000 min.*

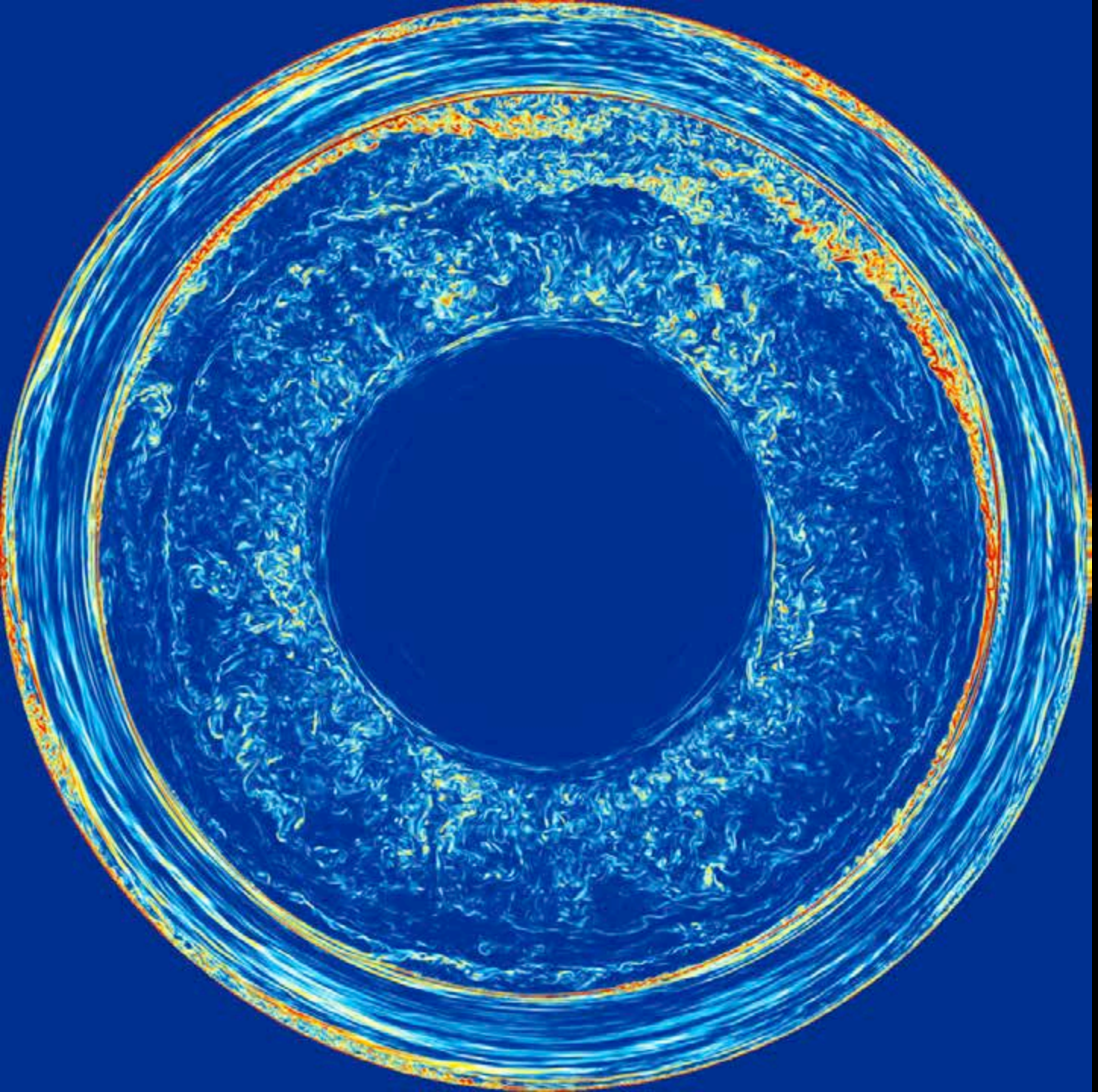

*These images of the magnitude of the vorticity show the flow field in a slice through the middle of the equator that is 1% of the domain's thickness.*

*Sakurai's Object H-ingestion simulation on Blue Waters machine in Jan., 2014, on a grid of $1536^3$ cells.*

*We look down the Y axis from Y = 1.5 using rho7lut with opacity 32*

*t = 1008 min.*

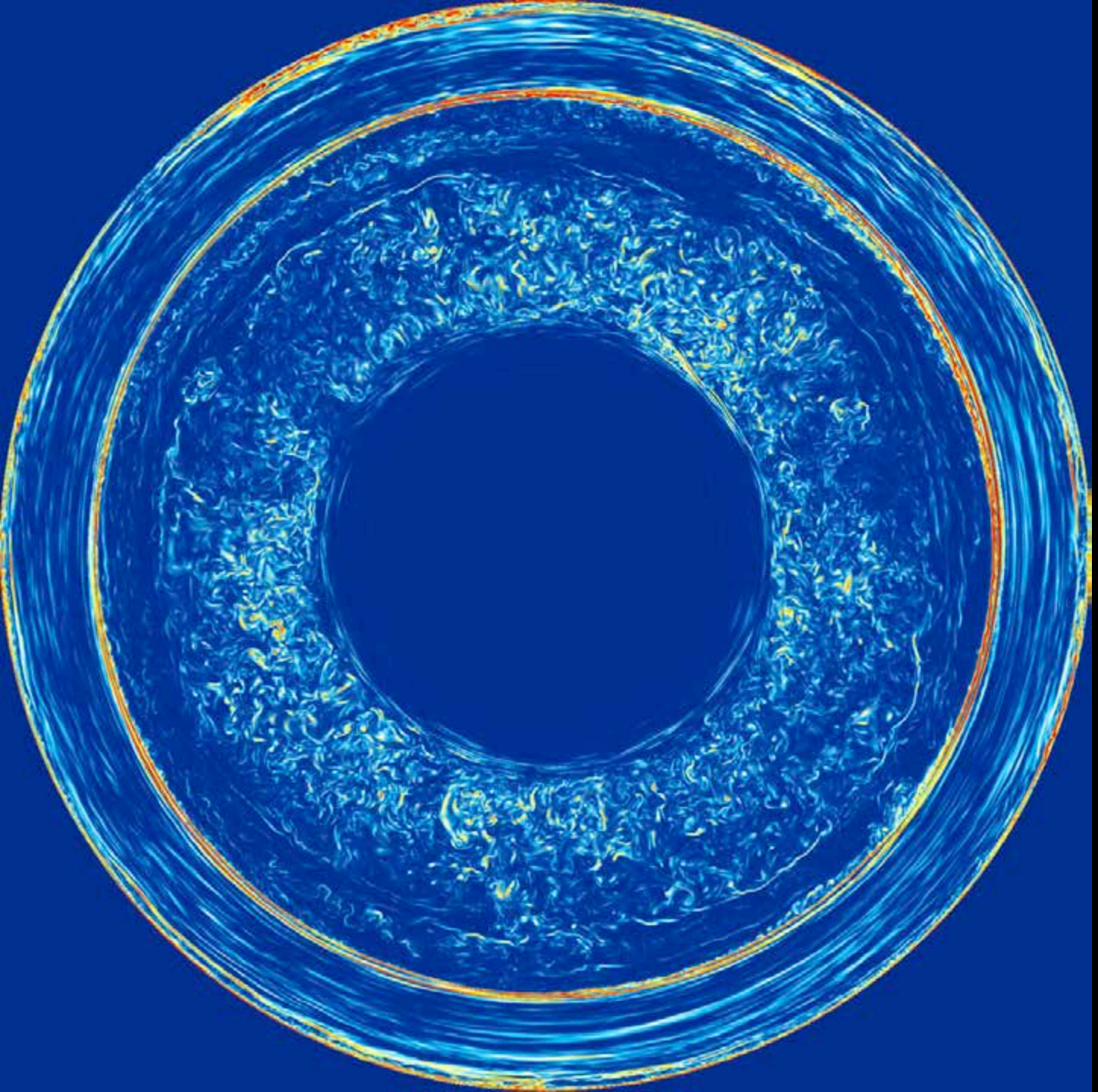

*These images of the magnitude of the vorticity show the flow field in a slice through the middle of the equator that is 1% of the domain's thickness.*

*Sakurai's Object H-ingestion simulation on Blue Waters machine in Jan., 2014, on a grid of $1536^3$ cells.*

*We look down the Y axis from Y = 1.5 using rho7lut with opacity 32*

*t = 1033 min.*

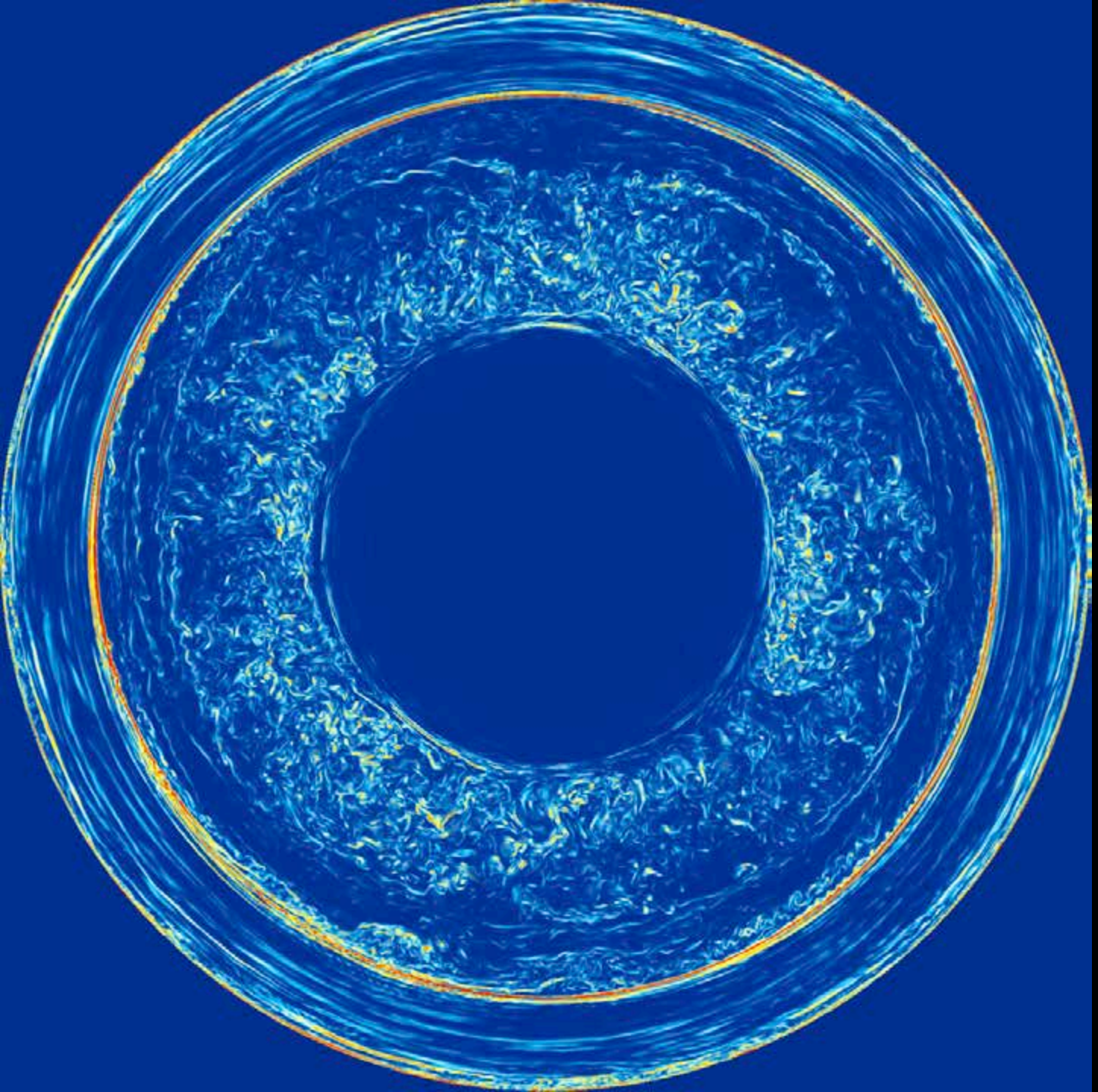

*These images of the magnitude of the vorticity show the flow field in a slice through the middle of the equator that is 1% of the domain's thickness.*

*Sakurai's Object H-ingestion simulation on Blue Waters machine in Jan., 2014, on a grid of $1536^3$ cells.*

*We look down the Y axis from Y = 1.5 using rho7lut with opacity 32*

*t = 1044 min.*

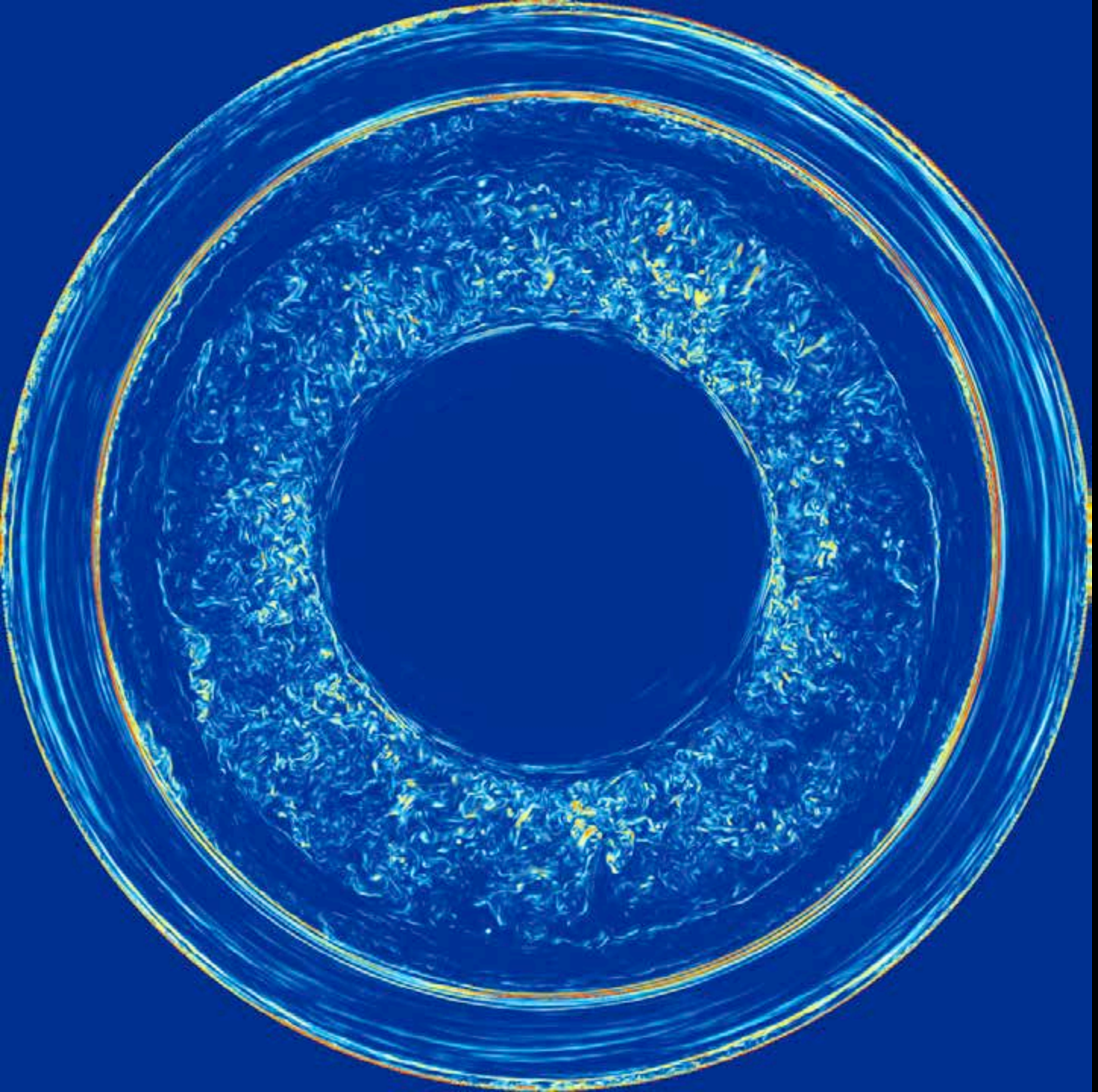

*These images of the magnitude of the vorticity show the flow field in a slice through the middle of the equator that is 1% of the domain's thickness.*

*Sakurai's Object H-ingestion simulation on Blue Waters machine in Jan., 2014, on a grid of $1536^3$ cells.*

*We look down the Y axis from Y = 1.5 using rho7lut with opacity 32*

*t = 1062 min.*

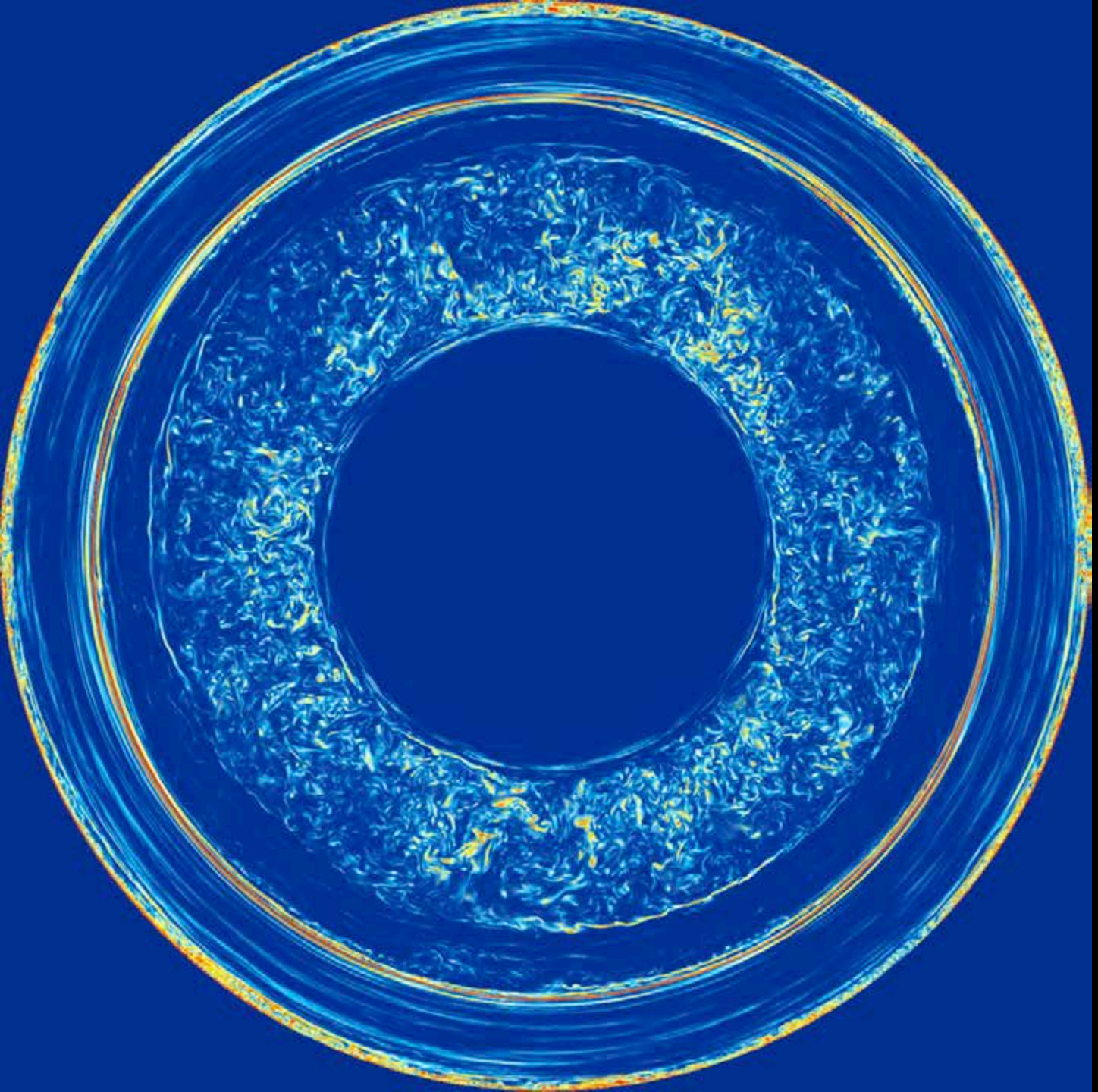

*These images of the magnitude of the vorticity show the flow field in a slice through the middle of the equator that is 1% of the domain's thickness.*

*Sakurai's Object H-ingestion simulation on Blue Waters machine in Jan., 2014, on a grid of $1536^3$ cells.*

*We look down the Y axis from Y = 1.5 using rho7lut with opacity 32*

*t = 1100 min.*

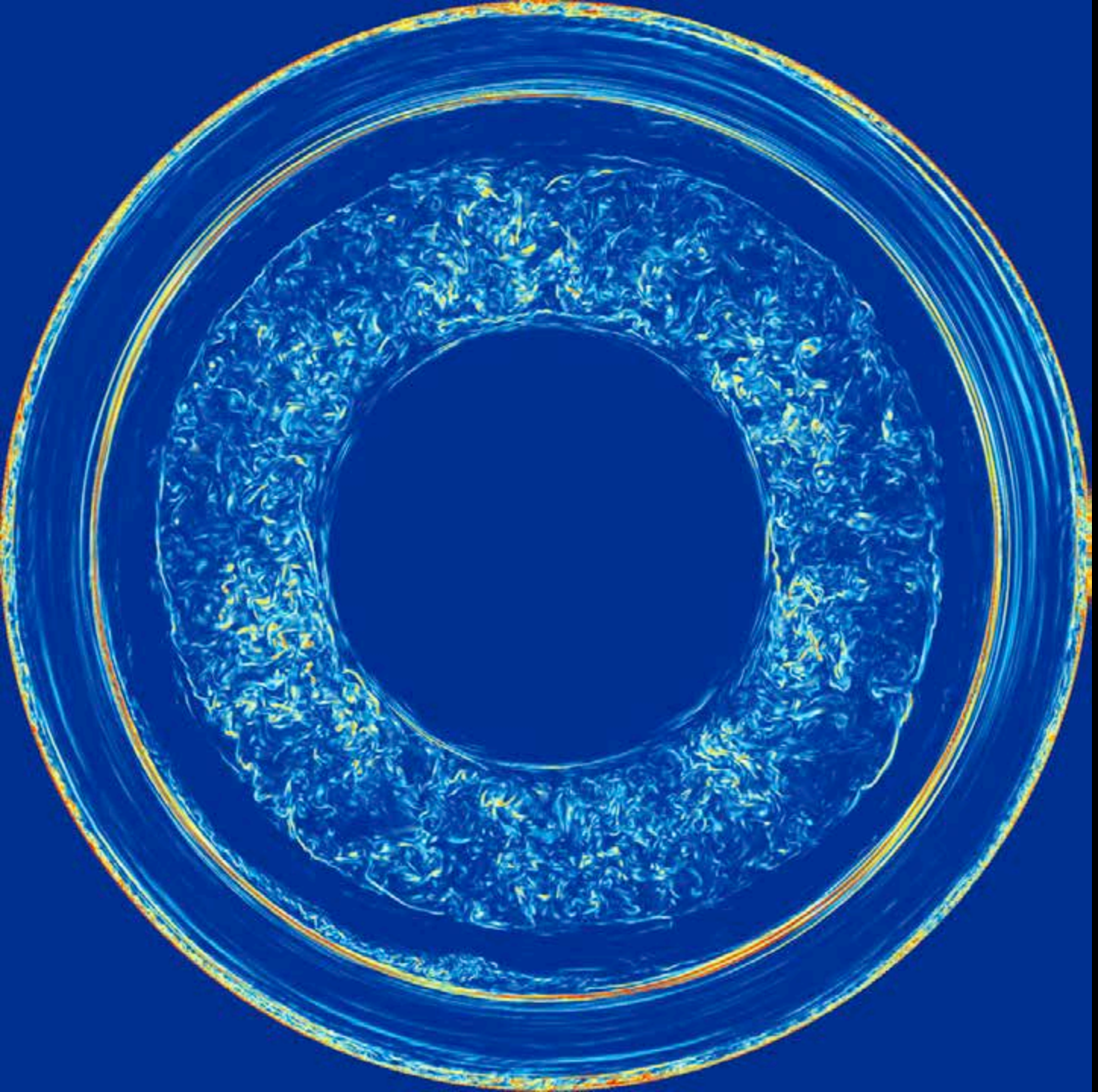

*These images of the magnitude of the vorticity show the flow field in a slice through the middle of the equator that is 1% of the domain's thickness.*

*Sakurai's Object H-ingestion simulation on Blue Waters machine in Jan., 2014, on a grid of $1536^3$ cells.*

*We look down the Y axis from Y = 1.5 using rho7lut with opacity 32*

*t = 1140 min. (actually 1100 min)*

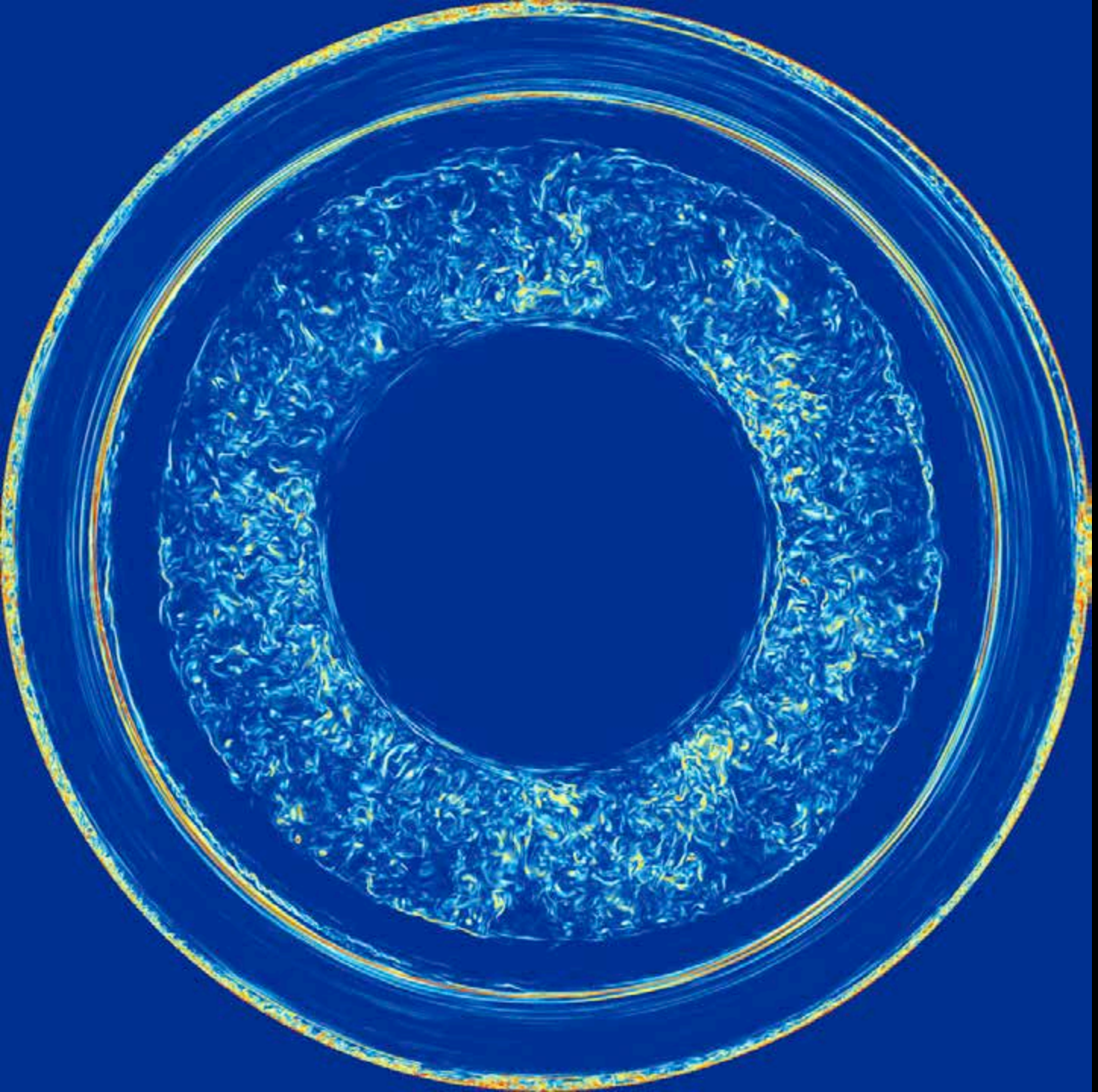

*These images of the magnitude of the vorticity show the flow field in a slice through the middle of the equator that is 1% of the domain's thickness.*

*Sakurai's Object H-ingestion simulation on Blue Waters machine in Jan., 2014, on a grid of $1536^3$ cells.*

*We look down the Y axis from Y = 1.5 using rho7lut with opacity 32*

*t = 1198 min. (actually XXXX min)*

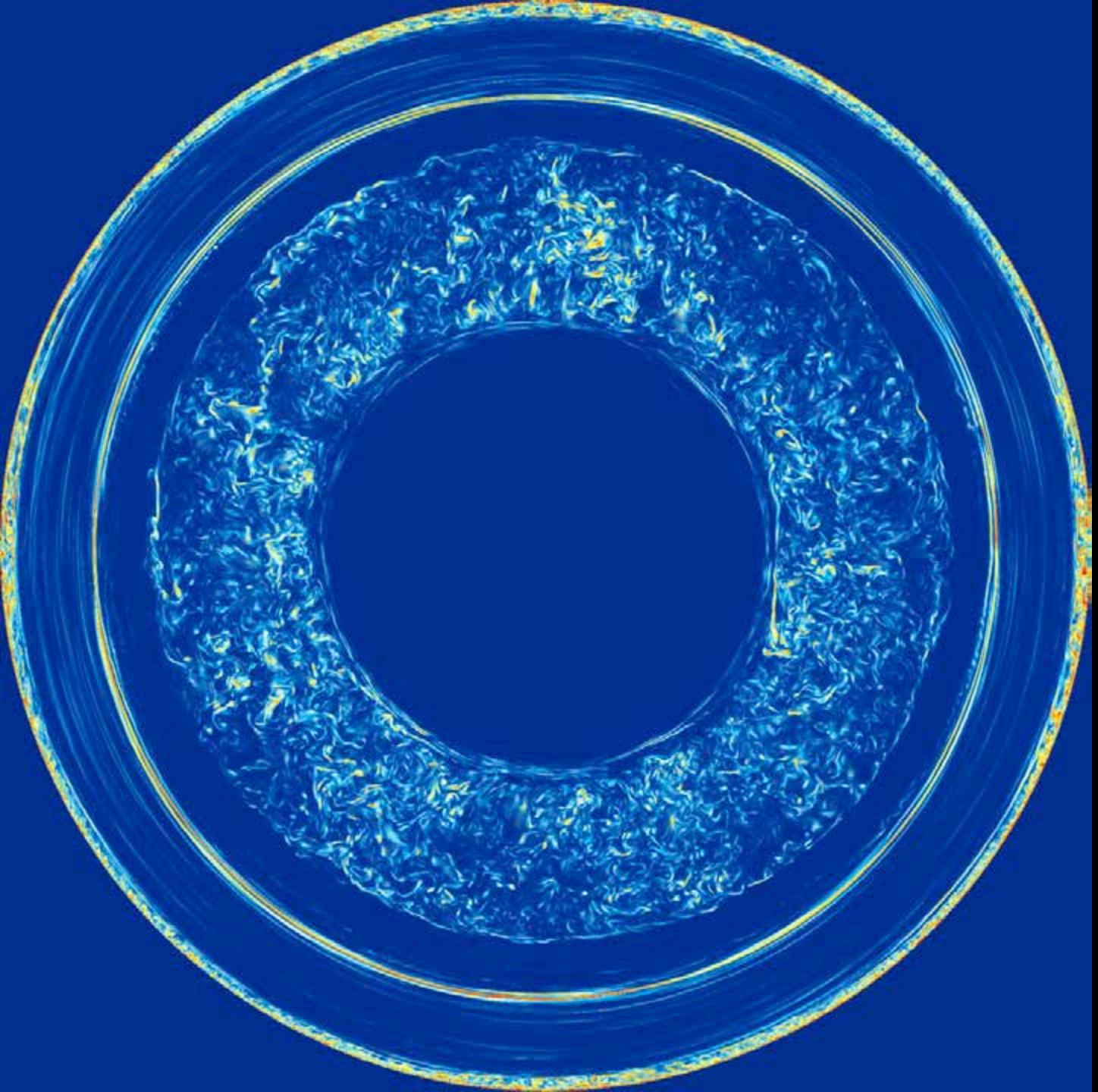

*These images of the magnitude of the vorticity show the flow field in a slice through the middle of the equator that is 1% of the domain's thickness.*

*Sakurai's Object H-ingestion simulation on Blue Waters machine in Jan., 2014, on a grid of $1536^3$ cells.*

*We look down the Y axis from Y = 1.5 using rho7lut with opacity 32*

*t = 1277 min. (actually XXXX min)*

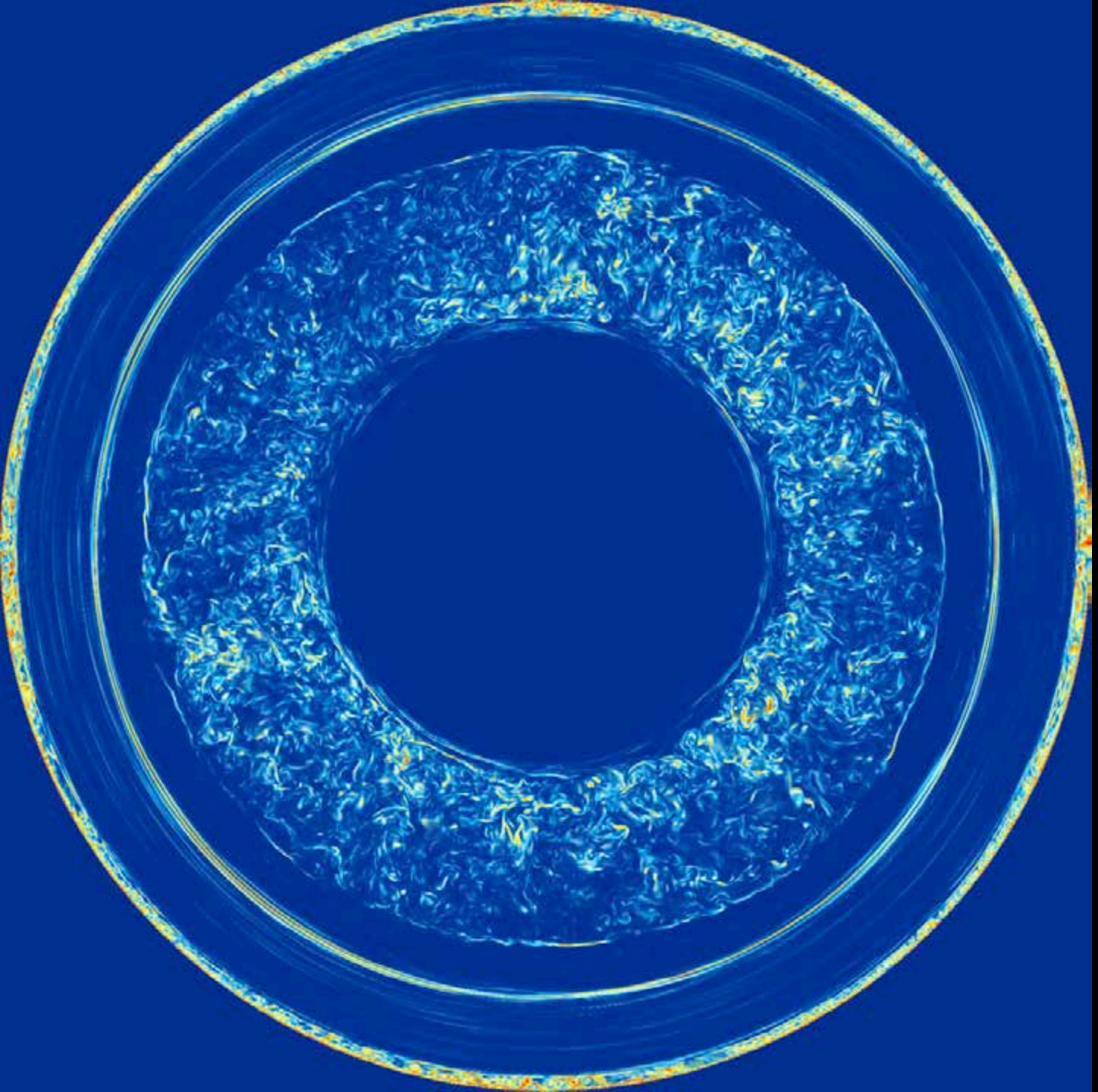

*These images of the magnitude of the vorticity show the flow field in a slice through the middle of the equator that is 1% of the domain's thickness.*

*Sakurai's Object H-ingestion simulation on Blue Waters machine in Jan., 2014, on a grid of $1536^3$ cells.*

*We look down the Y axis from Y = 1.5 using rho7lut with opacity 32*

*t = 1362 min. (actually XXXX min)*

## Experience with Intel MIC:

- As we did with the Cell processor, we put ALL our computational code onto the MIC card.
- The team leader (I/O) and timekeeper (global reduction) processes fit more naturally onto a host.
- At TACC, host <---> 114 Gflop/s
  and MIC <---> 103 Gflop/s.
- We give each $272^3$ cells to update, and MPI on the PCIe bus slows them each down to 87.4 Gflop/s.
- Thus one TACC node > 2 Blue Waters nodes.
- Whole TACC machine capable of 1.0 Pflop/s on PPM.
- Petaflop/s computation is therefore here and affordable on multiple NSF systems.
- Future systems will be significantly more powerful.

## Some History:

1. ***In 2008 a multifluid PPM code was built by Woodward, Jayaraj, Lin, and Knox at the University of Minnesota targeting the IBM Cell processor to demonstrate the potential of grid briquette data structures, massive code pipelining, and multithreaded SIMD processing for very high performance of hydrodynamics codes on multicore CPUs with small on-chip memories.***
2. ***The particular variant of the PPM gas dynamics scheme***

   *[* P. R. Woodward and P. Colella, "High-Resolution Difference Schemes for Compressible Gas Dynamics," *Lecture Notes in Phys*. **141**, 434 (1981); P. R. Woodward and P. Colella, "The Numerical Simulation of Two-Dimensional Fluid Flow with Strong Shocks," *J. Comput. Phys*. **54**, 115-173 (1984); P. Colella and P. R. Woodward, "The Piecewise-Parabolic Method (PPM) for Gas Dynamical Simulations," *J. Comput. Phys*. **54**, 174-201 (1984); P. R. Woodward, "Numerical Methods for Astrophysicists," in *Astrophysical Radiation Hydrodynamics*, eds. K.-H.Winkler and M. L. Norman, Reidel, 1986, pp. 245-326. Preprint available at www.lcse.umn.edu/PPB; P. R. Woodward, "The PPM Compressible Gas Dynamics Scheme," in *Implicit Large Eddy Simulation: Computing Turbulent Fluid Dynamics*, eds. F. Grinstein, L. Margolin, and W. Rider (Cambridge Univ. Press, 2006). Preprint available at www.lcse.umn.edu/ILES. *]*

   ***is described in the last of the references just given.***
3. ***The PPB method used for advection of the multifluid fractional volume is described in:***

   *[* P. R. Woodward, "Numerical Methods for Astrophysicists," in *Astrophysical Radiation Hydrodynamics*, eds. K.-H.Winkler and M. L. Norman, Reidel, 1986, pp. 245-326. Preprint available at www.lcse.umn.edu/PPB; Woodward, P. R., D. H. Porter, W. Dai, T. Fuchs, A. Nowatzki, M. Knox, G. Dimonte, F. Herwig, and C. Fryer, 2010, "The Piecewise-Parabolic Boltzmann Advection Scheme (PPB) Applied to Multifluid Hydrodynamics," report LA-UR 10-01823, available at www.lcse.umn.edu/PPMplusPPB; Woodward, P. R., J. Jayaraj, P.-H. Lin, G. M. Rockefeller, C. L. Fryer, G. Dimonte, W. Dai, and R. J. Kares, "Simulating Rayleigh-Taylor (RT) instability using PPM hydrodynamics at scale on Roadrunner," LA-UR 11-00061, Proc. NECDC 2010 conference, Los Alamos, Oct., 2010, preprint available at www.lcse.umn.edu/-NECDC2010; Woodward, P. R., Herwig, F., and Lin, P.-H., "Hydrodynamic Simulations of H Entrainment at the Top of He-Shell Flash Convection," submitted to the *Astrophysical Journal*, arXiv:1307.3821, (2013). *]*

## Some History:

4. ***This code was tested on Cell processor and Intel workstation equipment at the University of Minnesota's Laboratory for Computational Science & Engineering (LCSE).***
5. ***Then, with assistance from William Dai, Matt Sheats, Chris Fryer, and Gabe Rockefeller, a similar multifluid PPM code was run at scale on LANL's Roadrunner machine in 2010***
   ***(cf. LA-UR 11-00061, available at www.lcse.umn.edu/NECDC2010.)***
6. ***Multifluid PPM codes have been run on the Blue Waters machine achieving 1.5 Pflop/s sustained on 702,000 cores. (cf. LA-UR 13-20949, available at www.lcse.umn.edu/NECDC2012; also*** www.ncsa.illinois.edu/News/Stories/PFapps***)***
7. ***Multifluid PPM codes have achieved 104 Gflop/s on a single Intel Knights Corner (KNC) card, 114 Gflop/s on a dual-CPU Sandy Bridge (2xSB) node, and delivers 174 Gflop/s per KNC+2xSB node at scale.***
   ***Cf.*** Woodward, P. R., J. Jayaraj, P.-H. Lin, M. Knox, J. Greensky, S. D. Hammond, S. E. Anderson, "Scaling the Multifluid PPM Code on Blue Waters and Intel MIC," Proc. Extreme Scaling 2013 Workshop, Boulder CO, August, 2013.
   https://www.xsede.org/documents/271087/586927/Woodward.pdf

t = 0.045000

The uniform Cartesian grid moves steadily inward. We render the same portion of the grid in each view here so that the field of view includes roughly the entire part of the problem domain in which no boundary conditions are applied.

Dump 30

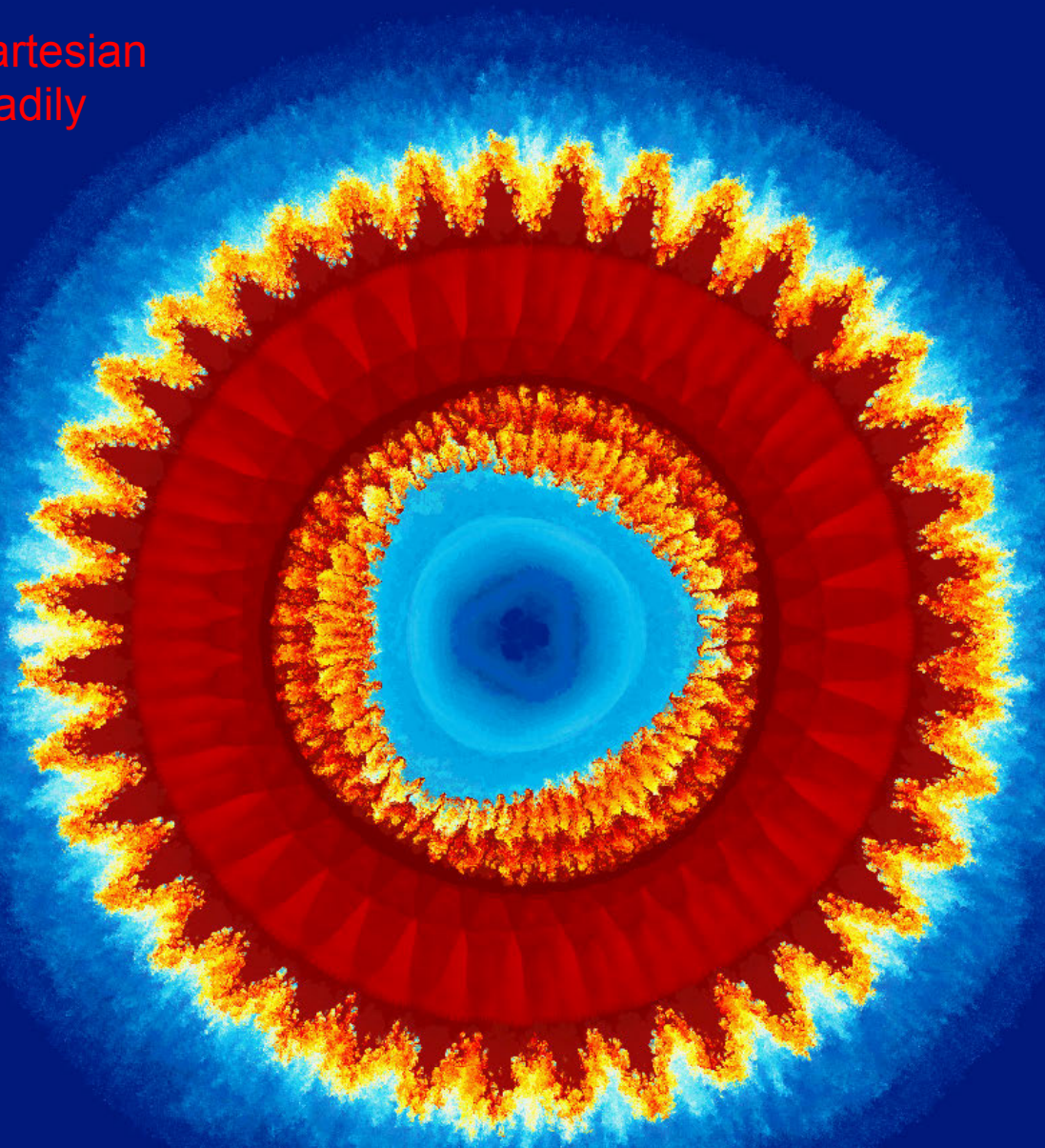

$\rho$

$10560^3$ grid

$22^{nd}$ $44^{th}$ in Y

rholut 7

opacity 48

distance from midplane 1.45

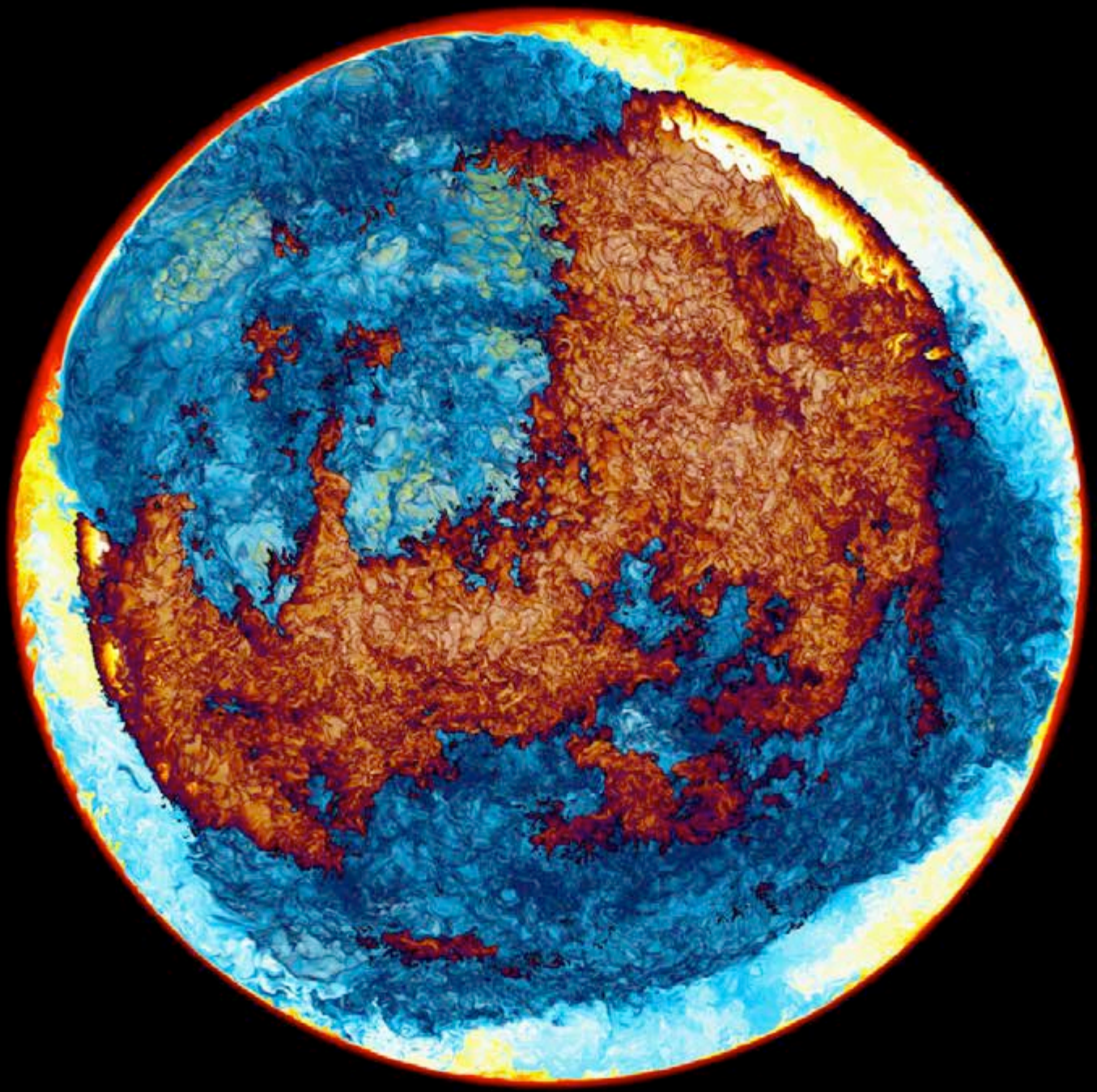

*Sakurai's Object H-ingestion simulation on Blue Waters machine in Jan., 2014, on a grid of $1536^3$ cells.*

*We see a hemisphere and make only mixtures of entrained hydrogen-rich gas with gas of the helium shell flash convection zone visible. The energy release rate from burning ingested H is shown in very dark blue, yellow, and white.*

*t = 1175 min.*

## Some History:

***8. The strategy of the code design used in multifluid PPM has been set out in:***


Woodward, P. R., Jagan Jayaraj, and Pei-Hung Lin, "Transforming Scientific Codes to Execute Efficiently on the IBM Cell Processor as well as on Other Multicore Microprocessor CPUs." LCSE Report, Nov. 9, 2006, available at www.lcse.umn.edu/F77-for-CELL.

Woodward, P. R., J. Jayaraj, P.-H. Lin, and P.-C. Yew, 2008, "Moving Scientific Codes to Multicore Microprocessor CPUs," *Computing in Science & Engineering*, special issue on novel architectures, Nov., 2008, p. 16-25. Preprint available at www.lcse.umn.edu/CiSE.

Woodward, P. R., J. Jayaraj, P.-H. Lin, and W. Dai 2009, "First Experience of Compressible Gas Dynamics Simula-tion on the Los Alamos Roadrunner Machine," *Concurrency and Computa-tion Practice and Experience*, **21,** 2160-2175 (2009), preprint available at www.lcse.umn.edu/RR-experience.

Woodward, P. R., J. Jayaraj, P.-H. Lin, P.-C. Yew, M. Knox, J. Greensky, A. Nowatzki, and K. Stoffels, "Boosting the performance of computational fluid dynamics codes for interactive supercomputing," Proc. Intntl. Conf. on Comput. Sci., ICCS 2010, Amsterdam, Netherlands, May, 2010. Preprint available at www.lcse.umn.edu/ICCS2010.

## Some History:

9. ***The motivation for and results of building automated tools to execute this code design strategy has been set out in:***

   Lin, P.-H., J. Jayaraj, and P. R. Woodward, "A Study of the Performance of Multifluid PPM Gas Dynamics on CPUs and GPUs," Proc. SAAHPC Conference, Knoxville, Tennessee, July, 2011. Preprint available at www.lcse.umn.edu/SAAHPC and presentation available at http://www-users.cs.umn.edu/~phlin/pub/SAAHPC2011.pdf ;

   P.-H. Lin, J. Jayaraj, P. R. Woodward, and P.-C. Yew, 2011, "A Code Transformation Framework for Scientific Applications on Structured Grids," Technical Report 11-021, UMN Computer Science and Engineering Technical Report, Sept., 2011, available at https://wwws.cs.umn.edu/tech_reports_upload/tr2011/old_files/11-021.pdf ;

   Jayaraj, J., P.-H. Lin, P. R. Woodward. And P.-C. Yew, "CFD Builder: A Library Builder for Computational Fluid Dynamics," to appear in Proceedings of 28th IEEE International Parallel & Distributed Processing Symposium (IPDPS): Programming Models, Languages and Compilers Workshop for Manycore and Heterogeneous Architectures (PLC2014), Phoenix, AZ, 2014, preprint available at www.lcse.umn.edu/IPDPS2014.

   Also the theses of Jagan Jayaraj and Pei-Hung Lin in 2013.